# NICASTRIN AS A NOVEL THERAPEUTIC TARGET IN BREAST CANCER

**by**

**Aleksandra Filipović**

**A thesis submitted for the degree of**

**Doctor of Philosophy at Imperial College London**

Imperial College London, Faculty of Medicine

Division of Surgery and Cancer

Department of Oncology

**Supervisor:** Prof. R Charles Coombes

**Co-supervisor:** Dr Ernesto Yagüe

Unless otherwise stated, the present thesis is the result of my own work.

*To my family*

# Abstract

Nicastrin is an essential component of the gamma-secretase (GS) enzyme complex, required for its synthesis and recognition of substrates for proteolytic cleavage. The purpose of this study was to investigate whether nicastrin has a prognostic value or the potential as a therapeutic target in breast cancer.

Tissue microarrays (TMAs) (n = 1050), and breast cancer cell line analyses confirmed that nicastrin expression was upregulated in breast cancer compared to normal breast cells. In TMA patient samples, high nicastrin expression was observed in 47.5% of cases and correlated with worse breast cancer specific survival in the ERα negative cohort.

Transient and stable gene silencing of nicastrin i*n vitro*, resulted in the disruption of the GS complex activity and a decrease in Notch1 cleavage. Nicastrin silencing in invasive MDA-MB-231 and HCC1806 cells resulted in the loss of vimentin expression and a reduction in cell invasion, which was concomitant with the formation of cell-cell junctions, as well as cellular repolarisation. In a population of breast cancer cells harbouring the cancer stem cell phenotype ($CD44^+/CD24^-$), nicastrin depletion abrogated expression of the epithelial to mesenchymal (EMT) markers, vimentin, SIP1 and Snail. Furthermore, nicastrin overexpression in the non-malignant MCF10A breast cells increased expression of other GS components, Notch activation, vimentin expression and invasive capacity. These data indicate that nicastrin can function to maintain the EMT transition during breast cancer progression. We have developed anti-nicastrin polyclonal and monoclonal antibodies and have shown that they are able to decrease the invasive and proliferative capacity of MDA-MB-231 breast cancer cells *in vitro*. In order to dissect the role of nicastrin within the GS complex from its presumed GS-independent signaling role in breast cancer cells, we have performed gene array analyses and identified a subset of genes that are nicastrin-dependent and are not affected by silencing of the Notch receptors. The data presented in this thesis therefore support our hypothesis that an antagonising monoclonal antibody could be suitable to inhibit nicastrin as a potential therapeutic target in invasive breast cancer.

# Acknowledgements

I wish to thank my supervisor, Prof R Charles Coombes for his continuous support, guidance and encouragement throughout my research work. Without his faith in me, and the freedom he gave me to be inspired by research, I wouldn't have developed into a truly passionate medical scientist. I would like to extend my gratitude to Dr Ernesto Yagüe for his guidance and intellectual help during the project. My sincere thanks go to my group members: Sabeena Rasul, Rachel Payne, Natasha Hava, and Bala Subramanian, who have helped me to acquire the technical skills required for the work. I would like to thank our new group member, Dr Ylenia Lombardo for her work on the 3D Matrigel culture assays, and mammosphere formation experiments and Dr Dongmin Shao for production of the NCT recombinant protein used for the generation of the anti-nicastrin polyclonal antibodies. Special gratitude goes to the Nicastrin Team: Dr Hayley Cordingley for her supreme project management, intellectual advice and scintillating summaries of our meetings; Dr Cathy Tralau-Stewart and Prof. Andrew George for their experienced advice; Dr Deonarain Mahendra for all his support and expertise with the BIACore experiments and advice on the characterisation of the monoclonal anti-nicastrin antibodies; Dr Jon Wilkinson for his guidance through the maze of intellectual property terminology and procedure, and his constant reminders that epitope mapping is of outmost importance. I would like to extend special gratitude to Prof Justin Stebbing for his professional guidance and for giving me the opportunity to feel like a part of his team as well. My gratitude extends to our collaborators: Prof. Ian Hart and Sabari Vallath for letting me join their team and perform the invasion assays at the Bart's School of Medicine; Dr Andrew Green for providing us with the priceless tissue arrays; Prof. Lucio Miele for continuous expert advice and assistance with the gene microarrays. I would like to thank Dr Justin Sturge and Julian Gronau for their help during this project. I wish to give credit to the Cancer Research UK for their financial support. Last but certainly not least, I would like to thank my friends, the ones in my home country, and new friends I have made at Imperial, who have whole heartedly supported me and shared with me the joys and the frustrations during the past four years. I would like to thank a special person in my life, Georgios Giamas, who has become my partner in every sense of that word, and without whose constant attention, affection and faith, I wouldn't have completed this work and grown as a person.

I would like to thank my parents for their generosity and making this life possible for me. I thank my father for handing me a pipette when I was five and my mother for being the greatest support a daugther could wish for and for opening the door to the world of oncology for me. But mostly, I am eternally grateful that they had the courage and faith in me to let me journey out on my own. It has been a great ride.

*Hvala vam !*

Ako mozes ostati miran kad na tvom putu
Svi izgube glavu i prstom pokazuju na tebe,
Ako sacuvas poverenje kad svi ostali sumnjaju,
Ali ako im ne zameris sto nemaju poverenja;
Ako ti cekanje ne predstavlja mnogo muke;
Ako ne lazes kad cujes lazi,
Ili ako ne mrzis kad tebe mrze;
Ako se ne pravis suvise dobar, niti govoris suvise mudro;
Ako snivas ali ti snovi nisu sve;
Ako mislis ali ti misli uvek ostaju ciste;
Ako znas da primis pobedu i poraz,
Da primis jednako i jedno i drugo;
Ako mozes podneti da tvoju istinu
Varalice iskrivljuju da bi lakse prevarili budale;
Ako vidis kako u komadice razbijaju tvoj cilj
I ako se sagnes da podignes i pokupis ostatke.

Ako mozes sakupiti sva tvoja dobra
I staviti ih na kocku, sve odjednom,
Ako si spreman da ponovo krenes, kao na pocetku,
Ne prosaptavsi ni reci, izgubivsi sve uz osmeh;
Ako prisilis svoje srce, svoje zivce, svoje misice
Da sluze tvojim ciljevima i kad su malaksali,
I aku ustrajes kada sve zaostane,
Izuzev volje koja naredjuje: "Drzi se dobro"
Ako se usred gomile ne ponosis,
I ne smatras se herojem, ako se druzis sa kraljevima;
Ako te ni prijatelj ni neprijatelj ne mogu pokvariti;
Ako svaki covek za tebe nesto znaci, ali ni jedan suvise;
Ako umes dobro ispuniti svaku minutu svog zivota,
I svakog trenutka ides pravim putem;
Tvoja ce biti zemlja i sve njeno blago,

Jer,

BICES COVEK, SINE MOJ

Rudyard Kipling

# Table of Contents

## Abbreviations

| | |
|---|---|
| °C | degree Celsius |
| 2D | two dimensional |
| 3D | three dimensional |
| aa | amino acid |
| amp | ampicillin |
| APS | ammonium persulfate |
| AD | Alzheimer's disease |
| Aph-1 | anterior pharynx defective-1 |
| APP | amyloid precursor protein |
| APP | amyloid Precursor Protein |
| ApoE | apolipoprotein E |
| Aβ | amyloid beta peptide |
| Bad | bcl2-associated agonist of cell death |
| BCA | bicinchoninic acid |
| Bcl-2 | b-cell leukaemia/lymphoma-2 |
| Bcl-XL | bcl2-related protein long isoform |
| bp | base pair |
| BSA | bovine serum albumine |
| Bub1 | budding uninhibited by benzimidazoles 1 |
| CHAPSO | [3-[(3-cholamidopropylldimethylammino-]-2-hydroxy-1-propanesulfonate] |
| CHO | chinese Hamster Ovary cell line |
| Cdk | cyclin-dependent kinase |
| $CO_2$ | carbon dioxide |
| DAPI | 4',6-diamidino-2-phenylindole |
| DMEM | dulbecco´s-modified Eagle's medium |
| DNA | deoxyribonucleic acid |
| dNTP | deoxyribonucleotide triphosphate |
| DTT | dithiothreitol |
| ECL | enhanced chemiluminescence |
| EDTA | ethylene-diamine-tetraacetic acid |

| | |
|---|---|
| EGTA | ethylene bis (oxyethylenenitrilo) tetraacetic acid |
| ECM | extracellular Matrix |
| ELISA | enzyme-linked immunosorbent assay |
| EOAD | early onset alzheimer's disease |
| ER | endoplasmic reticulum |
| ERα | estrogen receptor alpha |
| FACS | fluorescent activated cell sorter |
| FAD | familial alzheimer's disease |
| FCS | fetal calf serum |
| FGF | fibroblast growth factor |
| FGFR | fibroblast growth factor receptor |
| Fv | variable domain |
| g | gravity |
| G1,G2 | gap phases of cell cycle |
| GAPDH | glyceraldehyde 3-phosphate dehydrogenase |
| GFP | green fluorescent protein |
| GS | gamma-secretase |
| HEK293 | human embryonic kidney 293 cell line expressing swedish mutant APP695 |
| HeLa | Henrietta Lack Cells |
| HEPES | 4-2-hydroxyethyl-1-piperazineethanesulfonicacid |
| h | hour |
| $H_2O_2$ | hydrogen peroxide |
| HCl | hydrochloric acid |
| HRP | horse radish peroxidase |
| IgG | immunoglobulin G |
| IPTG | isopropyl N-phenylcarbanate |
| KCl | potassium chloride |
| kDa | kilodalton |
| $K_d$ | dissociation constant |
| *K*m | michaelis menten constant |
| KO | knockout |
| LB | Luria Bertani medium |

| | |
|---|---|
| LOAD | late onset Alzheimer's disease |
| M | molar |
| MAb | monoclonal antibody |
| mAmp | milliamp |
| MAPK | mitogen-activated protein kinases |
| MEK | mitogen-acivated Erk kinase |
| $MgCl_2$ | magnesium chloride |
| min | minutes |
| ml | mililiter |
| mM | milimolar |
| mTor | mammalian target of rapamycin |
| mRNA | messenger ribonucleic acid |
| MW | molecular weight |
| NaCl | sodium chloride |
| NaOH | sodium hydroxide |
| NCT | nicastrin |
| nM | nanomolar |
| NSAID | non-steroidal anti-inflammatory drug |
| NP40 | nonyl -phenoxypolyethoxy ethanol |
| nm | nanometer |
| ng | nano-gram |
| PAGE | polyacrylamide gel electrophoresis |
| PBS | phosphate-buffered saline |
| PcAb | polyclonal antibody |
| PCR | polymerase chain reaction |
| PDGF | platelet derived growth factor |
| PEN2 | presenilin enhancer protein-2 |
| PFA | paraformaldehyde |
| pH | negative decimal logarithm of hydrogen ion concentration |
| pI | isoelectric point |
| PI3K | phosphatidylinositol 3-kinase |
| PKA | cAMP-dependent protein kinase |

| | |
|---|---|
| PKC | protein kinase C |
| PS (1/2) | presenilin (1/2) |
| PTM | post-translational modification (s) |
| PVDF | polyvinylidene fluoride |
| RAS | sarcoma virus-associated oncogene |
| Rb | retinoblastoma |
| RIP | regulated intramembrane proteolysis |
| RNA | ribonucleic acid |
| RNAi | RNA interference |
| rpm | rounds per minute |
| RT | room temperature |
| RTK | receptor tyrosine kinase |
| RT-PCR | reverse transcription polymerase chain reaction |
| S phase | replication phase of cell cycle |
| SDS | sodium dodecylsulphate |
| SHSY5Y | human Neuroblastoma SH-SY5Y cell line |
| siRNA | small interfering RNA |
| SNP | single nucleotide polymorphism |
| SP | signal peptide |
| SPP | signal peptide peptidase |
| Ta | annealing temperature |
| TAE | tris acetate EDTA |
| Taq | thermus aquaticus |
| TBS-T | tris-buffered saline with Tween |
| TEMED | N,N,N',N' tetramethyl ethylenediamine |
| TMD(s) | transmembrane domain(s) |
| Tris | 2-amino-2 hydroxymethyl-1,3-propanediol |
| Triton X-100 | 4-octylphenol polyethoxylate |
| TWEEN-20 | polyoxyethylenesorbitan |
| UK | United Kingdom |
| USA | United States of America |
| VEGF | vascular endothelial growth factor |
| VEGFR | vascular endothelial growth factor receptor |

| | |
|---|---|
| VIM | vimentin |
| wt | wild type |
| β-ME | β-mercaptoethanol |
| µg | microgram |
| µl | microliter |
| µM | micromolar |

# CHAPTER 1

# Introduction

# 1. Breast Cancer

Cancer is the leading cause of death worldwide accounting for over 7 million deaths in 2010. Based on recent estimates, cancer incidence across the world will rise from 11 million cancer cases diagnosed in 2002, to predicted 17 million in 2020 and alarming 27 million by 2050 (1). Global mortality rates from malignant disease are also projected to increase from 7.1 million in 2002 to 11.5 million in 2030 (2).

## 1.1. Breast cancer incidence and mortality

Breast cancer is the most frequent neoplasm diagnosed in women, and accounts for 30% of all cancers in the female population. The cumulative lifetime risk of developing breast cancer is one in nine women (3), with the incidence rising by 1-3% yearly in most parts of the world (4). In 2002, there were 1.15 million cases of breast cancer diagnosed worldwide, while that number increased to 1.38 in 2010 (Figure 1a) (1). Known risk factors for developing breast cancer are related to:

i) Menstrual cycle (early menarche < 12 yrs; late menopause > 55 yrs);

ii) Pregnancy (nuliparity, late first birth > 30 yrs, multiple gestation > 35 yrs);

iii) Pre-menopausal hormonal therapy i.e. oral contraceptives for > 10 yrs and/or post-menopausal hormono-replacement therapy for > 5 yrs;

iv) Family history of breast cancer;

v) Genetic susceptibility: BRCA1 and BRCA2 mutation carriers;

vi) Lifestyle choices (alcohol intake, smoking, high body mass index, lack of physical activity etc.).

Joint effects of cancer-susceptibility genes and other endogenous and lifestyle risk factors are likely to account for the majority of diagnosed breast cancers (5). Use of screening programs in developed countries, enabling diagnosis of breast cancer at an early stage, as well as changes in exposure to risk factors and improvements in the post-operative adjuvant systemic and targeted therapies, have reduced overall mortality from breast cancer in the past three decades (Figure 1b) (2) (6, 7).

a)

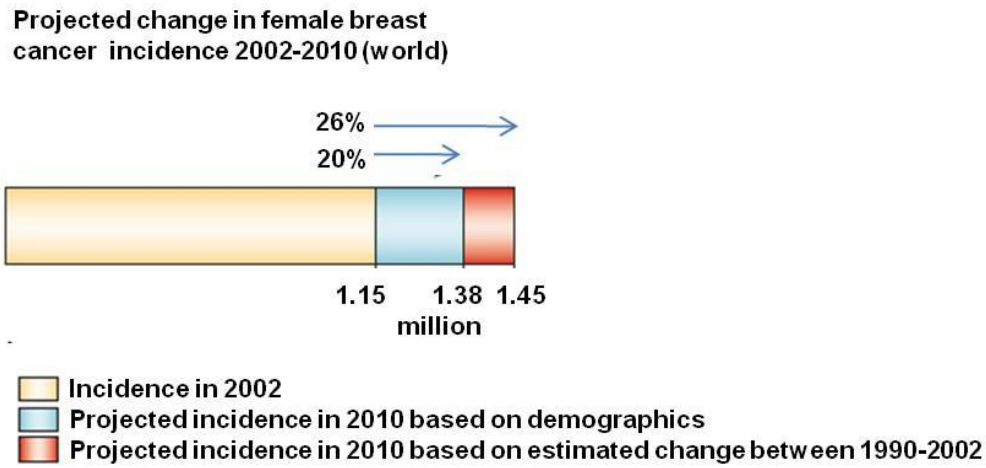


b)

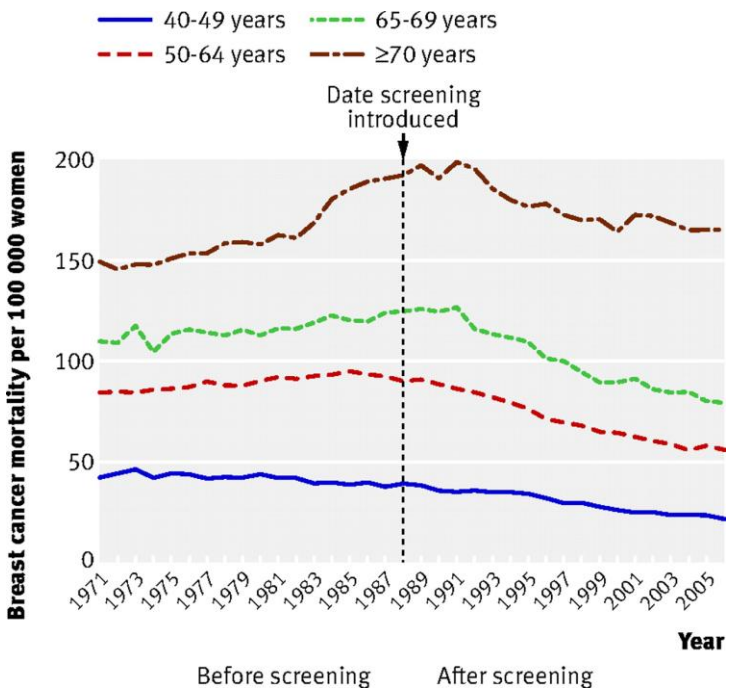


**Figure 1**.**Incidence of breast cancer. a)** Projected change in female breast cancer incidence. In 2002, the incidence of breast cancer was 1.15 million; 1.5 million new cases were diagnosed in 2010. Population growth and ageing alone would account for approximately two-thirds of the increase; **b)** Age adjusted breast cancer mortality rates in the United Kingdom for screened and non-screened age groups: (http://info.cancerresearchuk.org/cancerstats/types/breast/mortality).

Despite this obvious progress, there will still be women presenting with advanced and even metastatic disease at diagnosis, or will develop disseminated disease and eventually die.

### 1.1.2. Cellular pathways promoting breast cancer

In normal cells, a network of cellular signaling exists to maintain the homeostasis of cellular functions and balance tumour-suppressor versus oncogenic signals in favour of the former, to prevent cancer development.

Cancers arises from cells that have undergone a malignant transformation as a consequence of accumulating molecular alterations that lead to a disturbance of cell homeostasis (8). Characteristics commonly attributed to cancer cells are: a) uncontrolled cellular proliferation, b) insensitivity to negative growth regulation, c) evasion of apoptosis, d) lack of senescence, e) invasion, f) metastasis, g) neo-angiogenesis, h) genomic elasticity (Figure 2) (8).

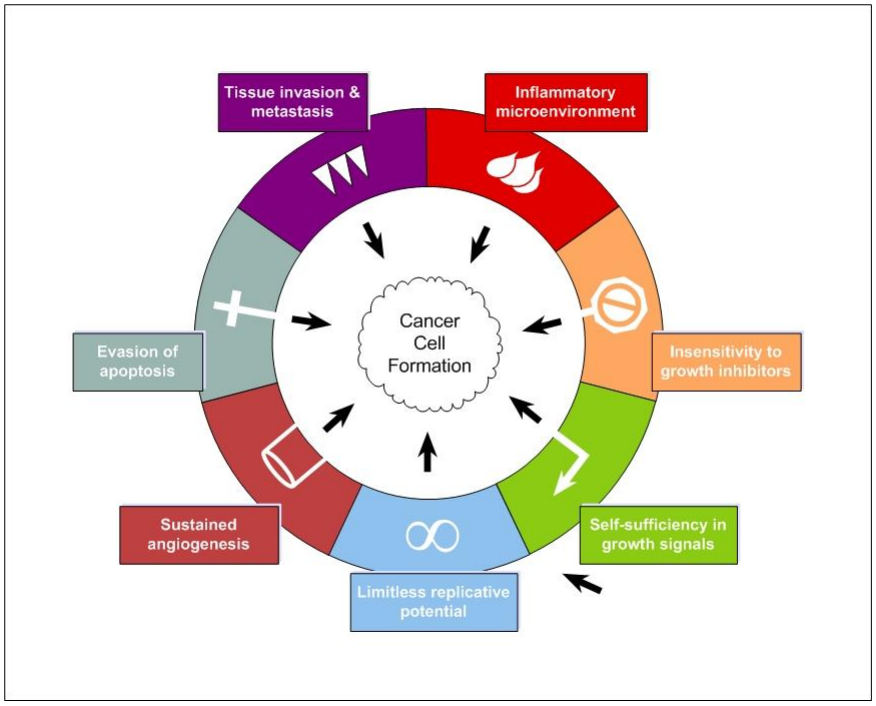


**Figure 2.The seven hallmarks of a cancer cell (8)**

Genes with highly diverse functions that are susceptible to alterations in cancer cells are grouped into three main categories: oncogenes, tumour suppressor genes and stability genes (9). Proteins encoded by these genes have complex roles in cellular processes and engage in the function of multiple cellular signaling networks (10). In cancer, oncogenes acquire so called ‘gain of function’ mutations that render these genes constitutively active in a cell (exp. Extracellular signal regulated kinase, ERK).

Conversely, tumour suppressor genes are targeted by the 'loss of function' alterations (e.g. p53). Stability genes are responsible for repairing damage caused in DNA replication, or damage of mutated genes (e.g. BRCA1). Mutations of these genes can occur in the germline or as somatic mutations. The former infer hereditary predisposition to malignant disease, while the latter underpin sporadic cancers. Molecular and gene signatures are novel tools that are used in the era of tailored patient treatment to determine the exact characteristics of a cancer and derive not only prognostic conclusions, but also predict response to certain types of treatment.

The complexity in the management of cancers lays in the heterogeneity of the disease, the ability of cancer cells to make the pathways that have been inhibited by therapy redundant, and the capacity to activate alternative routes for survival. In a fully transformed malignant cell, communications between oncogenic pathways ensure that once one pro-survival pathway has been inhibited by therapy, an alternative one is switched on to compensate, a phenomenon often referred to as 'oncogene addiction' (10).

### 1.1.3. Heterogeneity of breast cancer

Breast cancer is a heterogeneous disease that presents with a continuum of clinical, histological and molecular features. Several breast cancer characteristics provide insight into the biology of the disease and act as prognostic and predictive parameters, and guide treatment decision-making. These features are: histological type (Figure 3), histological grade, presence of lympho-vascular invasion, presence of sentinel and/or axillary lymph node invasion, and expression of markers like hormone receptors (ERα, PR), and the growth factor receptor, HER2 (11). The most recent classification by the World Health Organisation (WHO) recognises at least 18 distinct histological types of breast cancer (12), majority of which (50-80%) are invasive ductal carcinomas of non specific type (IDC-NST). Invasive lobular carcinomas (ILC) are the second most frequent subtype of breast cancer (5-15%). All other histological patterns constitute up to 25% of the breast cancer histological milieu (Table 1).

**Table 1.Prevalence of different breast cancer histological subtypes (12)**

| Histological type | Prevalence (%) |
|---|---|
| **Invasive ductal carcinoma-non special type** | 50-80 |
| **Invasive lobular carcinoma** | 5-15 |
| **Pure tubular carcinoma** | < 2 |
| **Invasive cribriform carcinoma** | 0.8-3.5 |
| **Medullary carcinoma** | 1-7 |
| **Mucinous carcinoma** | 2 |
| **Neuroendocrine tumours** | 2-5 |
| **Invasive papillary carcinoma** | 1-2 |
| **Invasive micropapillary carcinoma** | < 2 |
| **Apocrine carcinomas** | < 4 |
| **Metaplastic carcinomas** | < 1 |
| **Lipid-rich carcinomas** | < 1-6 |
| **Secretory carcinomas** | < 0.15 |
| **Adenoic cystic carcinomas** | 0.1 |
| **Glycogen-rich clear-cell carcinomas** | 1-3 |

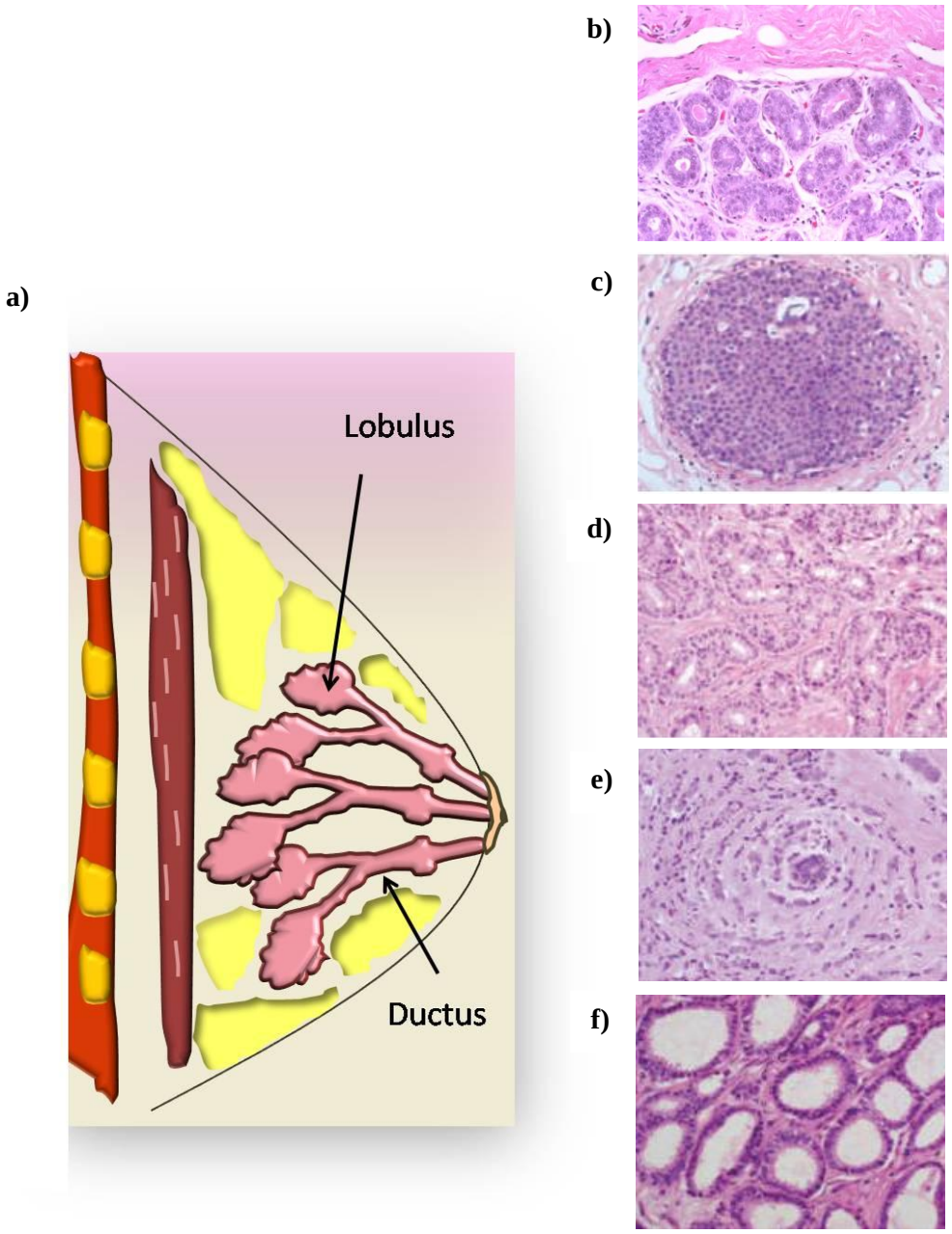


**Figure 3.Breast tissue composition and main histological representations of normal and malignant breast tissue. a)** Schematic of the breast architecture, and histological representation of **b)** normal breast tissue, **c)** ductal carcinoma *in situ*; **d)** invasive ductal carcinoma; **e)** invasive lobular carcinoma; **f)** tubular and cribriform breast carcinoma (13).

The seminal work of Wellings et al. suggests that all invasive breast carcinomas and their *in situ* precursor lesions stem from the terminal ducto-lobular unit. Hence, ductal and lobular denomination does not indicate the site of origin but rather implies distinct architectural patterns, cytological and immunohistochemical profiles (14).

### 1.1.4. Taxonomy of breast cancer

The era of microarray technology has yielded molecular signatures of breast cancer, which when compared to the histopathological surrogates and clinical features of the tumours reveal clear genetic-phenotypic correlations (15).

The majority of breast cancers are of the luminal type (60-70%). They are commonly estrogen receptor (ERα) positive, and highly dependent on the ERα driven signaling, while at the same time expressing low molecular weight cytokeratins, CK 8/18/19, as well as the cell-cell adhesion molecule E-cadherin. Within the luminal breast cancers, the luminal A type encompasses tumours with very high levels of the ERα, lower histological grade, lower mitotic index, and thus a favourable clinical prognosis. Luminal B and C type cancers have a lower ERα expression score and a less favourable prognosis, as their histological grade is usually higher, as is their rate of proliferation (Figure 4) (15).

Epidermal growth factor receptor 2 (ErbB2/HER2) positive tumours, which comprise 20-25% of all breast cancers are a separate entity, bearing overexpression of the HER2 protein (HER2 3+ by immunohistochemistry), and/or amplification of the HER2 amplicon on chromosome 17q12 (Figure 4). They are highly aggressive cancers, predominantly ERα negative, which rely on the HER2 signaling axis for their growth and spread. According to gene expression patterns, about 20% of the HER2 positive tumours jointly express the ERα protein and belong to the luminal type B (15).

Basal-like breast cancers are another group of ERα negative tumours, which represent ~15% of all breast cancers and resemble the luminal progenitor cells of the normal breast. They often express P-cadherin, caveolins, epidermal growth receptor 1 (EGFR), while they lack or have very low levels of ERα, PR and HER2 (Figure 4). For that reason basal tumours are commonly referred to as triple negative, although these are not overlapping entities. Both basal like and triple negative breast cancers are highly aggressive and are often underpinned by the existence of BRCA1 mutations. They display a distinct pattern of metastasis favouring brain and lung as secondary deposit sites, and the overall survival after detection of metastatic disease is often shorter in these types of cancer, than the luminal and HER2 positive. They often occur in younger women, before the age of 50, and are frequent in the African-American population (15).

Even though there are still many uncharacterised breast cancer subtypes, the molecular profiles, known histological types, clinical behaviour and the existing taxonomy of breast cancer, hold both prognostic and predictive value and drive disease management.

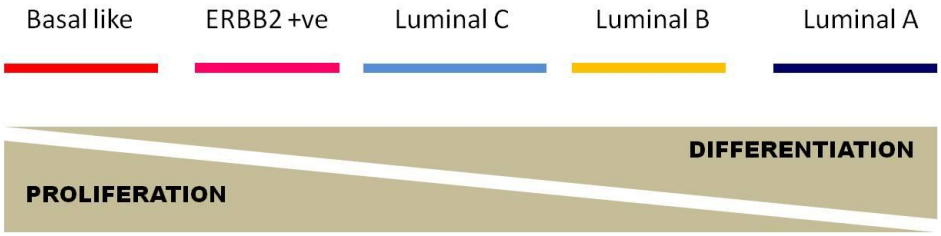


**Figure 4.Subtypes of breast cancer**. Schematic representation of the degree of cancer cell proliferation vs. cancer cell differentiation in the main breast cancer subtypes.

## 1.2. Targeted therapies for the treatment of breast cancer

Patient-tailored treatment entails taking into account the molecular makeup of an individual tumour in order to target the cancer driving pathways and ensure a maximal anti-tumour response. In this regard, introduction of monoclonal antibodies (MAbs) as therapies targeted against a specific oncogenic molecule expressed in cancer tissue, are one of the most significant recent advances in the treatment of leukaemias and solid tumours (16).

The vision of selective targeting was introduced a century ago by Paul Ehrlich who hypothesised that the 'magic bullet' could be developed to combat malignant disease (17). The development of the hybridoma technology by Köhler and Milstein has since revolutionised the field and enabled production of murine derived monoclonal antibodies (MAbs) (18). Poor immunogenicity and suboptimal recruitment of the immune system machinery, which represented a major hurdle in their implementation as therapeutics, were overcome by genetic manipulations and fitting these murine antibodies into the human IgG backbone (19). Several variants of MAbs were produced: i) chimeric MAbs, which are constructed from murine variable regions and human constant regions; ii) humanised MAbs where the murine complementarity-determining regions (CDRs) are fitted into the remainder of the human-source MAb construct, and; iii) human MAbs derived entirely from a human source (transgenic mice or phage display) (20).

Antibodies are Y shaped immunoglogulin (Ig) molecules, with a molecular weight of 150 kDa, which are composed of two paired polypeptide heavy- (50-70 kDa) and two light-chains (25 kDa) (Figure 5). Heavy chains are linked together and to the light chains by disulfide bonds. The heavy chains can belong to five distinct classes (A, E, M, D, G), based on their structural and functional properties, thereby determining the antibody isotype and functionality. Therapeutic antibodies are typically of the IgG class. Heavy and light chains contain compactly folded sequences, each of about 110 amino acids, which form repetitive regions ($C_H1$, $C_H2$ and $C_H3$). The first amino terminal region of both the heavy and the light chains greatly differ in their sequence amongst different antibodies, and are therefore termed as 'variable regions' (Fv, ($V_{H,}$ $L_H$)). The variable region is the one that determines the specificity of an antibody towards an antigen and thus harbours the antigen binding domain, while the remaining stable sequences form the constant region. Amino acid variability differs inside variable domains. The highest level of variability is in the so called hyper-variable regions, known as complementarity determining regions (CDR), which determine complementarity of the antigen-antibody interaction. Variable domains of heavy and light chains contain three CDRs (VLCDR1-3, VHCDR1-3) (21). Usually, $V_H$CDRs make a major contribution to contact formation with the antigen and the geometrical center of the antibody-antigen contact is usually located near the $V_H$CDR3 (21). The antibody molecule can be readily cleaved by proteolytic enzymes such as papain, into functionally distinct fragments. Digestion yields: i) the fragment antigen binding domains (Fab) that contain the variable parts of the heavy and the light chains, and ii) the fragment with no antigen binding activity but with a tendency to crystallise (Fc), which interacts with the effector molecules and induces a cellular response by activating the complement system molecules and macrophages (Figure 5).

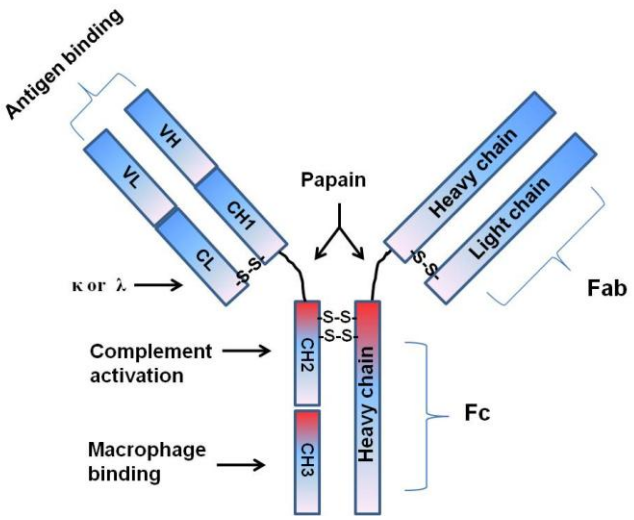


**Figure 5.Architecture of a monoclonal antibody molecule.** Antibodies are Y shaped molecules consisting of two paired polypeptides (heavy- and light-Ig chains). Heavy chains are linked by disulphide bonds. Heavy and light chains contain compactly folded sequences, which form repetitive regions ($C_H1$, $C_H2$, $C_H3$). The first amino-terminal region of both the heavy and the light chains are termed 'variable regions' ($V_H$, $L_H$). The antibody molecule can be cleaved by proteolytic enzymes such as papain into fragment antigen binding domains (Fab) and fragment crystallisable (Fc) domain. Antibody diagram reproduced from www.invitrogen.com

The structure of an antibody molecule is not rigid. The hinge regions that join the Fab domains and the Fc fragment are flexible, and allow the arms of the antibody to assume a range of angles and capture the cognate antigens. The type of antibody-antigen binding, which can be monovalent (one site of attachment) or bivalent (two interaction sites), influences parameters such as: i) antibody affinity (the strength with which an antibody molecule binds an epitope), and ii) avidity (functional affinity, combined strength of multiple bond interactions the effect of which is synergistic) (22).

A candidate target for MAbs is: i) a macromolecule overexpressed in cancer tissue compared to other vital organs, ii) whose overexpression relates to worse outcome of cancer patients given the ability of the antigen to confer oncogenic effects, such as cancer growth and invasion, iii) whose expression can be readily and reproducibly measured in obtained clinical samples, and iv) where interference with the MAb interrupts and inhibits antigen signaling yielding clinical response and survival benefit (23).

### 1.2.1. Factors influencing efficacy of therapeutic monoclonal antibodies

Clinical efficacy of MAbs depends on multiple parameters related to the antigen itself, the antibody, as well as the nature of the antibody-antigen interaction (24, 25). The interplay between pharmacokinetics, pharmacodynamics and the therapeutic efficacy is of paramount importance.

Antigen density and turnover at the cell membrane, affinity of the MAb, and the rate of MAb internalisation are all important determinants of MAb therapeutic efficacy. Minimal affinity is required for specific retention of MAbs in the tumour tissue (26). The off-rate of the MAb should ideally be faster than the antigen internalisation. If the MAb dissociation rate is slower than the antigen internalisation rate, MAb distribution is compromised as degradation of the MAb will occur faster than the equilibrium is achieved (27). Upon internalisation, the MAb is degraded in the endosomal/lysosomal compartment, but the antigen can be recycled and replaced by the newly synthesised protein. The rate of MAb internalisation is therefore dependent on the antigen recycling, while the rate of antigen endocytosis is unaffected by MAb binding (28, 29).

Affinity of a MAb affects tissue penetration in an inverse fashion, a phenomenon termed as the 'binding-site' barrier. This means that the majority of the antibody is taken up by the outer rim of the tumour, thereby limiting the diffusion into the tumour (30). The binding-site barrier is affected by multiple parameters: i) the tumour shape; ii) antigen density; iii) dose of the antibody; iv) vascularisation and lymphatic outflow of the tumour (31). Cross reactivity of the MAb with the antigen expressed in normal tissue (non-target pool of antigens) is involved in reducing the target effects, while the extravasation of MAbs is often compromised by heterogonous vasculature of the tumour and high interstitial pressure gradients.

Antibody half-life is a crucial parameter that depends on the antibody isotype as well as the rate of antibody clearance from the organism (pharmacokinetics) through the reticuloendothelial system (RES). Chimeric MAbs have a shorter half-life than the humanised MAbs (8-10 days vs. 2-3 weeks, respectively) (32). The $IgG_1$ and $IgG_2$ isotypes both have half-lives of three weeks and induce respectable antibody-dependent cellular cytotoxicity (ADCC) as well as complement dependent cytotoxicity (CDC) host responses, while the $IgG_3$

isotype has the same functional effects with the human serum half-life of only one week (33). Antibody clearance depends on the nature of the antigen as well as on the dose of the administered MAb. In the case of membrane associated antigens, as opposed to soluble antigens, the MAb clearance is influenced by the antigen kinetics at the membrane (as previously outlined), while reduced clearance is noted with increasing doses and repetitive administration of MAbs (32).

### 1.2.2. Mechanisms of monoclonal antibody action

Clinically effective MAbs deliver therapeutic effects using a combination of cytotoxic mechanisms and their effects on cancer cells can be direct and indirect. Direct effects of MAbs can be achieved by blocking ligand binding to the antigen and conjugation of MAbs to radioisotopes, drugs or toxins as vehicles to deliver these cytotoxic agents to tumour cells. In the case of indirect action, when the Fc domain of an antigen-bound MAb binds to an Fc receptor displayed on the surface of immune effector cells (macrophages, natural killer cells), it results in the activation of the ADCC cascade, inducing target-cell death. CDC is another indirect cell-targeting method of MAbs, believed to dominate the anti-tumour effects elicited by MAbs. The $C_H2$ region of the MAb heavy chains binds to C1q (component of complement C1) triggering a cascade leading to a proteolytic release of C3 and C5 and formation of a membrane-attack complex which induces target-cell death (19).

MAbs used for the treatment of malignant diseases are targeted against antigens expressed on tumour cells (in solid tumours and on circulating tumour cells), in the tumour-associated stroma as well as tumour vasculature. Most commonly targeted tumour-associated antigens are growth factor receptors which are overexpressed in many cancer types. In the 1980s, there was a surge of clinical initiations of MAb products. The official approval for clinical application in the USA and the EU was granted to a total of eighteen MAbs in the past decade (Table 2) (16). The majority are humanised MAbs with an application in oncology, followed by immunological and anti-infective MAbs.

Toxicities associated with MAb therapy can be mechanism-independent (hypersensitivity, allergic-type reactions) and mechanism-dependent. The latter arise from a MAb binding to its target antigen in non-malignant, normal tissue and interfering with the physiological antigen-driven cellular functions. The severity of the side-effects depend on the

level of antigen expression in organs other than the tumour bearing tissue, the relevance of the antigen-related signaling in these organs, as well the dose of the MAb (therapeutic window). For example, one of the side-effects of the anti-HER2 MAb is cardiac toxicity (34), while the anti-VEGF Ab can cause hypertension, bleeding and thrombosis (35).

**Table 2.Monoclonal antibodies approved for clinical implementation in the USA and EU (16)**

| Generic | Trade | Description | Therapeutic category |
|---|---|---|---|
| Muromonab-CD3 | Orthoclone OKT3 | Murine, IgG2a anti-CD3 | Immunological |
| Abciximab | ReoPro | Chimeric, IgG1 anti-GPIIb/IIIa; Fab | Hemostasis |
| Rituximab | Rituxan | Chimeric IgG1 anti-CD20 | Oncology |
| Daclizumab | Zenapax | Humanized IgG1 anti-CD25 | Immunological |
| Basiliximab | Simulect | Chimeric IgG1 anti-CD25 | Immunological |
| Palivizumab | Synagis | Humanized IgG1anti-respiratory syncytial virus | Anti-infective |
| Infliximab | Remicade | Chimeric IgG1 anti-TNFα | Immunological |
| Trastuzumab | Herceptin | Humanized IgG1 anti-HER2 | Oncology |
| Gemtuzumab | Mylotarg | Humanized IgG4 anti-CD33 | Oncology |
| Alemtuzumab | Campath-1H | Humanized IgG1 anti-CD52 | Oncology |
| Ibritumomab Tiuxetan | Biogen Idec | Murine IgG1 anti-CD20 radiolabeled | Oncology |
| Adalimumab | Humira | Human IgG1 anti-TNFα | Immunological |
| Omalizumab | Xolair | Humanized IgG1 anti-IgE | Immunological |
| Tositumomab | Bexxar | Murine IgG2aλ anti-CD20 radiolabeled | Oncology |
| Efalizumab | Raptiva | Humanized IgG1 anti-CD11a | Immunologial |
| Cetuximab | Erbitux | Chimeric IgG1 anti-EGFR | Oncology |
| Bevacizumab | Avastin | Humanized IgG1 anti-VEGF | Oncology |
| Natalizumab | Tysabri | Humanized IgG4 anti-α4 integrin | Immunological |

## 1.2. Epithelial to Mesenchymal Transition

Epithelial-to-mesenchymal (EMT) transition is a biological process which enables epithelial cells to acquire mesenchymal-like properties and behaviour. EMT is required during embryonal implantation and normal organ development (EMT type 1). This process is conserved in adult tissues where EMT facilitates wound healing and tissue repair after injury or inflammation (EMT type 2). However, EMT is also active in human malignancies (EMT type 3) (36).

Epithelial-to-mesenchymal transformation has first been described by Elisabeth Hay and colleagues who studied a model of chick primitive streak formation (37). The process has since been renamed transition instead of transformation, in order to reflect its reversibility, i.e. mesenchymal-to-epithelial transition (MET). Therefore, central to the dynamic concept of EMT-MET is the observation of cellular plasticity during development and adulthood, which exists in both normal and malignant tissue. This means that cells can evolve from epithelial to mesenchymal phenotypic and functional derivatives and back, in order to accomplish a given developmental or neoplastic program (36). Extensive studies investigating properties of primary cancer cells, circulating tumour cells and counterpart cancer cells from metastatic lesions, confirm that once cancer cells complete the invasion-metastasis cascade, they indeed shed their EMT traits through MET in order to colonise a distant organ and form secondary tumour deposits (38).

Hallmarks of EMT in cancer are:

1) Activation of EMT inducing transcription factors;
2) Expression of EMT cellular markers;
3) Stimulation of EMT promoting signaling pathways.

Finally, temporal interplay of these events results in completion of the EMT process, characterised by the dissociation of cell-to-cell junctions, disturbance of cellular connections to the basement membrane, production of extracellular matrix disintegrating factors and increased motility and invasiveness of the cells.

In cancer, therefore, EMT enables dissociation of epithelial cancer cells from the primary tumour, invasion into the surrounding stroma, extravasation and survival in systemic circulation, as well as homing in distant organs to form metastatic lesions. Genotypic, phenotypic and cell behavioural alterations imposed by the EMT promote resistance to apoptosis as well as anchorage independent growth, facilitating cancer cell survival during metastatic systemic spread through the circulation and evasion of cell death in response to certain anti-cancer therapies (39-41). To date, many EMT inducers originating from cancer cells, as well as from the tumour-surrounding stroma, and a spectrum of EMT markers and pathways driving EMT have been discovered.

EMT inducers are: i) transcription factors (TFs) such as *Snail* and *Slug*, which are zinc finger proteins; ii) the basic helix-loop-helix protein *Twist*; iii) homebox protein *Goosecoid*; iv) forkhead-box proteins *FOXC1* and *FOXC2*; v) E-box proteins *ZEB1* and *SIP1*. Their expression is upregulated in EMT. Individual overexpression of *Snail, Twist* and *Goosecoid* in a human mammary epithelial cell line was sufficient to induce a set of molecular alterations resulting in a complete EMT program (42, 43). Growth factors originating from the tumour-surrounding stroma, such as the hepatocyte growth factor (HGF), fibroblast growth factor (FGF), platelet derived growth factor (PDGF), epidermal growth factor (EGF), transforming growth factor β (TGF-β), appear to act through a paracrine loop to activate these EMT-promoting TFs in cancer cells (41, 44-48). Recently, an expanding field of micro RNAs is yielding data to implicate miRNAs in the regulation of the EMT (49). Presence of tumour hypoxia, a state induced by compromised blood supply to the tumour tissue also favours the migratory/invasive pattern of cancer cell behaviour (50). Matrix metalloproteinases (MMPs) are strong promoters of EMT. They can be either expressed on the surface of tumour cells or secreted as soluble factors by tumour cells for the purpose of degrading components of the extracellular matrix (collagen, gelatine, matrylisin etc.), as well as disintegrating cellular adhesions and facilitating migration of cancer cells (51).

Microarray gene analysis of the cells that have undergone EMT in response to these TFs has revealed a so called ‘EMT core signature’, comprising of 159 downregulated and 87 upregulated genes (43). Downregulation of E-cadherin and upregulation of N-cadherin and vimentin (52), the known hallmarks of EMT, were consistently reproduced in this core signature. The EMT transcriptome translates into an EMT proteome signature, which is

dominated by the expression of proinvasive, mesenchymal proteins: vimentin, fibronectin, laminin, collagens, SPARC (secreted protein acidic and rich in cysteine) protein, SMA (smooth muscle actin), MMPs (matrix metalloproteinases), proteoglycanes and their receptors etc. (53, 54). Expression of these proteins was found to be enriched in the so called 'basal B' subtype of breast cancer cell lines (e.g. MDA-MB-231, MDA-MB-435, BT-549), as opposed to the 'luminal' (e.g. MCF-7, BT-474, ZR75-1, T47D) and 'basal A' (e.g. MDA-MB-468, HCC1187, HCC3153) type cell lines, a taxonomy derived by Neve et al., which closely resembles the *in vivo* classification of breast cancer (15) (55).

Transcription factors and protein denominators of the EMT phenotype elicit their pro-migratory/invasive effects through multiple cellular signaling pathways in cancer cells, TGF-β (56), LEF/β-catenin (57), MAPK and PI3K/Akt (58), Rho-GTPases (59, 60), canonical and non-canonical Wnt pathway, as well as through the Notch receptors (61) .

Occurrence of EMT in clinical breast cancer samples has been somewhat debated, although more and more evidence is emerging to support this concept. Analysis of 490 human breast tumours for expression of the EMT markers has revealed stratification of these biological samples into two clusters (62); cluster A which is negative for EMT markers, encompassing both ERα positive and ERα negative tumours that express epithelial cytokeratins CK8/18/19; and cluster B, defined by cancers that are ERα negative, high grade tumours, expressing basal cytokeratins CK5/6/14 together with the EMT markers (N-cadherin, cadherin-11, vimentin, SPARC). When characteristics of the cluster B tumours were matched against the proposed markers defining basal breast cancers (63, 64), results strikingly demonstrated a positive correlation between basal like tumours and the presence of EMT markers.

### 1.3.1. Monitoring EMT in a 3D context

The majority of data regarding breast cancer cell lines' transcriptome, proteome and behavior, as well as the response to therapeutic drugs, has so far been derived from cell culture systems utilising 2D monolayers on a plastic substratum.

Even though these results are largely reproducible and informative, the 2D monolayer culture model precludes microenvironmental input of the extracellular matrix, an important

regulator of the cell phenotype and behaviour (65). Breast cell lines adopt one of the four distinct morphologies in 3D culture (round, mass, grape-like and stellate) (Figure 6), which reflect and correspond to their transcriptional profiles, proteome content and cellular behaviour. Comparative studies of these cellular aspects between monolayers in 2D plastic substrata and respective 3D matrigel cultures, have revealed marked differences in genes encoding signal transduction proteins in 25 different breast cancer cell lines (66), a collection which broadly covers the scope of distinct breast cancer subtypes found *in vivo* (15, 55). Non-malignant breast cells form round, growth arrested, polarised acini spheroids when cultured in 3D conditions, while the architecture of malignant breast cells is in the form of disorganised, proliferative, non-polarised colonies, as represented by grape-like and stellate structures (Figure 6) (67).

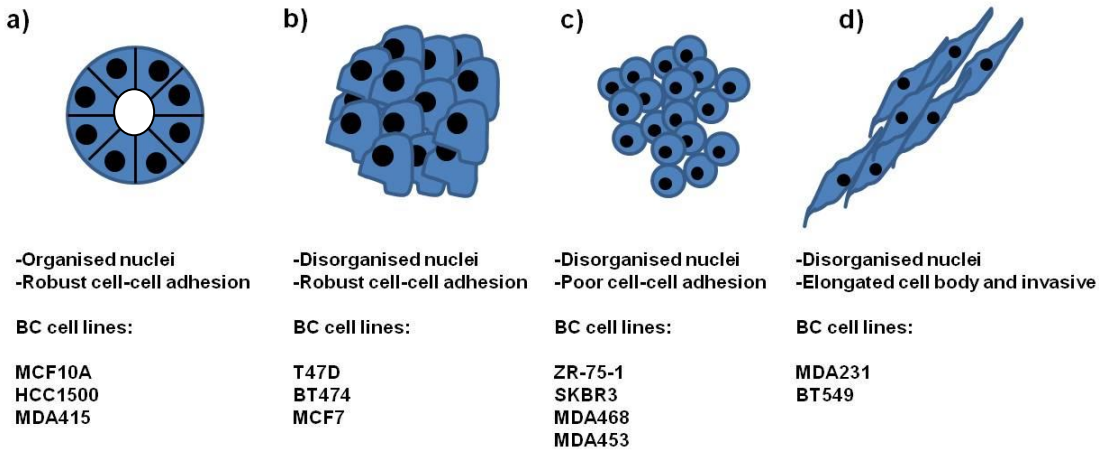


**Figure 6.Morphology of the three-dimensional acini structures derived from different breast cancer cell lines and non-transformed breast epithelial cells (66)**

The use of the 3D cell culture system allows for investigation of cellular pathways and oncogenes that are capable of inducing malignant transformation, and equally of the drugs potent enough to revert the invasive phenotype (68). For example, overexpression of cyclin D1 and the retinoblastoma (Rb) protein in MCF10A (non-malignant) breast cells grown in 3D, results in enhanced proliferation but retention of the original round, polarised organisation. In contrast, overexpression of the HER2 oncogene is capable not only to stimulate cell proliferation but also to disturb acini organisation and induce a marked loss of apico-basal polarity (68).

In support of the pathways previously shown to be important regulators of the EMT in 2D cultures, overexpression of E-cadherin as well as the inhibition of the PI3K/Akt and MAPK pathways is able to induce reversion of the EMT in a 3D model of invasive MDA-MB-231 and HMT-3522 cells (69, 70). Even though the traditional cell culture will always be utilised, the 3D cell cultures are rapidly becoming a preferred cellular model for studying the malignant cell behaviour, the inducers and inhibitors of the invasive phenotype, as they more closely recapitulate the *in vivo* conditions.

### 1.3.2. Epithelial-to-mesenchymal transition and stem cells

The EMT endowes cancer cells with invasiveness, ability to evade apoptotic stimuli, resistance to chemotherapeutic agents and sustainment of anchorage independent growth (Figure 7). These traits are commonly used as intrinsic attributes of cancer initiating cells, often referred to as cancer stem-cells (CSCs) (54, 71).

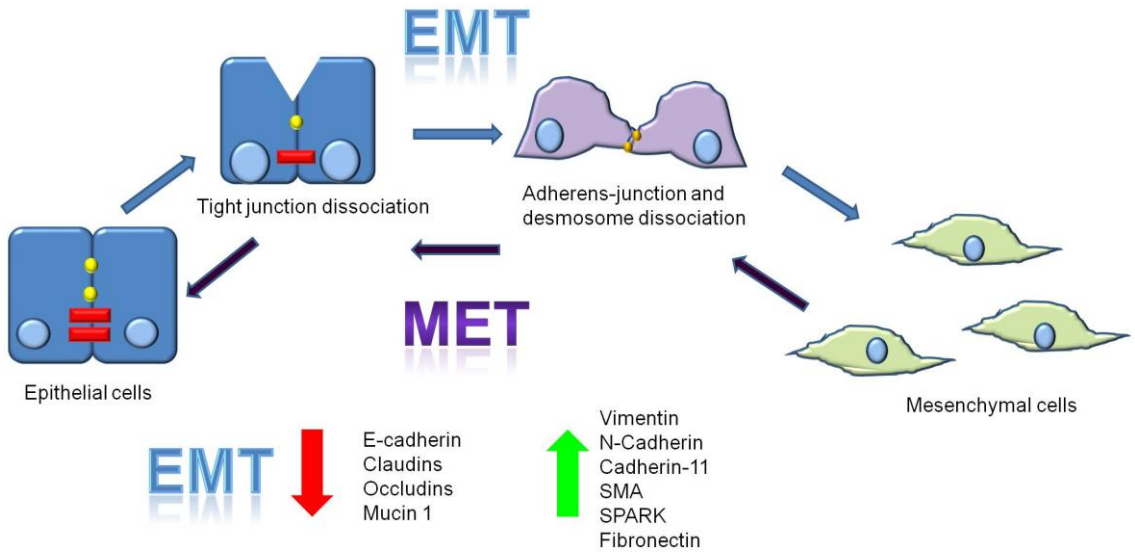


**Figure 7.Steps involved in epithelial-to-mesenchymal transition and cellular markers affected by this process.** Epithelial-to-mesenchymal transition (EMT) is characterised by the pro-migratory and proinvasive molecular, phenotypic and cell behavioural changes. During EMT, epithelial markers are lost, and invasion markers are upregulated. The reverse process is termed mesenchymal-to-epithelial transition (MET). Figure reproduced from (72).

## 1.4. Stem Cells and Breast cancer

The concept that cancers may arise from "stem cells" is 150 years old. In addition, over 40 years ago it has been suggested that cancer cells represent a maturation arrest of stem cells (73). This idea has been dormant for the past several decades, in which period substantial knowledge has been acquired on the molecular characteristics of cancer. Recently it has been reactivated in many studies, which have provided evidence that cancer cells and stem cells do share some similar traits.

Stem cells are defined as cells that have the ability to perpetuate themselves through self-renewal and to generate mature cells of a particular tissue through differentiation (74). The hallmark property of a stem cell is its ability to self-renew as well as to regulate the balance between self-renewal and differentiation. Loss of this hallmark also underpins the process of carcinogenesis. It is presumed that stem cells, being slow cycling with occasional bursts of proliferative activity, may be escaping effects of currently used cancer treatment modalities whenever they are not actively proliferating. Thus, the treatment is eradicating only well differentiated cancer cells, leaving the 'root' cells behind. This may be a compelling reason why chemotherapy induces remission, yet rarely cures, and why we are seeing relapses of cancer with no substantial benefit in overall survival in metastatic patients (Figure 8) (75, 76).

Given their purpose, stem cells are by nature long-lived. For that reason alone they are subject to accumulation of mutations that may potentially be carcinogenic. Other shared properties between stem cells and cancer cells, apart from self-renewal and differentiating capacity, are activation of anti-apoptotic pathways, increased transmembrane transport, ability to migrate and metastasise (77). Normal stem cells are dormant, predominantly in $G_0$ phase of the cell cycle, until they receive an appropriate signal from the cell surroundings (niche), when they go into asymmetric cell division producing one exact replica of itself and a daughter cell that further undergoes differentiation into cell lineages of the tissue in question (78). Another route of stem cell division is in a symmetric manner i.e. producing two stem cell progeny. Through such a disregulated self-renewal, the pool of stem cells expands.

The development of the human mammary gland during puberty, as well as pregnancy related cyclic involution and re-establishment of lactating function suggest that a mammary stem cell population resides within the mammary gland (79). The adult mammary gland has a tree-like structure comprised of three separate cell lineages: luminal epithelial cells, myoepithelial cells that secrete the basal lamina, which separates the mammary parenchyma from the stroma, and alveolar epithelial cells in the secretory acinar structures at the end of each branch that produce milk proteins (79, 80). Mammary stem cells may serve to give rise to more designated progenies that, at the end, form differentiated cell lineages of the breast, to allow for breast remodeling in and out of pregnancies, and possibly repair tissue damage.

### 1.4.1. Isolation of breast cancer stem cells

Led by the assumption that mammary stem cells are indeed present in the normal breast tissue and in breast cancer, substantial efforts have been invested into deriving optimal methodologies for their isolation and characterisation.

#### *1.4.1.1. Use of the Hoechst 33342 dye*

One such approach is using a Hoechst 33342 dye, which is an intercalating agent that binds to DNA (81). The use of the Hoechst 33342 dye technique resulted in isolating a unique cell staining profile from the bone marrow (81). The so called 'side population' (SP) was well separated from the other cells, as visualised by flow cytometry, due to an elevated rate of Hoechst efflux from the cells. Following this example, the presence of the SP was demonstrated in the mouse mammary epithelial preparations, where it represented 2-3% of the total epithelial cell preparations (82). Under mouse mammary epithelial clonal conditions, these SP cells grew as typical cytokeratin-expressing mammary epithelial cell clones (83). The same experiments were performed on human breast tissue obtained from reduction mammoplasty, with success rate of SP extraction varying across the groups from 0.2-5%. In *in vitro* cell culture, SP cells produced 2-7 times more colonies of both luminal and myoepithelial cells than the non-SP cells, suggesting that SP was indeed enriched for multi-potent stem cells (84).

On the other hand, a cultivation system was developed to support the propagation of mammary progenitors in an undifferentiated state. A neurosphere model was 'copied' into a 'mammary setting'. In 1992, Raynolds and Weis showed that rat neural cells proliferate in suspension culture, generating spherical colonies, termed neurospheres. The ability to generate neurospheres *in vitro* corresponded with the number of stem cells in the tissue of origin (85, 86). Mammary epithelial cells from reduction mammoplasty were cultured on a non-adhesive substratum in the presence of EGF and/or FGF. The rationale behind this approach was that stem cells do not undergo anoikis, i.e. are able to self-renew and form spherical structures in anchorage independent growth conditions. Single cells isolated from mammospheres, when cultured, went on to differentiate into ductal, alveolar and myoepithelial cells, and have also generated 3D functional structures in Matrigel.

#### *1.4.1.2. Breast Cancer Stem cell signature $CD44^{+}/CD24^{low/-}$*

A breakthrough in the field of breast cancer stem cells was delivered by the seminal work of Al-Hajj et al. who have identified a putative breast tumour stem-cell-like population that is defined by the presence or absence of two cell-surface markers, respectively: CD44 and CD24 (87). CD24 is a small mucine-type glycosylphosphatidylinositol-linked cell surface molecule expressed by hematological malignancies as well as a wide range of solid tumours. It is strongly expressed on the majority of human breast cancer cell lines and in fresh specimens of human breast carcinoma. The localisation (membranous/cytoplasmic) and intensity of its expression correlate with histological grade. Further research into the implications of CD24 positivity in breast cancer suggested that it may also enhance metastatic potential of the tumour, because CD24 has been identified as a ligand for p-selectin (an adhesion receptor on activated endothelial cells and platelets) (88). Combined expression of CD44 and CD24 in a $CD44^{+}/CD24^{low/-}$ phenotype is associated with the lack of differentiated breast epithelial cell lineage markers and has 10-50 fold increased ability to form tumours in xenografts compared to the bulk breast tumour cells (87, 89).

Following the footsteps of Al-Hajj et al., the group of Weinberg et al. elegantly recapitulated and expanded the characterisation of the $CD44^{+}/CD24^{low/-}$ population of cells. They have demonstrated a positive correlation between the stem cell phenotype and the EMT signature in breast cell lines, as well as in clinical specimens, and successfully converged

these two lines of research. Namely, as expected, human mammary epithelial cells stratified for the $CD44^{+}/CD24^{low/-}$ signature, were able to self-renew and form mammospheres with great efficacy. Single cell analysis of the mammospheres confirmed the presence of a mixed population of luminal (CK18 positive), basal/myoepithelial (CK14 positive) and a small fraction of bi-potential cells (CK18/14 positive). Conversely, $CD44^{low/-}/CD24^{high}$ counterpart population produced single cell clones predominantly positive for the luminal cytokeratin, CK18 (90). Importantly, cells harbouring the $CD44^{+}/CD24^{low/-}$ phenotype appeared to have pronounced mesenchymal features, and upon analysis of gene expression were shown to be significantly enriched for the EMT associated markers relative to the $CD44^{low/-}/CD24^{high}$ cells. E-cadherin (*CDH1*) levels were reduced 150 fold, while expression of vimentin (*VIM*), N-cadherin (*CDH2*), *Twist1*, Snail (*SNAI1)*, Fibronectin (*FN1*), *FOXC2* and *SIP1* were elevated between 20- and 200-fold. Overexpression of *Twist* and *Snail* in the $CD44^{low/-}/CD24^{high}$ cells was sufficient to induce a complete EMT program which resulted in the expansion of this pool of cells and production of the population with the stem cell $CD44^{+}/CD24^{low/-}$ features (90). Stem cells isolated from both reduction mammoplasties and primary breast cancer tissue confirmed enrichment in EMT markers.

Aldehyde dehydrogenase 1 (ALDH1) has been identified as another reliable breast cancer stem cell marker, as it was demonstrated that fewer $ALDH1^{+}$ than $CD44^{+}/CD24^{low/-}$ cells were needed to give rise to tumours in nude mice (91), while analysis of 577 clinical specimens yielded ALDH1 as a significant prognostic indicator of adverse survival and correlated with high cancer grade, stage and presence of metastasis. Furthermore, the population of $ALDH1^{+}$ cells, was cross-matched against the intrinsic characteristics of known breast cancer subtypes (15), and a striking overlap was observed between gene signatures obtained from $ALDH1^{+}$ cells and the basal like breast cancer cohort (92, 93).

Prevalence of breast cancer stem cells, either those identified by the $CD44^{+}/CD24^{low/-}$ or the aldehyde dehydrogenase 1 positivity (ALDH1) as a marker, was to date analysed in 12 clinical studies encompassing a total of 898 breast cancer cases. Meta-analysis confirmed that both the presence of $CD44^{+}/CD24^{low/-}$ cells and $ALDH1^{+}$ cells correlated with poor overall survival of breast cancer patients ($p < 0.001$) (94).

There are multiple lines of evidence supporting convergence of the two fields of research, the cancer stem cells and the EMT. Further reinforcement of this notion lies in the findings that the $CD44^{+}/CD24^{low/-}$ phenotype appears to be predominant in the basal B group of cell lines (55, 87, 95), which are enriched for EMT markers, as well as experimental approaches which showed that transplantation of EMT-like tumour cells from conditioned mutant BRCA1 mice, produced cells with the $CD44^{+}/CD24^{low/-}$ phenotype (96); while mammary cells undergoing EMT in response to treatment with TGF-β displayed enhanced mammosphere forming capacity (97). Conversely, mammosphere forming ability of normal breast stem cells and breast cancer stem cells was inhibited by shutting down the EMT program (98).

More evidence arises from the studies which demonstrate that standard anti-cancer treatment regimens (chemotherapy and hormonal therapy) result in an increase of $CD44^{+}/CD24^{low/-}$ stem cells in residual tumour tissue irrespective of the breast cancer subtype, as determined by analysing pre- and post- treatment biopsies (99). Furthermore, expression of the EMT hallmark, vimentin, was found enhanced at the leading edge of the tumours in the post-treatment biopsies, indicating simultaneous activation of the EMT process by the administered therapies (100), while this induction of EMT contributed to decreased efficacy of chemotherapy in solid tumours (101, 102).

Concomitant expression of EMT markers and cancer stem cell characteristics was also observed in the population of circulating tumour cells (CTCs) of cancer patients, implying that these cells have undergone an intrinsic modification of their phenotype to supports aggressive, metastatic behavior (103). CTCs are cancer cells detectable in the peripheral blood of both patients with primary cancer and metastatic disease. They provide evidence of the early dissemination of primary tumours through the systemic blood flow and represent an attractive therapeutic target. Considerable efforts are being made to identify markers for sensitive and specific detection, and thereby targeting of the CTCs, as these cells are perceived to be precursors of metastatic disease. A standardised method of CTC isolation from peripheral blood entails enrichment of CTCs by using cell surface markers, CD45 (lymphocyte marker), EpCAM (epithelial cell marker) and pan-cytokeratin (CK). The standard definition of CTCs is the $CD45^{-}/EpCAM^{+}/CK^{+}$ phenotype, however the loss of epithelial markers due to intrinsic EMT modifications that CTCs undergo, could be the reason why we may be underscoring the presence of CTCs by this conventional isolation

method. The fact that the activity of the PI3K/Akt pathway, as well as the expression of Twist, fibronectin, vimentin and ALDH1 are elevated in CTCs, proposes that these cells possess both the EMT and the cancer stem cell features (104). Furthermore, a proportion of $EpCAM^{+}/CK^{-}$ cells from the blood of breast cancer patients display equally high levels of the EMT markers, fibronectin and vimentin (105). Most of these cells originated from patients whose tumours were of the basal phenotype, where downregulation of luminal cytokeratins is not a rare feature. Furthermore, limitations in detecting accurate numbers of CTCs may stem from the loss of surface EpCAM due to its cleavage, and explain why we are sometimes not detecting CTCs in patients with aggressive disease (106).

Breast cancer stem cells and EMT derived metastasis-initiating cells share many commonalities in the cellular genotype, phenotype, aggressive behaviour (107), as well as in the signaling pathways which sustain them (Hedghog, Wnt, Notch) (108-111). Collectively, these data support the hypothesis of acquisition of stemness through the EMT. Therefore, an integration of the cancer stem cell hypothesis with the EMT model may best explain the origin of cancer progression and yield a working platform for investigation and elucidation of markers and pathways best suited as therapeutic targets for timely prevention of metastasis (112).

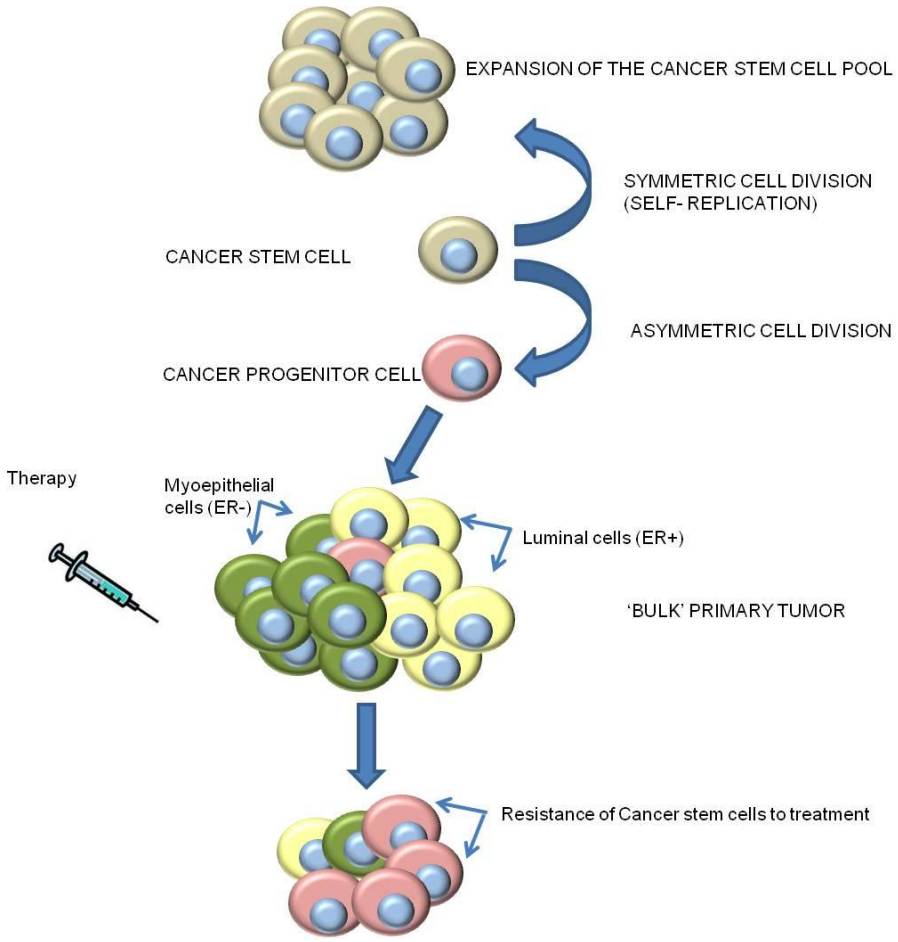


**Figure 8.Cancer stem cells.** Cancer stem cells undergo symmetrical cell division expanding the pool of cancer stem cells, as well as asymmetrical cell division giving rise to cancer progenitor cells. They are able to differentiate into distinct cell lineages of the breast tumour, i.e. luminal and myoepithelial cells. Anti-cancer therapies are successful in eradicating differentiated cancer cells, while the cancer progenitor/stem cells evade the therapeutic effects and act as a reservoir of disease recurrence.

## 1.5. Notch signaling

The Notch signaling pathway is referred to as the 'aristocracy' on the 'social ladder' of pathways, due to its preservation amongst the species and importance in both embryonal development and adult tissue function (113). Moreover, Notch signaling is found in a rare population of cancer stem cells that are proving to be a challenging target in oncology (110). Much of what we now know about Notch receptors and signaling comes from studies in *Drosophila* and *C.elegans* (114). Extensive data from studies on Notch in these two species served as a background to engage in the research about Notch in vertebrates.

Humans have four Notch receptors (Notch1-4). They are single-pass, type-I membrane proteins, composed of an extracellular (ECD), transmembrane (TMD) and intracellular (ICD) domains (115). Notch-ECD subunit contains a variable number of EGF-like repeats, and three Lin/Notch repeats (Lin being the Notch-related gene in *C.elegans*) (116). The three Lin/Notch repeats constitute the negative regulatory region (NRR) of the Notch-ECD, which preserves the Notch receptor in a cleavage resistant conformation before the ligand-induced Notch activation (117). It therefore acts as a Notch auto-inhibitor in order to maintain cellular homeostasis of Notch signaling. The EGF-like repeats mediate $Ca^{2+}$-dependent interaction between Notch-ECD and Notch-TMD. Notch-ICD also includes a "RAM23" sequence, which is composed of: i) a series of ankyrin repeats (ANK); ii) a nuclear localisation sequence; iii) a poly-glutamin stretch and; iv) a PEST sequence that modulates receptor half-life (114, 115).

Three ligands identified in invertebrates bind to Notch receptors: Delta, Serrate and LAG-2, forming a DSL family. A mammalian homologue of Delta ligands are Delta-like ligands (Dll-1, -2 and -4). Mammalian equivalent of Serrate ligands are Jagged 1 and Jagged2 (116). Hence, there are at least 5 separate Notch ligands in humans. Notch receptors and ligands are subject to N-linked glycosylation. In 1990, Irvine et al. identified a gene in flies called *Fringe*, and in 1997 a mammalian Fringe family was identified consisting of three genes: Lunatic-, Manic- and Radical-Fringe (116). Proteins encoded by these genes are homologues to bacterial glycolyltransferases, suggesting they might regulate glycosylation of Notch and its ligands. Fringe proteins add a β1 3-linked N-acetyl-Glucosamine to the O-linked Fucose residue of Notch and its ligands. Notch receptors acquire affinity ligand

binding through the O-fucosyltransferase 1 mediated fucosylation. Subsequently, Fringe acts to affect specificity of Notch for either ligand. It has not been elucidated yet which ligand activates which receptor. Most likely there is an overlap. There is also evidence that ligands other than Delta and Jagged, such as F3/contactin can also activate Notch in a CSL-independent manner (118).

### 1.5.1. Notch signaling begins in the plasma membrane and ends in the nucleus

Before ligand binding, the ECD of the Notch receptor is cleaved at the S1 cleavage site by a furine-like protease (117) (119). Ligand binding dissociates Notch-ECD from the TM domain, and the ECD-ligand complex is endocytosed into the neighbouring ligand-expressing cell (120). Dissociation also triggers a cleavage of the Notch-ECD by ADAM10 or ADAM17 enzymes at the S2 cleavage site, followed by the intra-membranous cleavage by the gamma-secretase (GS), at the S3 cleavage site. This releases the Notch-ICD, which then translocates to the cell nucleus and interacts with the DNA-binding, CSL (CBF1/Su(H)/Lag2) transcription factor and the transcriptional co-activator Mastermind (MML1) to modulate transcription of target genes (115). Notch target genes are transcriptional repressors such as *Hes* and *Hey* (121), as well as *cyclin D1* (122), *c-myc* (123, 124), *p21/WAF* (125), *Bcl-2* (126) etc. Cleavage of the Notch receptor by GS can occur at several positions within the 1743-1746 a.a. region of the protein, yielding distinct species of Notch-ICDs, with variable half-lives. Notch-ICD Val 1744 is the most stable one, and is the critical signaling component. Notch-ICD-Leu and -Ser are both short-lived species that, if generated, result in transient gene expression. However, at present, there are no reagents available to investigate the relative expression of these cleaved Notch variants in the tissue and determine their potential clinical significance (127).

### 1.5.2. Regulation of Notch signaling by Numb

Both in normal breast cell lines transformed by overexpression of Notch, and in cancer cell lines with innate Notch hyperactivation, a reduction or loss of Numb activity is noted. Numb is a negative regulator of Notch activity. It limits signaling through Notch, without altering receptor-ligand binding. Numb normally acts as an onco-suppressor and Notch/Numb antagonism controls proliferative/differentiation balance. When Notch is

overexpressed, Numb is lost through ubiquitination and proteasomal degradation. In normal breast tissue, staining for Numb is intense and homogenous, and in breast cancer samples Numb is lost, predominantly in high grade tumours (128). In support of the Notch-Numb biological antagonism, Numb overexpression targets Notch for polyubiquitination and proteosomal degradation (129).

In connection to the study of Stylianou et al., Numb overexpression in invasive breast cancer cell lines suppressed Notch, restored E-cadherin levels, and resulted in a change of cell morphology to a less invasive phenotype. Numb expression also correlated with stem cell markers in basal breast cancer, which are known for their dependency on Notch signaling (130). Furthermore, induction of Numb in breast cancer stem-cells, which exhibit the $CD44^{+}/CD24^{low/-}$ phenotype, impeded Notch-induced cell propagation (131).

Apart from the Notch/Numb signaling dependency, Notch is extensively related to other signaling pathways in the cell, where this cross-talk is certain to account for some of the effects of Notch activation. There is evidence that interactions between Notch and other pathways not only stimulate tumour development, but also tumour angiogenesis via the cross-talk between tumour and endothelial cells, as well as cellular motility and invasiveness by upregulation of the EMT-promoting factors (132, 133). For example, a so called 'love-hate' relationship between Notch and Ras has been explored in *Drosophila* and *C.elegans,* and to some extent in humans, revealing that both Ras and Notch may act as oncogenes and as tumour-suppressors. Their individual activity and nature of this cross-talk is highly context dependent (134). Ras-mediated activation of the p38 pathway is responsible for inducing Notch activity in Ras-transformed cells, while inhibition of Notch by genetic and chemical approaches partially reversed the Ras-transformed phenotype. Furthermore, the kinetics of Notch1 signaling is accelerated in Ras-transformed cells (135). The interaction between the Notch receptors is relatively unknown and may play a distinct role in maintaining the equilibrium of Notch signaling. It has been suggested that Notch2 activity may suppress Notch1 and Notch3, while Notch1 possessed the ability to induce expression of Notch4 (136).

### 1.5.3. Notch in human malignancies

Preclinical and clinical evidence support the role of Notch signaling in both hematological malignancies and solid tumours. Almost 60% of T-cell actute lymphoblastic leukemias (T-ALL) bear activating translocations in the Notch1 receptor, while constitutively active Notch is also present in B-cell chronic lymphocytic leukemia (B-CLL) (137, 138). Some studies report anti-tumour effects achieved by inhibiting Notch in Hodgkin lymphoma and multiple myeloma (139, 140). Aberrant Notch signaling has been discovered in 30% of non-small-cell lung cancers, concomitant with the loss of Numb expression, while 10% of these tumours were found to bear Notch activating mutations (141). Gene amplification of Notch3 causes its overexpression in non-small cell lung cancer and ovarian cancer (142, 143). In the latter, high Notch3 levels are observed in > 60% of squamous-cell carcinomas and correlate with advanced stage of disease, resistance to chemotherapy and worse overall survival (144). High Notch1 levels confer worse prognosis in head and neck cancer (145). Signaling via Notch1 contributes to the development of colon cancer, and chemotherapy-based regimens activate Notch1 in colon cancer as a means of developing resistance to treatment (146). Expression and activity of Notch are enhanced in metastatic prostate cancer compared to non-malignant prostate tissue (147). Targeted knockdown of Notch1 in prostate cancer cells results in inhibition of proliferation and invasion, mediated by Akt/mTOR pathways and MMP9/urokinase plasminogen activator (uPAR) (148, 149). Pancreatic cancer, being one of the most aggressive malignancies and certainly the one with the narrowest therapeutic spectrum, displays dependence on activated Notch1 and Notch3 for proliferation *in vitro* and in animal models. In addition, concomitant treatment of pancreatic cancer with Notch inhibitors and gemcitabine enhances response to chemotherapy (150). Glioblastoma multiforme is an aggressive brain tumour where Notch2 expression has been recorded. Inhibition of Notch 2 in this setting reduced tumour mass and enhanced response to both radiation treatment and chemotherapy (151).

Even though Notch behaves as a potent oncogene in the majority of human malignancies, there are certain cancer types (skin cancers, small cell lung cancer, hepatocellular carcinoma), where Notch has been attributed the role of a tumour-suppressor (152). In a breast cancer MDA-MB-231 xenograft model, overexpression of active Notch2 acted as an onco-suppressor and reduced tumour formation in nude mice (153).

The latest report suggests that silencing Notch1 and Notch2 in blood cells induces expression of genes specific for myelomonocitic lineage, resulting in a condition resembling chronic myeloide leukemia in mice. This study does not despute the oncogenic role of Notch in other hematological disorders such as lymphoma and T-ALL, but rather emphasises that the therapeutic window of Notch silencing may be dictated by the effects of Notch pathway inhibition on other cell types, such as myeloid progenitors (154).

### 1.5.4. Notch in breast tissue

In a study by Stylianou and coworkers, normal breast tissue from reduction mammoplasty and breast cancer tissue were analysed for the presence and localisation of Notch receptors and their ligands (155). Results have shown that Notch1 and 3, Dll4 and Jagged1 and 2 are expressed in normal luminal epithelial cells of the breast. Marked reduction of E-cadherin was noted in Notch expressing cells, but no change in CK 8/18 expression, confirming that these cells did not transform from luminal to myoepithelial, but rather that the observed change in cell morphology towards a spindle-like shape, occurred due to loss of cell-cell adhesions. Furthermore, viable single cells were seen, suggesting these cell lines were resistant to anoikis. Overexpression of Notch in normal breast cell lines abolished p53-mediated apoptotic response to cellular damage (155). In addition, in primary breast cancer tissue samples, colocalisation of Notch1 and Muc1 (luminal epithelial marker) confirmed upregulated Notch activation in luminal epithelial breast cancer cells. Increased Notch signaling was also found in premalignant breast lesions (156), while high Notch signaling in ductal carcinoma *in situ* (DCIS) was able to predict which lesions are likely to recur within five years (157). This suggests that aberrant Notch signaling may be an early event in breast tumour development. Particularly high levels of Notch activity have been associated with triple-negative breast cancers (158). Notch signaling was found activated in ERα positive breast cancers that possess *de novo* or acquired resistant to anti-hormonal agents (159). ERα positive breast cancers benefit from the well established treatment with tamoxifen (160). However, during the course of treatment ~50% of patients develop resistance and ultimately relapse. Notch has the capacity to activate ERα-related genes in both an estrogen-dependent and an estrogen-independent manner.

Notch achieves this through the IKKα transcription factor dependent chromatin recruitment of the CSL/MML1/Notch-ICD transcriptional complex to the close proximity of the estrogen response elements (EREs) of target genes (159). In ERα negative breast cancers, Notch achieves its tumour-promoting role by supporting cell survival and inhibiting apoptosis (161). In clinical samples, co-overexpression on Notch1-ICD and survivin was segregated to ERα negative, basal breast cancers, which displayed a marked Notch-survivin gene signature and unfavorable overall survival (158). Regulation of surviving signaling by Notch has also been described in non-small-cell lung cancer (162).

HER2 overexpressing/amplified breast cancers are candidates for targeted therapy with trastuzumab (anti-HER2 monoclonal antibody), where existence of *de novo* or acquired resistance is a major hurdle for therapeutic success. Activation of Notch signaling serves as one of the mechanisms of resistance to anti-HER2 therapies. Treatment with a gamma-secretase inhibitor in a murine model of breast cancer resensitised breast cancer cells to trastuzumab (163). In colon cancer, treatment with several chemotherapeutic agents (irinotecan, 5-Fluorouracile and oxaliplatin) induced Notch1-ICD overexpression by elevating the enzymatic activity of the gamma-secretase through enhanced expression of presenilin and nicastrin. A gamma-secretase inhibitor in this model served to resensitise cells to chemotherapy agents (146). Cross-talk of EGFR and Notch has been identified in basal-like breast cancers, lung and skin cancers, and glioma (164). Notch activation can also act to sustain Ras and PI3K/Akt and mTOR signaling (150, 165) in the presence of either EGFR or HER2 inhibition, thereby allowing cell survival and proliferation. These studies suggest that activation of Notch may be a means of resistance to both unselective (chemotherapy) and targeted therapies in multiple cancer types. Combinational therapies that would incorporate gamma-secretase or Notch inhibitors into existing protocols could deliver survival benefit to patients.

### 1.5.5. Notch in EMT

Downregulation of E-cadherin, the integral component of cell-to-cell adhesions, is one of the hallmarks of EMT, which occurs predominantly due to the transcriptional suppression of the *CDH1* gene via functional cooperation of the *bone fide* EMT promoting TFs (*Snail, Twist, Slug, SIP1*) (166). These TFs appear to be transcriptional targets of an active Notch pathway in the state of hypoxia.

Namely, the hypoxia induced factor HIF1α, acts to increase expression of Notch receptors, ligands and Notch target genes in breast cancer cells, concomitantly elevating the levels of *Snail* and *Slug*, which repress E-cadherin expression. This results in increased breast cell motility and invasion (167, 168). Interestingly, the same functional interplay between Notch and E-cadherin transcriptional regulators in the state of reduced oxygenation of tumour cells was noted in cervical, ovarian, colon and glioblastoma cancer cell lines (169). In these cell lines, hypoxia triggered Notch1 signaling and binding of Notch1-ICD to *Snail* and *Slug* promoters, confirming that these important EMT promoting TFs are direct transcriptional targets of Notch (169). Furthermore, genetic inhibition of Notch, as well as the treatment with a gamma-secretase inhibitor, abrogated *Snail*-mediated repression of *CDH1*. Furthermore, Notch signaling was able to induce HIF1α expression and activity through *Hes1*-mediated induction of Stat3 upon treatment of HeLa cells with doxycyclin (170).

Cooperation of TGF-β and Notch has been extensively studied in the context of EMT, since mammary cells exposed to TGF-β treatment demonstrate upregulated Notch activity, as well as increased expression of the Notch ligand Jagged1 (171). Notch inhibition limits TGF-β-induced stimulation of EMT (171), and FGF and PDGF execute their pro-EMT effects partly through Notch1 (172). Importantly, Notch was described as a participant in the Rho-GTPases signaling pathway known as potent inducer of cancer cell invasion (173, 174). In cervical cancer tissue Notch1 and RhoC expression colocalised, while inhibition of Notch signaling reduced RhoC levels (175). All of these results yield Notch signaling pathway as an important inducer and participant in the EMT program in cancer cells.

### 1.5.6. Notch in mammary cancer stem cells

Some of the most compelling evidence for the role of Notch signaling in the maintenance of cancer stem cells comes from the models of breast cancer. Utilising the $CD44^{+}/CD24^{low/-}/ESA^{+}$ phenotype, breast cancer stem cell (BCSC)-enriched population was isolated from MCF-7 and MDA-MB-231 cell lines, as well as clinical samples (cancer cells from pleural effusions of breast cancer patients) (176). The importamnce of individual Notch receptors was assessed for the survival and propagation of these cells. Interestingly, while expression of both active Notch1 and Notch4 were detected in the BCSCs from all three sources, signaling through Notch4 was notably more important, demonstrating 20-fold higher

levels in BCSCs than the non-stem cell counterpart. Inhibition of Notch signaling using a chemical compound DAPT (N-[N-(3,5- difluorophenacetyl)-L-alanyl]-S-phenylglycine t-butyl ester), was able to reduce the mammosphere forming capacity of the BCSCs by 30%; Notch1 gene silencing had negligible effects; while the most potent inhibition of sphere growth (60%) was achieved through targeted silencing of Notch4 (176). Similarly, in an independent study, mammosphere forming efficiency of breast DCIS was inhibited by a Notch4 neutralising antibody (157).

To further support the role of Notch in cancer stem cells, Notch3 and Jagged1 are upregulated in breast cancer stem cells due to increased p66Shc levels, where they cooperate to maintain survival of mammary stem cells in the state of hypoxia (177). Furthermore, inhibition of Notch signaling by DAPT significantly disabled the mammosphere forming potential of mammary stem cells bearing low levels of the p53 tumour suppressor gene (178). Overexpression of a constitutively active p63 (ΔNp63α) in MCF-7 breast cancer cells increased the $CD44^{+}/CD24^{low/-}$ stem cell population from 2.2 to 25 %, accompanied by an increase in Notch1 activity, enhanced cell proliferation, resistance to anoikis and potent xenograft growth (179).

Strong evidence exists, both from cell lines and patient tumours, supporting the importance of Notch signaling, not only in differentiated tumour cells but cancer initiating cells alike. The Notch pathway is therefore an attractive therapeutic target in hematological malignancies and many solid tumours, including breast cancer.

### 1.5.7. Targeting Notch signaling

Notch signaling is highly context dependent and the contribution of the four individual Notch receptors is not equal in all tissues. The dynamics of the Notch signaling is variable and complete abolishment Notch activity in cells may not be required for achieving therapeutic benefit. Given the stepwise activation pattern of the Notch axis, inhibition of this pathway can be achieved on multiple levels.

Since Notch receptors are activated by receptor-ligand binding, this step can be blocked by ligand blocking antibodies such as an antagonistic MAb against Dll-4. A peptide consisting of Notch1 EGF repeats that mimics the ligand binding site was also used in

keratinocytes to abolish Notch1 activation (180, 181). Prevention of the cleaved Notch-ECD-ligand trans-endocytosis can also attenuate Notch signal emission (182).

Given the severity of side effects that result from the simultaneous inhibition of Notch receptors, particularly Notch1 and Notch2, development of therapeutic MAbs against each individual Notch is a major breakthrough. Therapeutic antibodies directed against the NNRs of the individual Notch receptors interfere with conformational changes that are a prerequisite for cleavage by ADAM sheddases at the S2 cleavage site (183). Selective versus collective Notch targeting that these MAbs may achieve, could allow for a more specific treatment approach, reduced side effects and elucidation of discrete functions of individual Notch receptors. Next, the ADAM protease inhibitors can be used to prevent the sequential alpha cleavage that occurs in the Notch extracellular domain and renders it 'recognisable' for the gamma-secretase cleavage at the S3 site (184). GS modulators and inhibitors are therefore being widely explored as attractive therapeutic tools to achieve Notch inhibition (185, 186).

GS modulators are a subset of therapeutics whose mode of action relies on modifying the relative proportions of the Aβ isoforms, without changing the rate at which the amyloid precursor protein (APP) is processed (187). They can act either via targeting the gamma-secretase enzyme, interfering with its conformation and therefore ability to cleave the substrate (188), or with the substrate itself (189). GS modulators are predominantly being designed as anti-Alzheimer's drugs, targeting the Aβ while there are few GSMs which simultaneously hinder Notch processing.

Gamma-secretase inhibitors (GSIs) are another class of drugs used to inhibit Notch signaling. Several characteristics of the gamma-secretase (GS) enzyme represent an obstacle for the targeted drug design. Firstly, GS is a multi-protein enzyme complex. Secondly, detailed 3D structure and exact conformation of an active membrane embedded composite are unknown. Finally, there are over 60 described GS substrates apart from the Notch receptors (190), challenging the design of a substrate-specific GS inhibitor, which would be a desired notion in order to achieve therapeutic benefit while minimising side effects and toxicity.

## 1.6. Gamma-secretase inhibitors

Gamma-secretase inhibitors (GSI) can be classified into three categories based on the location where they bind the GS complex.

1) Transition-state analogues interact with the two aspartates in the active site of the enzyme, positioned at the internal interface of the presenilin N-terminal and C-terminal fragments (191). Immobilised transition-state analogues (peptide aldehydes) served to purify presenilin-accompanying molecules of the GS. However, since the APP substrate was copurified along with the enzyme complex, this implied that the active site and the substrate-binding site of the GS are in close proximity but nevertheless distinct (192).

2) Docking-site peptides (helical peptide inhibitors) were designed and affinity-labeled to mark the interaction point with the enzyme. It proved to be located on the outer presenilin N- and C- terminal interface (193).

3) A spectrum of other GSIs comprises of DAPT (dipeptide analogue) (194), compound E (a potent GSI derived by C-terminal modification of DAPT with benzodiazepine-like moieties) (195), and related benzodiazepine-like (LY-411,575) (196), and sulphonamide analogues (MRK-560) (197), all with enhanced and adjusted *in vivo* properties. Affinity labeling of all these compounds suggested that presenilin is the preferred binding component of the GSIs (195). Do date, there are no GSIs directed against other GS components: Aph-1, PEN2 or NCT.

Several non-competitive, orally administered GSIs are being investigated in clinical trials for the treatment of Azheimer's disease: LY-450139 (198, 199), BMS-299897 (200) etc.). Likewise, compounds like MK-0752 (Merck), PF-308414 (Pfizer), RO4929097 (Roche), are introduced into Phase I and II clinical trials in patients with malignant disease (Table 3). They are administered as single agents or in combination with existing therapies (chemotherapy, hormonal treatment, anti-angiogenic agents), proving a synergistic effect and an enhancement in cancer cell apoptosis (201). The trials have been designed to establish safety and tolerability, pharmacokinetics and pharmacodynamics of GSIs, tumour response and biomarkers of response.

**Table3.Clinical trials with gamma-secretase inhibitors** (www.clinicaltrials.gov)

| GSI | Trial Setting | Additional drug / Primary Endpoint | Phase |
|---|---|---|---|
| **RO4929097** | Relapsed or Refractory Solid Tumours, CNS Tumours, Lymphoma, or T-Cell Leukemia | Dexamethasone/ side effects and best dose | I and II |
| **RO4929097** | Advanced Solid Tumours | Cediranib maleate/Side effects Pharmacokinetic,Pharmacodynamic | I |
| **RO4929097** | Post-Menopausal Women With Hormone Receptor-Positive Stage II or Stage III Breast Cancer | Letrozole/ side effects and best dose | Neoadjuvant Ib |
| **RO4929097** | Advanced or Metastatic Sarcoma | Hedgehog antagonist GDC-0449/ side effects and best dose | I and II |
| **RO4929097** | Recurrent or Metastatic Melanoma | cisplatin, vinblastine, temozolomide/side effects and best dose | Ib and II |
| **RO4929097** | Advanced Solid Tumours | gemcitabine hydrochloride/ side effects and best dose | I |
| **RO4929097** | Stage IIIB, Stage IV, or Recurrent Non-Small Cell Lung Cancer | Erlotinib/ side effects and best dose | I |
| **RO4929097** | Pre- and Postmenopausal Patients With Advanced or Metastatic Breast Cancer | Exemestane/ dose escalation and efficacy | I and II |
| **RO4929097** | Previously Treated Prostate Cancer | Bicalutamide/efficacy | II |
| **RO4929097** | Previously Treated Metastatic Pancreatic Cancer | None/efficacy | II |
| **RO4929097** | Stage II or Stage III Triple-Negative Breast Cancer | Paclitaxel And Carboplatin/ side effects and the best dose | Neoadjuvant I |
| **RO4929097** | Advanced Non-Small Cell Lung Cancer Who Are Progression-Free After Finishing Treatment With Front-Line Chemotherapy | None/Pharmacodinamics | II |
| **RO4929097** | Recurrent Invasive Gliomas | None/ side effects and best dose | I |
| **RO4929097** | Multiple Myeloma after Autologous Stem Cell Transplant | Melphalan/efficacy | II |
| **RO4929097** | Advanced Solid Tumours (kidney and endometrial cancers) | Temsirolimus/ side effects and best dose | I |
| **RO4929097** | Recurrent and/or Metastatic Epithelial Ovarian Cancer, Fallopian Tube Cancer, or Primary Peritoneal Cancer | None/ efficacy | II |
| **RO4929097** | Advanced, Metastatic, or Recurrent Breast Cancer | None/ efficacy | II |
| **RO4929097** | Advanced Breast Cancer | Hedgehog antagonist GDC-0449/ Dose-escalation and side effects | I |
| **PF-03084014** | Advanced Cancer And Leukemia | None/Dose escalation and safety | I |
| **MK-0752** | Early Stage Breast Cancer | Combination with Tamoxifen or Letrozole/ safety and tolerability | Neoadjuvant Pilot Study |
| **MK-0752** | Treating patients With Advanced Cancer | Ridaforolimus/efficacy | I |
| **MK-0752** | Stage IV Pancreatic Cancer That Cannot Be Removed by Surgery | Gemcitabine hydrochloride/ side effects and best dose | I and II |

In terms of the mechanism of action by which the GSIs induce the anti-tumour effects, the compound PF-03084014 for example, induces a sub-G1 cellular arrest, cleavage of caspase-3 and PARP, and a robust regulation of the total Rb protein and p27/Kip1, which mediate apoptosis (202). The latest report from a pilot study using a GSI in breast cancer patients confirmed that a short exposure to MK-0752 in conjunction with tamoxifen or an aromatase inhibitor (AI) in ERα positive breast cancer patients, contributes towards significant biomarker changes in the tumour tissue, compared to hormonal treatment alone. Namely, the proliferative marker Ki67, as well as Notch1 and Notch4 were significantly decreased, while a pro-apoptotic marker NOXA was elevated in the combination arm compared to single agent AI or tamoxifen (203).

Clinical trials to date have demonstrated that GSIs maintain either stable disease or induce a partial response in patients with advanced solid tumours and leukemias. Intermittent dosing regimen is superior to continuous drug administration, as it sustains anti-proliferative potency while reducing side-effects (202). GSIs beare significant mechanism-based toxic properties, possibly derived from the insufficient GS-substrate specificity. Goblet cell metaplasia (increased number of Goblet cells in the crypts of the small intestine) is induced due to simultaneous inhibition on Notch1 and Notch2 receptors in the intestines, and results in nausea and diarrhea as notable GI side-effects (204). The mechanism behind the GSI-induced intestinal toxicity is *Hes1*-mediated transcriptional regulation of the Krüppel-like zink finger transcription factor (*Klf4*), functioning downstream of Notch in the intestines. *Klf4* is required for goblet cell differentiation and is a direct target gene of a transcriptional repressor *Hes1*. Inhibition of Notch signaling via a GSI, and thereby reversal of *Hes1* induced repression on *Klf4*, results in increased *Klf4* expression and disregulated cell differentiation in the intestinal crypts and villi. This is ameliorated by simultaneous administration of dexamethasone (205). Other adverse events recorded due to Notch inhibition have been fatigue and rash (hand-foot syndrome). If presented as grade 3/4, these adverse events are taken as dose-limiting toxicities. Further clinical investigations of GSIs and improvements in the dose and treatment scheduling regimens continue.

### 1.6.1. The GSI response signature

Molecular and gene signatures are novel tools used in the era of tailored patient treatment to determine the exact characteristics of the cancer and derive not only prognostic conclusions, but also predict response to certain types of treatment. Some of these assays are already incorporated into clinical practice (Oncotype DX, MammaPrint) (206, 207).

Watters et al. have conducted *de novo* analysis of gene expression patterns occurring in response to a GSI (MRK-003). They used a murine models of HER2-inducible breast cancer, where analysed tumours (n = 107) displayed a range of histological breast cancer subtypes (luminal, basal), variable stromal involvement and cytokine staining, as well as a heterogeneity of the Notch pathway activation, determined by mRNA levels of *Hes1* and *Jagged1*. The study unraveled 768 genes, termed the 'GSI sensitivity signature', differentially regulated between the group of responders and non-responders. Signaling pathways enriched at baseline in the tumours that did not benefit from the GSI treatment, were the canonical Notch pathway, interleukine (IL-10) and chemokine signaling. (208).

Another similar study used 15 T-ALL cell lines to determine the baseline activity of Notch and correlate it to the sensitivity to a GSI. The composite expression score, named the 10 Notch Target Score (*HES-1*, *HES-4*, *HES-5*, *HEY-L*, *HEY-2*, *DTX1*, *C-MYC*, *NRARP*, *PTCRA*, and *SHQ1*) was established, which predicted sensitivity to GSIs (209). Overexpression of IL-6 and IL-8 in lung cancer cell lines and in the A459 xenograft model rendered tumours resistant to RO4929097 and ablated GSI inhibition of Notch signaling. This proposed that the serum levels of IL-6 and IL-8 may serve in preselecting the patients eligible for RO4929097 treatment. Indeed, in a phase I clinical trial, low baseline serum levels of IL-6 and IL-8 predicted favourable response to RO4929097 (210). It remains to be tested whether the discovered gene signature sets or the interleukin serum level are able predict sensitivity to GSIs in other tumour types.

Another attempt to establish a robust, reproducible and reliable prognostic assay that would indicate tumour sensitivity to GSIs is the development of an *ex vivo* GS activity assay (EXO Assay) (211). The method entails processing an excised tumour tissue to obtain a concentrated cell membrane preparation which is then incubated with a labeled GS substrate that emits a fluorescent signal upon cleavage by the active enzyme. The level of fluorescence corresponds to the degree of cleavage, i.e. to the level of GS activity (211).

Some of these methodologies, alone or in combination, once further optimised and validated, may constitute a clinically approved GSI/Notch inhibition sensitivity test.

## 1.7. The gamma-secretase enzyme

The Gamma-secretase (GS) complex is one of the few known proteases capable of hydrolysing peptide bonds inside the membrane, where the hydrophobic environment excludes water molecules fundamental for peptide-bond cleavage. This process is termed the regulated intra-membrane proteolysis (RIP) (212).

Molecular identification of the GS complex occurred in the mid-1990s when the autosomal dominant forms of familial Alzheimer's disease were associated with underlying genetic abnormalities in the form of presenilin missense mutations (213). The hydrophobic Aβ42 peptide produced by the GS cleavage of the amyloid precursor protein (APP) is prone to aggregation and forms neurotoxic, extracellular, senile plaques, which are the causative factor of Alzheimer's disease (AD).

Gamma-secretase is a multi-protein complex formed by nicastrin (NCT), anterior pharynx defective homolog 1 (Aph-1), presenilin (PS) and the presenilin enhancer protein (PEN2) (Figure 9). Although PS is thought to be the catalytically active component of GS, all four proteins are necessary for full proteolytic activity (214).

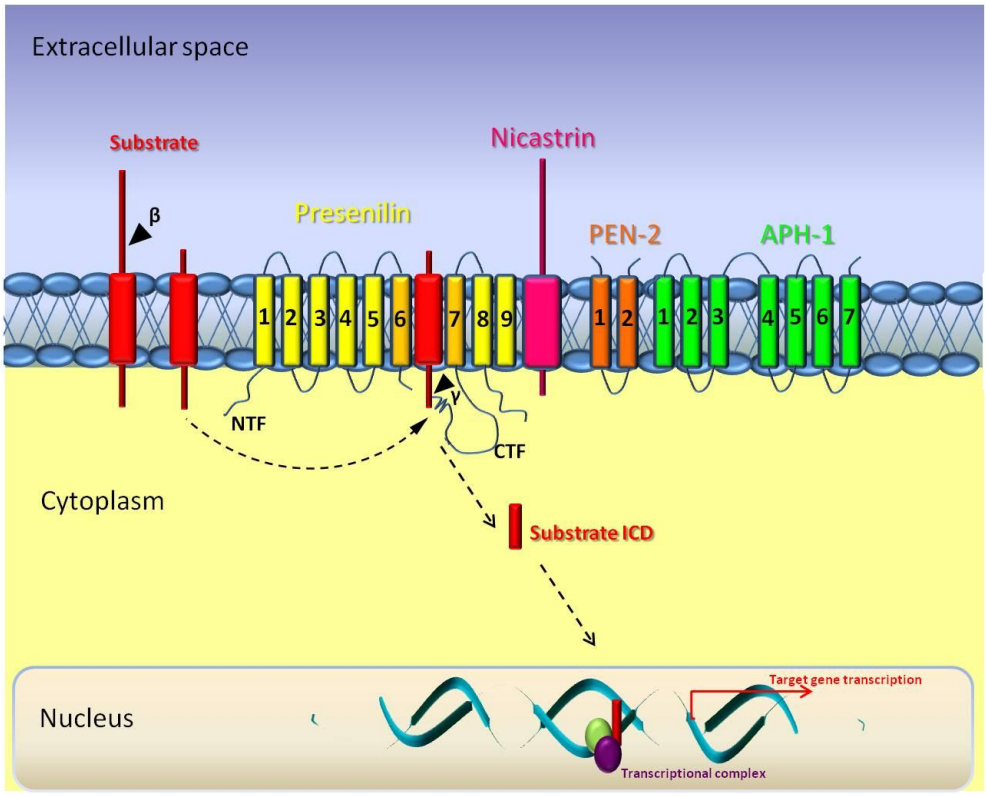


**Figure 9.Components of the gamma-secretase (GS) enzyme.** Presenilin (PS), PEN2 and Aph-1 contain multiple transmembrane (TM) spanning regions, whereas nicastrin (NCT) is the only GS member that has a single-pass transmembrane domain. In total, there are 19 transmembrane domains that contribute to the hydrophobicity of the GS enzyme. GS enzyme cleaves the substrates which are also transmembrane proteins. The extracellular domain of the GS substrates is shed by a sheddase before being eligible for GS recognition and cleavage. GS cleavage releases the intracellular domain (ICD) of the substrate, which is translocated to the cell nucleus, where it regulates target gene transcription (215).

Given the high degree of homology between the human and mouse subunits of the GS, the group of De Strooper et al. has performed an elaborate analysis of *in vivo* GS complex expression in mice. Cell membrane preparation, followed by coimmunoprecipitation and blue native electrophoresis was used in order to isolate and evaluate GS complex components in various mouse tissues. The GS enzyme was detected as a high molecular weight assembly which ranges in size between 380-550 kDa (average MW 440 kDa). The variability in the gel shift may be due to post-translational modifications of its components, or by the presence of additional cofactors binding the GS complex (216).

Since there are two Aph-1 isoforms (Aph-1a and Aph-1b), and two presenilin isoforms (PS1 and PS2) in mammalian cells, combinations of these components can yield different GS quartets (Figure 10) (213). It is unknown which cellular parameters influence the assembly of different GS complexes, and whether specific combinations of subunits yield an enzyme with substrate-preferences. Specific functional requirements and tissue distribution and expression levels of GS components and their isoforms may represent the determining factors. Recent evidence points that Aph-1a is the isoform required for Notch cleavage in mammalian cells, since Aph-1b/c knockout (KO) failed to exert Notch signaling failure in mice (217). However, Aph-1b and Aph-1c KO significantly decreased APP processing. Furthermore, the GS complex containing PS1 rather than PS2 is more efficient in processing the APP (218). Similarly, the PS2 KO mice suffer far less severe phenotypic malformations derived from deregulated Notch processing than the PS1 KO mice, indicating that PS2 may be dispensable for Notch cleavage by GS (219).

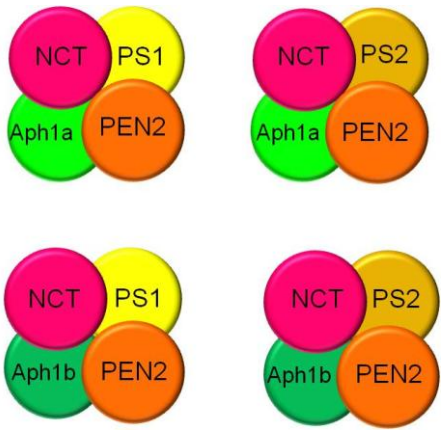


**Figure 10.Composition of distinct gamma-secretase complexes.** There are two Aph-1 (Aph-1a and Aph-1b), and two presenilin isoforms (PS1 and PS2). Combinations of these components with NCT and PEN2 can yield different GS quartets.

Coordinately high mRNA levels of GS components were detected in the liver, kidney and heart in the mouse models, while all four components were moderately transcribed in the testicles and weakly in the skeletal muscle. PS1 dominated over PS2 in the testis, with inverse levels of these PS isoforms in the liver (216). Surprisingly, protein levels did not reflect the abundance of the mRNA, as low expression of the GS members measured by western blotting was registered in liver, kidney and heart alike.

This suggests that post-translational regulation of GS components may be an important determinant of their protein expression and ultimately function. Interestingly, further analysis of PS1 and NCT expression in membrane preparations of various mouse tissues revealed that they are not coordinately regulated. PS1 was observed in the brain, lung and thymus, with low levels in the heart and skeletal muscle, while NCT was detected in the skeletal muscle, heart and brain, with lower levels in the liver, lung, spleen and kidnies (220). Disconcordance in mRNA levels of the PS1, PS2 and NCT were also detected in dog tissues, where NCT transcript levels were high in the liver, spleen, lungs and heart, in contrast to low mRNA levels of the PS1 and PS2 in the same organs. Protein levels were not examined, so it is plausible that the mRNA abundance did not translate to high levels of the functional protein (221). Notably, coimmunoprecipitation experiments using antibodies against PS isoforms confirmed that different GS complexes, i.e. one harbouring PS1 and another containing PS2, can coexist in the same cell line (216).

Gene expression profiling using a mouse cDNA microarray has also been carried out to identify genes that are transcriptionally susceptible to GS activity (222). The transcriptome of the Chinese hamster ovary (CHO) cells engineered to overexpress GS, was compared with CHO treated with a GS inhibitor DAPT, revealing that a broad spectrum of functional gene groups, pertaining to diverse downstream cellular pathways, were affected by the GS activity. These were GS substrates themselves (Notch3, Jagged1, CD44, E-cadherin etc.), as well as members of the Wnt signaling pathway, cellular cytoskeleton/adhesion molecules, neurotransmitters and transcriptional regulators (222). It remains to be established whether this differential gene signature translates to other cellular models, nevertheless the data of Magold et al. confirm an overall importance of GS activity in governing diverse cellular pathways and functions.

### 1.7.1. Assembly and cellular localisation of the gamma-secretase complex

Gamma-secretase complex assembly is a step-wise, dynamic and controlled process, which is characterised by intensive recycling/retrieval of the GS subunits and subcomplexes between the Golgi and the endoplasmic reticulum (ER) (190). GS composition is initiated in the ER, where all of the components are inserted after synthesis. Aph-1 binds the N-terminal sequence polar residues of the NCT-TMD to form the first subcomplex, a dimmer scaffold to which the other components are added (Figure 11) (223).

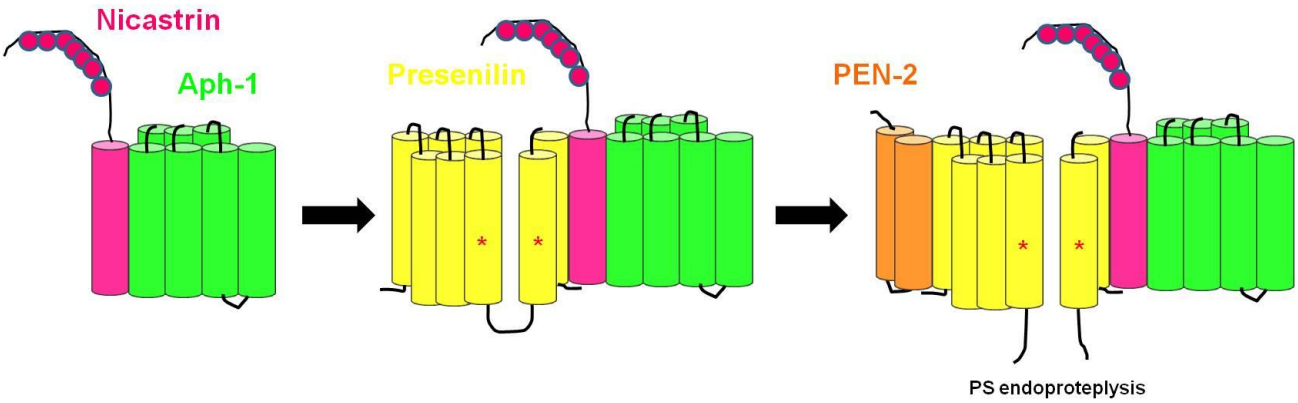


**Figure 11.Step-wise assembly of the gamma-secretase complex.** NCT and Aph-1 form a dimmer. Next, presenilin is added to produce a trimmeric intermediate complex. Finally, PEN2 joins the other components and executes PS endoproteolysis which renders the GS complex enzyimatically active.

Interestingly, the same TMD-site polar residues ($T_{670}$, $G_{674}$, $S_{681}$, $T_{685}$, $Y_{686}$) that are required for Aph-1 binding to NCT, are important for its interaction with the regulatory protein retrieval to the endoplasmic reticulum 1 protein (Rer1p). Rer1p is a 23 kDa mammalian homologue of a yeast cargo receptor which shuttles between the ER and the intermediate compartments/*cis*-Golgi, where it recognises polar TMD residues of escaped, target-ER proteins and unassembled subunits of multimeric complexes, executing a unique ER quality-control (224). Interaction with the Rer1p facilitates the transport of NCT between the early biosynthetic compartments (225). When the immature NCT leaves the ER, it is bound to Rer1p in the *cis*-Golgi and recycled back to the ER to bind Aph-1, which then sterically masks the binding site for Rer1p on NCT, allowing the NCT-Aph-1 dimmer to become independent from the Rer1p control mechanism.

Repetition of this recycling step also ensures that an adequate amount of the NCT-Aph-1 dimmer is formed in the ER, which influences the ultimate amount of the fully assembled GS complex. Another GS component possessing a Rer1p binding site is PEN2 (226), suggesting that unassembled PEN2 is also kept in the ER.

The following steps in GS assembly are subject to two hypotheses. According to the first, the PS holoprotein joins the NCT-Aph-1 scaffold (227), by binding to NCT-TMD, and forms a trimmeric intermediate subcomplex, most likely in the ER or during the ER-Golgi cycling. Since PS contains an ER-retention signal in its C-terminus domain (228) (229), this motif is most likely covered by the interaction with NCT-Aph dimmer, securing a maturing complex. Lastly, PEN2-TMD1 interacts with the PS-TMD4 to form a complete tatrameric assembly, and subsequently PEN2 executes PS endoproteolysis, to yield the PS-C-terminal fragment (CTF) and the PS-N-terminal fragment (NTF) (230). PS endoproteolysis takes place in the loop domain linking the PS-TMD6 and PS-TMD7. This loop domain may very well be blocking the GS substrate interaction with the PS exosite (docking site), explaining why the GS remains inactive prior to PS endoproteolysis (231). The second hypothesis prioritises the PEN2-mediated PS endoproteolysis before merging with NCT-Aph-1, since NCT-Aph-1-PS CTF and NCT-Aph-1-PS NTF subcomplexes have also been identified, and PEN2 has been shown to bind the PS holoprotein independently of the NCT-Aph-1 dimmer (Figure 11) (232).

Collectively, generation of the tetrameric GS is achieved during the ER/*cis*-Golgi recycling. Further maturation and initial GS activity are detected in the Golgi/*trans*-Golgi network, finally allowing for the transport and localisation of the competent GS enzyme at the plasma membrane. Analyses of the isolated active complex show that the GS contains one of each component, i.e. that the GS is a monomeric enzyme with the NCT: Aph-1: PS: PEN2 stochiometry that has a 1:1:1:1 ratio, respectively (233).

Apart from Rer1p being the limiting factor which negatively regulates assembly and function of the GS, there are other reported endogenous GS-interacting molecules, like the CD147 (234) and the transmembrane protein 21 (TMP21) (235), which execute GS regulatory roles. CD147 is a transmembrane glycoprotein and a potent extracellular matrix-metalloprotease inducer, with two Ig-like domains. It coimmunoprecipitates with NCT and

the PS1-CTF in a cervical cancer cell line (HeLa) cells, as well as a neuronal cell line HCN-1A, and human embryonic kidney cells (HEK293) (234).

CD147 genetic ablation did not influence NCT or PS1 protein levels, although the cleavage rate of Aβ was mildly increased (from 25% to 38%). TMP21, a type I transmembrane protein involved in vesicular protein transport, was also reported to be an accessory to the core GS complex, engaging its TMD segment to bind mature NCT and the PS1-NTF, thereby decreasing Aβ42 production (235). These cofactors, however capable of modulating GS activity, are not stably associated with the active GS complex (236).

### 1.7.2. Segregation of GS on the plasma membrane

Plasma membrane is composed of the phospholipid bilayer and contains specialised floating compartments rich in cholesterol and sphingolipids, termed lipid rafts (237). Lipid rafts serve as organising centres for signaling molecules and compartmentalisation of cellular processes. Lipid rafts can be planar (in continuum with the plasma membrane) or invaginated, caveolin-rich structures (caveolae) (238). Lipid rafts are detergent insoluble, hence can be isolated from the rest of the membrane (239). Detergent solubilisation method using Triton X-100 and 3-[(3-Cholamidopropyl) dimethylammonio]-1-propanesulfonate (CHAPSO) has been utilised to separate lipid from non-lipid membrane domains.

Active GS complex, containing all four protein members, associates with lipid rafts in a human neuroblastoma cell line (SH-SY5Y) (240). A non-ionic CHAPSO detergent was used in order to dissociate these detergent resistant membrane domains, since the treatment with the ionic Triton X-100 abolishes GS activity (241). In a PS1 and PS2 KO cells line, NCT and PEN2, but not Aph-1 shifted to non-lipid rafts, indicating that localisation of NCT and PEN2 in detergent resistant membrane domains is dependent on the presence of PS1/PS2, and that Aph-1 may therefore be important for the recruitment of other components to the lipid rafts. Since both the immature and the mature NCT equally localise in the lipid rafts, NCT glycosylation does not seems to be a requirement for its lipid raft topology. Cholesterol-sequestration which renders lipid rafts detergent soluble, induced a shift of GS components (mature NCT, PS1-CTF, Aph-1 and PEN2) to the ER compartment, while cholesterol depletion by statins, although preserving protein levels of GS components, caused relocation to the non-lipid rafts.

Experimental photo-labeling of the PS-CTF by the covalently bound photo-reactive derivative of a potent transition-state analogue GSI (LY-685,458) in adult mouse brain tissue, identified that preferential, but not exclusive localisation of the active GS, are indeed the lipid raft-membrane microdomains (242). However, this group also proposed that certain GS substrates, like the Notch receptors, N-cadherin and deleted in colon cancer (DCC), are located and cleaved in the non-lipid rafts, and further suggested that this shift in membrane segregation of the GS substrates and the GS activity may be interchangeable between the embryonic and adult state.

Since the support system of the lipid structure plays an important role in modulating GS function, reconstitution of the GS in complex lipid mixtures has revealed the contribution of individual lipid species in the regulation of GS activity (243). The most abundant phospholipid in cellular membranes is phosphatidylcholine (PC), with a lesser and variable contribution of phosphatidylethanolamine (PE), phosphoserine (PS), phosphatidylinositol (PI) and phosphatidic acid (PA). Removal of the detergent from the GS preparations increased the baseline GS activity by 2-fold, while still preserving the purity of the enzyme and the formation of the proteoliposomes closely resembling the native membrane environment. In such experimental conditions, GS activity was increased by addition of PE, PS and PA to the PC, while the addition of PI caused a decrease in GS activity. GS activity was greatly stimulated in an environment containing a combination of PC and sphingomyelin (SM), and even more with the addition of cholesterol to the PC/SM mix, which is the innate composition of the lipid rafts. Undoubtedly, the phospholipid content of the membrane, and more precisely the lipid raft sub-compartments where the GS resides, contribute greatly to the level of GS activity, presumably by influencing lipid packing and fluidity of the membrane and influencing GS conformation.

### 1.7.3. Functional gamma-secretase and the spatial paradox

The fact that all four GS members are synthesised in the ER, which is theoretically the earliest cellular compartment where assembly can take place (244), and yet GS activity is restricted to later secretory compartments and plasma membrane, a spatial paradox surrounding the composition and function of GS has been postulated (245).

A functional GS complex has been identified in multiple cellular compartments, like the Golgi/*trans*-Golgi network, lysosomes, phagosomes, and even mitohondria (246-248). Subcellular fractionation and analysis of the membrane vesicles in CHO cells, which express endogenous, mature NCT, and were stably transfected with human PEN2, Aph-1, PS and APP, revealed enrichment and functional interaction amongst the four components, as well as proteolytic generation of the Aβ in the Golgi/*trans*-Golgi compartment, compared to the ER.

Interestingly, proteomix analyses have also identified active GS in the purified phagosomes (a vacuole formed by the cell membrane around the particle absorbed by phagocytosis) of murine macrophage cells (249). GS members were detected in the maturing and mature phagosomes, excluding the option that GS is targeted for phagosomal degradation. Glycosylated NCT, processed PS fragments (PS1-CTF and PS1-NTF), Aph-1 and PEN2 were all enriched in the CHAPSO resistant phagosomal lipid rafts, compared to the total membrane preparations. Two GS substrates, CD44 and the low density lipoprotein (LDL) are also integral members of the phagosomes, which further corroborates the likelihood of GS presence in these specialised membrane organelles. Furthermore, treatment with interferon γ (IFN-γ) increased GS activity in the phagosomes, indicating that GS activity may be important in the phagocyte-mediated immune response of macrophages (249, 250).

The endosomes and lysosomes are predominantly catabolic cellular organelles, although they are also involved in repairing plasma membrane tears, and are capable of exocytosing the proteins which have reached them. Endocytic vesicles can recycle membrane resident proteins multiple times before they are finally targeted for lysosomal degradation. PS1 possesses a lysosomal sorting sequence unlike NCT, but both were found to be major components of the outer lysosomal membranes. NCT is a resident lysosomal protein in its mature state. It colocalises with PS1-CTF, and forms a functional GS complex, executing cleavage of the APP to yield the Aβ peptide at the permissive pH of 4.5 in the lysosomes. Indeed, lysosomes were found to harbour 30% of the total cellular GS activity (251, 252). Another line of work has suggested that the precision of the GS cleavage inferred on its substrates may vary between the lysosomes and the plasma membrane due to diverse pH conditions (253).

It was first determined that PS1 possesses a mitochondrial targeting sequence and is present in this cell compartment in the rat brain and liver cells. Likewise, NCT has a mitochondrial targeting sequence in the N-terminus. Tissue preparations from the rat brain confirm NCT localisation in the mitochondria, and its colocalisation with PS1, Aph-1 and PEN2. Therefore, mitochondria contain a fully assembled GS complex that migrates at the molecular weight of approximately 500 kDa, in line with previous studies (254). Mitochondria are cellular organelles central in the regulation of the cell energy pool but also cell death. The GS complex is capable of cleaving the APP in the mitochondria. This is relevant in Alzheimer's disease where an Aβ42-induced increase in reactive oxygen species contributes to neuronal cell death (254).

Taken together, GS activity is not only restricted to the plasma membrane, but seems to be widely distributed in other cellular compartments as well. Further research would be required to investigate the potential substrate specificity of the GS in distinct organelles, as well as to determine whether this is a uniform finding across all tissues.

### 1.7.4. Three-dimensional structure of the gamma-secretase

The GS enzyme is a unique multimeric complex as it contains 19 TM domains across its four subunits (NCT, Aph-1, PS and PEN2), which are embedded in the hydrophobic lipid milieu of the plasma membrane. Confoundedly, GS executes the proteolytic cleavage of substrates for which hydrophilic environment is preferred, probing the need for elucidation of its structure. Two independent predictions of the GS 3D structure came from performing negative stain electron microscopy (EM) and 3D reconstruction by Lazarov et al. and Ogura et al. They have revealed, albeit in low resolution, a glimpse of the GS three-dimensional structure (255, 256).

Ogura et al. have identified that the assembled GS enzyme assumes a flattened heart shape with a boat-like bottom and two outward protruding arms, essentially hanging over the putative GS transmembrane domain. The 41,000 x EM magnification identified small cavities on the surface and a low-density area in the centre of the visualised structure, corroborating the speculation of the existence of the inner enzyme cavity (Figure 12a). Antibody labeling revealed that NCT predominantly binds to the arms of the structure and that PS1-CTF is closer to the inner pore (256).

In more detail, Lazarov et al. performed GS purification, single particle image analysis and 3D EM of the GS, identifying the following: i) a large 120 Å long, 70-80 Å wide, multi-globular structure, with a 60 Å high circumferential belt corresponding to the membrane embedded portion of the GS; ii) an interior cylinder chamber 20-40 Å in length, occluded from the hydrophobic surroundings; iii) four individual pores. The pores were localised to the top (the exit for the substrate's N-terminus into the extracellular space), bottom (the cytosolic release door for the cleaved substrate ICD), and at the two side pores of the complex postulated to enable entry for the substrates into the inner GS chamber. Labeling with lectin, which binds to mannose and glucose residues, localised NCT ectodomain, and therefore provided a top-to-bottom orientation of the complex. Likewise, it gave an indication that the NCT-ECD, which protrudes into the luminal space, may be shielding the upper pore and acting as a control lid that allows entry of the water molecules and exit of the substrate N-terminus upon GS cleavage (Figure 12b) (255).

These data served as a stepping stone for a more detailed analysis utilising the cryo-EM technique at the resolution of 12 Å. It was confirmed that the GS assumes a globular structure with a belt-like motif surrounding the complex, corresponding to the membrane imbedded portion of the GS oligomer, and multiple areas of low density depicting the predicted communication pores of the inner chamber. The cytoplasmic surface was visualised as smooth, while the dominating extracellular part exhibited irregular contours. The diameter of the complex was measured at 8-9 nm. A striking novel observation was the membrane facing side groove thought to harbour the substrate docking site (Figure 12c) (257). Finally, in order to propose a 3D reconstruction of the mature, catalytically active GS complex using single particle cryo-EM and a resolution of ~18 Å, the purified GS complex has been labeled with an established transition-state analogue GSI (L-685,458), which bound to, and annotated the location of the enzyme active site (258). The purified GS enzyme corresponded to a mass of ~200 kDa, and had dimensions of: 100 Å in width (x-axis); 70 Å in depth (y-axis), and; 105 Å in height (z-axis). The 40-50 Å high, belt-like structure, considered to be the GS-TMD, corresponded to the thickness of the eukaryotic cellular membrane. Nicastrin ECD was observed covering most of the membrane surface of the enzyme and measuring 50 Å in maximal height.

A single central chamber was apparent spanning from the concave surface of the NCT- ECD into the membrane, lead to a lateral opening and harboured the region mapped by the L-685,458, i.e. the GS active site (Figure 12d). Renzi et al. took a step further and compared the relative 3D structures of the NCT-Aph-1-PS trimmeric intermediate and of the fully assembled and active GS containing PEN2. PEN2 is required to execute PS endoproteolysis, a step which facilitates NCT glycosylation/maturation and conformational adjustment, establishing a functional GS enzyme (227). The above comparison indeed noted subtle rearrangements in the 3D region of NCT-ECD, corresponding to its conformational change, as well as the widening of the central chamber and formation of the lateral opening. These are important new information which may also be considered markers of GS functional capacity.

There are some subtle differences between reports of the 3D GS structure, mostly derived from different map resolutions and varying detergent solubilising conditions. Nevertheless, the postulated 3D structure is intriguing. Much laborious work involving cryo-EM with resolution < 10 Å and X-ray crystallography is still pending. The current model, although somewhat vague in delineating the exact particle position and boundaries, precise contours of the outer envelope and the inner pore, as well as the organisation of the active site, provides us with a solid GS 3D working model (259).

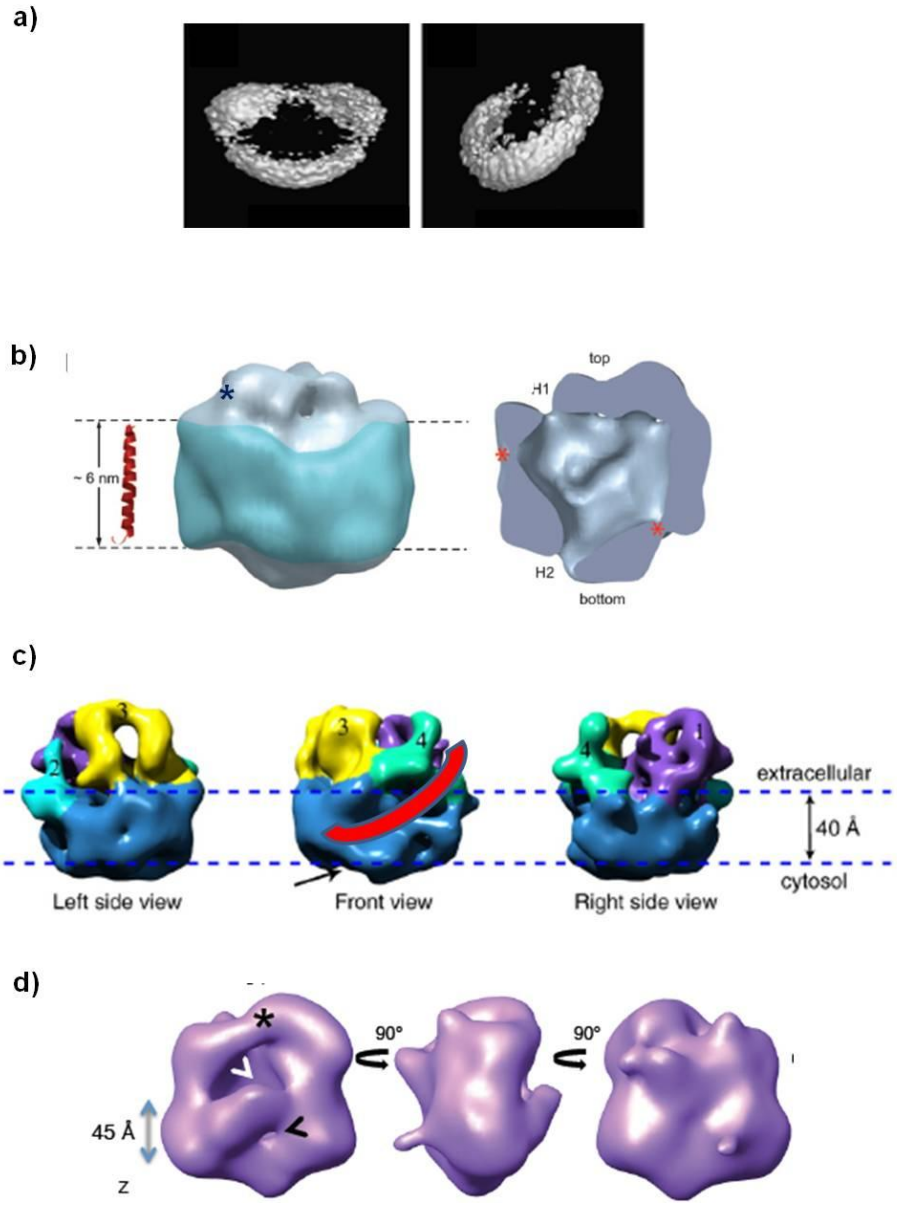


**Figure 12.Three-dimensional representation of the GS complex. a)** 3D reprojections: boat-like bottom and two outward protruding arms of the GS complex, in bright shades. **b)** Potential transmembrane, belt-like structure is outlined. Two openings are labeled: H1-top and H2-bottom connecting the inner GS chamber, * NCT ECD. **c)** 3D cryo-EM structure of the GS. Images from left to right correspond to the left-, front- and right-side views. Red line designates a potential substrate docking site. **d)** A double-headed arrow indicates the proposed location of the GS transmembrane region; the star depicts location of NCT-ECD; white arrow marks the cavity in the extracellular region that extends to the transmembrane region ending in a lateral opening (black arrow).

### 1.7.5. Gamma-secretase degradome and substrate requirements

The gamma-secretase degradome represents a subset of the membrane proteome, encompassing substrates eligible for GS cleavage. Thus far, over 60 different candidates prone to GS cleavage have been identified, and the list is ever growing (190). The range of substrates is cell context dependent, which explains why the searches for GS substrates in different cell lines yield similar, but not overlapping results. Even though there isn't a consensus motif in the interaction domain of the substrates with the GS, the enzyme is not indiscriminate, as some requirements characterising the putative GS substrates are known.

Firstly, GS substrates are type-I, intra-membrane proteins whose ECD is truncated by ADAM10 or ADAM17 preceding the GS cleavage, while a restricted group of substrates undergo BACE1 sheddase cleavage of their ECD. This may be influenced by the presence or absence of a cognate ligand in a particular cell context which stimulates the substrate-ECD shedding. Generated peptides, annotated as Xβ, analogous to the Aβ denomination, are released into the cytosol to execute their specific roles. For example, the Nβ (Notch derived peptide) undergoes trans-endocytosis into the neighbouring cells, upon binding to Notch ligands, Jagged and Delta. The sequence is known only for a limited number of the cleaved peptides, like the Aβ, Nβ, CD44β (212). Secondly, the remaining stub, i.e. the C-terminal fragment (CTF) of the substrates needs to be smaller than 40 amino acids. Thirdly, certain determinants in the TMD and the cytoplasmic region of the substrates may be needed to allow complete endoproteolysis by GS, like a particular conformation of these regions that masks possible presence of GS cleavage inhibitory domains. Other determinants could be the proximity between the GS and the substrates, i.e. spatial segregation on the membrane, as well as accelerated trafficking of the substrates to the cell membrane and turn-over rate at the membrane. Some substrates' post-translational modifications (palmitoylation of p75) are prerequisites for GS processing (260).

After the substrate is recognised by NCT, the role of the GS active site, which contains the highly conserved GxGD sequence motif with the PS C-terminal active site aspartate (PS-TMD6 and PS-TMD7), is crucial for the final substrate selection prior to cleavage (261). Small side chains of glycin within the GxGD sequence are a structural requirement of GS, whichs serve to minimise steric hindrance and allow the formation of the permissive conformation for docking of the substrates, and for the active site-substrate

interaction (262). There are indications as well, that the PS-TMD regions may play a role in GS substrate selectivity, as the I437 mutation in the PS-TMD9 blocked the cleavage of the APP while sparing Notch (263).

### 1.7.6. Other gamma-secretase substrates

#### *1.7.6.1. E-cadherin and its role in regulating cellular junctions*

E-cadherin is the most important molecule in cell-cell adhesion in epithelial tissues. Classical cadherins, including E-cadherin and N-cadherin are single-pass, transmembrane, cell-surface proteins that enable formation of cell-cell adhesions and control of other cellular behaviours such as differentiation and tissue development. This is mediated by the $Ca^{2+}$ dependent homophilic interaction of cadherin extracellular domains on adjacent cells. Conserved regions on the E-cadherin cytoplasmic tail interact with beta- and gamma-catenins, that in turn bind to alpha-catenin, docking the whole structure into the actin cytoskeleton (264).

Besides having a role in normal cells, E-cadherin plays a major role in the malignant cell transformation, since the control of cellular adhesion and motility represents the crucial mechanism in tumour initiation and progression. Loss of E-cadherin is the hallmark and a requisite of EMT. It allows for the tumour cells to detach from the primary site and engage in migration and invasion, finally homing themselves as secondary deposits (metastasis) in distant sites. In culture models, E-cadherin cDNA transfection converts invasive tumour behaviour to a markedly less invasive phenotype (265). Loss of E-cadherin in breast cancer is particularly notable in the *in situ* and the invasive lobular breast carcinomas, as well as basal and triple negative breast cancers that exhibit invasive behaviour. E-cadherin is lost in the high invasive ductal carcinomas, while it is still retained in almost 70% of the low grade ductal cancers (266).

Expression levels of E-cadherin are regulated by multiple mechanisms. E-cadherin gene (*CDH*-1) is often inactivated in human malignancies due to germline gene mutations or epigenetic changes (hypermethylation). Transcription of the *CDH-1* is further regulated by several transcriptional factors, namely *Twist1, Snail1* and *Slug* (267), all of which act as its

transcriptional repressors. Messenger RNA levels of the *CDH-1* regulators are upregulated in cancer cells that have lost E-cadherin expression (268).

Post-translational regulation of E-cadherin also plays an important role in its expression and function on the cell surface. E-cadherin turn-over at the cell membrane is a dynamic process that determines the level and the availability of the functional E-cadherin. In this context, the GS enzyme which cleaves E-cadherin at the cell membrane emerges as an important regulator of the E-cadherin function. Cleavage of E-cadherin is stimulated by apoptosis or $Ca^{2+}$ influx and occurs between the Leu731 and Arg732 residues at the membrane-cytoplasm interface. GS recognises both the full-length E-cadherin and the stub left after E-cadherin is cleaved extracellularly by a metalloprotease. The product of GS cleavage of E-cadherin is the 33kDa E-cad-CTF2 (269).

#### *1.7.6.2. E-cadherin, p120ctn and gamma-secretase: the super-complex*

The p120 catenin (p120ctn) is the prototypic member of the family of armadillo-like proteins that include delta p0071, delta-catenin, NPRAP and ANCF. P120ctn exists predominantly in the cadherin-bound form where its core function is regulation of E-cadherin turnover at the cell membrane. P120ctn increases the half-life of E-cadherin, directly influencing its adhesive strength and the amount of E-cadherin available at the cell surface. The p120ctn binding site on E-cadherin (604-615 a.a.) is distinct from the β-catenin binding site, localised at the far end of the cytoplasmic tail (270).

The p120ctn catenin is also required for the binding of E-cadherin CTF2 to DNA in the nucleus, where it translocates after it has been cleaved by the GS. The E-cadherin CTF2/p120ctn dimmer regulates the transcription of not well characterised target genes. Thus far, it is known that E-Cad/CFT2-p120ctn dissociate transcriptional repressor Kaiso from the DNA, relieving the repression it enforces on its target genes, hence reactivating their transcription. One such gene that is driven by E-cad-CTF2/p120ctn is MMP-7 or matrylisin metalloprotease (269). Furthermore, p120ctn has emerged recently as a key linker protein and the pre-requisite for the formation of the E-cadherin/GS super-complex. The binding site on the E-cadherin-ICD involved in the binding of both p120ctn and PS, overlap. Interestingly, p120ctn can also colocalise with NCT at the site of cell-cell contact in HEK293 cells (270).

The other form of p120ctn in the cells is its E-cadherin unbound fraction. It is generated in one of two ways: by dissociation from E-cadherin and by preventing p120ctn degradation. Cytosolic p120ctn assumes signaling function via regulation of Rho GTPases, RhoA and Rac1. Soluble p120ctn, in contrast to the p120ctn within adherence junction (AJ) complexes, promotes cellular motility and invasion by inducing lamellipodia and filopodia formation, and induction of MMP-7 (matrylisin) through its effect of displacing Kaiso transcriptional repressor from the DNA (271).

#### *1.7.6.3. CD44 as the gamma-secretase substrate*

CD44 is belongs to a family of transmembrane glycoproteins. It is a receptor for hyaluronan that exists as a standard isoform (CD44s) and in multiple splice variants (CD44v2-10). Cell surface expression of CD44 is closely related to clinic-pathological parameters of breast tumours, such as grade, stage, presence of metastasis and survival. CD44s, CD44v3 and CD44v6 are upregulated in both *in situ* and invasive breast carcinomas, indicating a role of CD44 in early stages of breast cancer pathogenesis (272). CD44 is a substrate for GS cleavage upon the initial shedding of its extracellular domain by a metalloproteinase (273). The cleavage releases the CD44-ICD which binds unique downstream signaling effectors like the RhoA-ROCK, c-Src, p185 HER2, etc., and sets off tumour cell growth, invasion and migration, leading to breast cancer progression (274). A two-step processing of CD44 is initiated by $Ca^{2+}$ influx and 12-O-tetradecanoylphorbol-13-acetate (TPA) treatment of the cells, similar to the triggering conditions for the GS cleavage of E-cadherin. Therefore it seems likely that the GS activity on the cell membrane is one of the key mechanisms that regulates the function of the cell-cell and cell-matrix adhesion proteins.

#### *1.7.6.4. Vascular endothelial growth factor receptor 1 and gamma-secretase*

In opposition to its anti-angiogenic role in vascular endothelial cells, the vascular endothelial growth factor receptor 1 (VEGFR1) stimulates tumour cell growth and invasion when expressed in non-endothelial, cancer cells (275). In response to VEGF stimulation and tyrosine phosphorylation, VEGFR1 undergoes shedding of its ECD which generates the soluble peptide (sVEGFR), a marker of disease progression in several malignancies, while the remaining membrane bound CTF fraction becomes a substrate for GS cleavage (276). The

exact role of the intracellular VEGFR1 remains to be elucidated. However, an indication arises from a recent report highlighting that the form of VEGFR1 predominantly expressed in invasive MDA-MB-231 breast cancer cells is its intracellular isoform, which promotes tumour cell invasion through a Src-mediated pathway (277).

#### *1.7.6.5. HER4 receptor and gamma-secretase*

HER4 (ErbB4) is a receptor tyrosine kinase member of the epidermal growth factor family of receptors, which also includes EGFR1, HER2 (ErbB2) and HER3 (ErbB3). These are growth factor dependent tyrosine kinases, which regulate a myriad of cellular functions including apoptosis, proliferation, invasion etc. (278). Stimulation of HER4 by the growth factor heregulin, as well as a protein kinase C (PKC) stimulator TPA, known to induce signals associated with cancer cell differentiation and apoptosis, causes shedding of the HER4-ECD by a metalloprotease and generation of the soluble, 80 kDa, HER4 peptide. Consequently, HER4 binds presenilin (279), facilitating GS cleavage, which liberates the HER4-ICD and is required for HER4-ICD nuclear translocation (280). HER4 indeed possesses a nuclear localisation and export signal in its cytoplasmic domain (281), indicating its ability to localise to the nucleus.

HER4-ICD can mediate a range of cellular responses which is greatly dependent on its subcellular context and shuttling (282). Cytosolic HER4-ICD can negatively influence cell growth, i.e. exert pro-apoptotic effects, mediated by its mitochondrial, ER compartmentalisation and BH3 apoptotic initiating domain (279, 283). Conversely, HER4-ICD growth stimulating effects seem to be associated with its successful nuclear translocation and cross-talk with ERα in breast cancer cells. Indeed, the proteolytic processing of HER4 can be stimulated by the estrogen treatment in ERα positive breast cancer cell lines, and is involved in potentiating estrogen stimulated growth (284). HER4-ICD is therefore a potent physiological coregulator that forms a complex with the ERα on promoters of ERα inducible genes, such as PR, where HER4-ICD is sufficient and necessary for estrogen induced expression of PR (285). Furthermore, HER4-ICD nuclear localisation may be important for predicting response to hormonal therapy in ERα positive breast cancer patients (286). *In vivo* studies have indicated that nuclear HER4-ICD associates with worse patient outcome (282).

#### *1.7.6.6. The epithelial cell adhesion molecule (EpCAM) and gamma-secretase*

The epithelial cell adhesion molecule (EpCAM) is a transmembrane glycoprotein overexpressed in human malignancies (breast, prostate, colon, pancreatic cancer etc.), as well as in cancer initiating cells, and serves an important role in cancer cell adhesion, differentiation, migration and proliferation (106). Recently, EpCAM has been identified as a substrate for GS cleavage in colon and hypopharinx cancer cells, as well as in HEK293 cells. Interestingly, EpCAM was found to interact with PS2- and not PS1- containing GS complex. Even though EpCAM and Notch share a high TMD sequence homology, GS cleavage sites do not overlap between these two substrates. The EpCAM-ECD shedding, which precedes the GS-mediated release of the EpCAM-ICD, liberates the soluble EpCAM-β peptide, which is capable of further promoting receptor proteolysis in an autocrine, positive feed-back loop manner. Upon generation, the EpCAM-ICD associates with the members of the Wnt signaling pathway to regulate target gene transcription (*c-myc*, *cyclins etc.*), and to promote cancer growth and invasion, both *in vitro* and *in vivo* (287). High expression of the nuclear EpCAM-ICD was detected in the aggressive thyroid carcinoma *in vivo*, where it conferred worse overall survival (288).

#### *1.7.6.7. N-cadherin as a gamma-secretase substrate*

N-cadherin, like E-cadherin, is an important cell surface glycomolecule, which regulates cell contact, motility and invasion via $Ca^{2+}$-dependent homophilic interactions. Cadhrin switching, a phenomenon characterised by a downregulation of E-cadherin with concomitant overexpression of N-cadherin, is one of the hallmarks of EMT and tumour progression (289). N-cadherin has been identified as a GS substrate in neuronal cell lines, where its role in the formation and function of the hypocampal synaptic contact is paramount (290). N-cadherin-ICD accelerates proteosomal degradation of a transcriptional co-activator CBP (cAMP response element binding (CREB) binding protein), thereby affecting expression of many CBP-dependent transcriptional systems (291). The role of N-cadherin-ICD in cancer remains to be explored.

## 1.8. Nicastrin

The human nicastrin (NCT) gene is located on the chromosome 1 (1q22-q23) and encodes a type-I, single-pass, transmembrane, glycoprotein of 709 amino acids, which shares a high degree of homology with other vertebrate orthologs. There are two isoforms of the human nicastrin (Figure 13). The sequence of the isoform 2 lacks the first 20 a.a., and the sequence 21-29 a.a. is changed from LSFCVLLAG to MDFNLILES. Functional consequences or tissue distribution differences of these distinct NCT isoforms remain to be explored. Nicastrin has a putative signal peptide (1-33 a.a.), an epitope presumed to be subjected to proteolytic cleavage (292), a long N-terminal hydrophilic domain harbouring the GS substrate recognistion/binding site (ECD), a 20-residue, hydrophobic, putative transmembrane domain (TMD), and a short hydrophilic carboxyl terminus of 20 residues (Figure 14). The estimated half-life of NCT is 30 hours in mammalian reticulocytes (*in vitro*), > 20 hours in yeast (*in vivo*), > 10 hours in *E. coli* (*in vivo*), and > 24h in mouse embryonic fibroblast (*in vitro*) (248). The predicted isoelectric point based on the amino-acid content is pI 5.8 (http://expasy.org/cgi-bin/protparam).

```
Q92542   MATAGGGSGADPGSRGLLRLLSFCVLLAGLCRGNSVERKIYIPLNKTAPCVRLLNATHQI 61
Q92542-2 --------------------MDFNLILESLCRGNSVERKIYIPLNKTAPCVRLLNATHQI 41
                           :.* ::* .******************************

Q92542   GCQSSISGDTGVIHVVEKEEDLQWVLTDGPNPPYMVLLESKHFTRDLMEKLKGRTSRIAG 121
Q92542-2 GCQSSISGDTGVIHVVEKEEDLQWVLTDGPNPPYMVLLESKHFTRDLMEKLKGRTSRIAG 101
         ************************************************************

Q92542   LAVSLTKPSPASGFSPSVQCPNDGFGVYSNSYGPEFAHCREIQWNSLGNGLAYEDFSFPI 181
Q92542-2 LAVSLTKPSPASGFSPSVQCPNDGFGVYSNSYGPEFAHCREIQWNSLGNGLAYEDFSFPI 161
         ************************************************************

Q92542   FLLEDENETKVIKQCYQDHNLSQNGSAPTFPLCAMQLFSHMHAVISTATCMRRSSIQSTF 241
Q92542-2 FLLEDENETKVIKQCYQDHNLSQNGSAPTFPLCAMQLFSHMHAVISTATCMRRSSIQSTF 221
         ************************************************************

Q92542   SINPEIVCDPLSDYNVWSMLKPINTTGTLKPDDRVVVAATRLDSRSFFWNVAPGAESAVA 301
Q92542-2 SINPEIVCDPLSDYNVWSMLKPINTTGTLKPDDRVVVAATRLDSRSFFWNVAPGAESAVA 281
         ************************************************************

Q92542   SFVTQLAAAEALQKAPDVTTLPRNVMFVFFQGETFDYIGSSRMVYDMEKGKFPVQLENVD 361
Q92542-2 SFVTQLAAAEALQKAPDVTTLPRNVMFVFFQGETFDYIGSSRMVYDMEKGKFPVQLENVD 341
         ************************************************************

Q92542   SFVELGQVALRTSLELWMHTDPVSQKNESVRNQVEDLLATLEKSGAGVPAVILRRPNQSQ 421
Q92542-2 SFVELGQVALRTSLELWMHTDPVSQKNESVRNQVEDLLATLEKSGAGVPAVILRRPNQSQ 401
         ************************************************************

Q92542   PLPPSSLQRFLRARNISGVVLADHSGAFHNKYYQSIYDTAENINVSYPEWLSPEEDLNFV 481
Q92542-2 PLPPSSLQRFLRARNISGVVLADHSGAFHNKYYQSIYDTAENINVSYPEWLSPEEDLNFV 461
         ************************************************************

Q92542   TDTAKALADVATVLGRALYELAGGTNFSDTVQADPQTVTRLLYGFLIKANNSWFQSILRQ 541
Q92542-2 TDTAKALADVATVLGRALYELAGGTNFSDTVQADPQTVTRLLYGFLIKANNSWFQSILRQ 521
         ************************************************************

Q92542   DLRSYLGDGPLQHYIAVSSPTNTTYVVQYALANLTGTVVNLTREQCQDPSKVPSENKDLY 601
Q92542-2 DLRSYLGDGPLQHYIAVSSPTNTTYVVQYALANLTGTVVNLTREQCQDPSKVPSENKDLY 581
         ************************************************************

Q92542   EYSWVQGPLHSNETDRLPRCVRSTARLARALSPAFELSQWSSTEYSTWTESRWKDIRARI 661
Q92542-2 EYSWVQGPLHSNETDRLPRCVRSTARLARALSPAFELSQWSSTEYSTWTESRWKDIRARI 641
         ************************************************************

Q92542   FLIASKELELITLTVGFGILIFSLIVTYCINAKADVLFIAPREPGAVSY 710
Q92542-2 FLIASKELELITLTVGFGILIFSLIVTYCINAKADVLFIAPREPGAVSY 690
         *********************************************
```

**Figure 13.Human nicastrin isoforms.** Human nicastrin isoform 1 (Q92542) and human nicastrin isoform 2 (Q92542-2), which lacks the first 20 a.a. and has the sequence LSFCVLLAG replaced by MDFNLILES (http://www.uniprot.org/uniprot/Q92542).

Nicastrin was named after an Italian village, Nicastro, home to the members of an extended family diagnosed with familial Alzheimer's disease (FAD) (293). It was first identified as a PS-binding partner within the GS complex, participating in the cleavage of APP and generation of the toxic Aβ42 peptide, which inherently has a tendency to form aggregates in senile neuronal plaques as the underlying neuropathologic feature of Alzheimer's disease.

Nicastrin does not exhibit a high degree of homology with other functionally characterised proteins. However, the tendency of assigning function to protein sequence, and the fact that a region of NCT resembles aminopeptidase receptor family of proteins, has led to the assumption that NCT possess catalytic activity. In the true aminopeptidases, the 'fingerprint' amino-acid sequence denoting their peptidase activity is composed of six residues (His85, 247; Asp87, 97, 160; and Glu132). Even though the central region of NCT (Asn263-Ala483) bears significant sequence homology and structural equivalence to human non-protease transferin receptor and *Streptomyces griseus* aminopeptidase, only one of the six residues is preserved (Asp87), while other critical zinc-binding residues have been lost through evolutionary changes. This implies that NCT does not possess catalytic activity, but retains the capacity to bind proteins (294, 295). Human NCT has 89% homology with the mouse NCT protein (708 a.a), 30% with the *Drosophila* (695 a.a.) and 22% with the *C. elegans* orthologues. The highest sequence conservation lies within the following regions: 306-360 a.a., 419-458 a.a. and 625-662 a.a. (296). The DYIGS domain (336-340 a.a.) encompasses the putative 'catalytic' residue (Glu333; E333) of the aminopeptidase superfamily. Of note is also the conservation of the cystine residues in the ECD of NCT (Cys195, Cys213, Cys230, Cys248). A NCT missense mutation (N417Y) identified in AD patients is not, however, conserved amongst the species (297). The least conserved domain of NCT, which also lacks any known functional sequence, is its C-terminus, the amino acid sequence of which is divergent among the species (mammals, *C.elegans, Drosophila*) (298).

### 1.8.1. Functional domains of nicastrin

The DYIGS (336-340 a.a.) domain is a highly conserved region of NCT, located in the so called domain (261-502 a.a.) with aminopeptidase-like activity (DAP). It possesses a GS substrate binding function (Figure 14) (299). Missense mutations in this conserved domain (DYIGS to AAIGS) result in a marked increase in the Aβ42 production in HEK293 cells, while deletions constructs encompassing the same region, in particular the NCTΔ312-369, inhibit predominantly Aβ generation and to a lesser extent Notch cleavage (296) (300). The DAP domain also harbours the anionic E333 residue, which does not participate in the formation of the GS enzyme active site, but has a role in maintaining the intrinsic GS activity, both in terms of: i) participating in NCT maturation, and; ii) enabling the interaction between the α-amino group of the GS substrates and NCT. Nicastrin protein baring a Ser to Ala mutation (E333A) has been studied in several models: the Sf9 cell model (derived from *Spodoptera frugiperda* (Fall Armyworm)) (301), as well as in a mouse embryonic fibroblast cell line model (MEFs) (302). In both systems, NCT-E333A failed to undergo full maturation through glycosylation. The divergence was noted when NCT-E333A failed to incorporate into the GS complex in MEFs. In Sf9 cells, this mutation diminished GS activity by 50% (302). This reduction was not inferred through impaired PS catalytic function, since PS endoproteolysis, as well as the GS complex stochiometry, were mostly preserved in the NCT-E333A mutants, but rather because of lower affinity of NCT-E333A to bind GS substrates (302). An elaborate set of NCT mutation constructs E333A, E333R, E333S and E333T in HEK292 cells resulted in GS substrate (APP) cleavage inhibition, unlike the conserved E333Q mutation (299). Altered substrate binding affinity was not noted in NCT-E333A MEFs. Therefore, it appears that the specific role of the E333 residue of the NCT DAP domain may be cell context dependent. Collectively, loss of this negatively charged residue impairs nicastrin maturation, thereby affecting GS activity, and in some cell systems additionally prevents GS substrate binding.

Despite the prevailing scenario where the mature NCT binds GS substrates at the plasma membrane, immature NCT has been found coupled to GS substrates as well (300). In experiments where the chimeric constructs were generated by replacement of the NCT-TMD with the TMD of E-selectin, the APP-CTF was still pulled down together with NCT, indicating that that the NCT-TMD, although important for its binding to Aph-1, PS and PEN2

during GS assembly, is not required for substrate binding (302). The N-terminal, third portion of NCT-TMD, encompassing Thr3, Gly7, Ser14 and Thr18, is of particular importance for its interation with other GS components (223). Furthermore, specific mutations of the evolutionary conserved residues in this part of the NCT-TMD domain, S623A and W648A, prevented appropriate NCT glycosylation, interfered with the stability of NCT-Aph-1 interaction and ultimately resulted in impaired GS function, as measured by reduced production of cleaved APP (303). Nicastrin C-terminus though appears dispensable for these interactions but may facilitate NCT membrane anchoring (223). Nicastrin signaling peptide was also attributed the function of facilitating membrane anchoring (292).

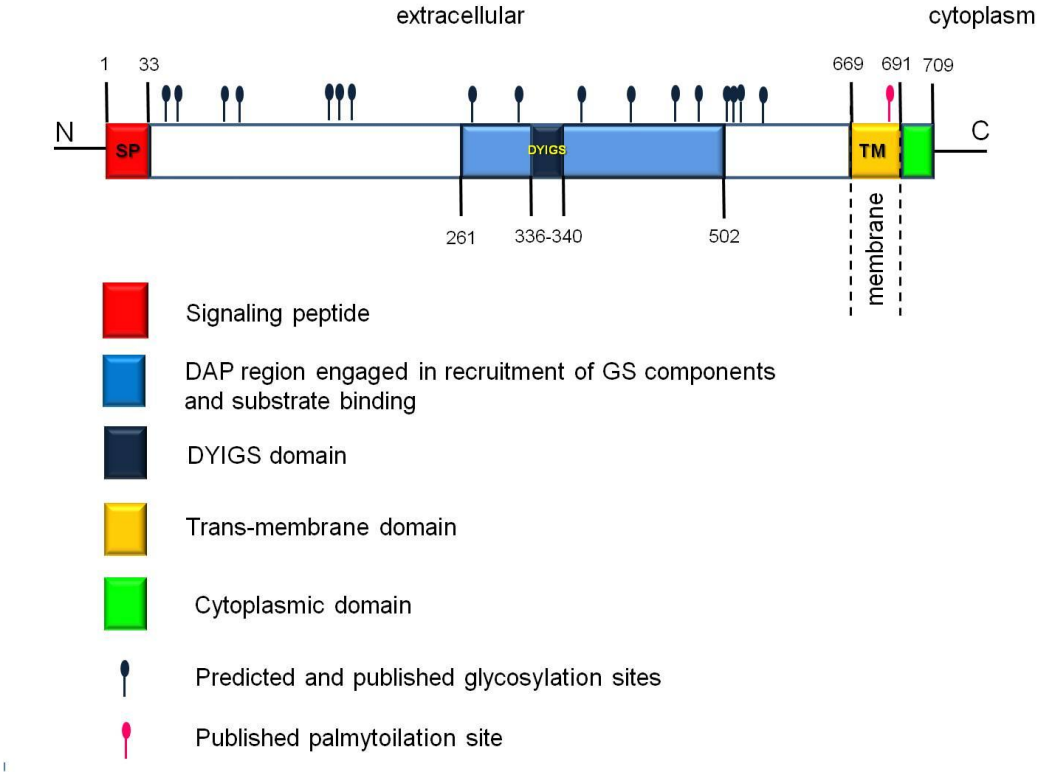


**Figure 14.Schematic of the nicastrin protein architecture.** Nicastrin signaling peptide (SP), extracellular, transmembrane and cytoplasmic domains are annotated. The DAP domain containing the DYIGS is labeled blue. Blue balloons represent reported and predicted glycosylation sites while the pink balloon marks the reported palmytoilation site.

### 1.8.2. Contribution of nicastrin genetic mutations in Alzheimer's disease pathogenesis

Contribution of PS mutations in the pathogenesis of Alzheimer's disease has been well documented. There are 43 identified missense mutations in the coding regions of PS1 that relate to presenile Alzheimer's disease, and only one splice site mutation resulting in the in-frame skipping of the exon 9, additionally brings on the symptoms of spastic paraplegia (304). Extensive efforts have been invested in analysing potential NCT mutations and polymorphisms in different populations, in the hope of deciphering whether NCT genetic perturbations may bear a causative role in Alzheimer's disease as well.

Analysis of NCT genetic variations in a Dutch population-based study of patients with EOAD and late onset Alzheimer's disease (LOAD), revealed 14 NCT single nucleotide polymorphisms (SNPs), of which 10 intronic and 4 in the coding regions, 3 silent mutations and one missense mutation (N417Y), which however is not evolutionary conserved and was found at the same frequency in healthy controls. A similar NCT SNP haplotype distribution was noted between patients and controls (297). However, in the apolipoprotein epsilon 4 negative group (APOE ε4, a known Alzheimer's susceptibility gene (305)) suffering from EOAD but not LOAD, the NCT haplotype B (IVS6+18C→G; GCGC) conferred an increased risk of developing the disease. A subsequent Finnish study reiterated this finding, however the association here was noted in the presence of the NCT haplotype D (IVS16-119G→C, ACCC), rather than haplotype B (306). The French study failed to replicate these results, suggesting a potential population specific contribution of NCT genetic mutations in the development of AD (307).

A Chinese population study investigated a distinct SNP, rs10752637 (-922T/G), located in the promoter region of *NCT*. They found that the -922T allele (TT or TG genotype vs. GG genotype) significantly increased *NCT* promoter activity relative to the -922G, while its frequency was also increased in sporadic AD patients vs. controls, suggesting that the rs10752673 SNP may influence increased NCT expression, which in turn may play a role in the pathogenesis of AD (308). Ma et al. analysed the promoter region of *NCT* and identified a set of three SNPs (rs2147471, -1216C/A; rs10752637, -796T/G; rs1324738, -436C/T), where the frequency of the first two were associated with the risk for developing sporadic AD, regardless of the APOE ε4 allele status (309).

Namely, genotypes -1216CC and -796TT and -796TG were carriers of increased risk, while the -1216AA and -796GG seemed to be protective against developing AD. Most recently, a novel DNA pooling approach was used to perform deep sequencing of the *NCT* gene in order to identify genetic abnormalities in the coding regions, and it identified a previously reported non-synonymus SNP (N417Y) which was associated with Alzheimer's disease occurrence in the Greek population (310). Finally, an elaborate meta-analyses of genetic association studies in AD reported a SNP 119 in the intron 16 of the *NCT* gene as being significantly associated with occurrence of AD (305).

In aggregate, genetic variations of NCT are evident in population based studies. Lack of data reproducibility in certain cohorts may be addressed by recruiting more patients into the studies. It would be equally important to investigate functional implications of the NCT genetic variations in terms of their impact on NCT expression and activity.

### 1.8.3. Expression of nicastrin in various tissues

Expression of NCT has predominantly been studied in rat and mouse tissues. Limited data is available on distribution of NCT in normal and diseased human tissues. Studies of the rat NCT gene have revealed the existence of a splice variant lacking exon 3, which encodes for a protein truncated by 62 amino acids. While the full length NCT was ubiquitously expressed, the spliced variant was preferentially found in embryonic and adult rat neurons, but not astrocytes and microglial cells. It was also detected in a human neuroblastoma cell line (LAN-5), suggesting it may be evolutionary conserved, hence possessing a distinct cellular function (311). Eukaryotic cells have a tight regulatory mechanism to distinguish between the normal and the premature termination codons, thereby assessing whether an mRNA transcripts is suitable for translation (312). This surveillance mechanism sends potentially harmful transcripts for accelerated degradation. The depleted exon 3 NCT variant may therefore have physiological, tissue-specific relevance since its expression is preserved in embryonic and adult rat neuronal cells.

Analysis of NCT expression in membrane preparations of various mouse tissues using antibodies against the N- and the C- terminus of NCT highlighted, for the first time, that the glycosylation pattern of NCT may differ across organs, hinting that the N-terminal NCT glycoforms may even infer tissue-specific function of this protein (312).

Namely, the C-terminal NCT antibody detected mature and immature nicastrin forms (140 kDa and 125 kDa), with strong expression in the muscle, brain and heart. Low expression was noted in the lung and kidneys. Antibody recognising the N-terminal domain of NCT equally picked up the deglycosylated NCT (~80 kDa) form, which was absent in the heart preparations, while prominent in the brain and muscle (220). In aggregate with high mRNA levels of NCT found in the skeletal muscle, and the fact that NCT was detected within complexes of ~290 kDa as opposed to PS-containing complexes migrating at ~400 kDa, it was proposed that NCT may have a PS/GS-independent role in the skeletal muscle tissue. Measuring mRNA and protein expression of GS components in mouse whole tissue extracts, De Strooper et al. observed that transcriptional levels of the NCT are not necessarily translated to equally high protein levels. For example, a disconcordance was noted between high NCT mRNA but low protein levels in the heart, and low NCT mRNA but high protein levels in the spleen. In contrast to Ilaya et al., higher protein levels of NCT were found in the liver, spleen, kidneys and lung than in the heart and muscle, while widely reported high levels of NCT mRNA and protein in the mouse skeletal muscle were low, but still exceeding those of PS1 and PS2, as previously reported (216, 220). Furthermore, mass spectrometry analysis of isolated murine lympocytes and murine primary splenocyte membrane preparations, revealed NCT as one of the integral plasma membrane constituents in these cells (313). Analysis of the canine brain and peripheral tissues for expression of NCT by means of RT-PCR confirmed the abundance of the NCT transcript in the brain and skeletal muscle, while NCT mRNA was also detected in the liver, spleen and lungs (221). Collectively, analysis of NCT mRNA and protein levels in various animals tissues, although mainly in agreement, still propose that it is highly plausible that the post-translational modulation is indeed the critical step determining the actual levels of the functional protein, which may not necessarily be directly correlated with the abundance of the transcriptional template.

### 1.8.4. Nicastrin cellular localisation

Coimmunofluorescence (co-IF) analysis of NCT and the protein markers of subcellular compartments, calnexin (ER) and GM130 (Golgi), revealed that the cellular localisation of NCT in neuronal cells is predominant peri-nuclear and adopts a punctuated pattern. Additional cytolpasmic distribution of NCT implies its presence in the late secretory pathways. Colocalisation IF studies confirm that the full length NCT undergoes glycosylation dependent cellular localisation, with immature species colocalising with the ER, and the higher molecular weight, mature NCT, being visualised in the Golgi. In invertebrates (*C.elegans)*, NCT IF also demonstrated localisation at the cell membrane (314).

### 1.8.5. Effects of nicastrin depletion on other GS components

In the absence of NCT, stability of other GS components (Aph-1, PS and PEN2) is diminished, their protein levels reduced, and the remaining amounts are predominantly sequestered in the ER (315-317). Hence, NCT appears to be required to support GS-members' stability, as well as to regulate their exit from the ER and further cellular trafficking and maturation through the *cis*-Golgi/*trans*-Golgi network to the cell membrane (315). Interestingly, some amounts of the PS1 holoprotein-PEN2 complex are still delivered to the plasma membrane independently of NCT deficiency. Additionally, even though NCT depletion induces downregulation of GS components, PEN2 levels are partially NCT-independent as they can be restored just by overexpression of exogenous PS1 and/or Aph-1 (315). Even though the scaffold backbone in the GS complex assembly is the NCT-Aph-1 dimmer (214), Aph-1 can also associate with the full length PS and PEN2 in NCT knockout cells (315). Since the products of PS endoproteolysis are not observed in cells lacking NCT, it is unlikely that the Aph-1/PS1/PEN2 trimmeric intermediate complex is able to execute intrinsic GS-like activity, so it is plausible that NCT contributes to the catalytic cleavage of PS, rendering the complex proteolytically competent. However, an absolute requirement of NCT for GS activity has recently been challenged by two independent reports. Presenilin mutations in MEFs, namely the S438P located in the PS-TMD8 and the F411Y mutation in the PS-TMD9, reduced NCT levels while not impairing the production of PS-NTF and PS-CTF, nor affecting the levels of PEN2 and Aph-1, thereby sustaining wild-type GS protease

activity (cleaving APP and Notch). Also, a PS/PEN2/Aph-1 trimmer, not harbouring the above PS mutations was found to possess GS activity, albeit at lower levels compared to a fully assembled GS (318). However, the stability of the S438P/F411Y mutant PS-CTF, as well as the PS/PEN2/Aph-1 trimmer was severely shortened, re-emphasising the relevance of NCT for GS complex stability and maintenance of required cellular levels of GS activity (318) (319).

### 1.8.6. Nicastrin post-translational modifications

Post-translational modifications (PTMs) are chemical alterations in the form of covalent additions at particular amino acid residues, which affect the majority of the total cellular proteome, and regulate how a particular protein sequence will behave and what final folded structure it will assume in eukaryotic organisms. Understanding the protein's PTM pattern facilitates deciphering its involvement in the underlying cellular molecular processes. PTMs of one protein may vary across cellular types and organisms, enabling protein's participation in the context-designated cellular processes. PTMs enable protein shuttling between cellular compartments, as well as incorporation of the integral residential proteins into appropriate cellular organelles (lysosomes, mitochondria, plasma membrane). Similarly, protein PTMs may vary between normal and diseased conditions, inducing a differential expression pattern, as well as altered cellular localisation profile of the protein. There are multiple forms of PTMs: glycosylation, phosphorylation, palmitoylation, acetylation, methylation etc (320).

#### *1.8.6.1. Glycosylation*

Glycosylation is the most common PTM affecting ~ 50-70% of the protein pool in eukaryotic cells. It involves covalent linking of oligosaccharide chains to certain amino acid residues of the primary protein, mainly asparagines, serines and threonines (320). A wide range of protein's properties can be affected by glycosylation: folding, localisation, trafficking, solubility, activity, antigenicity, half-life, as well as protein-protein interactions.

There are two main types types of glycosylation: N-linked (addition of a sugar to the amino group ($NH_2$) of an asparagine at the Asn/X a.a./Ser consensus sequence, where X can be any amino acid except Proline), and O-linked (linkage of *N*-acetylgalactosamine, *N*-

acetylglucosamine, mannose, fucose, phosphodiester linked *N*-acetylglucosamine, glucose, galactose or xylose to the hydroxyl -$OH^-$ group of a Serine or Threonine, not requiring a consensus motif). N-linked glycoforms fall into three main categories: high mannose, hybrid and complex. N-linked glycosylation predominantly occurs in the ER, influencing protein folding, and is followed by the O-linked glycosylation, which takes place on the folded protein in the *cis*-Golgi network, and influences properties of the secreted and membrane glycoproteins (321).

Newly synthesised proteins gain 'core-oligosaccharides', including mannose residues in the ER, and only when properly folded they traffic to the Golgi, where some of the mannose residues are trimmed and replaced with terminal sugars. In order to understand the rationale behind using specific deglycosylating agents to monitor the PTM efficiency and stage, it is of note that glycoproteins within the ER and the *cis*-Golgi still contain mannose residues that can be removed by EndoH, while in the medial and distal Golgi, they become EndoH resistant (Figure 15) (322).

The enzyme endoglycosidase H (Endo-β-N-acetylglucosaminidase H; EndoH), is a highly specific endoglycosidase which cleaves asparagine-linked high mannose moieties. EndoH is an enzyme widely used to follow the conversion of oligosaccharides from EndoH sensitive to EndoH resistant, as a means of following the transit of a glycoprotein from the ER to the Golgi. Endo H resistance is acquired through modification of the oligosaccharide portion of the glycoproteins in the medial Golgi apparatus (323). It is an important parameter in measuring whether the transport of glycoproteins from the ER to the Golgi is accomplished. Proteins that are processed aberrantly fail to escape from the ER, making them unable to gain EndoH resistance in the Golgi. Thus, the acquisition of EndoH resistance is an indication that the glycoproteins are folded and processed correctly. A peptide-N4-(N-acetyl-beta-glucosaminyl) asparagine amidase (PNGase) is an enzyme that catalyses cleavage of all carbohydrate chains attached to asparagine residues.

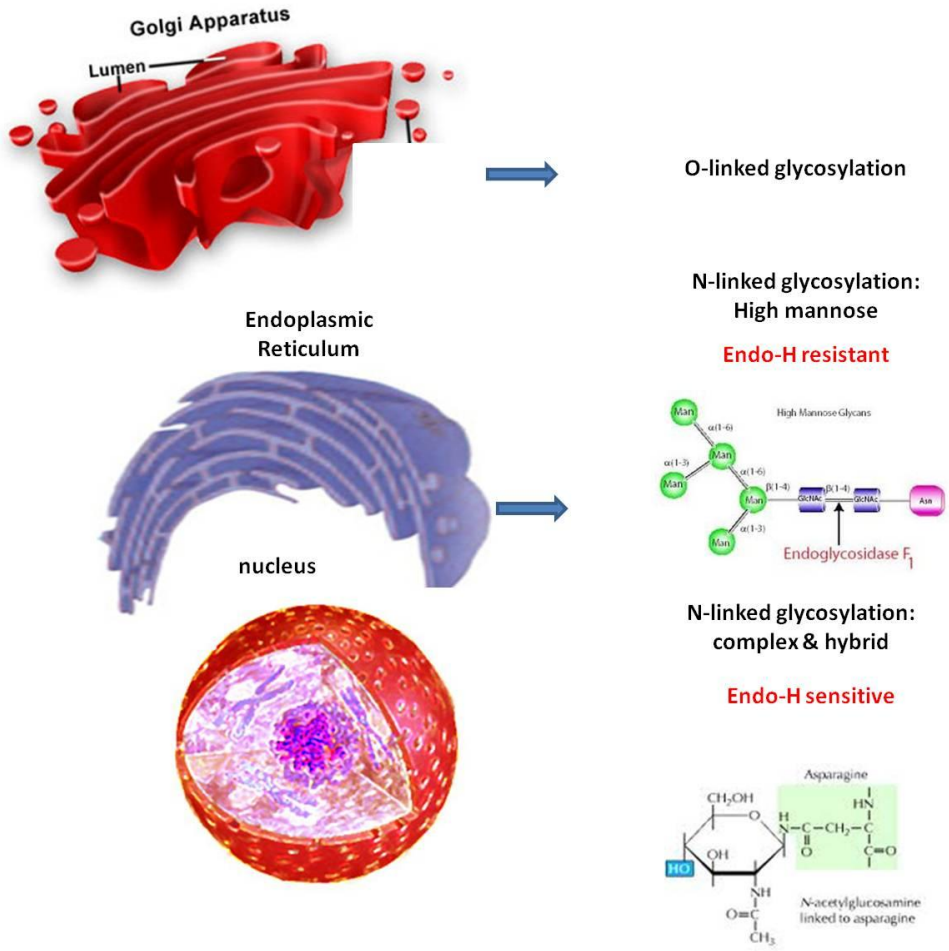


**Figure 15.Sequential glycosylation steps occurring in the endoplasmic reticulum and the Golgi apparatus.** N-linked glycosylation (complex and hybrid) predominantly occurs in the ER, influencing protein folding. O-linked glycosylation takes place on the folded protein in the *cis*-Golgi network and influences properties of the secreted and membrane glycoproteins. Glycoproteins within the ER and the *cis*-Golgi contain mannose residues that can be removed by EndoH, while in the medial and distal Golgi, they become EndoH resistant.

The primary amino-acid sequence of NCT translates to a ~80 kDa protein, which contains 16 putative N-glycosylation consensus sequences in the hydrophilic N-terminal domain (Figure 16). Nicastrin is a heavily glycosylated protein, and this PTM significantly affects its cellular localisation, function, as well as molecular weight, as determined by the western blotting experiments using the common deglycosylating agents: EndoH, PNGase, neuramidase and O-glucosidase.

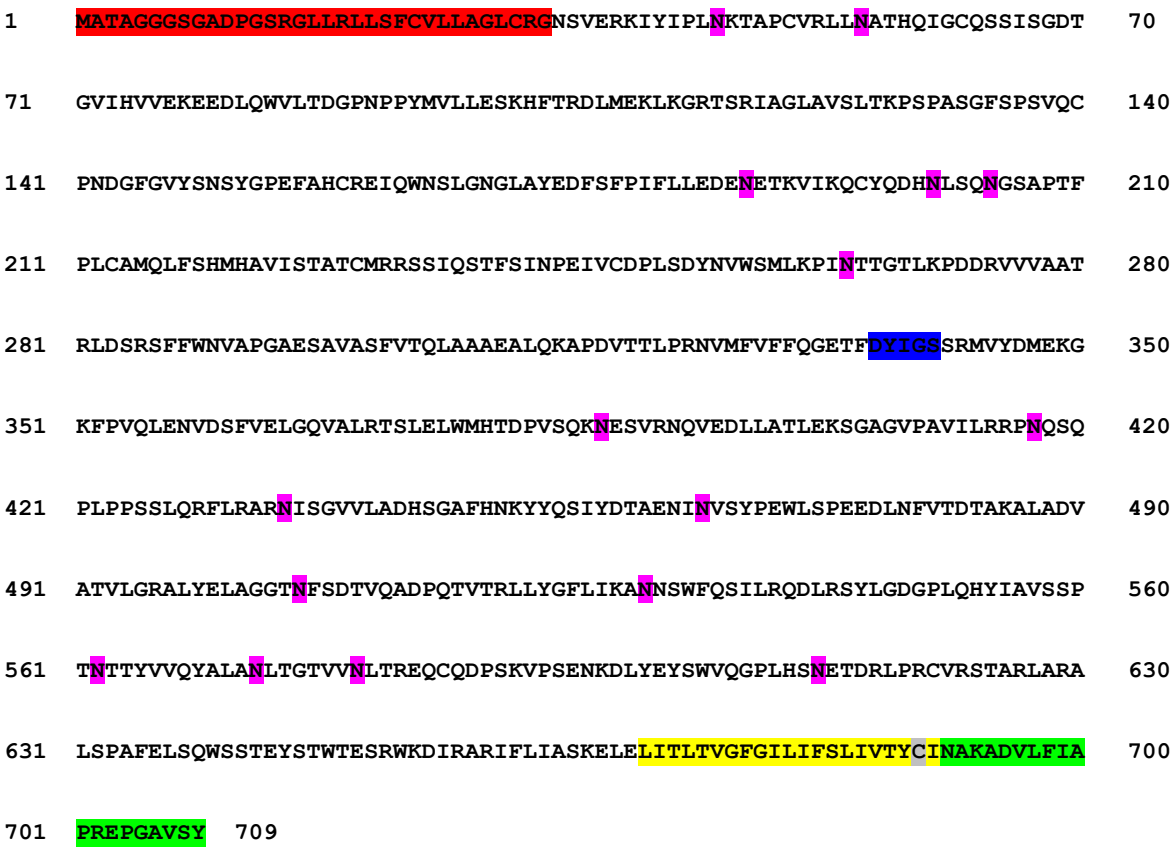


**Figure 16.Nicastrin protein sequence with annotated regions and residues which are post-translationally modified**

- Nicastrin signaling peptide
- Nicastrin transmembrane domain
- Nicastrin cytoplasmic domain
- Nicastrin DYIGS domain
- Nicastrin glycosylation residues: reported (45 and 187 (324), 387 (324, 325), 612 (325)), and predicted (55, 200, 204, 264, 417, 435, 464, 506, 530, 562, 573, 580, 612)
- Nicastrin palmitoylation residue

In a wide spectrum of cell lines (247, 292, 326, 327), and in *ex vivo* cell preparations from the mouse brain tissue extracts (216, 247), endogenous NCT can be visualised as a close doublet band at molecular weights of ~140 kDa and ~125 kDa, corresponding to mature and immature NCT. The immature NCT contains high-mannose oligosaccharides and is gradually turned into mature NCT that contains a mix of EndoH sensitive and EndoH resistant oligosaccharide chains. Both forms contain one or more high-mannose moieties, as EndoH treatment induces a mobility shift of the mature and the immature NCT by ~15 kDa and ~40 kDa, respectively, indicating that the mature NCT contains both high-mannose, EndoH resistant moieties, which persist at ~125 kDa, as well as Golgi-derived complex

oligosaccharides which are removed by EndoH (248, 292). Complete disappearance of the ~140 kDa band after the EndoH treatment, without affecting the ~125 kDa band, is achieved by the addition of neuramidase which removes the sialic acid residues. This indicates that the fully mature NCT may be terminally sialyted as well as glycosylated (247). PNGase treatment, however, which removes all asparagine-linked glycoforms, including the high mannose linkages, reveales minor NCT bands at ~110 kDa and ~80 kDa, corresponding to incomplete and complete deglycosylation, respectively (326). O-glucosidase treatment doesn't affect the mature, nor the immature NCT species, confirming that NCT is post-translationally modified by N-liked and not O-linked glycolylation (247 499, 326). Glycosylation pattern of NCT was analysed in MEFs by means of specific binding of lectins to carbohydrates. Reactivity of the immature NCT with *Galanthus nivalis* agglutinin recognising high mannose residues was higher than that of the mature NCT, indicating that the immature NCT is richer in these oligosaccharide moieties. Mature NCT reacted with *Datura stramonium* and *Maackie amurensis* agglutinins, which bind to complex and hybrid N-glycans, and sialic residues, respectively, while the immature NCT showed no reactivity. Absence of O-glycan modifications of immature and mature NCT was confirmed by the absence of reactivity with the peanut agglutinin (248). This data is in agreement with the EndoH sensitivity reports. Occasional discrepancies in molecular weight of NCT glycoforms reported in the literature are minor and most likely caused by cell-type specific PTM patterns of NCT, or the interpretation of gel mobility patterns due to the use of alternate protein ladders.

Of note is that in the cells transfected with exogenous NCT, accumulation of the immature species is predominant, pointing out the inefficiency of the exogenous wild-type NCT protein glycosylation. In terms of interaction with PS, coimmunoprecipitation and GS activity experiments confirm the existence of tight cellular regulatory features, where it is the fully mature NCT that preferentially binds to PS. This indicates the necessity of NCT maturation for its full functionality within the GS. Furthermore, NCT fails to undergo full glycosylation in PS knockout cells, more so in PS1/PS2 double knockout cells than PS individual knockout cells (248), indicating that the presence of PS, but not its ability to form proteolytically functional heterodimers (PS-CTF/PS-NTF) (326), is a requirement for proper maturation and stabilisation of NCT (247, 298, 322).

Nicastrin mutants which affect the function of the protein and by inference of the GS enzyme, as measured by the generation of the Aβ42 peptide, also show a differential glycosylation pattern. NCT mutation (DYIGS→AAIGS) which induces increased Aβ42 production, indicating enhanced GS activity, indeed confirmed that this double missense mutation lead to NCT trafficking-dependent glycosylation in the Golgi and full maturation of the protein, mimicking that of the wild type NCT. The Δ312-369 a.a. loss of function mutation of NCT caused a proportionate trafficking/glycosylation arrest of NCT and its accumulation in then ER (292) (327). The immature NCT possesses the ability to bind Aph-1 forming a structural scaffold in the GS assembly process. This is also largely unaffected by PS or PEN2, since the immature NCT-Aph-1 dimmer persists even in the absence of PS and PEN2 (317).

Conformational change of the NCT-ECD is another feature coupled to glycosylation, which is also a pre-requisite for complete structural activation of NCT (316). Nicastrin ECD plays a pivotal role in the GS function, and appears to do so by undergoing a conformational switch during the process of maturation and GS complex assembly (316). Mature, fully glycosylated NCT is mainly trypsin resistant like PEN2, but unlike its immature counterpart and the other GS components (PS-CTF, PS-NTF and Aph-1). The presence of PS seems to be necessary for the acquisition of NCT trypsin resistance, suggesting that this is a feature characteristic of a GS-associated NCT. Furthermore, NCT retains trypsin resistance, membrane localisation and association to PS, PEN2 and Aph-1 even upon kifunensine treatment (inhibition of mannosidase I, i.e. N-linked complex glycosylation) (248), which yields immature NCT, migrating to ~125 kDa. This, and the fact that functionally inactive NCT mutants are digested by trypsin, rules out the possibility that the branched oligosaccharide chains added through glycosylation are fully responsible for trypsin resistance, and emphasises that NCT assumes degradation resistant conformation upon full maturation and assembly into an active GS complex (316).

Expression of NCT N-terminal domain mutants (Cys248, Pro262, Asp283, Glu333, Gly339) in a NCT knockdown background of HEK293 cells, which induces downregulation of all other GS components (PS1, PS2, PEN2 and Aph-1), demonstrated that the P262L, D283N, and the missense DY/AA mutations, largely restored GS component levels and activity, as well as NCT glycosylation and conformational maturation, unlike the C248S, E333Q and G339A mutants.

Maturation of the latter group of NCT mutants was severely impaired, and GS activity was not restored, despite a partial rescue of Aph-1 and formation of the NCT-Aph-1 dimmer, indicating that these residues of the NCT-ECD may be important for the NCT-Aph-1 dimmer binding to PS and PEN2 and/or are necessary for NCT to assume active conformation (316). Additionally, deletion of the NCT C-terminus has the capacity to impair glycosylation and maturation of the protein, despite the lack of known functional domains located in this part of NCT (298). In light of the differential cellular localisation, binding partners and functional importance of NCT glycosylation species and mutants forms (292), it can be concluded that this PTM of NCT is not only a marker of its cellular trafficking but also an important marker of its activity.

#### *1.8.6.2. Nicastrin palmitoylation*

Protein S-palmitoylation is a PTM which involves covalent addition of the 16-carbon fatty acid palmitate to the cysteine residue(s) of proteins. It is a reversible PTM that facilitates dynamic protein shuttling between cellular compartments, increases protein's hydrophobicity and contributes to the protein's membrane localisation (328). There are four groups of proteins subject to this type of PTM: a) G-protein coupled receptors (GPCRs) and likes thereof, that are palmitoylated on cysteine residues close to their transmembrane domains; b) Gα subunits, which are palmitoylated near their N-terminus; c) H-Ras and N-Ras that are modified near the C-terminus, and; d) peripheral membrane proteins, which are modified with a palmitate only (Figure 17) (329).

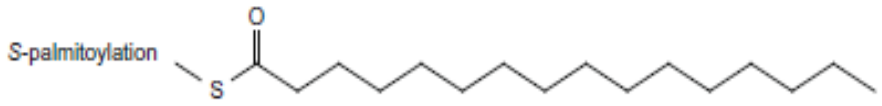


**Figure 17.Palmitate acid chain added in the process of S-palmitoylation to a cysteine residue of a protein.**

Nicastrin undergoes S-palmitoylation at the Cys689 residue in the ER. Another S-palmitoylated member of the GS enzyme is Aph-1, at residues Cys182 and Cys245 (330). This PTM of NCT is not required for proper interaction with other GS components, nor does it greatly affect the enzymic potency of the GS *in vitro*, while in transgenic mouse models,

absence of NCT and Aph-1 palmitoylation reduces Aβ42 neuronal deposits. Furthermore, S-palmitoylation affects protein stability of the immature NCT, as the C689S NCT mutants degrade much more rapidly than the palmitpylated protein, presumably as this PTM is thought to shield proteins from proteasomal degradation. S-palmitoylation also facilitates membrane anchoring of NCT, and by inference the GS complex into the membrane lipid-rafts (330).

#### *1.8.6.3. Nicastrin phosphorylation*

Phosphorylation is a key PTM which occurs in the cell nucleus or in the cytosol, and entails a transfer of a phosphate moiety from an adenosine-triphosphate (ATP) molecule to a threonine, serine or a tyrosine residue of a receptor molecule (320). Protein kinases catalyse cellular phosphorylation events which are of fundamental importance in the regulation of cell proliferation, differentiation, apoptosis, invasion etc. A protein kinase recognises acidic, basic or hydrophobic residues in the vicinity of the phosphorylation site as a determinant of its specificity (320).

The first indication that NCT may be undergoing phosphorylation came from Kim et al., who reported that the extracellular signal regulated kinase 1/2 (ERK1/2) acts as a negative regulator of endogenous GS activity in HEK293 cells engineered to stably overexpress GS components, and in primary murine cortical neurons (331, 332). Inhibition of ERK1/2, a downstream effect of tyrosine kinase inhibitors (333), which are extensively used in the treatment of cancers, induced a marked increase in GS activity. Both the immature and the mature NCT were found to interact with ERK1/2, regardless of its phosphorylation status, and this interaction was able to increase the phosphorylation of NCT (331) and full length PS1 (332) in the *in vitro* kinase assays. Tumour-necrosis factor α (TNF-α) elicits regulation of GS activity through c-Jun N-terminal kinase 2 (JNK2)-mediated serine-threonine phosphorylation of NCT and PS1 (334). Specific NCT phosphorylation sites have not yet been identified. However, it is known that JNK2-mediated phosphorylation of PS1 occurs at Ser319/Thr320 residues and stabilises PS1-CTF cellular levels (334). In contrast to ERK1/2-induced NCT phosphorylation, which attenuates GS activity, TNFα/JNK2-mediated phosphorylation of NCT and PS1 augments GS activity (334).

This indicates that NCT and PS1 harbour phosphorylation sites, which when activated, can act as both positive and negative regulators of GS activity in response to respective stimuli. Elucidation of these sites would be of paramount importance in the clinical settings where tyrosine kinase inhibitors are used, as the proposed increase in GS activity in this context may serve as a mechanism of resistance to the treatment modalities which induce ERK1/2 inhibition. This was corroborated by the finding by Osipo et al., where HER2 inhibition in breast cancer cells resulted in a marked increase in the Notch pathway activity, possibly in part due to the above described mechanism (163). Predicted phosphorylation sites of NCT and their respective kinases are included in Table 4.

**Table 4. Predicted nicastrin phosphorylation sites using high stringency analysis (http://scansite.mit.edu/motifscan)**

| | |
|---|---|
| **Tyrosine kinase** | **EGFR** |
| **Site** | Sequence |
| **Y94** | TDGPNPP**Y**MVLLESK |
| **Basophilic Ser/Thr kinase** | **PKA** |
| **Site** | Sequence |
| **S235** | ATCMRRS**S**IQSTFSI |
| **Basophilic Ser/Thr Kinase** | **PKC** |
| **Site** | Sequence |
| **S632** | ARLARAL**S**PAFELSQ |
| **Kinase binding site** | **ERK1** |
| **Site** | Sequence |
| **P179** | AYEDFSF**P**IFLLEDE |
| **Kinase binding site** | **PDK1** |
| **Site** | Sequence |
| **S177** | GLAYEDF**S**FPIFLLE |

Biological significance of NCT phosphorylation may be discussed for the putative phosphorylation sites located in the NCT domain facing the cytosol. As the extracellular domain of NCT is facing the lumen of the secretory vesicles during ER-Golgi-plasma membrane transport, when it is reported not to be in contact with the cytosolic milieu that contains the intracellular kinases (214), it remains to be determined where the NCT phosphorylation sites are actually located, and how they are being post-translationally modified.

### 1.8.7. Nicastrin interactome

Extensive analyses of the protein-protein interactions within the GS complex have demonstrated that Aph-1, PS and PEN2 interact with the N-terminal part of NCT-TMD and are able to coimmunoprecipitate upon isolation of the active GS complex (223). As the GS-substrate recognition 'device', NCT also interacts with the C-terminal fragments of the GS substrates (300). Furthermore, NCT is able to interact with BACE1 *in vitro* (335), promoting its catalytic function, required for the enzymic cleavage of the GS substrates' extracellular domains. Another binding partner of NCT is Neprilysin (MME), an enzyme which degrades the Aβ peptide (336). Nicastrin deficiency lowers MME expression and membrane-bound activity, while NCT overexpression restores this loss in a GS-dependent manner. The main cluster of NCT interacting partners is shown below (Figure 18).

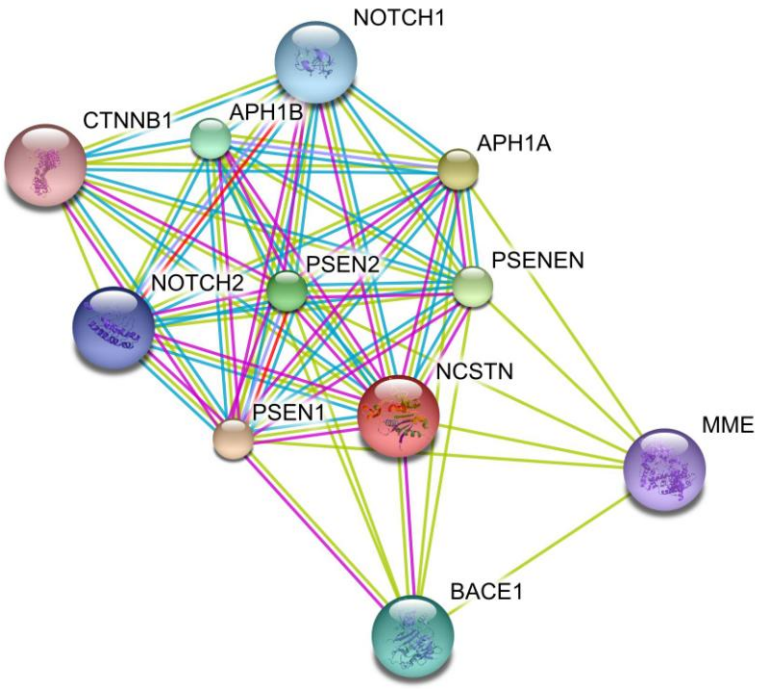


**Figure 18.Nicastrin interacting partners**. A schematic depicting nicastrin interacting partners. Adopted from: http://string.embl.de/newstring_cgi/show_network_section.pl. Data obtained via —textmining; —database derived information; —experimental data.

### 1.8.8. Consequences of the loss of nicastrin in various system models

Nicastrin expression is not eliminated upon inhibition of other GS components, rather NCT fails to fully mature under these circumstances. NCT silencing, however, results in a coordinated reduction of expression of all other GS components: PS, PEN2 and Aph-1 (317). This fact reinforces the notion that NCT is indeed a pivotal component of the GS complex (317). Genetic inhibition of NCT using the RNA silencing (siRNA) approach in *C. elegans* proved embryonically lethal and induced a phenotype comparable to that of the simultaneous loss of both PS orthologues (sel-1 and hop-1), and Notch inhibition (296, 337). In *Drosophila* (fruit fly), embryos lacking both maternal and zygotic NCT display a severe neurogenic phenotype, consistent with impaired Notch signaling (hyperplastic embryonic nervous system, wing notching, thickening of wing veins etc.) (338). Mice lacking NCT suffer severe growth retardation, vascular deformities and embryonic mortality with an onset at 10.5 days, all consistent with a pronounced 'Notch phenotype', underlined by formation of extensive apoptotic areas in the brain and heart (339, 340). However, in mice with a double PS1 knockout genotype, two distinct phenotypic outcomes were observed: i) the Notch-severe and; ii) the Notch-mild phenotype, the latter baring milder skeletal deformities. The modifier between the two was mapped to the distal chromosome 1, or more precisely to the NCT gene (341). The coding region of NCT in the Notch-severe vs. Notch-mild phenotype harboured two missense substitutions at residue 21 (Phe21 vs. Ser21) in the NCD-ECD, and at residue 678 (Iso678 vs. Thr678), within the membrane-spanning region.

### 1.8.9. Gamma-secretase independent function of nicastrin

Even though NCT is largely viewed as the structural and functional requisite and an integral component of GS, it has recently been proposed that it may possess certain GS-independent cellular activity. This has been observed in the context of p53-regulated cell death (342). Namely, overexpression of NCT in HEK293 and neuronal cell lines supported cell survival, inhibited activation of the proapoptotic caspase cascade, promoted Akt pathway activation and induced evasion of the staurosporin induced p53-mediated cell death via decreasing p53 transcriptional and phopho-protein levels.

Nicastrin mutants, AAIGS and Δ312-340 a.a., known to increase and inhibit GS catalytic activity, respectively, as well as NCT expression in the PS1-depleted fibroblast cells, and in cells treated with a GS inhibitor, were still able to exert the same protective effect on cell viability in a p53 dependent manner (342). P53 has previously been implicated in the bidirectional transcriptional and functional crosstalk with the members of the GS complex: Aph-1, PS and PEN2. Namely, overexpression of Aph-1, PS and PEN2 was also able to rescue cells from staurosporin induced apoptosis, but this feature was dependent on GS integrity (343). PS2 exerted predominantly a proapoptotic cellular response (344). Therefore, it is evident that p53 mediates GS dependent cellular functions. Importantly, NCT-mediated effects do not require full molecular integrity of the GS enzyme. Thereby, Pardossi-Piquard et al. demonstrated a GS-independent NCT cellular function in exerting both transcriptional and post-translational control of the p53 tumour suppressor (342). In support of NCT engagement in the control of cell-death, but in contrast to the above data, NCT DYIGS-AAIGS mutation known to increase GS activity and promote cell survival, was able to induce apoptosis in a neuroblastoma cell line, an effect accompanied by BAX expression as well as mitochondrial cytochrom C release (345). Therefore, one must bear in mind that NCT involvement in regulating cellular apoptotic machinery may be cell context dependent.

### 1.8.10. Nicastrin degradation

Protein degradation is executed through two major cellular pathways, the proteasome and the lysosome. It is critical for the regulation of the proteins' turn-over and half-lives, thereby maintaining homeostasis of cellular processes like proliferation, differentiation, apoptosis etc. Proteasomal degradation is a characteristic of the cytosolic and nuclear proteins, while lysosomes degrade long-lived, membrane proteins and endocytosed material (346). In cell lacking NCT, other GS components are destabilised and targeted for cellular degradation, as determined by their reduced half-lives. PS1 and PEN2 are subjects of proteasomal mediated digestion, while Aph-1 and NCT seem to be degraded by both the ubiquitin-proteasome pathway and the lysosome (315, 347). Apart from being localised in the ER, Golgi, mitohondria and the plasma membrane, NCT was recently named the residential protein of lysosomal membranes with properly orientated, cytoplasm-facing ectodomain, verifying its presence in this cellular organelle (252).

Nicastrin protein targeted for degradation is ubiquitinated, and cellular levels of ubiquitin and mature NCT are inversely correlated (348). Proteasomal inhibition using MG132 and lactacystin, and a lysosomal inhibitor chlorochin, increased cellular levels of NCT (moreso of the mature form), and also induced NCT accumulation in the ER and the lysosomes, respectively. Levels of the immature NCT were found elevated in cells lacking E3 ubiquitin ligase (Synoviolin), implicated recently in the quality control of proteins through the ER, as well as in ER and proteasomal-mediated protein degradation. Immature NCT and Synoviolin were found to interact, indicating that immature NCT is a Synoviolin substrate (349). Furthermore, plasma membrane levels of both immature and mature NCT were increased in E3 ligase-null, cells implicating the importance of this ligase for the cellular trafficking of NCT (349).

### 1.8.11. Nicastrin in other diseases

Nicastrin polymorphisms have been analysed in the context of age related cognitive decline (350). Nicastrin haplotype B, previously linked to increased susceptibility to EOAD in the absence of the APOE ε4 allele, proved to impact on the general cognitive levels, rather than to induce cognitive changes with age. In a post-natal forebrain conditioned NCT knockout mouse model, animals displayed severe, age-related learning and memory impairment due to neuronal cell apoptosis (351).

Acne inversa is a chronic inflammatory condition of the hair follicles characterised by the formation of skin abscesses and draining sinuses. Like Alzheimer's disease, it can be hereditary and sporadic. The fact that genetic inhibition of Notch via inhibiting the GS enzyme in mice resulted in skin changes resembling those occurring in acne inversa, prompted investigations into the possible genetic modifications of the GS components in this condition. Indeed, the haploinsuficiency of GS component genes was found as the underlying genetic basis for a subset of this disease. More precisely, distinct NCT mutations, one resulting in the formation of a premature termination codon (p.E584DfsX44), and another nonsense mutation at codon 117 (p.R117X), both yielded reduced *NCT* mRNA transcript levels and loss of function. The abnormal splice variant (skipping of exon 13) led to 32a.a. residue loss in the NCT protein (352).

It has previously been established that neurons are the predominant cell type of NCT localisation in the brain (311). Furthermore, it appears that the levels of NCT in murine neuronal cells *in vivo* are saturated to the extent that a 50% reduction of NCT mRNA levels, which induces a marked inhibition of APP processing in fibroblast cells, had no effect on APP cleavage in neurons (353). Traumatic brain injury (blunt head trauma, penetrating brain injury, intracranial hemorrhage, infarction or inflammation) induces a set of responsive, repair-intended reactions in the brain tissue, such as edema, accumulation of inflammation infiltrates and activation of astrocytes and microglial cells. In mice, it resulted in a marked increase of NCT levels, both in neurons and non-neuronal cells in the proximity of the wound, across the cerebral cortex, hippocampus, thalamus, hypothalamus, striatum and amygdala (354). The increased expression of NCT was maximal after 4-7 days after injury, and gradually declined thereafter. Since PS levels followed the same trend of increase and distribution, and colocalisied with NCT, this suggests that GS activity may regulate important healing processes after brain trauma (354). This possibly provides a mechanism for the finding that traumatic brain injury is also followed by increased Notch activity in cortical neurons (355).

Analysis of NCT expression and function in human malignancies is still sparse. Treatment of a colon cancer cell line with a standard chemotherapy agent, oxaliplatin, induced activation of the Notch pathway, through increasing both NCT and PS1 protein levels, and thereby elevating cellular GS activity, potentially as a means of developing resistance to treatment (146). In the context of breast cancer, stable NCT depletion in a triple negative, but EGFR positive breast cancer cell line, HCC1806, resensitised these breast cancer cells to EGFR inhibition, by means of impeding Notch pathway and Akt activity (164).

### 1.8.12. Targeted inhibition of Nicastrin

An experimental means of interfering with the GS activity via inhibition of NCT has been proposed via the introduction of a single chain variable fragment (scFv) against NCT into the cells, i.e. the NCT intrabody (356). The intrabody 5201F was constructed based on a template monoclonal anti-NCT ECD Ab. It consisted of the light and heavy chain variable regions which bound specifically to the NCT-ECD during the process of GS biosynthesis and assembly, thereby interfering with the enzymes catalytic maturation and function. The intrabody also arrested NCT maturation by inhibiting its glycosylation and ECD conformational change, rendering NCT readily degradable by trypsin digestion. All of this resulted in an overall loss of endogenous levels of the the mature NCT and of other GS components (356). This approach in inhibiting GS activity opens room for consideration of NCT inhibition as a valid modality to interfere with the GS enzyme.

# CHAPTER 2

# Materials and Methods

# 2. Materials

## 2.1. Suppliers:

Abcam (Cambridge, UK)

Amersham (Buckinghamshire, UK)

Applied Biosystems (Warrington, UK)

BD Bioscience/VWR International (Hitterworth, UK)

BDH Chemicals (Poole, UK)

Bio-Rad Laboratories (Hampsted, UK)

DAKO (Ely, UK)

Dharmacon (Lafayette, CO, USA)

eBioscience (San Diego, CA, USA)

Eurofins Genetic Services (London, UK)

Fermentas (St. Leon-Rot, Germany)

FirstLink (Birmingham, UK)

GE Healthcare (Chalfont St. Giles, UK)

Gibco/Invitrogen (Paisley, UK)

GURR (High Wycombe Bucks, UK)

Invitrogen (Paisley, UK)

Leinco Technologies (Missouri, USA)

Lonza Sales AG (Basel, CH)

Millipore (Southampton, UK)

New England Biolabs/Cell Signaling (Hertfordshire, UK)

Origene (Rockville, USA)

PAA Laboratories (Somerset, UK)

Qiagen (West Sussex, UK)

R&D Systems (Minneapolis, USA)

Roche Diagnostics (Burgess Hill, UK)

Santa Cruz (Heidelberg, GE)

Sigma-Aldrich (Gillingham, UK)

US Biomax/Insight Biotechnologies (Wembley, UK)

Vector Laboratories (Peterborough, UK)

## 2.2. Reagents

Small interfering RNA (siRNA) against nicastrin was obtained from Dharmacon. HiPerfect transfection reagent, AllStars Cell Death siRNA positive control, the RNAeasy RNA extraction kit, PAHS-013 gene array, RT² First Strand Kit, RT² qPCR SYBR Green/ROX Master Mix, cDNA Maxi and Mini Preparation Kits were all purchased from Qiagen. Dulbecco's Modified Eagel Medium (DMEM), RPMI-1640 medium (developed at Roswell Park Memorial Institute), trypsin, EDTA, L-glutamine, isopropanol, ethidium bromide, ampicilin, bovine serum albumin (BSA), TEMED, heparin, XP725 Protein array were all from Sigma. Penicillin-streptomycin solution, Lipofectamine 2000, puromycin, EGF, FGF, TA cloning kit were from Invitrogen. Foetal calf serum (FCS) was obtained from FirstLink. Matrigel, CycleTEST Plus DNA Reagent Kit and Dispase were obtained from BD Bioscience. Ethanol, methanol, agarose were from Fisher Scientific. Paraformaldehyde was purchased from BDH Chemicals. Mammary epithelial basal cell media was from Lonza. Protein kaleidoscope ladder and Bradford protein determination reagent were from Bio-Rad and 1kb DNA loading marker from Fermentas. The ECL western blotting detection reagent, the high performance chemiluminescent films and the Cy3 and Cy 5 dyes were obtained from GE Healthcare. Enhanced Immobilon Western chemiluminescent HRP substrate was from Millipore. BM Blue POD substrate, the First Strand CDA Synthesis Kit, PCR Grade Water and the Protease Inhibitor Cocktail were from Roche Diagnostics. SYBR Green PCR Master Mix and the green fluorescent protein (GFP) negative control siRNA were from Applied Biosystems. Nicastrin Blocking peptide (N164) was from Leinco Technologies. The α-MEM

media was from PAA Laboratories. Secondary antibodies were from DAKO, Sigma and eBioscience. Primary antibodies are listed below.

## 2.3. Antibodies

**Abcam:** nicastrin (ab2474), Aph-1a (ab19390), PEN2 (ab24743), Presenilin C-terminus (ab12272), β-actin (ab8226), GM130 (ab52649), Numb (ab4147), α6-integrin (ab20142), CD147 (MEM-M6/1; ab666), Akt (ab8805).

**New England Biolabs/Cell Signaling:** Notch1 cleaved-D3B8/Val 1744 (4147), pAkt Ser473 (193H12), eIEF4 (9742), rabbit IgG isotype control (3900).

**Santa Cruz:** Notch4 C-19 (sc-644), Vimentin clone V-9 (sc-6260), Bcl-2(sc-23960).

**BD Biosciences**: p21Cip/WAF1 (610234), p120-catenin (610133), β-catenin (C19229), E-cadherin (610182), CD44-FITC (555478), CD24-PE (555428).

**Millipore**: Ki67 (MAB4190)

**Sigma**: nicastrin (N-1660), Anti-MAP kinase ERK1&2 (M5670), Anti-MAP Kinase, Activated-Diphosphorylated ERK-1&2 (M8159), monoclonal Anti-Rat IgG2b clone R2B-8, Monoclonal Anti-Rat κ & λ light chain clones RT-39 and RL-6, Goat Anti-Rabbit IgG-Peroxidase, Rabbit Anti-Rat-Peroxidase

**eBioscience**: Rat IgG2b isotype control, Anti-Rat IgG-FITC, Anti-Rabbit IgG-FITC

**DAKO:** Polyclonal Goat Anti-Mouse HRP, Polyclonal Goat Anti-Rabbit HRP.

**Molecular Probes/Invitrogen**: anti-rabbit and anti-mouse IgG Alexa Flour® -488 and -555, phalloidin Alexa Fluor®-633.

## 2.4. Cell culture

Breast cancer cell lines (MCF-7, MDA-MB-231, SKBR3, BT474) were from the American Type Culture Collection (ATCC). NCT $^{+/+}$ and NCT $^{-/-}$ mouse embryonic fibroblasts (MEFs) were obtained from Dr Philip Wong (Department of Neuropathology, Johns Hopkins University, ML, USA). HCC1806-Luc1 and HCC1806-NCTsh cells (generated as described below *)were a kind gift of Prof Michel Loren, (Department of Cell Biology and Physiology, Washington University School of Medicine). All tumourigenic cells were cultured in DMEM, except HCC1806-Luc1 and HCC1806-NCTsh cells that were cultured in the RPMI-1640 media, both supplemented with 10% FCS and 2 mM L-glutamine, 100 U/ml penicillin, 0.1 mg/ml streptomycin in 5% $CO_2$ at 37 °C. The non-tumourigenic immortal breast cell lines 184A1 (CRL-8798, ATCC) and MCF10A were cultured in basal mammary epithelial cell growth medium supplemented with bovine pituitary extract (13 μg/ml), EGF (10 μg/ml), hydrocortisone (500 μg/ml), insulin (5 μg/ml), transferrin (0.005 μg/ml), cholera toxin (1ng/ml), penicillin (100 U/ml), and streptomycin (0.1 mg/ml).

*Short hairpins targeting human nicastrin with the sequences:
5′-CCCATCTTTCTTCTTGAAGAT-3′;
5′-GCTCTACTGAATACTCTACAT-3’, were cloned into the lentiviral vector pLKO-puro. Lentiviral infections were carried out using FuGENE 6 transfection reagent (Roche) according to the manufacturer's instructions. Infected cells, HCC1806-NCTsh were selected in medium containing 2 μg/ml puromycin (164).

## 2.5. RNA interference

Double-stranded synthetic 21-mer RNA oligonucleotides (siRNA) were from Dharmacon. si GENOME set of 4 upgrade duplexes was used in deconvoluted and pooled analysis (Figure 19).

siRNA1: D-008043-01: 5’-UAUCUUUCCAGCGGCUCUCUU-3’
siRNA2: D-008043-02: 5’-UACUGUACAACAUAAGUGGUU-3’
siRNA3: D-008043-03: 5’-AUAGUGGGAAGGUUGGUGCUU-3’
siRNA4: D-008043-04: 5’-UACUCAUACAGAUCCUUGUUU-3’

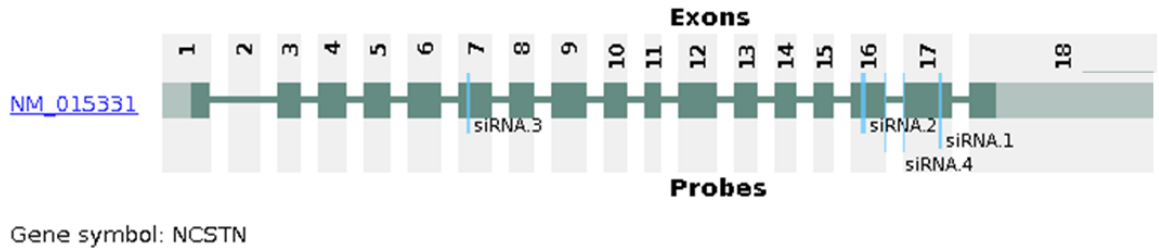


**Figure 19.Display of nicastrin gene regions targeted by the siRNA oligos.** Image adopted from: http://www.tigerteamconsulting.com/SpliceCenter/siRNACheck

The siRNA was used at a final concentration of 40 nM. HiPerfect transfection reagent (Qiagen) was used to transfect the cells. The combination of the D-008043-02 and D-008043-04 siRNA oligos was the most efficient and was used in all experiments. Following each siRNA transfection experiment, the efficiency of downregulation of the targeted mRNA was assessed by RT-qPCR. GFP siRNA (AM4626, Ambion) was used as a negative control.

## 2.6. RNA isolation and quantitative RT-qPCR

Isolation of total RNA was performed using the RNeasy kit (Qiagen). Total RNA concentration was measured using a NanoDrop ND1000 spectrophotometer (Labtech international, East Sussex, UK). RNA (1 μg) was reverse transcribed using oligo dT and Transcriptor First Strand cDNA Synthesis Kit (Roche). RT-qPCR reactions were carried out in a 20 μl reaction volume containing 3.5 nM of each primer and SYBR Green PCR Master Mix (Applied Biosystems). The RT-qPCR amplification conditions were set up as follows: 10 min at 95 ºC, followed by 40 cycles of 60 sec at 95 ºC, 30 sec at $T_a$ (60 ºC), 30 sec at 72 ºC, on a 7900HT Thermocycler (Applied Biosystems, Warrington, UK). The PCR cycle number that generated the first fluorescence signal above a threshold (threshold cycle, CT; 10 standard deviations above the mean fluorescence generated during the baseline cycles) was determined, and a comparative CT method was then used to measure relative gene expression.

**Table 5.Primer sequences**

| Gene | Forward primer | Reverse primer |
|---|---|---|
| ***GAPHD*** | 5'- TGAAGGTCGGAGTCAACGGATTT-3' | 5'- GCCATGGAATTTGCCATGGGTGG-3' |
| ***NCT*** | 5'- GGAGAACCAGCCGAATTG-3' | 5'- GGAGTAAACACCAAACCCA-3' |
| ***PS1*** | 5'-TCACAGAAGATACCGAGACT-3' | 5'-GGATGACCTTATAGCACCTG-3' |
| ***NOTCH1*** | 5'-ACTGTGAGGACCTGGTGGAC-3' | 5'-TTGTAGGTGTTGGGGAGGTC-3' |
| ***NOTCH4*** | 5'-CTAGGGGCTCTTCTCGTCCT-3' | 5'-CAACTTCTGCCTTTGGCTTC-3' |
| ***CDH1*** | 5'- GATTCTGCTGCTCTTGCT-3' | 5'-GTCAAAGTCCTGGTCCTC-3' |
| ***VIM*** | 5'-ACATTGAGATTGCCACCT-3' | 5'- TCCAGATTAGTTTCCCTCAAG -3' |
| ***SIP1*** | 5'-TCATATCGGCTTGTGGAAT-3' | 5'-TCTGTGGCTCAATACGTTT-3' |
| ***PEN2*** | 5'-TTCCTTGTCCCAGCCTACAC-3' | 5'-CAGGGGTATGGTGAAGGAGA-3' |
| ***SNAI1*** | 5'-CCTAGCGAGTGGTTCTTC-3' | 5'-CTGGAAGGTAAACTCTGGATT-3' |
| ***TWIST*** | 5'- CGGAGACCTAGATGTCATTG-3' | 5'- ACGCCCTGTTTGTTTGAAT-3' |
| ***SPRY1*** | 5'-ATGGATCCCCAAAATCAACA-3' | 5'-CGAGGAGCAGGTCTTTTCAC-3' |
| ***CDH2*** | 5'-GACAATGCCCCTCAAGTGTT-3' | 5'-CCATTAAGCCGAGTGATGGT-3' |
| ***SPANXB2*** | 5'-AATGAGGCCAACAAGACGAT-3' | 5'-TCGGGGTTGATTCTGTTCTC-3' |
| ***HES1*** | 5'- CACAGAAAGTCATCAAAGCC-3' | 5'- CAGAATGTCCGCCTTCTC-3' |
| ***CST4*** | 5'-ACTTGGACACCTGTGCCTTC-3' | 5'-CCACATGCACACCTAAATGC-3' |
| ***CTGF*** | 5'-GGAAAAGATTCCCACCCAAT-3' | 5'-TGCTCCTAAAGCCACACCTT-3' |
| ***COL14A1*** | 5'- CACGACCACCAACTTTTCCT -3' | 5'- GCAACTTGGGTTCCATCTGT -3' |
| ***ITGA4*** | 5'- GAGTGCAATGCAGACCTTGA -3' | 5'-TGGATTTGGCTCTGGAAAAC-3' |
| ***ITGB2*** | 5'- CAAGCTGGCTGAAAACAACA -3' | 5'- ATTGCTGCAGAAGGAGTCGT -3' |

## 2.7. Cell lysis for protein extraction

Cells were lysed in NP40 lysis buffer. Lysates were incubated on ice for 20 min and vortexed every 2-3 min to facilitate lysis. Lysates were cleared of insoluble material by centrifugation at 15,000 *g* for 15 min at 4 °C, and protein concentrations were determined.

*NP40 lysis buffer*: 50 mM Tris-HCl, pH 8.0, 150 mM NaCl, 10% glycerol, 0.5% NP40, 5 mM DTT, 1 mM EDTA, 1 mM EGTA, 50 µM leupeptin, 30 µg/ml aprotinin.

### 2.7.1. Total protein measurement

Total protein concentration in each sample was determined by the Bradford (Bio-Rad Protein Assay, Bio-Rad Laboratories) assay procedure. Briefly, 160 µl of appropriately diluted bovine serum albumin standards and samples were placed in wells of a microtiter plate and 40 µl of dye reagent concentrate added to each well. After mixing and incubation for at least 5 min at room temperature (RT), the absorbance was measured at 595 nm.

### 2.7.2. Sodium dodecyl sulphate polyacrylamide gel electrophoresis (SDS-PAGE)

Samples were denatured in sample buffer containing sodium dodecyl sulfate (SDS). After heating the samples at 95 ºC for 5 min, samples (20 µg protein) were loaded onto SDS-polyacrylamide gels (8-12%). Electrophoresis was performed at 80 V for 90 min using the appropriate running buffer.

*SDS running buffer*: 25 mM Tris-HCl, 200 mM glycin, 0.1% SDS
*SDS stacking gel*: 0.1% SDS, 4% acrylamide, 130 mM Tris HCl pH 6.8, 0.09% APS, 0.12% TEMED
*SDS running gel*: 0.1% SDS, 12.5% acrylamide, 130 mM Tris HCl pH 8.8, 0.09% APS, 0.12% TEMED
*SDS sample buffer*: 130 mM Tris-HCl pH 6.8, 10% β-mercaptoethanol, 20% glycerin, 4.6% SDS, 0.2% bromphenol blue was used to prepare loading samples.

### 2.7.3. Western blotting

After separation on SDS-polyacrylamide gels, proteins were transferred onto a PVDF membrane (Hybond C super, Amersham Biosciences) using a wet-blot chamber (Mini Trans blot chamber, Biorad). Unspecific bindings were blocked by incubating the membrane in blocking solution for 1 h at RT. The membranes were then probed with the primary antibodies (diluted in blocking solution) and incubated for 12 h at 4 °C. Next, the membranes were washed 3 times for 10 min and incubated with the secondary antibodies (conjugated with horseradish peroxidase) for 1 h at RT, followed by 3 washing steps as previously described. Immunocomplexes were detected by chemiluminescence detection (GE, Healthcare), by mixing equal volumes of ECL solution A and B and incubating the membrane for 5 min. The intensity of bands was quantified using Image J software (NIH, Bethesda, MD).

*Blocking solution*: 5% milk powder in 0.05% Tween-20 in PBS

*Washing buffer*: 0.05% Tween-20 in PBS

*ECL solution A*: 2.5 mM luminol, 0.4 mM paracumaric acid, 100 mM Tris-HCl pH 8.5

*ECL solution B*: 5.4 mM $H_2O_2$, 100 mM Tris-HCl pH 8.5

## 2.8. Cell Proliferation assay (Sulphorhodamine B, SRB)

The sulphorhodamine B (SRB) assay was used to monitor the effects of various treatment conditions on cell proliferation. The assay relies on the ability of SRB to bind to protein components of cells that have been fixed to tissue culture plates by trichloroacetic acid (TCA). SRB is a bright pink aminoxanthene dye with two sulphonic groups that bind to basic amino-acid residues under mild acidic conditions, and dissociate under basic conditions. As the binding of SRB is stoichiometric, the amount of dye extracted from stained cells is directly proportional to the cell mass. To determine the effect of different treatment modalities on cell number over time, SRB assays were performed as described. Cells were seeded in flat-bottomed 96-well plates ($3x10^3$ cells/well). The cells were allowed to adhere overnight, and then media containing treatment was added. One plate was assayed at this time point (Day 0) and further plates were assayed at 1 or 2-day intervals. The cells were fixed by

adding 100 µl per well of ice-cold 40% TCA to each well for 60 min. The plates were washed five times in running tap water and stained with 100 µl per well of the SRB reagent (0.4% w/v SRB in 1% acetic acid) for 30 min. The plates were washed five times in 1% acetic acid and allowed to dry overnight. SRB was solubilised with 100 µl per well 10 mM Tris-base, shaken for 30 min and the optical density was measured at 492 nm.

## 2.9. Gamma-secretase activity assay

GS activity was measured using the Gamma-secretase Activity Kit (R&D Systems, FP-003) following the manufacturer's instructions. Briefly, cells were transfected with control or nicastrin siRNA, or the GSI1, and harvested after 72 h in cell extraction buffer followed by incubation on ice for 10 min. Lysates were centrifuged at 10,000 x *g* for 1 min and supernatants were collected with a total protein yield of 0.5–1.0 mg/ml. Pierce BCA Protein Assay was used to determine protein concentration. Protein (200 µg) was incubated with the GS fluorogenic substrate for 1 h at 37 °C and fluorescence was measured at 355/460 nm.

## 2.10. Cell migration and invasion

Cells ($1 \times 10^4$) were plated on glass bottomed 24-well plates and imaged by digital recording at a time-lapse interval of 10 min for 16 h in an environmentally controlled ImageXpress Micro microscope (Molecular Devices, UK). The average speed of cell migration (mean ± s.e.m.; n > 100 cells) was determined (357). Cell invasion assays were performed using Matrigel-coated polycarbonate transwell filters (8 µm pore size) (Beckton Dickinson). 70 µl Matrigel (diluted 1:1 in α-MEM) was added to the upper chamber and allowed to polymerise for 1 h at 37°C. Keratinocyte growth medium consisted of α-MEM supplemented with 10% FCS, 100 IU/ml penicillin, 100 µg/ml streptomycin, 250 ng/ml amphotericin B (Gibco), $1.8 \times 10^{-4}$ M adenine, 5µg/ml insulin, 0.5µg/ml hydrocortisone, 10 ng/ml EGF, and $1 \times 10^{-10}$ M cholera toxin. 500 µl of this medium was placed in the lower chamber to act as a chemoattractant.

Cells were plated in the upper chamber of triplicate or quadruplicate wells per treatment condition, at a density of $5 \times 10^4$ in 200 µl of α-MEM and incubated at 37 °C for 72 h. Cells in the lower chamber (including those attached to the under surface of the membrane) were trypsinised and counted using a Casy 1 counter (Sharfe System GmbH, Germany). Mean and standard error of the mean (SEM) of independent experiments were calculated. Statistical analysis was performed using a two-tailed Student's *t*-test to determine the statistical significance of the differences observed. A *p*-value below 0.05 was considered significant.

## 2.11. Immunofluorescent staining and confocal microscopy

Immunostaining and confocal imaging were carried out as previously described (358). $1 \times 10^4$ cells were seeded on 13 mm diameter glass cover slips, fixed in 4% w/v paraformaldehyde at 37 °C and incubated in immunofluorescent blocking buffer (2% v/v FCS and 1% BSA) followed by incubation with 1/100 nicastrin pAb, 1/100 E-cadherin, or 1/100 p120 catenin antibodies. Incubation with 1/1,000 anti-rabbit or anti-mouse-IgG Alexa Fluor®-488 or -555 or phalloidin Alexa Fluor®-633 (Molecular Probes, UK). Nuclear counterstaining was carried out using TO-PRO-3 and coverslips were mounted using Vectashield H-1200 (Vector Laboratories). Images were captured using a Zeiss LSM 410 confocal microscope (63× lens; 1.40 NA oil; Leica) using Immersol 518F oil (Zeiss). Image composites of ~20 × 0.5 µm *z*-stacks were obtained using Axiovision LE software (Zeiss). Photoshop 8.0 (Adobe Software) was used for post-acquisition editing of images.

## 2.12. Fluorescence Activated Cell Sorter (FACS) analysis

### 2.12.1. Cell cycle analysis

For flow cytometry analysis approximately $1 \times 10^6$ adherent cells (treated with control siRNA, nicastrin siRNA, Rabbit IgG Isotype control, anti-NCT PcAb) were washed with ice-cold PBS and lysed as per CycleTEST Plus DNA Reagent Kit protocol. Analysis was performed on a FACS LSR II flow cytometer using the CELLQuestPro software 3.0 (Becton-Dickinson, Belgium), counting 10,000 events per experiment. Detection of DNA fragmentation with done with PI as fluorescent indicator.

### 2.12.2. FACS analysis using fluorescein isothiocyanate (FITC)-conjugated antibodies

MDA-MB-231 cells and MCF-7 cells were used to investigate the capacity of the developed anti-nicastrin polyclonal and monoclonal antibodies to bind endogenous, cell surface expressed nicastrin. Cells were cultured to 70-80% confluence and detached from the cell culture flasks using EDTA. Cell pellets were obtained and washed with cold PBS containing 0.1% BSA and 0.02 % sodium-azide ($NaN_3$). All further steps were performed on ice and all centrifugation steps at 4 ºC. Anti-nicastrin antibodies were added and incubated on an orbital shaker at 4 ºC for 1 h. Cells were washed three times in cold PBS + BSA+ $NaN_3$, and the secondary, species specific anti-rabbit (rat) IgG-FITC-conjugated Abs were added at 1:100 dilution for 45 min, and incubated on the orbital shaker in the dark. Cells were then washed twice in PBS+BSA+NaN3 and finally resuspended in 400 µl of PBS. Immunofluorescent staining acquisition and analysis of 10,000 gated, live cells was done using FACSCanto II (Becton-Dickinson, Belgium) and FlowJo software, Version 7.1 (Tree Star, Inc., Ashland, OR, USA).

## 2.13. Affymetrix gene array performance and analysis

MDA-MB-231 cells were transfected with nicastrin siRNA (40 nm final concentration) for the period of 72 h. GFP siRNA was used as a negative control. Cells were harvested and processed for mRNA extraction. Nicastrin knockdown was confirmed by RT-qPCT (> 90%) and mRNA was sent for gene expression analysis. The gene arrays were done on an Affymetrix 2.0 platform by the Northwestern University Genomics Core Facility in Chicago, IL, USA. Each sample was run in biological duplicates. Data analysis was performed by the bioinformatics group at Northwestern University and revised by Dr. Chindo Hicks, Director of Cancer Bioinformatics, University of Mississippi Cancer Institute.

## 2.14. RT² Profiler™ PCR Array: Extracellular Matrix and Adhesion

The PCR Array PAHS-013 (Qiagen) consisted of a set of optimised real-time PCR primers on a 96-well plate. The array included built-in positive control elements for: i) proper data normalisation, ii) detection of genomic DNA contaminations; iii) quality of the mRNA samples. HCC1806-Luc1 and HCC1806-NCTsh cells were cultured and 1 x $10^6$ cells were

lysed using the RNAlater (Qiagen), and mRNA was prepared as previously described. cDNA was made using the RT² First Strand Kit (Qiagen). RT² qPCR SYBR Green/ROX Master Mix was used in the reactions according to the manufacturer's protocol. The PCR Array Data Analysis Portal automatically performed the calculations and interpretation of the control wells including thresh-hold cycle data from the real-time instrument. The RT² Profiler PCR Array Data Analysis Template v3.3 software was used. Calculations were based on the $\Delta\Delta C_t$ fold-change. Genes of interest were validated by RT-qPCR.

Genes incorporated on the array were:

**Cell Adhesion Molecules:**

Transmembrane Molecules: CD44, CDH1, HAS1, ICAM1, ITGA1, ITGA2, ITGA3, ITGA4, ITGA5, ITGA6, ITGA7, ITGA8, ITGAL, ITGAM, ITGAV, ITGB1, ITGB2, ITGB3, ITGB4, ITGB5, MMP14, MMP15, MMP16, NCAM1, PECAM1, SELE, SELL, SELP, SGCE, SPG7, VCAM1.

Cell-Cell Adhesion: CD44, CDH1, COL11A1, COL14A1, COL6A2, CTNND1, ICAM1, ITGA8, VCAM1.

Cell-Matrix Adhesion: ADAMTS13, CD44, ITGA1, ITGA2, ITGA3, ITGA4, ITGA5, ITGA6, ITGA7, ITGA8, ITGAL, ITGAM, ITGAV, ITGB1, ITGB2, ITGB3, ITGB4, ITGB5, SGCE, SPP1, THBS3.

Other Adhesion Molecules: CNTN1, COL12A1, COL15A1, COL16A1, COL5A1, COL6A1, COL7A1, COL8A1, VCAN, CTGF, CTNNA1, CTNNB1, CTNND2, FN1, KAL1, LAMA1, LAMA2, LAMA3, LAMB1, LAMB3, LAMC1, THBS1, THBS2, CLEC3B, TNC, VTN.

**Extracellular Matrix Proteins:**

Basement Membrane Constituents: COL4A2, COL7A1, LAMA1, LAMA2, LAMA3, LAMB1, LAMB3, LAMC1, SPARC.

Collagens & ECM Structural Constituents: COL11A1, COL12A1, COL14A1, COL15A1, COL16A1, COL1A1, COL4A2, COL5A1, COL6A1, COL6A2, COL7A1, COL8A1, FN1, KAL1.

ECM Proteases: ADAMTS1, ADAMTS13, ADAMTS8, MMP1, MMP10, MMP11, MMP12, MMP13, MMP14, MMP15, MMP16, MMP2, MMP3, MMP7, MMP8, MMP9, SPG7, TIMP1.

ECM Protease Inhibitors: COL7A1, KAL1, THBS1, TIMP1, TIMP2, TIMP3.

Other ECM Molecules: VCAN, ECM1, HAS1, SPP1, TGFBI, THBS2, THBS3, CLEC3B, TNC, VTN

## 2.15. Panorama® Antibody Microarray - XPRESS Profiler725 Kit

The Panorama® Antibody Microarray - XPRESS Profiler725 Kit, a proteomics tool that measures the relative level of protein expression (protein microarrays) in cell or tissue extracts was used for comparing protein expression profile between two samples (reference samples vs. test). The Panorama Antibody Microarray-XPRESS Profiler725 Kit contains 725 different antibodies, each spotted in duplicate on nitrocellulose-coated glass slides. These antibodies represent families of proteins known to be involved in a variety of different biological pathways. Each sample was labeled with a different Cy Dyes (Cy3 or Cy5) and the two paired samples were applied simultaneously at equal protein concentrations on the array. Fluorescent signal intensity for each sample was then recorded individually at the wavelength corresponding to the dye label of the sample and compared. Cy3 and Cy5 Monofunctional Reactive dyes were from (GE Healthcare). Two independent experiments were performed. One including MDA-MB-231 cells treated with NCT siRNA and control GFP siRNA, and the other using HCC1806-NCTsh and HSS1806-Luc1 cells. Control samples were labelled with the Cy3 and treated samples with the Cy5 dye, and the 2 samples were applied simultaneously on the array. Treated and control cells were washed twice with cold 0.01 M PBS, pH 7.4. 3 and 1 ml of Buffer A was added directly onto each plate and incubated for 5 min on ice. The plates were scraped using a rubber policeman and samples were collected into a microcentrifuge tube. Samples were centrifuged for 10 sec at 10,000 *g*. Supernatants were transferred to a new microcentrifuge tube and protein concentration was determined by the Bradford protein assay. Samples were diluted to 1 mg/ml in Buffer A and 1 ml of extract (1 mg/ml) was used for labeling with Cy3 or Cy5. Vials were mixed thoroughly and the reaction was incubated for 30 min at RT, mixing the solution every 10 min. Free Cy3/Cy5 from the labeled sample was removed using SigmaSpin columns. 150 µl of the labeled protein sample solution was applied directly onto the center of the SigmaSpin column and centrifuged for 4 min at 750 *g*. Before hybridisation, the dye-to-protein molar ratio was determined followes by the calculations supplied with the antibody microarray kit. Only samples with a dye-to-protein molar ratio >2 were applied to the antibody microarray as

recommended. Each of the Cy3 and Cy5 labeled samples (150 mg), at equal protein concentrations (30 mg/ml), were mixed with 5 ml of Array Incubation Buffer and slides were incubated for 30 min at RT on a rocking shaker at a moderate shaking frequency of ~30 rpm. Slides were then washed, dried and scanned at 532 nm and 635 nm excitation wave lengths, respectively (Molecular Devices Axon 4000B). The software used for data analysis was GenePix 6. Each array contained spots with a monoclonal antibodies specific for Cy3/Cy5, which served as positive control. Normalisation was done using the housekeeping protein β-actin. F635/F532 ratio was calculated according to the manufacturer's protocol, and values of interest were those with a Cy5/Cy3 ratio higher or lower than 2.

## 2.16. Mammosphere culture

HCC1806-Luc1 and HCC1806-NCTsh cells were plated as single cells in ultralow attachment plates (Corning) at a density of 5 x $10^3$ viable cells/well in a 6-well plate. Cells were grown in a DMEM:F12 (1:1) culture medium supplemented with 0.4% bovine serum albumine (BSA), 5 μg/ml insulin, 10 ng/ml basic FGF and 20 ng/ml EGF. Mammospheres were grown for 10-14 days and phase contrast images were obtained using the ImageXpress Micro microscope (Molecular Devices, UK). Cells were collected by gentle centrifugation (800 rpm) and processed for mRNA extraction (359).

## 2.17. CD44/CD24 Cell Sorting

HCC1806-Luc1 and HCC1806-NCTsh cells were grown to 70-80% confluence, washed once with PBS and harvested using 0.02% EDTA. Detached cells were washed and resuspended in PBS containing 1% FCS and 1% penicillin/streptomycin ($10^6$ cells/100 μl). Combinations of fluorochrome-conjugated monoclonal antibodies against human CD44-FITC and CD24-PE or their respective isotype controls were added to the cell suspension at concentrations recommended by the manufacturer and incubated at 4 °C in the dark for 40 min. The labeled cells were washed and fixed in PBS containing 1% paraformaldehyde, and then analysed on a FACSAria (BD Biosciences).

### 2.17.1. Overlay three-dimensional culture on Matrigel

Matrigel is considered as the basement membrane and is generated from EHS sarcoma cells. Matrigel contains not only basement membrane components (collagens, laminin, and proteoglycans), but also matrix degrading enzymes, their inhibitors and growth factors. Invasion of tumour cells into Matrigel has been used to characterise involvement of extracellular matrix receptors and matrix degrading enzymes which play roles in tumour progression (Figure 20).

Matrigel was thawed on ice overnight at 4 ºC. Matrigel (40 µl/well) was added into each of the wells of the eight-well glass slide chambers, and spread evenly in the well to form a 1 mm thick bed using the tip of a P-200 pipette tip while monitoring for air bubbles or overspread so no to form a high meniscus on the border. Matrigel was left to solidify at 37 ºC for 45 min. Then, cells (5 x $10^3$/well) were plated in medium containing 2% Matrigel and allowed to grow in a 5% CO2 humidified incubator at 37 ºC. The day that the assay was set up corresponds to Day 0; addition of treatment was every 2 days. The cells formed clusters by Day 10.

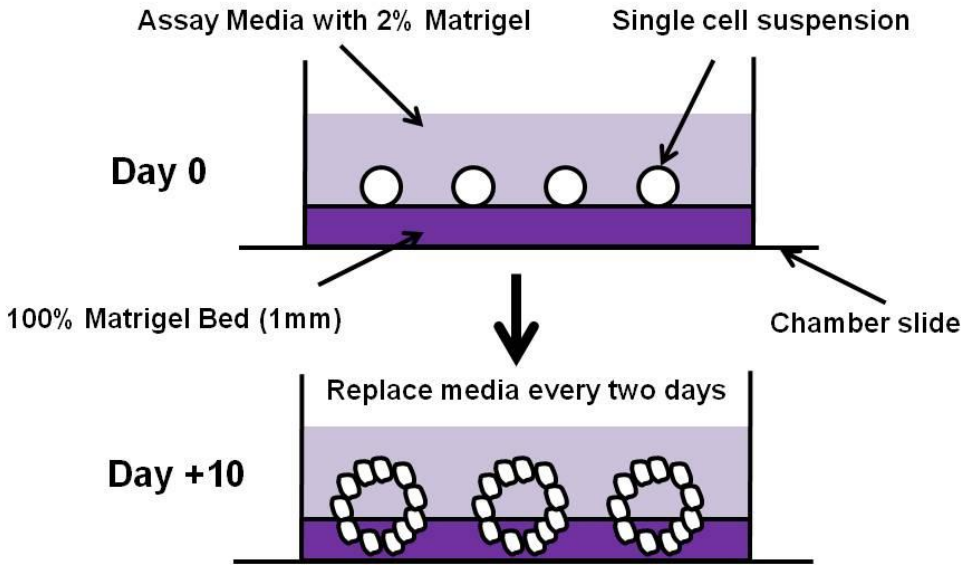


**Figure 20.Overlay method of 3D Matrigel cell culture**

### 2.17.2. Immunofluorescent staining of the 3D cultures

Media was aspirated from the chambers and cells were rinsed twice with ice-cold PBS. Cultures were fixed using 4% paraformaldehyde at RT for 20 min. Fixation was stopped by aspirating 4% paraformaldehyde, and cells were then washed three times with PBS. Blocking was done using 10% human-AB serum (Sigma-Aldrich), followed by 1 h incubation with the primary antibody. Cells were then washed three times with PBS and secondary antibody was added for 1 h. Staining was done at RT. Secondary antibody was removed and cells were washed three times with PBS. DAPI was dissolved in water to produce 20 mg/ml stock solution which was then added to the chamber wells at 1:5000 dilution for 5 min; washed three times with PBS and the chamber slide was mounted using VECTASHIELD Mounting Medium without DAPI (H-1000) (Vector Laboratories)**.**

### 2.17.3. Recovery of the cells from the Matrigel matrix

In order to recover cells cultured in 3D Matrigel, the culture media was removed and the cells in each chamber were washed 3 times with cold PBS. Dispase (Invitrogen) was used to disintegrate the cells from the Matrigel. Dispase was dissolved in PBS at the final concentration of 2 U/ml, and pre-warmed to 37 ºC. Dispase solution was added to the wells and incubated at 37 ºC for 30 min. Dispase solution containing the cells was pipetted out from the wells and the solution was centrifuged to obtain a cell pellet. Dispase solution supernatant was discarded. Cells were used to isolate mRNA and protein.

## 2.18. Purification of malignant epithelial cells from primary breast tumours

Fresh breast cancer tissue was obtained from the Department of Pathology, Charing Cross Hospital, London, UK. Required ethic approval was in place (RREC3386). The tissue was minced to small pieces and digested by incubation with Collagenase A (1 mg of Collagenase A in 1 ml of DMEM containing 5% FBS), at 37°C for 2-5 h on a shaking platform, to obtain a single-cell suspension. The digestion reaction was stopped by the addition of 10 ml of cold DMEM-5% FBS, and the preparation was then subjected to serial filtration steps using 50 μm-, 38 μm- and 28 μm- pore nylon meshes sequentially.

The filtered preparation was centrifuged at 1,200 *g* for 5 min at 4 °C, and the cell pallet was washed twice with PBS containing 2% FBS. Epithelial cells were immunoaffinity purified using super-paramagnetic, polystyrene beads (Dynal Ltd, New Ferry, Wirral, UK) coated with an epithelial membrane antigen (EMA) antibody (marker of epithelial cells), on a rotating platform for 1 h at 4 °C. After the incubation, epithelial cells bound to the magnetic beads were separated by placing the cell preparation on a magnetic holder for 5 min. Cells pallets were obtained and processed for mRNA or protein extraction.

## 2.19. Clinical specimens and tissue microarrays

Archival formalin-fixed, paraffin-embedded (FFPE) blocks of normal breast tissue from reduction mammoplasty, fibroadenoma and paired primary breast tumour and metastatic lymph node samples were obtained from the Pathology Department, Charing Cross Hospital, London. No patient identifiers were used. For the purpose of analysing Nicastrin expression in other normal tissue, the TMA (BN-481) was obtained from US Biomax. Images were taken on the Chromavision Automated Cellular Imaging System II.

Primary operable breast cancer cases from the previously validated Nottingham Tenovus Primary Breast Carcinoma Series were employed with the ethics approval (REC202313). A 13-slide series breast cancer TMA (n = 1050 cases) comprising 4 μm thick formalin fixed paraffin embedded tissue cores was immunostained for nicastrin expression. The cohort comprised women aged up to 70 years, who presented between 1986 and 1999. This well-characterised resource contains information on patients' clinical and pathological data including histological tumour type, primary tumour size, lymph node status, histological grade and data on other breast cancer relevant biomarkers. These include ERα, PR, HER2, cytokeratins (CKs: 5/6, 7/8, 18), Ki67 and E-cadherin. Patients within the good prognosis group (Nottingham Prognostic Index (NPI) ≤ 3.4) did not receive adjuvant therapy. Hormonal therapy was prescribed to patients with ERα positive tumours and NPI scores > 3.4 (moderate and poor prognostic groups). Pre-menopausal patients within the moderate and poor prognosis groups were candidates for chemotherapy. Conversely, postmenopausal patients with moderate or poor NPI and ERα positive were offered hormonal therapy, while ERα negative patients received chemotherapy. Data collected are presented here in line with the REMARK criteria (360). Clinical data were maintained on a prospective basis with a median follow-up of 124 months (range 1 to 233).

Anti-nicastrin Ab (N-1660, Sigma) was optimised to a working concentration of 2 μg/ml on full-faced excisional breast cancer tissue sections, and further used for all the tissue samples. The anti-nicastrin pAb was incubated for 3 h at room temperature without antigen retrieval. Secondary labelling using indirect streptavidin-avidin-biotin was performed followed by detection with diaminobenzidine chromogen. Negative controls were performed by omission of the primary antibody. Immunostained sections were counterstained with hematoxilin. Nicastrin immunoreactivity was detected in the cytoplasm and cell membrane and was scored based on staining intensity ranging from 0 to +3; 0 = null, +1 = low, +2 = intermediate and +3 = high level of staining intensity. All cases were scored without prior knowledge of the clinic-pathological or outcome data. Images from the breast cancer TMAs were analysed using the high resolution digital imaging (NanoZomer, Hamamatsu Photonics, Welwyn Garden City, UK) at 20x magnification with a web-based interface (Distiller, SlidePath Ltd., Dublin, Ireland). Standard cut-offs were used for established prognostic factors: ERα, PR and cytokeratins 5/6, 7/8 and 18, positive if ≥ 10%; E-cadherin positive if H-score ≥45. Cut-off values for different biomarkers included in the study were chosen before statistical analysis.

### 2.19.1. Statistical analysis of patient samples

Statistical analysis for TMAs was performed using SPSS 16.0 statistical software (SPSS Inc., Chicago, IL, USA). Analysis of categorical variables was performed with the appropriate statistical test. Survival curves were analysed using the Kaplan-Meier method with significance determined by the Log rank test; multivariate analysis was performed by Cox hazards regression analyses. Overall survival (OS) was defined as the time from the date of the primary surgical treatment to the time of death from breast cancer, death being scored as an event, and patients who died as a result of other causes or were still alive were excluded at the time of last follow-up.

### 2.19.2. Statistical analysis of other experiments

Standard deviation (SD), mean and standard error of the mean (SEM) of independent experiments were calculated for proliferation assays, cell migration and invasion assayas as well as RT-qPCR analysis. The applied statistical method, as well as number of independent

experiments is outlined in the figure legends. Statistical analysis was performed using a two-tailed Student's *t*-test to determine the statistical significance of the differences observed. A *p*-value below 0.05 was considered significant.

## 2.20. Polyclonal Antibody Production (Biogenes, GE)

RNA from a breast cancer cell line (MDA-MB-231) was reverse transcribed using randon hexamers (Dr Dongmin Shao, Imperial College, London).

5'-GGATCCGAAGCCTATAAATACAACTGGGA-3' and

5'- GCGGCCGCTCACTGAACTGTGTCGCTGAAGTTG-3,

The above primers were used to amplify a DNA fragment corresponding to the nicastrin 261-512 a.a. domain using the LongRange PCR kit (Qiagen), ligated to pET-duet (Novagen), which introduces a His-tag in the recombinant protein, and transformed into Rosetta *E. coli* cells. His-tagged protein was isolated using denaturing conditions (soluble protein conditions: 100 mM Na phosphate, 10 mM Tris, 8 M urea pH 8.0 with protease inhibitors; inclusion body conditions: extraction with 20 mM Tris; pH 8.0; 150 mM NaCl; 1% NP40; 1 mg/ml lysozyme; 0.01% v/v protease inhibitors), purified on a nickel column and eluted (20 mM Tris; 300 mM imidazole; 300 mM NaCl, pH 8.0). Protein was dialysed in PBS and the precipitate collected and resuspended in PBS (1 mg/ml). Protein (4 ml) was dialysed against 500 ml of PBS overnight. Precipitate was collected and washed 3 times with 3 ml of PBS. Protein in PBS was then measured by UV. The net weight protein in the pellet (8.1 mg) was resuspended in 8 ml PBS. Purity of the recombinant NCT protein (261-502 a.a.) that was used as an immunogen was 90-95% and concentration 0.5-1 mg/ml.

The immunisation protocol was:

Day 1: 1st immunisation/ collection of pre-immune serum
Day 7: 2nd immunisation
Day 14: 3rd immunisation
Day 28: bleeding/ boost
Day 35: final bleeding (20 ml/animal)

Animals were intramuscularly immunised using BioGenes' proprietary adjuvant. The adjuvant was mixed 2:1 with the provided antigen. Monospecific antibody purification was carried out from the bleeding preparations. Nicastrin protein used for immunisation was also used to prepare the antigen column (CNBr-Sepharose), for affinity purification of the bleedings. The purified antibodies were dialysed against PBS, sterile-filtered and provided without preservatives.

## 2.21. Monoclonal antibody production and purification (Genovac, GE)

A DNA fragment corresponding to nicastrin amino acids 34-669 a.a. was generated as in Section 2.20. using the following primers (Dr Dongmin Shao, Imperial College London):

5'-GCTAGCATGGCTACGGCAGGGGGTGGC-3' and

5'-GCGGCCGCTCAGTATGACACAGCTCCTGGC-3'.

Amplified DNA was cloned into pIRES-neo2 (Clontech) and sent to Genovac. Antibodies were raised by genetic immunisation of WISTAR rats using a cDNA, encoding for the extracellular domain of nicastrin (34-669 a.a). This cDNA was cloned into proprietary GENOVAC expression vectors specially developed to maximise an immune response in mammals and to allow screening of the resulting immune sera. The immunisation constructs were introduced into the animals using a Genegun. Following several DNA boosts test sera were taken from the animal and tested for the presence of antibodies in a transient transfection assay in flow cytometry against the corresponding GENOVAC screening vector. Once an immune response had been identified, lymphocytes were removed for further processing (fusion with mouse myeloma cell line, screening, subcloning by limited dilution). Monoclonal antibodies were purified by Protein G affinity chromatography from cell culture supernatant after cultivation in serum free medium (ISF-1 from Biochrom).

### 2.21.1. Monoclonal antibody sequencing

Hybridoma cells from the 1E2, 2H6, 10C5 and 10C11 clones were cultured and 1 x $10^7$ cells/clone were harvested. Cells were lysed for mRNA extraction which was conducted using the Qiacube, Qiagen, UK. RNA (1 μg) was reverse transcribed using the First Strand

cDNA Synthesis Kit (Roche), to yield 20 µl of the final volume. 5 µl of cDNA/clone was used in the PCR reactions. Kappa light chain DNA was isolated by the polymerase chain reaction (PCR) using primers that hybridise to the 5' end of the kappa chain constant domain and the framework 1 region of the r chain variable domain. The 3' heavy chain variable region DNA was isolated using primers that hybridize to the framework 1 region of the heavy chain variable domain and to the amino-terminal portion of the y chain constant 1 domain (361).

| **Priming region** | **Name** | **Sequence** |
|---|---|---|
| K chain variable domain | Bi6 | 5'-GGTGATATCGTGAT( A/G)AC(C/A)CA( G/A)GATGAACTCTC |
| a.a. 1-10 | Bi7 | 5'-GGTGATATC(A/T)TG(A/C)TGACCCAA(A/T)CTCCACTCTC |
| | Bi8 | 5'-GGTGATATCGT(G/T)CTCAC(C/T)CA(A/G)TCTCCAGCAAT |
| K chain constant domains | Bi5 | 5'-GGGAAGATGGATCCAGTTGGTGCAGCATCAGC |
| a.a. 116-109 | Bi5b | 5'-C'I'C'I'AGATTAATGATGATGGTGATGGGATCCACq~I'GGTGCAGCAACAGC |
| Heavy chain variable domain | Bi3 | 5'-GAGGTGAAGCTGCAGGAGTCAG GACCTAGCCTGGTG |
| a.a. 1-8 | Bi3b | 5'-AGGT(C/GXA/C)AACTGCAG(C/G)AGTC(A/T)GG |
| | Bi3c | 5'-AGGT(C/GXA/C)AGCTGCAG(C/G)AGTC(A/T)GG |
| 3'chain constant domain | Bi3d | 5'-AGGT(C/G)CAGCTGCAG(C/G)AGTC(A/T)GG |
| a.a. 127-15 | Bi4 | 5'-CCAGGGGCCAGTGGATAGACAAG C'I'I'G G GTGTCG'VITI" |

Each primer (10 pmol) and 2.5 µg of cDNA were used in a 100 µl reaction mix containing 250 M of each dNTP, 10 mM Trisaminomethane/ HCl, pH 8.3, 2.5 mM $MgCl_2$, 50 mM KCI, 0.01% gelatine and 1.25 U *taq* DNA polymerase. 35 cycles of 1 min at 94 °C, 2 min at 52 °C and 2 min at 72 °C were carried on the Veriti Thermal Cycler, Applied Biosystem. The PCR reaction (10 µl) was run on a 1.2% agarose gel. Band at 350 kb indicated the amplified variable region. The TA cloning kit (Invitrogen) was then used to perform the ligation. Ligation was performed in a 10 µl volume containing 1 µl fresh PCR reaction, T4 DNA ligase. The reaction was performed over-night at 14 °C. LB-agar plates with 100 µg/ml Ampicilin were allowed to set and dry at 37 °C. X-gal (5-bromo-4-chloro-3-indolyl-b-D-galactopyranoside) was dissolved in dimethlylformamide (DMF) to a final concentration of 40 mg/ml. X-gal (40 µl/plate) was spread on LB/Amp plates and allowed to dry for 30 min at 37 °C the following day and prior to seeding the competent cells. Transformation of TA competent cells, INVαF´, with the ligated DNA was performed as follows. INVαF´ cells were thawed on ice and 2 µl of the ligated reaction was added and allowed to incubate for 30 min on ice. The cells were heat shocked by transferring the tubes into a preheated thermo-mixer (42 °C) for 45 sec. The tubes were then immediately placed back into ice. S.O.C medium (250 µl) was added to each tube and then transferred to a shaking incubator, set at 37 °C, for 1 hour in order to allow the bacterial cell growth. Finally,

200 µl of each reaction was plated onto agar plates (1.5% Bacto-Agar in LB medium) containing 100 µg/ml Ampicillin and X-gal. The plates were incubated at 37 °C overnight. *LB medium*: 1% Bacto tryptone, 0.5% Bacto yeast extract, 20 mM NaCl. The next day, six white colonies were picked per each condition and grown overnight in LB media supplemented by 100 µg/ml Ampicilin at 37°C. Mini-preps (Qiagen) were performed and cDNA quantified. Presence of an appropriate insert was assessed by digesting the DNA with *Eco*RI enzyme for 2 h at 37 °C.

### 2.21.2. Restriction endonuclease analysis of DNA

The recombinant plasmids were cut with the use of specific endonucleases. The reaction was performed in 20 µl containing 500 ng plasmid DNA, 1 x buffer (specific for each endonuclease), 100 µg/ml BSA and 5 units of restriction enzyme. The reaction was incubated at 37 °C for 3 h.

*EcoRI buffer*: 100 mM Tris-HCl pH 7.4, 10 mM $MgCl_2$, 50 mM NaCl, 0.025% Triton-X 100

### 2.21.3. Principle of blue/white selection of positive recombinant colonies

The pCR21 plasmid that contains bacterial *lac*Z gene can produce β-galactosidase (β-gal) if its open reading frame isn't interrupted by insert DNA. β-galactosidase can turn X-gal into a blue colour product. When a foreign DNA is inserted into the multiple cloning site within the *lac*Z gene, the open reading frame of *lac*Z is changed and will not produce β-galactosidase, therefore the recombinant colony of interest will be in white colour.

### 2.21.4. Agarose gel electrophoresis

The DNA products from the PCR reactions and from restriction-enzyme digestions were separated on a 1.5% agarose gel (1.5 g agarose in 100 ml of 1x TE buffer). Ethidium bromide 1 µl was added to the solution. Samples were loaded with 10% of DNA loading buffer. Along with the samples a DNA marker (1 Kb ladder) was also loaded in order to estimate the size of the DNA products. The electrophoresis was carried out at 80 V for 45 min. The current was derived from a controlled power supply (Biorad, Model 200/2). Detection of DNA was performed under UV light (254 nm) and pictures of the gels were

taken using a fluorescent gel imager). The PCR products were sequenced by GATC-Biotech AG, Konstanz, Germany.

*TAE buffer*: 1 mM EDTA, 40 mM Tris-acetate pH 8.0

*DNA loading buffer*: 50 % glycerin, 0.05% bromophenol blue

Sequences of M13 forward and M13 reverse primers:

M13 Forward primer sequence*:* 5' GTAAAACGACGGCCAG 3'
M13 Reverse primer sequence: 5' CAGGAAACAGCTATGAC 3'

### 2.21.5. Fab fragment preparation

Fab fragments were purified from whole IgG2b molecules (1E2, 2H6, 10C5 and 10C11), using papain digestion (Fab preparation kit, Pierce) according to manufacturer's protocol. This kit uses papain, a nonspecific thiol-endopeptidase, immobilised on an agarose resin. Whole IgG2b (1 μg/clone) was incubated with the immobilised papain resin for 4 h at 37 °C on a tabletop shaker, producing Fab and Fc antibody fragments. Fab fragments were bound to protein A column and purified using PBS. Concentration of purified Fab fragments was determined using nanodrop spectrophotometer at 280 nm wavelength (mass extinction coefficient value of 1.4). For typical antibody solutions: Absorbance $(A)_{280\ nm}^{1\ mg/ml} = 1.4$. (www.piercenet.com/files/TR0006-Extinction-coefficients).

### 2.21.6. Protein Gel Interpretation and Coomassie staining

The separation of Fab from the Fc fragment was analysed by reducing SDS-PAGE. After electrophoresis, gels were stained for 10 min in Coomassie-blue staining solution, and then destained for 20 min in Coomassie destaining solution.

*Coomassie-blue staining solution*: 1.2 g Coomassie Brilliant blue, 450 ml methanol, 90 ml acetic acid, 450 ml $H_2O$

*Coomassie destaining solution*: 10% isopropanol, 10% methanol, 80% $H_2O$

Whole, undigested IgG2b molecules were used as negative controls for respective clones. Boiling the IgG2b digest before gel loading resulted in a reduced sample. Present Fab fragments migrated near 25 kDa, and Fc fragments migrated at ~30 kDa.

The presence of Fc at ~30 kDa confirmed digestion of IgG2b. Also, an additional band, which is likely the undigested IgG2b heavy chain, appeared at ~50 kDa.

### 2.21.7. Titration FACS and antibody $K_d$ determination

Cell-based FACS titration was performed using MDA-MB-231 cells. Non-permeablised cells were incubated with each IgG (1E2, 2H6, 10C5 and 10C11) as the primary antibody in two fold serial dilution (1 mM to 0.01 nM), followed by the secondary FITC-conjugated antibody. This allowed MAb binding the endogenous, native, cell surface nicastrin antigen and determination of a cell-based $K_d$. As well as being physiologically relevant, this helped to show whether the binding of the MAbs is monovalent or bivalent. Cells were analysed on the FACSCalibur, BD Bioscience. The mean fluorescent intensity was obtained by analysis the Results using WinMDI 2.8 program (Verity Software House, Inc., Topsham, ME, USA).

### 2.21.8.$K_d$ determinantion of full IgG and Fab fragments by ELISA

The binding of Fab fragments from all four clones as well as whole IgG2b molecules was measured directly by ELISA. Recombinant human nicastrin-Fc antigen was coated on 96-well microtiter plates (5 μg/ml). The purified antibodies (IgG2b and Fab) were used as the primary antibody with a two-fold serial titration (1 mM to 0.01 nM), followed by the secondary detecting antibodies and colorimetric POD substrate The dissociation constant ($K_d$) was determined by fitting the binding curve to a sigmoidal four parameter logistic curve and calculating the 50% binding concentration from the $X_o$ value (SigmaPlot software).

### 2.21.9. BIACore Surface plasmon resonance technology

BIAcore 3000 was used to determine the affinity of MAbs and Fabs. BIACore was also used to epitope-map the antibodies by determining which ones compete for binding. The preferred, direct immobilisation of NCT onto the chip, led to a non-binding protein. Therefore, each MAb was immobilised using NHS-EDC coupling on the surface of a separate BIAcore CM5 chip, followed by the flow of the human NCT-Fc antigen (1 μM). This resulted in formation of antigen-antibody binding. Next, each IgG chip was subjected to the flow all four Fabs (10 μM) for the purpose of deciphering the degree of competitive binding

between the antibodies. The rational behind this method is that if two MAbs bind the same or overlapping epitopes, addition of a Fab will compete off the pre-existing complexes on the chip. This is seen as a dissociation curve. Any additional increase in the binding curve will indicated the antibodies bind distinct, non-overlapping epitopes. All experiments were carried out on flow cell-2 (Fc2) and flow cell-1 (Fc1, blank chip) values were substratcted (Fc2-1 net binding).

#### *2.21.9.1. Production of the nicastrin extracellular domain Fc fusion protein (Fusion Antibodies, UK)*

HEK293 cells stably expressing human nicastrin extracellular domain Fc-fusion protein (hNECD-Fc) were generated by Dr Dongmin Shao (Imperial College) and supplied to Fusion Antibodies. Cells were adapted to serum free cultures in shaker flasks. A large scale 1 litre volume culture was seeded and grown for 12 days. hNECD-Fc was then purified via Protein A affinity chromatography. Final quality control was performed using SDS-PAGE, BCA and endotoxin detection. Cells were thawed at 37 °C and transferred to 12 ml of complete DMEM supplemented with 10% IgG serum, 1% non essential amino acids, 2 mM L-glutamine and 150 mg/ml Zeocin (all Invitrogen). Cells were incubated in a 75 $cm^2$ tissue culture flask at 37 °C until subconfluent before passage by trypsinisation. Following two passages in complete DMEM adaption of cells to growth in serum free medium (Ex Cell 293 serum free medium (Sigma), supplemented 150 g/ml Zeocin (Invitrogen)) was commenced. Once cells were considered adapted to serum free culture cells were seeded in one litre of Ex Cell 293 medium at a concentration of 5 x $10^5$ cells/ml in disposable Erlenmeyer shake flasks (Corning Inc, MA, USA) shaking at 130 rpm, 37 °C, 8% $CO_2$. A sandwich ELISA to detect the presence of human IgG Fc in the culture supernatants was performed. The Fc fusion protein was then purified from medium supernatant using an Amersham Biosciences AKTA Chromatography system (AKTA Prime). Purification method was affinity using a 1ml protein A column. The fractions were analysed by a Bradford. Only the positive samples were combined and dialysed against PBS. After overnight dialysis, the purity of the final product was checked by SDS-PAGE analysis. Final quantification was performed using BCA. Purified hNECD-Fc (1.45 ml) was produced. According to the BCA, it corresponded to a total of 1.546 mg of the Fc fusion protein.

| Purity | Concentration | Volume | Quantity | Endotoxin Level | Final Buffer |
|---|---|---|---|---|---|
| >90% | 1.066 mg/ml | 1.45 ml | 1.546 mg | 1.35E U/mg | PBS |

### 2.21.10. Small scale preparations of plasmid DNA (Miniprep)

A single bacterial colony was picked up and inoculated in 5 ml of LB medium containing 50 µg/ml ampicillin in sterile 15 ml tube. Then the tubes were incubated at 37 °C while shaking (200 rpm) overnight. 2 ml of the overnight culture was transferred into a new tube and centrifuged at 5,000 rpm for 5 min. The pellet was then resuspended by vortexing in 200 µl of resuspension solution. Subsequently, 200 µl of lysis solution (0.2 M NaOH, 1% SDS) was added. The solution was mixed by gently inverting the tube. Neutralisation solution (3M potassium acetate pH 5.5) (200 µl) was added and mixed again by inverting the tube several times, incubated at 4 °C for 10 min and then centrifuged at 14,000 rpm for 10 min. The supernatant (cleared lysates containing plasmid DNA) was carefully transferred to a new tube and the DNA was precipitated by 700 µl of isopropanol. After centrifugation at 14,000 rpm for 10 min, the supernatant was aspirated and the pellet was washed with 100 µl of 70% ethanol. After a final centrifugation at 14,000 rpm for 5 min, the pellet was dried and eluted into 30 µl of $H_2O$.

*Resuspension solution*: 50 mM Tris-HCl pH 8.0, 10 mM EDTA, 100 µg/ml RNase A

## 2.22. Large scale preparations of plasmid DNA (Maxiprep)

*E. coli* bearing the control pCMV6-XL4 and the full length human nicastrin cloned into the pCMV6-XL4 vector (Origene) were cultured in LB for 18 h at 37 ºC with shaking. The cultures were centrifuged at 6,000 rpm for 15 min at 4 °C in Sorvall® GSA centrifuge. All traces of supernatant were removed by inverting the open centrifuge tube until all medium had been drained. Bacterial pellet was resuspended in 10 ml Buffer P1 and pipetted up and down until no cell clumps remained. 10 ml of buffer P2 was added, mixed thoroughly by inverting 4-6 times, and incubated at RT for 5 min. 10 ml of chilled buffer P3 was added, mixed by inverting 4-6 times, incubated on ice for 15 min, and centrifuged at 13,000 rpm for 30 min at 4°C. Supernatant containing plasmid DNA was removed promptly. QIAGEN-tip 500 was equilibrated by applying 10 ml buffer QBT, and columns were allowed to empty by gravity flow. The supernatant was applied to the QIAGEN-tip and allowed to enter the resin

by gravity flow. QIAGEN-tip was washed with 2 x 30 ml of the buffer QC. DNA was eluted with buffer QF. DNA was then precipitated by adding of 10.5 ml (0.7 volumes) RT isopropanol to the eluted DNA, mixed and centrifuged at 11,000 rpm for 30 min at 4 °C. Supernatant was decanted, DNA pellet washed with 5 ml of RT 70% ethanol, and centrifuge at 10,000 rpm for 10 min. Supernatant was decanted without disturbing the pellet. The pellet was air-dried for 5-10 min, and DNA re-dissolved in a suitable volume of TE buffer (pH 8.0, or 10 mM Tris-Cl, pH 8.5).

*Resuspension buffer P1*: 50 mM Tris-Cl, pH 8.0; 2–8°C, 10 mM EDTA; 100 μg/ml RNase

*Lysis buffer P2 :* 200 mM NaOH, 1% SDS

*Neutralisation buffer P3* : 3.0 M potassium acetate

*QIAfilter washing buffer FWB2* : 1 M potassium acetate

*Equilibration buffer QBT* :750 mM NaCl; 50 mM MOPS, pH 7.0; 15% isopropanol; 0.15% Triton X-100

*Wash Buffer QC* : 1.0 M NaCl; 50 mM MOPS, pH 7.0; 15% isopropanol

## 2.23. Generation of nicastrin stably overexpressing MCF10A cell line

The cDNA encoding full length human nicastrin was subcloned into a retroviral expression vector pMXs-puro and the construct was kindly provided by Prof. Gopal Thinakaran, University of Chicago, USA (330). The pMXs-puro-nicastrin retroviral vector was used to infect MCF10A cells (Dr Ylenia Lombardo, Imperial College, London). Control cells were generated by retroviral transduction of the empty vector pMXs-puro (Cambridge Bioscience). Stable, polyclonal cell populations were established after puromycin selection (0.5 μg/ml) by Dr Ylenia Lombardo, Imperial College London.

# CHAPTER 3

# Results

# Nicastrin expression in breast cancer cells and consequences of its genetic silencing

## 3.1. Introduction

Tumour progression and metastatic spread involve upregulation of molecular components that constitute numerous proteolytic and cell migration pathways and help drive cell invasion into the surrounding tissue (362). Gamma-secretase (GS) is a unique multi-protein complex with activity as a cell surface protease that directly cleaves a variety of transmembrane proteins to modify their function. The proteolytic targets of GS include a number of proteins involved in tumour cell proliferation, adhesion and invasion (363).

Small molecule GS inhibitors are currently being used in the clinic, however ongoing patient trials in advanced and metastatic solid tumours have indicated multiple side effects (364), which suggests the need for more controlled and tissue specific regulation of GS-associated biological activities. This could potentially be achieved by targeting nicastrin (NCT), which provides critical structural support for GS complex assembly and facilitates molecular recognition of multiple substrates for cleavage by the catalytic component of the complex, presenilin.

A recent report that implicated NCT to function independently of the GS complex in the control of p53-mediated cell death (235), as well as observations that its expression was upregulated following treatment of colon cancer cell lines with chemotherapeutic agents, and that overexpression of NCT is sufficient to enhance GS activity (365), serve as an indication that NCT could be specifically targeted when it is upregulated during disease pathology. We have therefore focused our attention on elucidating the expression pattern and functional implications of NCT expression in breast cancer cells. RNA interference (siRNA) has become a powerful approach to characterise gene function. In this chapter we investigated the expression of NCT in breast cancer cells and used transient NCT gene silencing as a method to derive information about its functional role in breast cancer cells.

## 3.2. Results

### 3.2.1. Nicastrin expression in breast cell lines and functional effects of nicastrin gene silencing in breast cancer cells

Given that NCT expression had not yet been explored in breast cells, we initially performed western blotting analysis of NCT protein levels in the non-tumourigenic breast epithelial cell line, 184A1 (366), and breast cancer cell lines (MCF-7, MDA-MB-231, BT474, SKBR3) (Figure 21) (367). Nicastrin expression was weak in the non-tumourigenic breast cell line 184A1, while breast cancer cell lines expressed markedly upregulated NCT levels. Both the immature and the mature NCT were detected, as noted by the close doublet band migrating at ~140 kDa and ~125 kDa. This result promted us to to investigate differential expression of NCT between normal breast tissue and primary breast cancers (described and discussed in detail in Chapter 5), which confirmed that NCT was indeed absent from normal breast tissue while being present in abundance in malignant breast disease. Furthermore, high NCT levels were predictive of overall survival in ERα negative patients (Chapter 5, Figure 43). This suggested that NCT might play a role in more aggressive breast cancer cells. The triple negative (ERα-, PR-, HER2- negative), basal B type, MDA-MB-231 cells were therefore chosen for subsequent experiments in order to investigate the functional role of NCT in invasive breast cancer, and the luminal A, MCF-7 cell line (368) was used for comparison of NCT functional role in the non-invasive cell line counterpart.

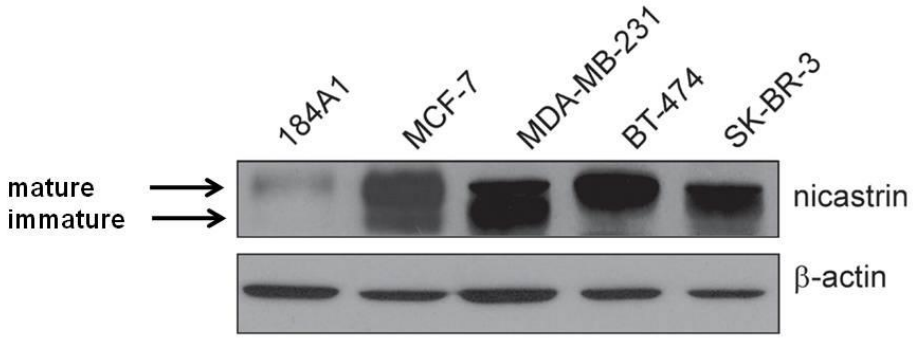


**Figure 21.Nicastrin expression is upregulated in breast cancer cell lines compared to normal breast cells. a)** Western blotting of nicastrin protein levels in a normal breast cell line 184A1 and four breast cancer cell lines (MCF-7, MDA-MB-231, BT-474 and SK-BR-3). Cell lines were cultured to 70-80% confluence and whole cell protein lysates were prepared. 20 μg of protein was loaded per lane. Both mature and immature nicastrin forms are detected. β-actin was used as the loading control.

### 3.2.2. Titration and functional analysis of NCT silencing in MDA-MB-231 cells

In order to determine the appropriate concentration and combination of the four *NCT* siRNA oligos (Dharmacon), we have transfected MDA-MB-231 cells with each individual siRNA and a pool of all four oligos at 10 nmol and 40 nmol concentrations, and measured *NCT* mRNA levels after 48 h of treatment. In deconvoluted analysis, siRNA1 had no effect, while siRNA3 reduced NCT mRNA only by 10-20%. siRNA2 and 4 induced a potent inhibition of *NCT* gene transcription, peaking at 40 nmol concentration. In pooled analysis, the combination of siRNA2 and 4 was the most effective, inhibiting *NCT* mRNA levels by > 95 % (Figure 22a). We have therefore used a combination of siRNA2 and 4 in all subsequent experiments, from here on referred to as '*NCT* siRNA'. In order to further confirm the optimal dose, we next investigated whether *NCT* siRNA would affect proliferation of MDA-MB-231 cells in a dose-dependent manner that would reflect the degree of gene inhibition observed in the previous experiment. We have transfected MDA-MB-231 cells with increasing concentrations of *NCT* siRNA, and measured cell proliferation after 96 h of treatment. The dose of 40 nmol was the most potent, inducing a marked reduction of cell proliferation (Figure 22b). Control siRNA against the green fluorescent protein (GFP) was used at an equivalent concentration as the negative control in all experiments, and did not induce significant cell toxicity. Therefore the dose of 40 nmol of *NCT* siRNA was taken forward to all subsequent experiments. Silencing efficiency was monitored and achieved (> 90%) for both *NCT* mRNA (Figure 24a) and protein levels (Figure 25a) in all reported experiments.

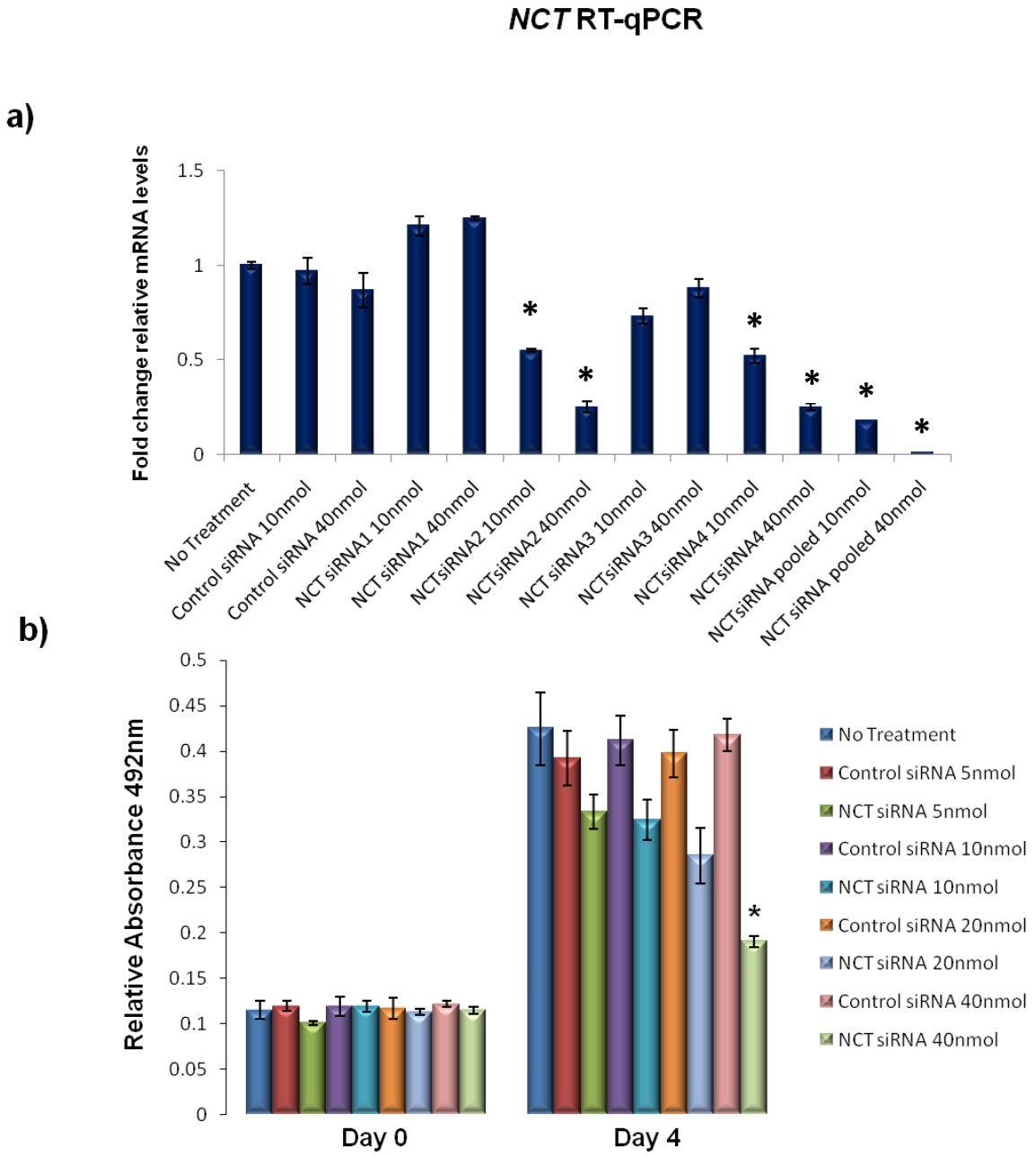


**Figure 22.Selection of the optimal *NCT* siRNA concentration. a) Titration of *NCT* siRNA.** MDA-MB-231 cells were transfected with 10 nmol and 40 nmol of *Control* siRNA (non targeting) and four *NCT* siRNA oligos. RT-qPCR for *NCT* was performed 48 h after transfection. GAPDH was used for normalisation. Error bars represent SEM of two separate experiments, each in triplicate; changes observed throughout these experiments were statistically significant * $p < 0.01$. **b) Cell proliferation assay.** MDA-MB-231 cells were transfected with increasing concentrations of *Control* siRNA and *NCT* siRNA and cell viability was measured at Day 4. Error bars represent SEM of two separate experiments, each done in quadruplicate, * $p < 0.01$.

### 3.2.3. Nicastrin silencing inhibits proliferation of breast cancer cells by inducing a sub-G1 cell cycle arrest

In order to investigate the impact of NCT silencing on breast cancer cell proliferation we have transfected MDA-MB-231 and MCF-7 cells with *NCT* siRNA and monitored cell viability in two-day intervals using the SRB assay. Nicastrin depletion markedly inhibited proliferation of both MDA-MB-231 cell (82±6.2%) and MCF-7 cells (75±8.1%) (Figure 23a). Furthermore, cell cycle analysis following *NCT* silencing in both cell lines confirmed that cells were accumulating in the sub-G1 phase of the cell cycle, i.e. undergoing apoptosis. More precisely, 37 % and 48% of cells were registered in the sub-G1 phase upon *NCT* siRNA vs. 2.4 % and 17 % in the *Control* siRNA treated MDA-MB-231 and MCF-7 cells, respectively (Figure 23b). Interestingly, treatment of these cells with a small molecule GSI (GSI1, Calbiochem), which inhibit the proteasome in addition to inhibiting the GS enzyme, also inhibited breast cancer cell proliferation although by inducing a G2/M arrest (369). This suggests that the inhibition of cell proliferation by interfering with the GS complex via NCT silencing may be more specific, and hence infers a different profile of the cell cycle arrest.

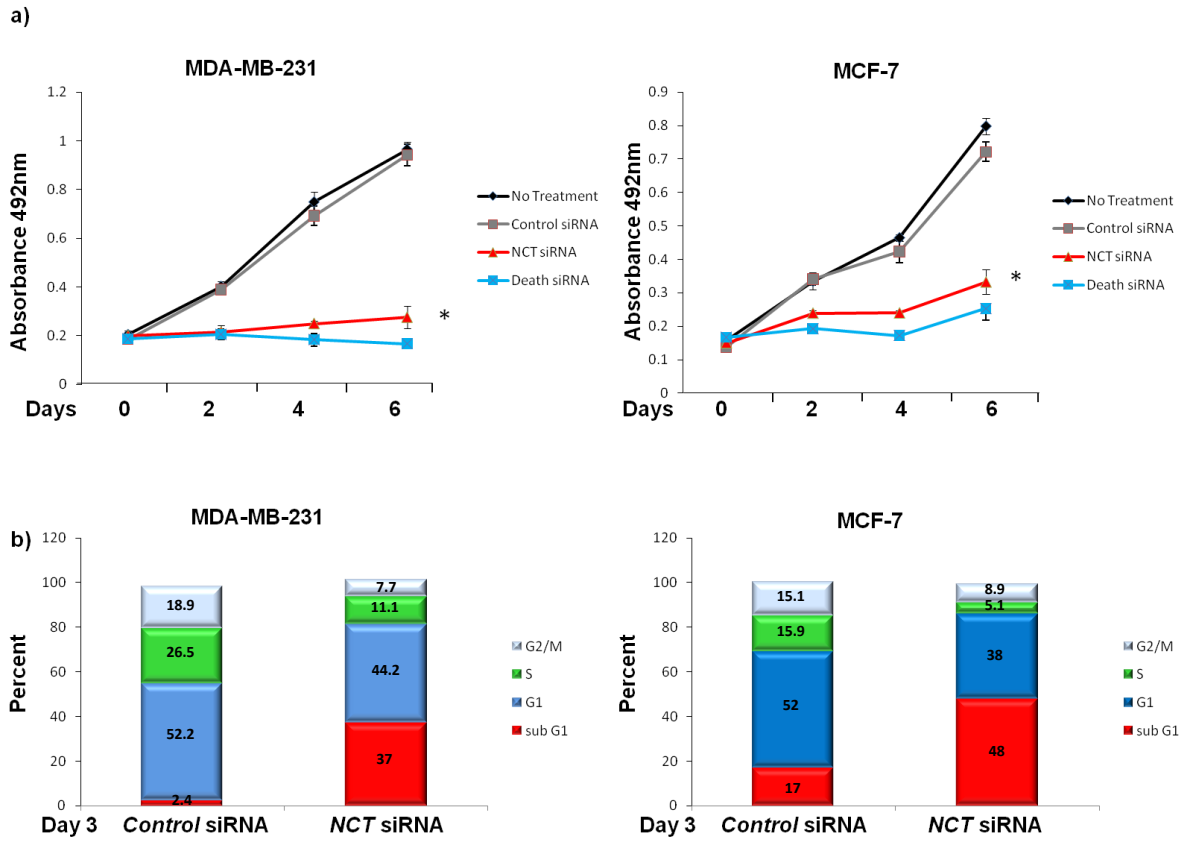


**Figure 23.Nicastrin siRNA inhibits breast cancer cell proliferation. a)** Cell proliferation assay. MDA-MB-231 and MCF-7 cells were treated with 40 nmol of the *Control* siRNA, *NCT* siRNA and the positive control *Death* siRNA. The day of transfection was annotated as Day 0. Proliferation (SRB) assay was performed every 2 days until Day 6, *p = 0.005. Error bars represent SEM of two separate experiments, each done in triplicate. **b)** Cell cycle analysis. MDA-MB-231 and MCF-7 cells were treated with 40 nmol of the *Control* siRNA and the *NCT* siRNA and cell cycle profile was analysed after 72 h.

### 3.2.4. Nicastrin silencing inhibits the gamma-secretase complex in breast cancer cells

We next investigated whether *NCT* genetic silencing disrupts the GS complex in breast cancer cells, by monitoring GS activity levels and *Hes1* mRNA levels upon transfection of breast cancer cells with *NCT* siRNA. Nicastrin silencing was sufficient to significantly reduce GS complex enzymatic activity ($p<0.001$) (Figure 24b), equally so as the GSI1. Furthermore, *NCT* siRNA reduced the transcription of a direct target gene of the Notch signaling pathway, *Hes1* ($p<0.001$) (Figure 24a).

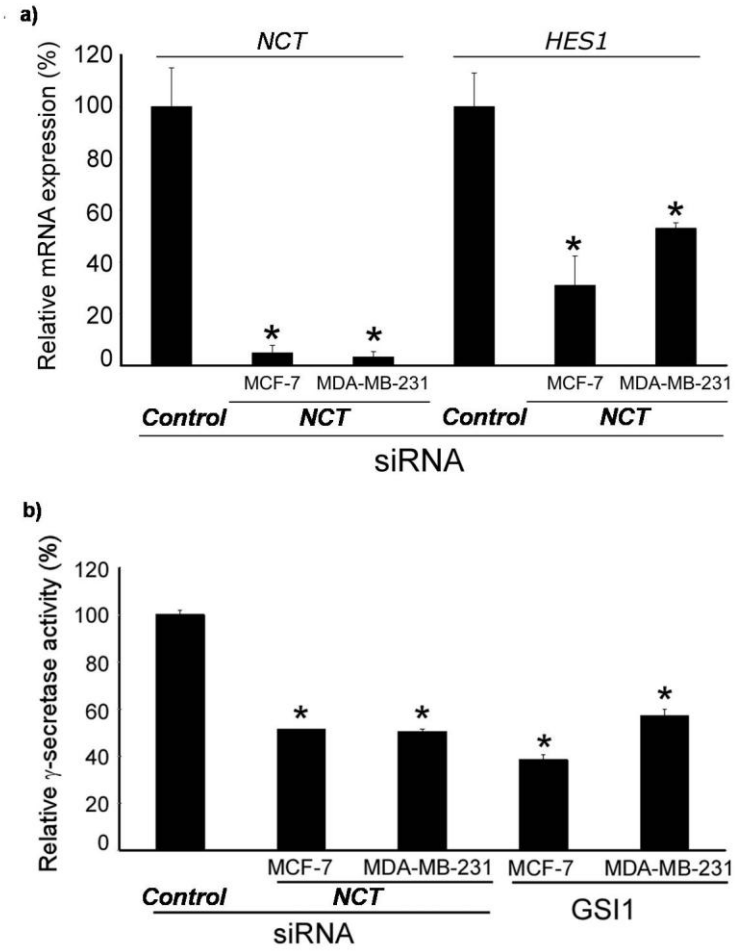


**Figure 24.Nicastrin silencing disrupts GS complex activity. a)** RT-qPCRs were carried out to determine fold changes in expression of *NCT* and *Hes1* in *NCT* siRNA treated samples compared to *Control* siRNA samples in MDA-MB-231 and MCF-7 cells. Data are the mean fold change in expression compared with *Control* siRNA samples. Error bars represent SEM of duplicate samples in three independent experiments, *$p < 0.001$. **b)** GS activity assay upon *NCT* silencing in MCF-7 and MDA-MB-231 cells. GS inhibitor (GSI1) (Calbiochem) at 1 μmol concentration was used as a positive control in this experiment, *$p < 0.001$. Degree of inhibition is comparable to that of a GSI in both cell lines.

In accordance with a previous report (370), NCT depletion appears to affect GS activity by inducing a concomitant loss of the PS1 protein in breast cancer cells as well (Figure 25a). Importantly, *NCT* silencing reduced protein levels of both the PS1 holoprotein and its N- and C- terminal fragments that are derived upon PEN2-mediated PS1 endoproteolysis, which yields an active GS complex. Interestingly, mRNA levels of neither PS1 nor PEN2 were significant changed in response to NCT siRNA in MDA-MB-231 cells, while PS1 mRNA levels were only mildly reduced in MCF-7 cells (35±10.1%) (Figure 25b), suggesting a post-translational regulatory effect of NCT on PS. As previously demonstrated in mouse embryonic fibroblast cells and neuronal cell lines, where NCT knockdown results in the abolishment of PS1, NCT appears to be equally important for PS1 stability in breast cancer cells (315). Collectively, these data demonstrate that the loss of NCT is sufficient to destabilise the GS complex in breast cancer cells.

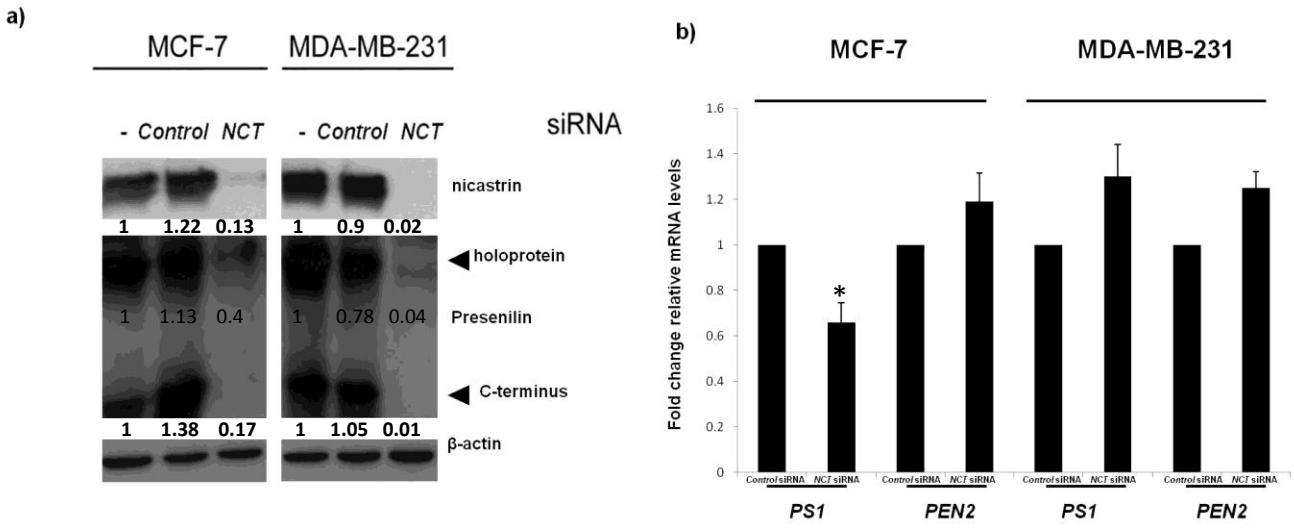


**Figure 25.Nicastrin silencing downregulates presenilin protein levels. a)** Western blotting analysis using indicated antibodies after 72 h of treatment with *Control* siRNA and *NCT* siRNA. β-actin was used as loading control. The intensity of bands was quantified using Image J software. Numbers below the bands represent fold change compared to the non-treated samples, relative to the loading control. **b)** RT-qPCR of *PS1* and *PEN2* upon *NCT* silencing. GAPDH was used for normalization, *p = 0.04. Error bars represent SEM of two separate experiments, each in triplicate.

## 3.3. Nicastrin silencing affects breast cancer cell adhesion and invasion

To investigate if NCT is able to functionally contribute to breast cancer cell adhesion/invasion, an siRNA targeting approach was used in MCF7 and MDA-MB-231 breast cancer cell lines, which represent luminal and basal breast cancer phenotypes respectively (368). The GS substrate E-cadherin is required for the formation of stable cell-cell adhesions in the normal breast epithelium. To investigate whether NCT affected the stability of breast cancer epithelium, the E-cadherin positive MCF-7 cell line was treated with *NCT* siRNA. *NCT* silencing in MCF-7 monolayers increased the total cellular levels of E-cadherin mRNA and protein (Figure 26 a & b), and facilitated its enhanced localisation to the cell membrane (Figure 27). This suggests that NCT may play a role in the regulation of breast cancer cell-cell adherence junctions. A potential mechanism of adherence junction regulation by NCT might be via the release of the transcriptional repression upon *E-cadherin (CDH-1)* by *Snail1 (SNAI1),* since the levels of this pivotal transcriptional factor in the EMT program were significantly reduced following *NCT* silencing ($p<0.001$) (Figure 26b).

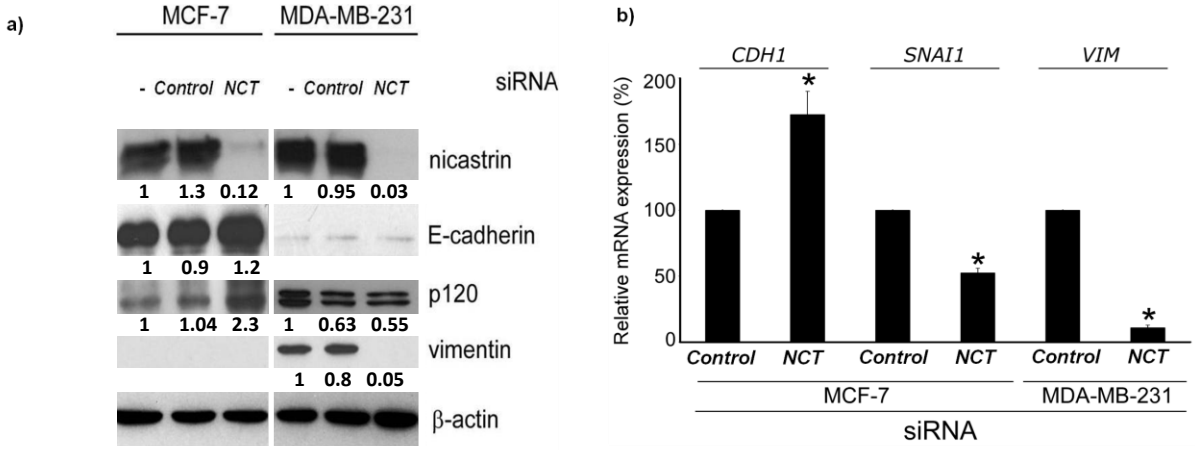


**Figure 26**.**Nicastrin silencing affects cell adhesion and invasion molecules in MDA-MB-231 and MCF-7 cells**. **a)** Western blotting analysis using indicated antibodies in *Control* siRNA and *NCT* siRNA treated cells. β-actin used as loading control. The intensity of bands was quantified using Image J software. Numbers below the bands represent fold change compared to the non-treated samples, relative to the loading control. **b)** Nicastrin silencing regulates transcription levels of E-cadherin, Snail and vimentin. Quantitative RT-PCRs were carried out to determine fold changes in expression of E-cadherin (*CDH1*), Snail (*SNAI1*) and vimentin (*VIM*) in *NCT* siRNA treated samples compared with control (*Control* siRNA) samples , *$p < 0.001$. GAPDH was used for normalisation. Error bars are SEM of the mean percent change in expression compared with control siRNA samples from duplicate samples in three independent experiments.

Additional evidence suggests that NCT-dependent regulation of E-cadherin may involve p120ctn, a molecule that is responsible for regulating E-cadherin turnover from the plasma membrane (371), thereby stabilising E-cadherin localisation to adherence junctions (372, 373). This regulatory mechanism may be modulated by the presence of a stable GS complex at the plasma membrane where PS1/GS can compete with p120ctn for binding to E-cadherin (372). Following *NCT* silencing, we observed an increase in p120ctn protein expression (Figure 26a) and localisation to MCF-7 cell membrane (Figure 27), suggesting that there may be multiple levels at which NCT can regulate the stability of luminal epithelial cell-cell adhesions. Although expression levels of the β-catenin and phalloidin were not affected, their alignment at the cell membrane upon NCT silencing was observed, corroborating the possibility of the formation of functional cell-cell adhesions (Figure 27).

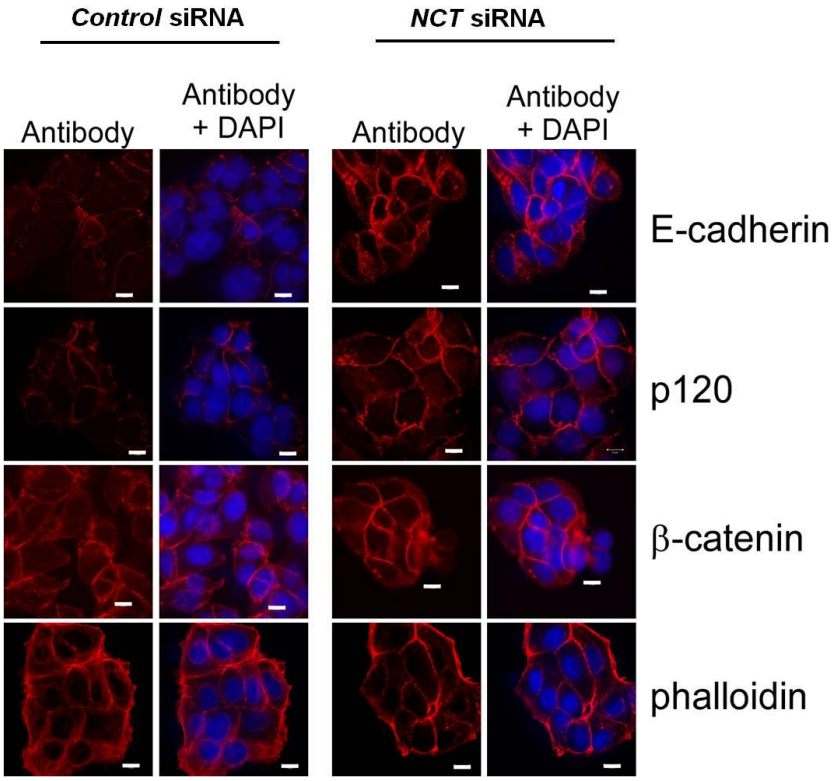


**Figure 27.Nicastrin silencing affects E-cadherin and p120 in MCF7 breast cancer cells.** Cells were transfected with *Control* siRNA and *NCT* siRNA and after 72 h fixed, permeabilised and stained with anti-E-caderin, anti-p120, anti-β-catenin MAbs. Polymerised actin was visualised with a tetramethylrhodamine isothiocyanate-phalloidin conjugate. The E-cadherin antibody was labeled with Zenon Alexa Flour 488 (Invitrogen), while the staining with the anti-p120, anti-β-catenin Mabs was followed by Alexa Flour 594 goat anti-mouse IgG (H+L) (Invitrogen). Nuclei were counterstained with DAPI (Vector Laboratories). Bar = 10 μm.

### 3.3.2. Nicastrin silencing inhibits breast cancer cell motility and invasion

Given a differential role of the membrane-associated p120ctn in cell-cell adhesions and the proinvasive role of the cytoplasmic p120ctn, we investigated the effect of NCT silencing on p120ctn in MDA-MB-231 cells. Although p120ctn protein expression following *NCT* siRNA was only mildly reduced (Figure 26a), p120ctn became associated with F-actin fibers at the sites of cell-cell contact in these cells (Figure 28). This signified that the loss of NCT could promote formation of cell-cell junctions in cells such as MDA-MB-231 that have previously undergone progressive transformation towards a scattered, single cell distribution. Furthermore, immunofluorescence staining has demonstrated that MDA-MB-231 cells intrinsically assume the elongated morphology (Figure 28, white stars), as well as a more rounded shape, consitent with the amoeboid cell motility (Figure 28, while circles).

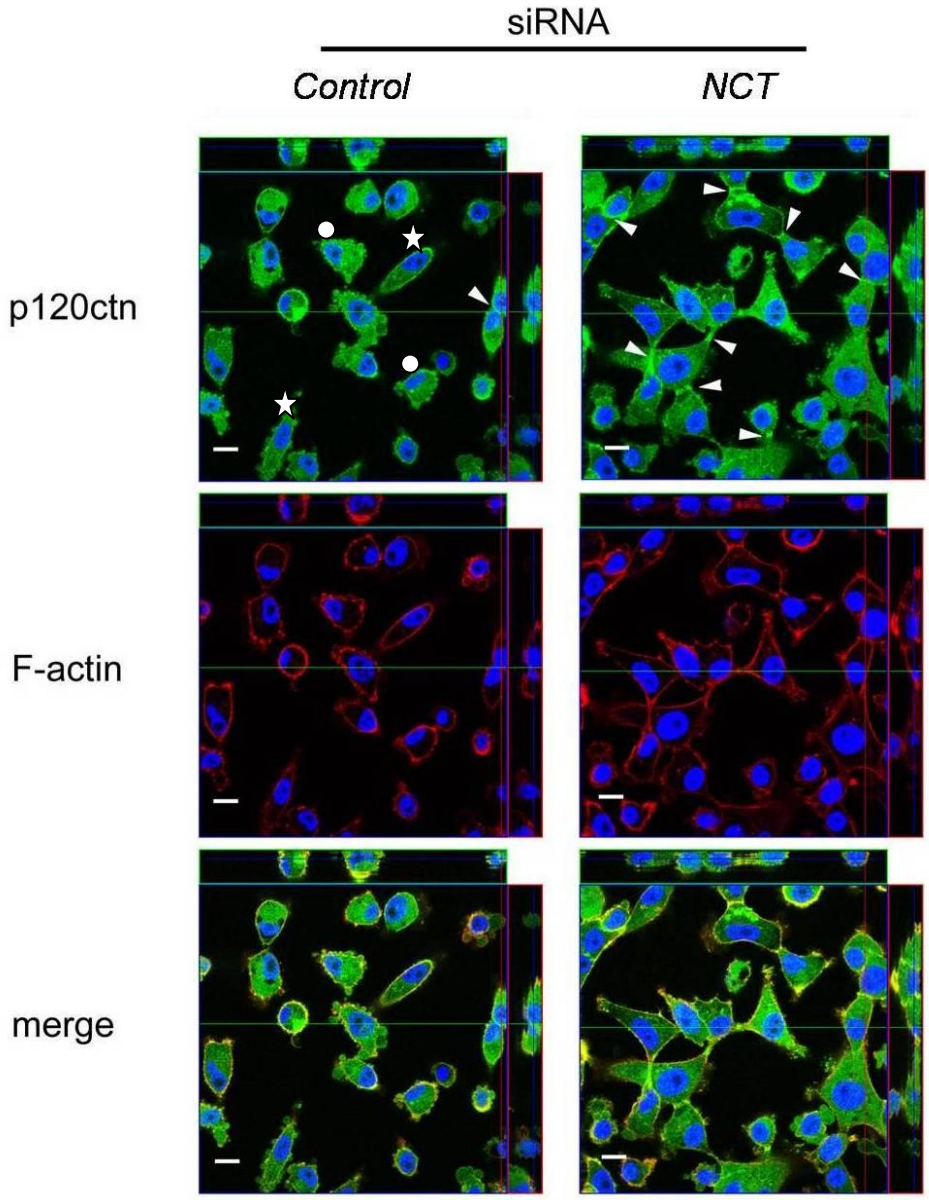


**Figure 28**.**Nicastrin silencing promotes formation of cell junctions in MDA-MB-231 cells.** MB-MDA-231 cells were transfected with *Control* and *NCT* siRNA and after 72 h cells were fixed, permeabilised and stained with anti-p120 MAb followed by Alexa Flour 488 goat anti-mouse IgG (H+L) (Invitrogen). Polymerised actin was visualised with a tetramethylrhodamine isothiocyanate-phalloidin conjugate (red). Nuclei were counterstained with TO-PRO-3 (blue). Bar = 10 μm. White arrow heads indicate cell-cell junctions. White star indicates mesenchymal shaped cells which move in an elongated fashion. White circle indicates round cells with membranous bleb-like protrusions, which are characteristics of the amoeboid-type motility.

Since this result suggested that NCT silencing may play a role in the loss of cellular features which are characteristic of a migratory behavior, we decided to investigate the effect of *NCT* siRNA on a well established promoter of cell migration and invasion, vimentin (374). Interestingly, NCT depletion was sufficient to reduce transcription and protein expression of the mesenchymal marker and promigratory cytoskeletal protein vimentin (Figure 26). Given the observed phenotypic and molecular changes in MDA-MB-231 cells upon NCT knockdown, all consistent with a decrease in the cellular invasive features, we next performed two-dimensional (2D) and three-dimensional (3D) analyses of cellular motility and invasiveness. This allowed us to monitor the functional consequences of NCT depletion on breast cancer cell motility and invasion. Motility can be studied using 2D experimental systems, which provide insights into cell movement patterns and can also give insight into the molecular machinery driving cell motility/migration (375). We have monitored the effects of *NCT* siRNA on motility of MDA-MB-231 cells, by treating the cells with *Control* or *NCT* siRNA for 72 h, after which the cells were imaged for 12 h in an environmental chamber (37 °C, 5% $CO_2$) by means of video time-lapse microscopy. This allowed us to obtain information regarding the motility of the cells in the 2D environment. Although informative, the mechanical properties of 2D motility assays on rigid surfaces are not fully comparable to those found in a 3D, *in vivo* setting. Epithelial cells *in vivo* are supported by both the basal membrane and the extracellular matrix. These structures play a key role during the invasion process by providing both a mechanical barrier preventing the invasion of the deeper tissues, as well as a substratum allowing malignant cells to migrate. Tumour cells leaving the primary tumour must therefore acquire the ability to invade the surrounding matrix in order to disseminate. To investigate the cellular invasive capacity in a 3D system, we used the trans-well invasion chamber method, where the cells are introduced into the upper chamber and allowed to invade through the Matrigel-coated porous filter, mimicking the basement membrane and the extracellular matrix, into the lower chamber containing the chemo-attractant, where they are collected from and counted. Matrigel does not only contain the basement membrane components (collagens, laminin, and proteoglycans), but also matrix degrading enzymes, their inhibitors and growth factors. Invasion of tumour cells into Matrigel has been used to characterise involvement of extracellular matrix receptors and matrix degrading enzymes which play roles in tumour progression (376).

Time-lapse microscopy experiments indeed revealed a decreased migratory speed of MDA-MB-231 cells upon *NCT* siRNA (Figure 29a). This was consistent with a reduction of the cell invasive capacity by 32±9.2% MDA-MB-231 cells upon NCT siRNA treatment in the trans-well invasion assay (Figure 29b).

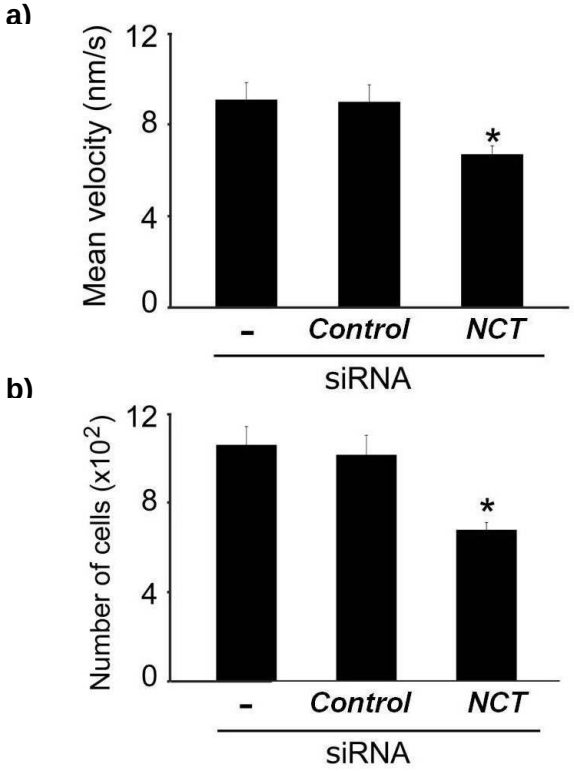


**Figure 29.Nicastrin silencing inhibits migration and invasion of MDA-MB-231 cells. a)** Effect of *NCT* silencing on the migration of MDA-MB-231 cells. Bars represent mean of cell migratory speed nm/sec ± SD from three separate experiments. **b)** Effect of nicastrin silencing on invasion of MDA-MB-231 cells. Bars represent mean number of invaded cells ± SD from three separate experiments. Statistical difference from control levels, *p = 0.01.

To validate the phenotypic and behavioural changes associated with *NCT* silencing in breast cancer cells, and also to address the issue that the inhibition of cell invasion in the trans-well assay might have been observed due to the acute cytotoxic effects of NCT siRNA treatment, we repeated the live imaging and motility analysis using the mouse embryonic fibroblast cells (MEFs), where NCT has been stably depleted ($NCT^{-/-}$) (Figure 30a) (370). Unlike $NCT^{+/+}$ MEFs, which displayed a typical fibroblastic spindle-like morphology with a scattered distribution, $NCT^{-/-}$ MEFs were rounded (377), and formed dense aggregates (Figure 30b), with a marked reduction in migratory speed (Figure 30c).

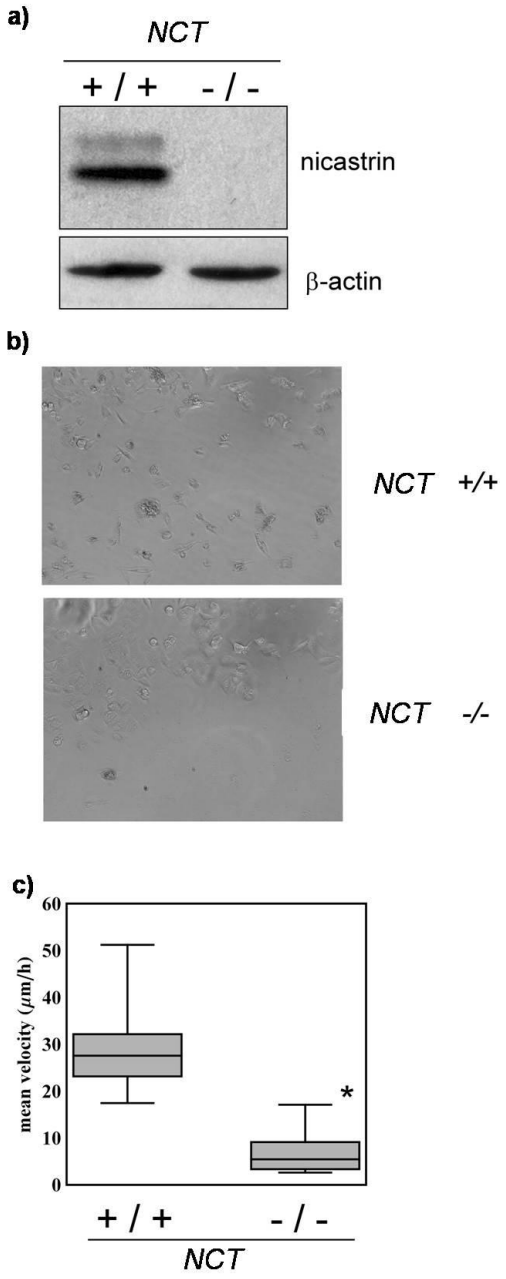


**Figure 30.Stable NCT knockdown in mouse embryonic fibroblast cells induces profound morphological and functional changes. a)** Western blotting for nicastrin in *NCT* $^{+/+}$ and *NCT* $^{-/-}$ MEFs. **b)** Phase contrast microscopy image of *NCT* $^{+/+}$ and *NCT* $^{-/-}$ MEFs. **c)** Cell migration assay (μm/h ± SD) of *NCT*$^{+/+}$ and *NCT*$^{-/-}$ MEFs. Magnification x10. * $p < 0.01$.

The evidence that genetic ablation of NCT in stromal fibroblasts of true mesenchymal origin induces a marked phenotypic and behavioural conversion towards a less motile cell model, strengthened our emerging hypothesis that silencing NCT may be able to induce restoration of a less invasive phenotype, thereby reversing the EMT-like program that has been proposed to promote breast cancer progression.

### 3.3.3. Nicastrin silencing inhibits cell proliferation machinery in MDA-MB-231 cells

In order to further examine the downstream signaling effectors that may be modulated by NCT inhibition in MDA-MB-231 cells, we assessed the protein levels of some of the mediators of cancer cell invasion and proliferation, which have also been implicated the Notch-dependent cellular processes. Nicastrin silencing in MDA-MB-231 cells induced an upregulation of the p21 cell cycle regulator and a concurrent inhibition of the nuclear proliferation marker Ki67 and of the anti-apoptotic protein Bcl-2. Furthermore, two established oncogenic pathways were inhibited in the NCT siRNA treated cells, namely the ERK1/2 and the Akt, as demonstrated by reduced protein levels of their respective phosphorylated/activated forms. Corroborating the impaired function of the Akt pathway, its direct effector, the translation initiation factor 4E (eIF4E) protein, was equally inhibited. Interestingly, protein levels of the CD147, a recently established accessory protein to the GS complex, were downregulated in NCT siRNA treated cells (Figure 31).

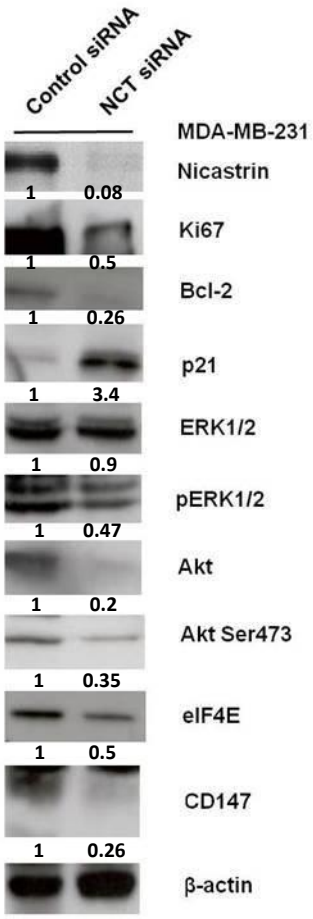


**Figure 31.Nicastrin silencing affects cell proliferation markers as well as the ERK1/2 and the Akt pathway.** Western blotting showing expression of marked proteins in MDA-MB-231 cells treated with *Control* siRNA and *NCT* siRNA for 72 h. β-actin was used as the loading control. The intensity of bands was quantified using Image J software. Numbers below the bands represent fold change compared to the *Control* siRNA treated samples, relative to the loading control.

These data indicated that NCT could be mediating its anti-proliferative and anti-invasive effects by cooperating with established cellular oncogenic pathways. The observed effects may be mediated through the NCT siRNA-induced reduction of GS activity, PS1 and activated Notch proteins. The cross-talk of Notch and MAPK signaling pathways has already been described in a number of cell types, playing a vital role in determining the context-specific functional outputs in the cell. Transformation by Notch requires active signals from the MAPK/ERK and PI3K/Akt (378). Also, activated Notch4 mediates anchorage-independent growth through the MAPK/ERK pathway (378), while primary tumours from Notch4 transgenic animals have been shown to express active forms of ERK. This co-operation is also reflected *in vivo*, as a subset of Notch positive human breast tumours

express phopsho-ERK1/2 in the nuclei. Such cases exhibit high node positivity, suggesting that Notch-ERK co-operation may lead to poor prognosis (165). Furthermore, a synergism exists between Notch and Akt in malignant disease (379), and Notch inhibition via targeted siRNA or GS inhibitors leads to concomitant downregulation of the cellular Akt activity (146). The deficits in Akt and ERK activation are also observed in cells deficient in both PS1 and PS2 (380).

The proliferation inhibitory and apoptotic effects resulting from NCT siRNA may be due to the downregulation of Notch activity and mediated through the expression of cell cycle regulatory proteins Bcl-2 and p21, and the activity of Akt signaling. It has been previously reported that the GS activity-regulated apoptosis is mediated via the Bcl-2-dependent cell death machinery (369, 381, 382), while the inhibition of Notch and Akt have been known to inhibit nuclear expression levels of the proliferation marker Ki67 (383). The eukaryotic initiation factor 4E (eIF4E) is a translational regulator that acts downstream of Akt and mTOR, and recapitulates the action of Akt in tumourigenesis (384). It is a major effector of the mTOR axis in Notch-mediated cell survival (385). Knockdown of eIF4E has been implicated in inhibition of proliferation via decreased expression of Bcl-2 in breast cancer xenografts (386).

We have analysed the effect of NCT knockdown on CD147 protein because it has recently been identified as one of the accessory proteins able to regulate GS activity (234). CD174 also plays a critical role in the invasive and metastatic activity of cancer cells by stimulating the tumour-surrounding fibroblasts to express matrix metalloproteinases (MMP2 and MMP9), as well as the VEGF, which promote tumour neoangiogenesis in malignant melanoma, prostate and bladder cancer. CD147 expression also is linked to development of multidrug resistance in breast cancer (387) (388). We have observed that NCT silencing downregulates CD147, suggesting this may be an accessory mechanism of NCT-mediated effects on cell invasion.

### 3.3.4. Overexpression of nicastrin is sufficient to increase GS activity in MCF-7 cells

Having observed that transient NCT silencing in both MDA-MB-231 and MCF-7 cells disrupts the GS complex and inhibits its activity, we wanted to investigate whether transient NCT overexpression would have the capacity to induce an opposite effect. For this experiment, we have transiently overexpressed NCT in non-invasive, MCF-7 cells, using a full-length NCT construct cloned into a pCMV6-XL4 expression vector. Nicastrin mRNA levels were significantly increased (Figure 32a), which translated to an upregulation of the NCT protein. This increase of NCT was sufficient to induce a concurrent upregulation of PS1, as well as an enhancement of the active, cleaved forms of GS substrates (Notch1, Notch4 and E-cadherin) (Figure 32b). This result indicated that NCT overexpression could indeed promote GS activity in breast cancer cells. The fact that we have observed an increase in E-cadherin-ICD, which is a nuclear chaperone of the p120ctn required for the activation of the proinvasive MMP7 gene and the disassembly of adherence junctions (269, 373), indicated that NCT overexpression may be acting in direct contrast to the NCT siRNA-induced effects in MCF-7 cells, where membrane E-cadherin levels were increased, suggesting a re-enforcement of cell-cell junctions.

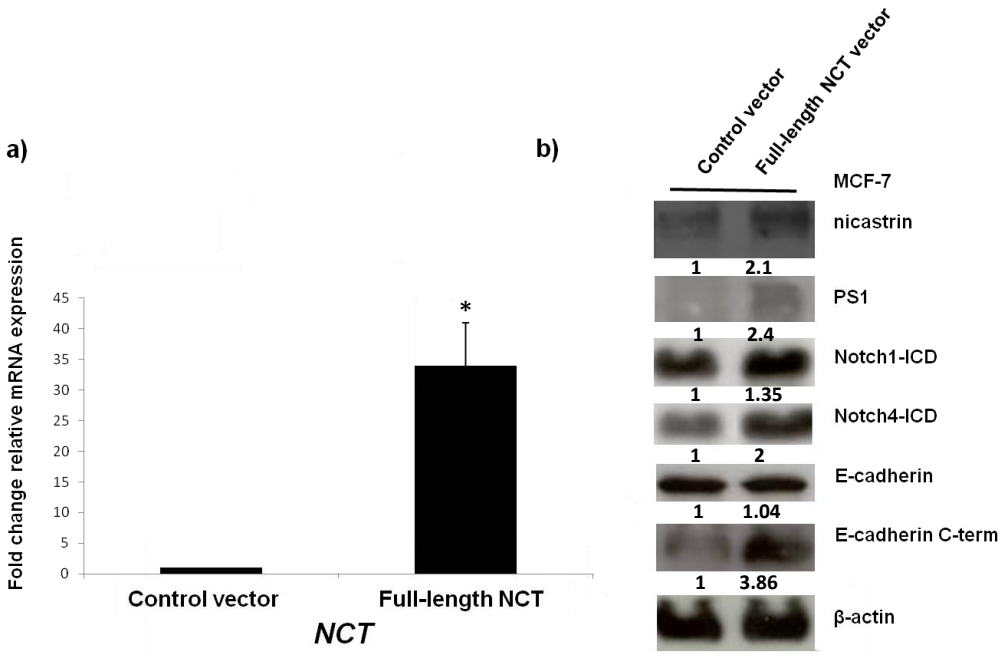


**Figure 32.Nicastrin overexpression in MCF-7 cells.** MCF-7 (2 x $10^5$) cells were plated in a 6 cm Petri dish and transfected with 1.5 ng of full-length NCT cDNA (SC100655, Origene) and the pCMV6-XL4 empty vector control, using Lipofectamine 2000 (Invitrogen). Cells were incubated for 48 h and then lysed for mRNA and protein extraction. **a)** RT-qPCR of *NCT* showing a marked increase of *NCT* mRNA levels. GAPDH was used for normalizing. GAPDH was used for normalisation. Error bars represent SD of two separate experiments, each in triplicate; changes observed throughout these experiments were statistically significant * p = 0.0006. **b)** Western blotting of marked proteins showing the effects of transient NCT overexpression in MCF-7 cellsonPS1, Notch1, Notch4 and E-cadherin proteins. β- actin was used as the loading control. The intensity of bands was quantified using Image J software. Numbers below the bands represent fold change compared to the control vector transfected samples, relative to the loading control.

In order to further validate these findings in a system where NCT overexpression would be able to yield more robust effects, we used non-transformed, non-invasive immortalised MCF10A breast cells that do not express abundance of NCT, and generated an MCF10A cell line stably overexpressing NCT. Nicastrin overexpression was achieved by infecting the cells using a retroviral vector pMXs-puro, containing full length human NCT (NCT-pMXs-puro), kindly provided to us by Prof. Gopal Thinakaran, University of Chicago, USA (330). As previously reported, overexpression of NCT resulted in a predominant accumulation of its immature form at ~125 kDa (326, 365, 389). Nicastrin overexpression in MCF10A cells induced more rapidly proliferating acini-like structures in 3D Matrigel (Figure 33a). At the same time, protein levels of PS1, Aph-1 and PEN2, as well as of the cleaved Notch1 were induced, indicating that NCT-induced synthesis and activity of the GS complex Furthermore, Numb, the negative regulator of Notch, was downregulated (Figure 33b).

Dowstream of active the Notch1, we also show that the transcription of the Notch target gene, *Hes1* was stimulated (Figure 33c). Importantly, we observed a marked elevation of vimentin, both at the protein and mRNA levels (Figure 33b, d). At the same time, proinvasive genes *SIP1*, *Twist* and *Snail*, were induced in the context of NCT overexpression (Figure 33e). Interestingly, NCT affected matrix-metalloproteinases, as observed by the induction of MMP7 transcription, which may be a consequence of an increase in E-cadherin cleavage (269), which is currently under investigation. The induction of EMT promoters inferred a functional consequence, since the invasive capacity of MCF10A NCT-expressing cells was enhanced, compared to control cells (Figure 33f). Collectively, these data confirm that overexpression of NCT is able to promote breast cell invasiveness.

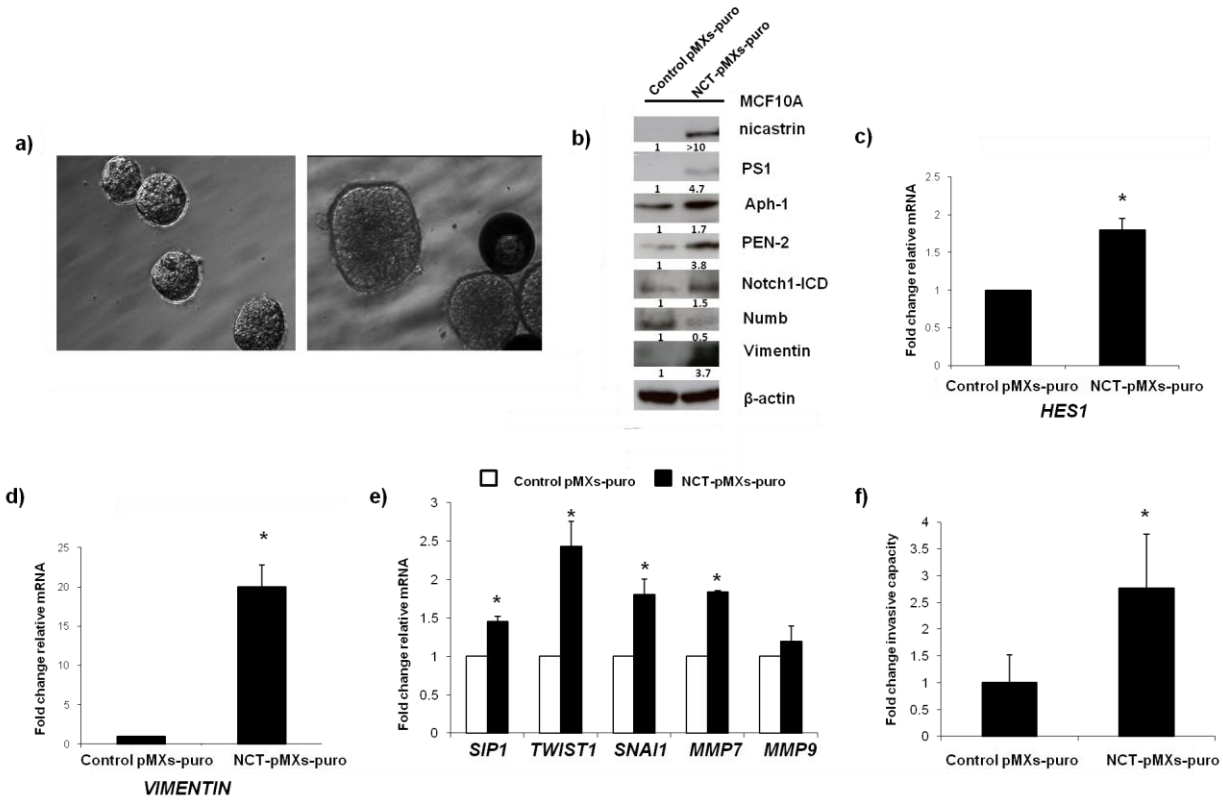


**Figure 33.Nicastrin overexpression in MCF10A non-transformed breast cells induces cell growth and invasion. a)** Phase contrast microscopy image of acini-like structures formed by culturing MCF10A Control pMXs-puro and NCT expressing NCT-pMXs-puro cells in the 3D Matrigel overlay assay. The pictures were taken at day 12. Original magnification x20. **b)** Western blotting analysis of MCF10A Control pMXs-puro and NCT expressing NCT-pMXs-puro whole cell lysates with indicated antibodies. β-actin was used as a loading control. The intensity of bands was quantified using Image J software. Numbers below the bands represent fold change compared to MCF10A Control pMXs-puro cells, relative to the loading control. RT-qPCR depicting fold change of quantitative mRNA levels of: **c)** *HES1*, *p =0.02; **d)** *Vimentin*, *p = 2.56E-06; **e)** *SIP1*, *p = 0.003; *TWIST*, *p = 2.26E-05; *SNAIL1*, *p = 0.0002; *MMP7*, *p = 0.004; *MMP9*, *p = 0.19. GAPDH was used for normalising. Error bars represent SEM of the fold change from two separate experiments, each in triplicate. **f)** Trans-well invasion assay. Bars represent fold change of the invasive capacity ± SD from two separate experiments, each in triplicate. Statistical difference from control cells, *p = 0.01.

## 3.4. Discussion

Most studies to date have focused on the expression and function of GS substrates, such as the Notch proteins, E-cadherin, CD44 and HER4, and have reported altered expression and function of these proteins in normal and diseased human tissues. Limited attention has been given to investigating the expression of individual GS components in breast cancer cells, with a general notion that the function of all four GS members is united within this enzyme complex. We have demonstrated a marked upregulation of NCT in human breast cancer cell lines compared to normal breast cells. Our efforts to characterise the functional implications of NCT expression in breast cancer cells by employing the siRNA targeting approach have indicated that NCT is important in maintaining breast cancer cell invasive and proliferative capacity.

Both of these aspects of the NCT function may be related to its role within the GS complex, and may be mediated through *NCT* siRNA-induced impairment of GS activity, causing inhibition of the GS substrate cleavage and activation, particularly that of Notch. Indeed, we have shown that mRNA levels of *Hes1,* an immediate target of the Notch pathway is inhibited by *NCT* silencing. Nicastrin inhibition was able to inhibit proliferation of both the basal-like (MDA-MB-231) and the luminal (MCF-7) breast cancer cell lines. However, in patient samples, high NCT expression predicted for worse overall survival only in the ERα negative patients. This fact indicates that NCT may be a particularly significant molecule in aggressive breast cancer, and proposes that a correlation exists between NCT overexpression and breast cancer aggressiveness.

We next demonstrated that targeting NCT in breast cancer epithelial monolayers and metastatic breast cancer cells *in vitro,* was sufficient to promote cell-membrane localisation of the principle cell-cell adhesion proteins and reduce cellular invasive capacity. The mechanism underlying these newly identified properties of NCT appears to involve the regulation of E-cadherin and p120ctn localisation to the cell membrane and downregulation of vimentin as part of an EMT-like program in breast cancer cells. The upregulation of E-cadherin protein and mRNA levels, as well as the enhanced cell membrane localisation upon *NCT* silencing could involve several mechanisms. The first mechanism could relate to the fact that the absence of NCT inflicts impaired GS activity, hence may reduce GS cleavage of E-cadherin, which consequently may reduce E-cadherin turnover from the cell membrane.

A secondary mechanism of regulation could occur via the activation of the transcriptional targets. Mechanistically, this could in part represent a Notch-mediated event. This is corroborated by reduced transcription of the Notch target *Hes1* in MCF7 cells upon *NCT* silencing. Notch-mediated effects on *Snail* were previously shown in an ovarian cancer model (169). Nicastrin-dependent E-cadherin regulation could also involve p120ctn, which stabilises E-cadherin localisation to adherence junctions by regulating its turnover or competing with PS for direct binding to E-cadherin (372, 373). Nicastrin overexpression in MCF10A cells induced a more rapid proliferation of acini-like structures grown in Matrigel. This is an effect already observed upon Notch1-ICD overexpression in MCF10A cells (390), and may very well be a Notch-mediated consequence in our experiment as well. Treatment of MCF10A NCT-expressing cells with a gamma-secretase inhibitor would help discern the extent to which the proliferation induction is dependent on GS/Notch activation or NCT-dependent cellular signaling. Should a GSI revert the growth rate to basal levels, it will indicate that NCT overexpression exerts its pro-proliferative function mainly via GS/Notch activity. Regulation of vimentin by *NCT* silencing appears to occur at the transcriptional level, as suggested by a marked decrease in vimentin mRNA levels upon NCT siRNA and increase upon NCT overexpression. Inhibition of vimentin, a *bona fide* EMT denominator, has previously been shown to reduce cellular invasive capacity in the reversal of an EMT program (374). Notch receptor-mediated regulation of vimentin has thus far been examined in human salivary gland (HSG) epithelial cells in the context of salivary acinar growth and differentiation (391), and in rat alveolar epithelial cells in the context of examining Notch signaling in the process of pulmonary fibrosis (392). It has been demonstrated that only simultaneous inhibition of all four Notch receptors in capable of inducing a reduction of vimentin protein (391). We have demonstrated a profound inhibition of vimentin protein upon NCT silencing in MDA-MB-231 cells. In alveolar epithelial cells, ectopic expression of active Notch induced an EMT phenotype accompanied by E-cadherin inhibition, induction of the smooth muscle actin and migratory behavior of cells (392). Although the authors state that vimentin mRNA levels were equally elevated, this increase was 1.3-fold from baseline levels, while we have observed a ~20-fold increase in vimentin transcription upon NCT overexpression in MCF10A cells.

Given the degree of vimentin inhibition and induction upon NCT silencing and overexpression, respectively, our data suggest that while to some extent vimentin may be regulated by Notch signaling in breast cancer cells, there may also be an additional layer of Notch-independent/NCT-dependent regulation of vimentin. Metastatic invasion in breast cancer is a critical event leading to patient mortality, and the identification of molecular contributors specific to metastasis is essential for the development of effective targeted therapies. Our data suggest that NCT upregulation may have an important mechanistic role underlying the increased risk of dissemination of breast cancer cells.

# CHAPTER 4

# Results

# Effects of stable nicastrin depletion in the invasive breast cancer cells

## 4.1. Introduction

Molecular profiling of the HCC1806 breast cancer cell line has revealed that they represent an *in vitro* model of basal-like breast cancers, as they are triple negative and EGFR positive cells, derived from the squamous cell primary breast tumour (367). EGFR is commonly expressed in basal-like breast cancers, as are the Notch receptors that have been recognised for their hyper-activation in this breast cancer subtype (158).

The group of Prof. M. Loren et al. has generated a stable HCC1806 cell line lacking NCT expression (164). Short hairpins targeting human NCT with the sequences: 5′-CCCATCTTTCTTCTTGAAGAT-3′ and 5′-GCTCTACTGAATACTCTACAT-3', were cloned into the lentiviral vector pLKO-puro. Control cells were generated by lentiviral transduction of a short hairpin targeting the luciferase gene, which contains coding sequences not present in the human genome. Stable, polyclonal knockdown cell populations were established after infection and drug selection. Cells harbouring the NCT short hairpins showed a significant decrease of NCT protein levels (164). GS inhibition in HCC1806 cells significantly disabled the Notch signaling pathway, which in conjunction with EGFR inhibition using gefitinib, resulted in a potent inhibition of cell viability, exceeding the anti-proliferative effects of gefitinib and the GS inhibitor DAPT as single treatments (164). Mechanistically, this loss of cell viability was due to Notch1-mediated effects on the Akt pathway, whose activation is an established mechanism of resistance to treatment with EGFR inhibitors (393). To rule out the possibility that off-target (toxic) effects of the GSI (DAPT) have contributed to the observed additive cytotoxicity upon gefitinib and DAPT combined treatment, this group has generated a stable HCC1806 cell line lacking GS activity by knocking down NCT, and has replicated the data obtained with the use of the DAPT (164).

The HCC1806 control and NCT knockout cells represented an advantageous tool to use in our experiments as well, and were obtained as a kind gift from Prof. M. Loren, University of Washington, USA. It is important to emphasise that the HCC1806 cells are, like the MDA-MB-231 cells used to transiently silence NCT, a triple-negative, basal-like, breast cancer cell line, the fact that enabled us to compare and contrast the results obtained from these two cell line models.

Furthermore, given the nature/durability of the stable NCT depletion, these cells allowed us to investigate the impact of NCT inhibition on cellular invasion in the trans-well assays, while avoiding the possible hindrance of acute cytotoxic effects and lack of durability of the transient siRNA.

## 4.2. Results

### 4.2.1. Stable nicastrin depletion impairs proliferation and invasion of breast cancer cells

In order to investigate the impact of the stable NCT depletion in HCC1806 breast cancer cells on cell behaviour and morphology, we have performed phase contrast microscopy of the HCC1806-Luc1 and HCC1806-NCTsh cells cultured in a 2D assay, allowing us to monitor cell shape and distribution, as well as in the 3D Matrigel-overlay assay, enabling us to examine the acini-forming capacity of HCC1806-NCTsh vs. control cells.

Absence of NCT had a profound effect on cell morphology, since the spindle shape and scattered distribution of HCC1806-Luc1 cells were notably changed to a rounded phenotype and compact cell clusters in the HCC1806-NCTsh cells (Figure 34a). The more physiologically relevant 3D Matrigel-overlay model, which allows integration of the crucial extracellular matrix signaling components, showed that control HCC1806 cells formed grape-like complex acini structures, which are characterised by the absence of functional cell-cell adhesions and increased migratory behaviour (67). Conversely, NCT depleted cells yielded significantly smaller acini and their shape was more rounded (Figure 34a), suggesting that the cells lacking NCT expression may have undergone a reversal of the EMT. Since the size of the cellular acini was greatly affected in a 3D assay, we speculated that the rate of proliferation might be reduced in HCC1806-NCTsh cells. Therefore, we conducted a 2D proliferation assay with HCC1806-Luc1 and HCC1806-NCTsh cells in 96-well plates and detected that the rate of proliferation in NCT depleted cells was indeed reduced by 47±4.1% ($p < 0.01$) over the period of 6 days (Figure 34b).

Furthermore, the invasive capacity of the HCC1806-NCTsh cells was reduced by 51.4±1.7% compared to control cells (Figure 34c), which compared to the reduction of invasion in MDA-MB-231 cells upon transient *NCT* silencing, indicates that stable NCT depletion is more potent in interfering with the aggressive behaviour of breast cancer cells. This was further confirmed by a marked downregulation of vimentin protein levels in HCC1806-NCTsh cells (Figure 34d).

In order to explore the downstream signaling pathways responsible for inferring the observed functional effects in HCC1806-NCTsh cells, we prepared whole cell lysates of HCC1806-Luc1 and HCC1806-NCTsh cells and firstly examined the effect of NCT depletion on other GS components. Protein levels of PS1, Aph-1 and PEN2 were reduced, suggesting that the GS complex has been impeded, which was in line with reduced levels of the cleaved Notch1 (Figure 34d). As previously reported by Dong et al., we have also observed that the Akt pathway was inhibited in NCT depleted cells, as measured by the levels of phosphorylated Ser473 residue. Furthermore, the EGFR protein was markedly downregulated, which could help explain the additive effect that gefitinib and NCT inhibition had on cell proliferation (164). Slower proliferation rate of HCC1806-NCTsh cells we have observed (Figure 34d) is in line with the lower levels of the proliferative marker, Ki67, as well as with the noted increase in p21 (Figure 34d), the expression of which mediates the cell cycle $G_1$ phase arrest in response to a variety of stimuli (394).

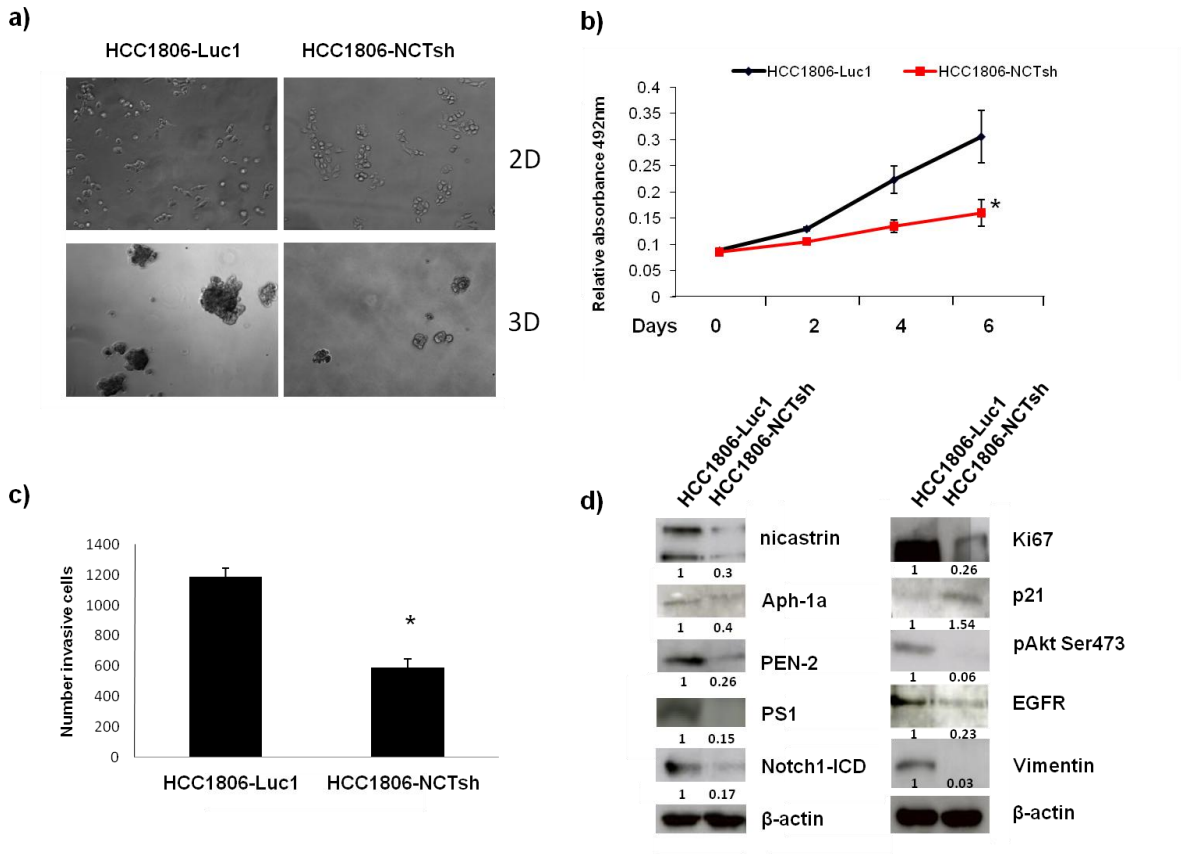


**Figure 34.Stable NCT depletion impedes proliferation and invasion of HCC1806 cells.**
**a)** Phase contrast microscopy image of HCC1806-Luc1 and HCC1806-NCTsh cells cultured in 2D (upper panels) and in the 3D Matrigel-overlay chambers (lower panels); Magnification x10. **b)** HCC1806-Luc and HCC1806-NCTsh cells were plated (3 x $10^3$/well) in 96-well plates and allowed to adhere over-night, when one plate was fixed and annotated as Day 0. Cells were grown and SRB assay was performed every 2 days until Day 6. Error bars represent SEM of two independent experiments, each in quadruplicate, *p = 0.017. **c)** Trans-well invasion assay. Bars represent mean number of invaded cells ± SEM from three separate experiments, each in triplicate. Statistical difference from control levels, *p = 0.001. **d)** Western blotting analysis of HCC1806-Luc1 and HCC1806-NCTsh whole cell lysates with indicated antibodies. β-actin was used as a loading control. The intensity of bands was quantified using the Image J software. Numbers below the bands represent fold change compared to HCC1806-Luc1 cells, relative to the loading control.

### 4.2.3. Nicastrin depletion affects the breast cancer stem-cell like population

The role of Notch signaling has recently been implicated in the maintenance of the stem cell pool, both in the normal mammary epithelium, and in the cancer stem cells (395). Notch4 has been described as the key downstream effector of the Notch signaling axis, and also the main receptor of this family whose expression levels are elevated in breast cancer stem cells (BCSCs) (176). We sought to investigate whether NCT expression was altered in BCSCs compared to non-CSC population, as well as to explore the effect of NCT depletion on the Notch pathway in the BCSCs population.

Cancer stem cells are characterised by the multi-potency to give rise to various cellular lineages within the primary tumour, as well as to survive and form mammospheres, which are structures enriched in cells with functional characteristics of stem/progenitor cells, in anchorage independent conditions (396). We tested the mammosphere forming capacity of HCC1806-Luc and HCC1806-NCTsh cells by culturing them on a non-adherent surface in the presence of growth factors. We demonstrated that the mammospheres were more abundant in NCT expressing cells (Figure 35a & b), suggesting that NCT depletion may play a role in inhibiting the pool of stem/progenitor cells in the HCC1806 breast cancer cell line. Therefore, we next wanted to examine in more detail the impact of NCT inhibition in breast cancer stem cells. In order to isolate the appropriate cell population, we employed a stem-cell enrichment protocol which relies on immunosorting and the use of antibodies against cell-surface proteins. Based on the phenotypic signature of BCSCs proposed by the work of Al Hajj et al. (87), we used CD44 and CD24 as the relevant cell surface markers. Both the HCC1806-Luc and HCC1806-NCTsh cells were sorted according to the expression of cell surface CD44 and CD24, and the percent of the BCSCs baring the $CD44^{+/}CD24^{-}$ signature were compared. A reduction of the BCSC pool in the HCC1806-NCTsh cells (4.2±1.5% in NCT depleted cells vs. 10.1±2.3% in the control cell line) was observed (Figure 35c & d). This further strengthened our hypothesis that NCT may be important for the maintenance and function of BCSCs.

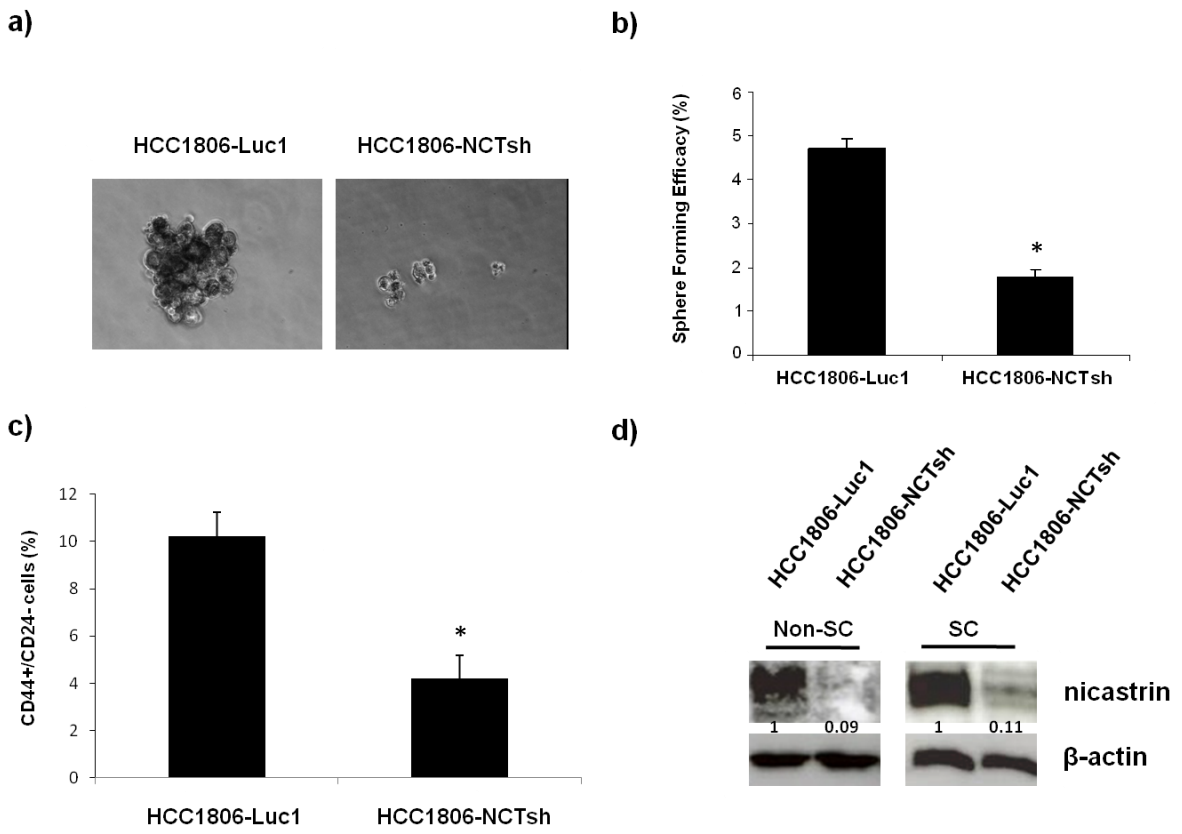


**Figure 35.Stable NCT depletion reduces stem-cell-like properties of HCC1806 cells. a)** Phase contrast microscopy of HCC1806-Luc1 and HCC1806-NCTsh cells grown in low attachment 6-well plates and cultivated in serum-free mammary epithelial growth medium, supplemented with 20 ng/ml EGF, 20 ng/mL FGF and 4 μg/mL heparin. Images were taken 10 days after cell plating. HCC1806-Luc1 cells form mammospheres (> 60 μm in size), while HCC1806-NCTsh cells predominantly form doublets, triplets and small-cell aggregates. Magnification x20. **b)** Bar graph represents the sphere forming efficiency mammosphere forming efficacy of HCC1806-Luc1 and HCC1806-NCTsh. Sphere forming efficacy was calculated as the number of spheres formed in 10 days divided by the original number of single cells seeded and expressed as a percentage. Bars represent mean percent of mammospheres ± SD from two separate experiments. Statistical difference from HCC1806-Luc1 cells, *$p < 0.01$. **c)** HCC1806-Luc1 and HCC1806-NCTsh cells were dual-labeled with fluorochrome-conjugated monoclonal antibodies against human CD44 (CD44-FITC) and CD24 (CD24-PE), and subjected to cell sorting on the FACSAria, BD. The bars represent percent of isolated stem-cell-like cells ($CD44^+/CD24^-$) ± SD from three separate experiments. Statistical difference from HCC1806-Luc1, *$p < 0.01$. **d)** Western blotting showing protein levels of NCT in the HCC1806-Luc1 and HCC1806-NCTsh non-stem cell (non-SC) and the stem-cell (SC) populations derived from the cell sorting. β-actin was used as the loading control. The intensity of bands was quantified using Image J software. Numbers below the bands represent fold change compared to the HCC1806-Luc1cells, relative to the loading control.

### 4.2.4. Nicastrin depletion inhibits Notch4 protein levels in breast cancer stem cells

To investigate the impact of NCT depletion on the Notch pathway, we performed RT-qPCR analysis of *Notch1*, *Notch4*, *Hes1* and *Numb*. Firstly, we confirmed that the *NCT* gene was silenced in both the BCSC and the non-SC fractions of the analysed cell lines (Figure 36a). *Notch1* transcription displayed a trend of elevation, although not statistically significant, between non-SC and BCSC pools, in both the control and NCT depleted cells. This trend was mirrored by the *Hes1* mRNA levels (Figure 36b & c). Interestingly, transcription of the negative regulator of the Notch pathway, *Numb*, was increased in the BCSC fraction of HCC1806-Luc1 cells compared to the non-SC population, even though *Notch* mRNA levels were still upregulated (Figure 36c & e). This may represent a negative feed-back mechanism as a tendency to counteract the activation of Notch in the BCSCs. Increased levels of *Numb* were maintained at this higher level in both the BCSC and the non-SC of the HCC186-NCTsh cells (Figure 36d).

As previously reported (176), we also found that the *Notch4* was most markedly upregulated in the BCSC population of both HCC1806-Luc1 (6.5-fold) and HCC186-NCTsh cells (8-fold) compared to their respective non-SC counterparts (Figure 36e). Upon analysis of the cleaved Notch4 protein levels, we have observed that Notch4-ICD was indeed markedly upregulated in BCSCs in the HCC1806-Luc1 cells, mimicking the increase in mRNA levels (Figure 36f). Strikingly, even though *Notch4* transcription still remained high in the NCT depleted BCSCs, the increase of the activated Notch4 protein was partially prevented by NCT depletion in the BCSCs as well as in non-SCs (Figure 36f).

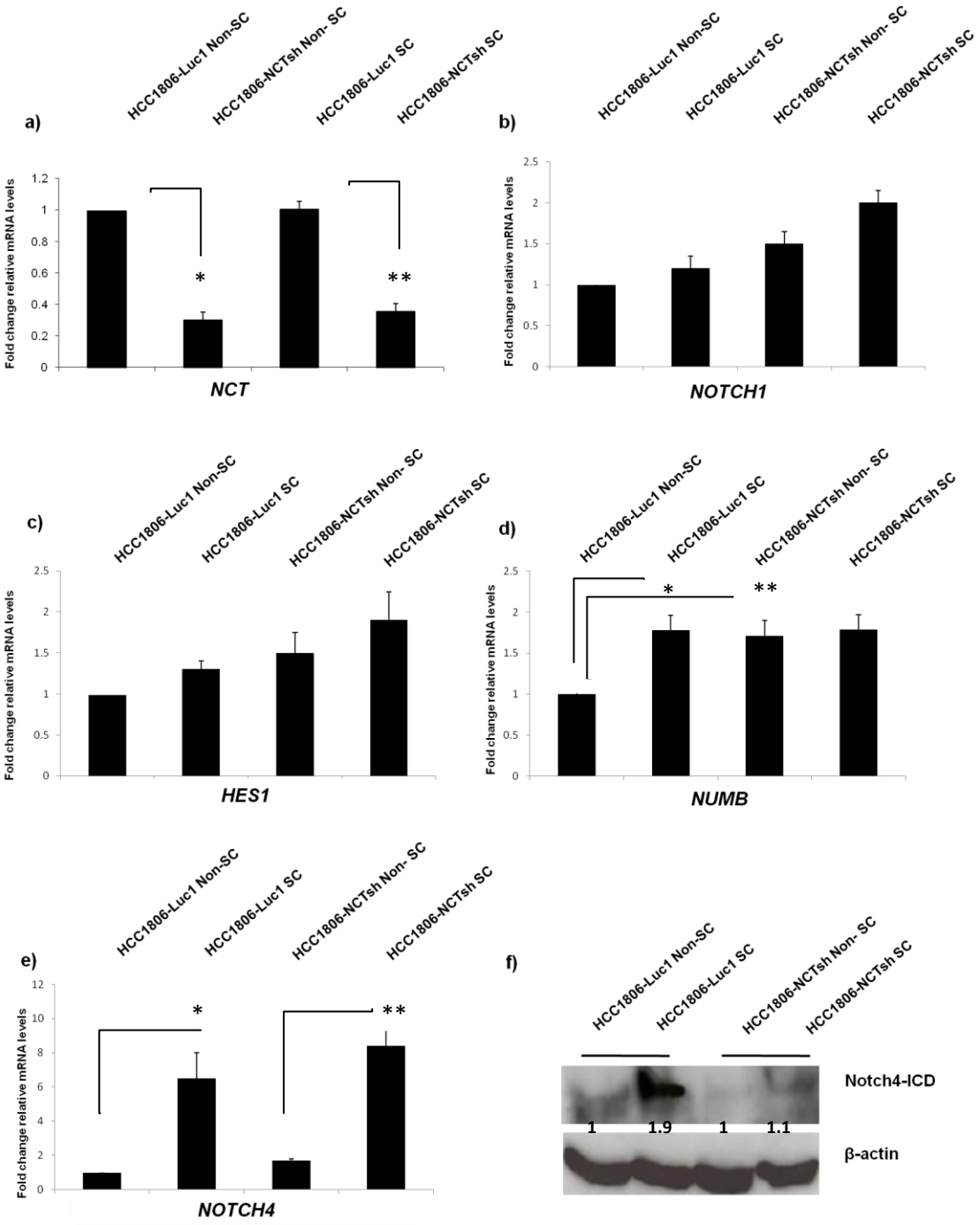


**Figure 36.Stable NCT depletion affects the Notch pathway in non-SC and in the SC populations of HCC1806-Luc1 and HCC1806-NCTsh cells.** RT-qPCR depicting fold change of quantitative mRNA levels of: **a)** *Nicastrin*, *p = 0.0002 and **p = 0.004; **b)** *Numb*, *p = 0.02 and **p = 0.02; **d)** *Notch4*, *p = 0.009 and **p = 0.001. GAPDH was used for normalising. Error bars represent SEM of the fold change from two separate experiments, each in triplicate. **f)** Western blotting of the Notch4-ICD. β-actin was used as the loading control. The intensity of bands was quantified using Image J software. Numbers below the bands represent fold change compared to the HCC1806-Luc1cells, relative to the loading control.

### 4.2.5. Nicastrin depletion inhibits proinvasive genes in breast cancer stem cells-like cells derived from HCC1806 cell line

Genes commonly associated with basal breast cancer cell lines which are upregulated in EMT include *SIP1, Vimentin, Twist, Snail, FOXC2, N-cadherin* and *Fibronectin* etc. (54). Breast cancer stem cells display higher expression levels of the proinvasive genes. Furthermore, the 'invasiveness gene signature' of the breast cancer cells expressing the $CD44^{+}/CD24^{-}$ phenotype was found to be predictive of patient outcome (397). Emphasising the relationship between the EMT and BCSCs, recent evidence proposed that passage of mammary epithelial cells through an EMT program has the capability to generate cells with stem cell properties (90).

Considering the inhibitory effect of NCT depletion on cell invasion, as well as on vimentin protein levels, and the fact that EMT is a concept that is increasingly gaining recognition within cancer stem cells, we next checked whether NCT inhibition modulated transcription of the proinvasive genes in non-SCs and BCSCs in the HCC1806-Luc1 and HCC1806-NCTsh cell lines. We subjected HCC1806-Luc1 and HCC1806-NCTsh cells to immunosorting and generated non-SC and BCSC populations for each of the two cell lines. The mRNA was then isolated from the cells and NCT mRNA levels were proven to be downregulated in respective HCC1806-NCTsh populations (Figure 36a).

As previously observed upon transient NCT knockdown in MDA-MB-231 cells, vimentin mRNA levels were 10-fold downregulated between the non-SC populations of the HCC1806-Luc1 and HCC1806-NCTsh cells. As expected, vimentin was markedly overexpressed (8.5-fold) in the BCSC pool of the NCT expressing cell line, compared to the non-SC counterpart (Figure 37a). NCT depletion, however, was able to prevent a similar increase of vimentin mRNA levels in the BCSCs of the NCT depleted cell line, maintaining the levels comparable to those in the HCC1806-NCTsh non-SCs. The same trend was observed for the *SIP1* (Figure 37b) and *Snail1* (Figure 37c), while NCT inhibition had negligible effects on *Fibronectin* and *N-cadherin* (Figure 37e & f). *Twist1* transcription was elevated in the HCC1806-Luc1 BCSCs compared to the non-SC counterpart, however, NCT inhibition did not confer a reduction of *Twist1* mRNA levels (Figure 37d).

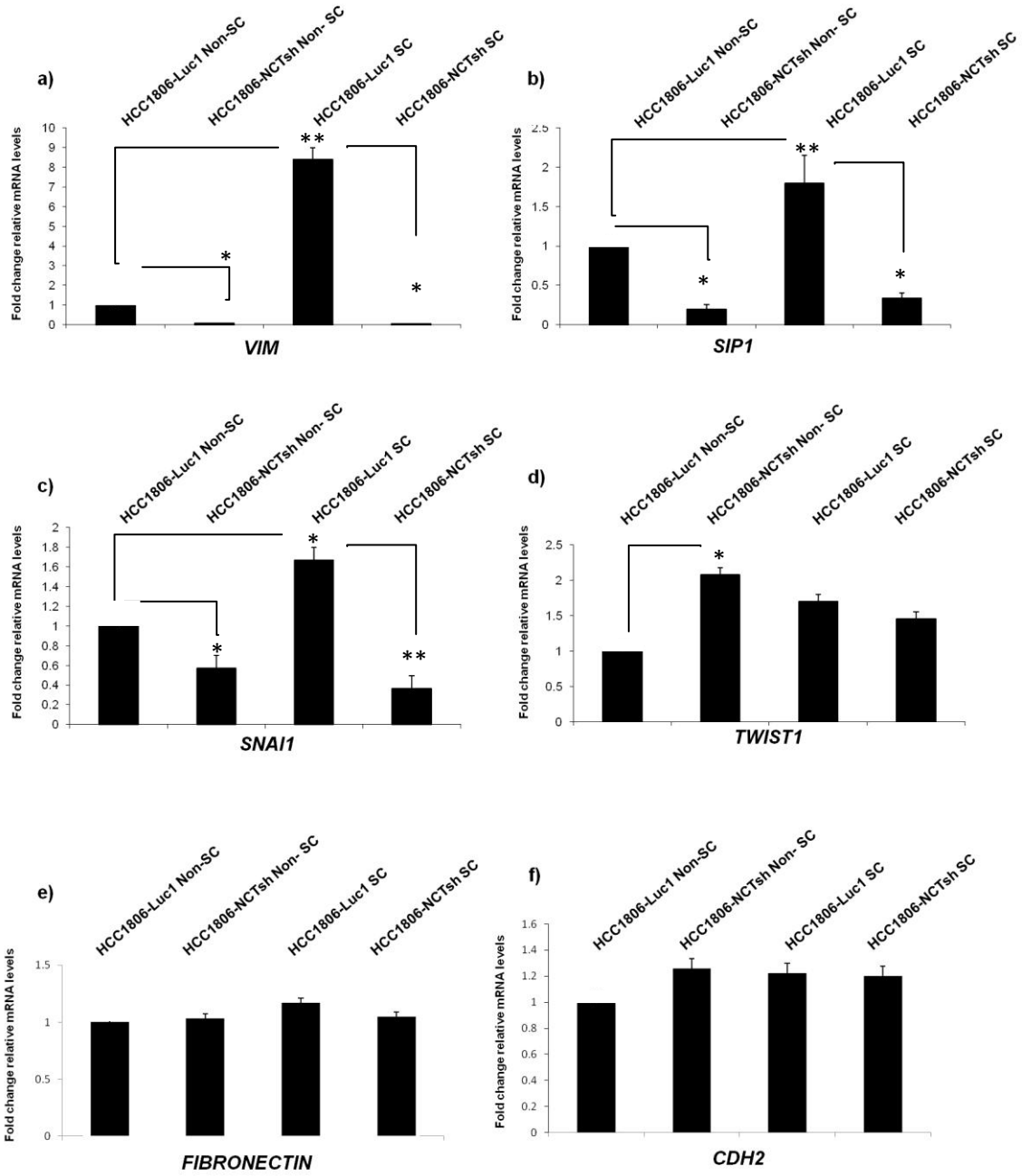


**Figure 37.Stable NCT depletion inhibits the expression proinvasive genes in non-SC and in the BCSC populations of HCC1806-Luc1 and HCC1806-NCTsh cells.** RT-qPCR depicting fold change mRNA levels of **a)** *Vimentin,* *p < 0.001 and **p = 1.84E-05. **b)** *SIP1,* *p = 0.0005 and **p = 2.11E-05. **c)** *Snail1* *p <0.01 and **p = 0.001. **d)** *Twist,* *p = 0.003. GAPDH was used for normalising. Error bars represent SEM of two individual experiments, each in duplicate.

### 4.2.6. The Human Extracellular Matrix and Adhesion Molecules PCR Array

Having demonstrated that stable nicastrin depletion inhibits proinvasive genes, we have next used HCC1806Luc-1 and HCC1806-NCTsh cells to perform a gene array that profiles the expression of 84 genes important for cell-cell adhesion and cell-matrix interactions. This array contained genes encoding for basement membrane constituents, collagens, and other genes defining extracellular matrix structure: integrins, selectins, cell-cell adhesion molecule family members (full gene list is included in Chapter 2).

Nine genes were upregulated in the HCC1806-NCTsh compared to HCC1806-Luc1 cells: *COL14A1*, *COL15A1*, *COL5A1*, *VCAN*, *ITGA4*, *ITGA7*, *ITGAL*, *LAMA1*, *VTN*. According to the analysis software, seven of these were ruled out due to a high threshold of detection (> 30 cycles), or variations between replicate wells. The two upregulated genes that passed the internal quality control were *COL14A1* and *ITGA4*, while the two downregulated genes were *ITGB2* and *SELL* (Table 6).

**Table 6.PAHS-013 cell-adhesion and cell-matrix gene array**

| **Genes Overexpressed in HCC1806-NCTsh vs. HCC1806-Luc1** | | | | |
|---|---|---|---|---|
| **Position on array plate** | **Gene Symbol** | **Fold Regulation** | **Comments** | **RT2 Catalog** |
| **A09** | COL14A1 | 4.2203 | OKAY | PPH02129B |
| **C08** | ITGA4 | 7.2858 | OKAY | PPH00659E |
| **Genes Under-Expressed in HCC1806-NCTsh vs. HCC1806-Luc1** | | | | |
| **Position on array plate** | **Gene Symbol** | **Fold Regulation** | **Comments** | **RT2 Catalog** |
| **D05** | ITGB2 | -5.967 | OKAY | PPH00679E |
| **F08** | SELL | -20.5478 | OKAY | PPH00677E |

The PCR Array PAHS-013 (Qiagen) consisted of a set of optimised real-time PCR primers on a 96-well plate. The array included built-in positive control elements for: i) proper data normalisation, ii) detection of genomic DNA contaminations; iii) quality of the mRNA samples. HCC1806-Luc1 and HCC1806-NCTsh cells were cultured and 1 x $10^6$ cells were lysed using the RNAlater (Qiagen), and mRNA was prepared. HCC1806-Luc1 and HCC1806-NCTsh cDNA was made using the RT² First Strand Kit (Qiagen, UK). RT² qPCR SYBR Green/ROX Master Mix was used in the reactions according to the manufacturer's protocol. The PCR Array Data Analysis Portal automatically performed the calculations and interpretation of the control wells, including thresh-hold cycle data from the real-time instrument. The RT² Profiler PCR Array Data Analysis Template v3.3 software was used. Calculations were based on the $\Delta\Delta C_t$ fold-change**.**

We have then validated *COL14A1*, *ITGA4* and *ITGB2* genes in an independent experiment (Figure 38). The *SELL* gene validation is pending. Collagen XIVA1 (*COL14A1*), upregulated 4-fold in NCT depleted cells, is a large extracellular matrix glycoprotein that associates with mature collagen fibrils. Frequent absence of COL14A1 is recorded in the vicinity of invading tumours, such as the Kaposi sarcoma and oral squamous cell carcinoma. This gene is often methylated and silenced in renal cancer (398). Integrin alpha 4 (*ITGA4*), upregulated 4-fold in HCC1806-NCTsh cells compared to control, is a cell surface integrin whose downregulation has been associated with tumour invasiveness (399), while expression of integrin beta 2 (*ITGB2)*, which was inhibited > 4-fold by the stable NCT knockdown, facilitates tumour cell migration. The *SELL* gene encodes the cell surface adhesion molecule L-selectin that belongs to a family of homing receptors. It is required for binding and subsequent rolling of leucocytes on endothelial cells, facilitating their migration into lymphoid organs and inflammation sites (400). It has been shown that experimental metastasis were significantly reduced in the absence of L-selectin (401).

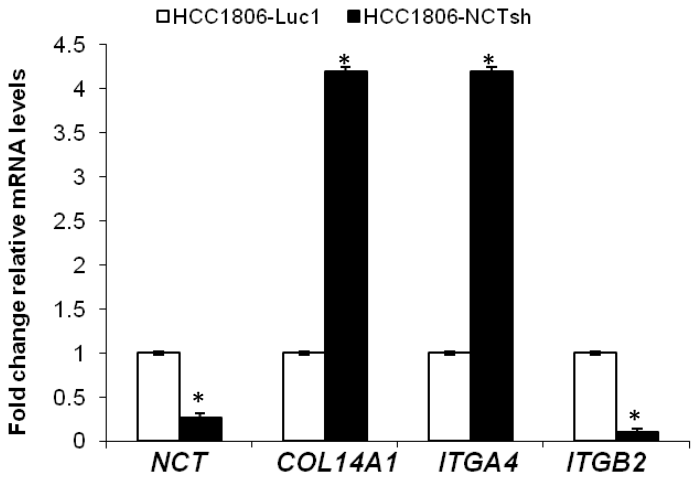


**Figure 38.Validation of the PAHS-013 gene array.** RT-qPCR confirming *NCT* knockdown in HCC1806-NCTsh cells as well as demonstrating the same trend and level of regulation of the cellular matrix and adhesion genes yielded as hits in the PAHS-013 gene array. *NCT*, *p = 0.0005; *COL14A1*, *p = 0.0004; *ITGA4*, *p = 0.0004; *ITGB2*, *p = 2.57E-05. GAPDH was used for normalising. Error bars represent SEM from two independent experiments, each in triplicate.

## 4.3. Identification of proteins affected by nicastrin silencing in MDA-MB-231 and HCC1806 cells using XP725 Profiler Antibody Array (Sigma)

Having demonstrated that both the transient and the stable nicastrin gene silencing result in inhibition of cell invasion and proliferation, we chose to perform an antibody array analysis in order to try and identify protein networks which are responsible for these effects upon nicastrin depletion in invasive breast cancer cells.

Protein arrays, for which antibodies are printed onto array surfaces, are designed to capture and measure the relative abundance of their cognate antigens in the applied samples (402). Protein profiles obtained by the antibody arrays, represent comprehensive means of analysing the signaling cellular proteome content and deriving information about the governing signaling cellular networks. A combination of complex changes involving multiple proteins is required for malignant transformation of normal cells. For this reason, profiling of the cancer-associated alterations requires simultaneous measurement of many proteins in a single sample (403). Investigation of the proteomic changes is also important since there is not always a direct correlation between the mRNA levels and protein expression. Furthermore, post-translational modifications, which cannot be detected at the mRNA level, may play an important role in the level of expression of the oncogenic proteins. Multiple studies so far have utilised antibody arrays to investigate protein expression profiles in breast cancer cells, conditioned media, or tumour infiltrating interstitial fluid, and have derived significant conclusions regarding:

- differential protein expression in malignant and adjacent normal breast tissue, such as a decrease in the protein 14-3-3e, and an increase in casein kinase Ie, annexin XI, CDC25C, eIF4E and MAP kinase 7 (404);
- association of IL-8 with the ERα negative status, vimentin expression and breast cancer invasiveness (405);
- identification of E-cadherin as an MDM2 interacting proteins targeted for proteasomal degradation in MDA-MB-453 breast cancer cell extracts, as a part of the MDM2-mediated promotion of cell adhesion disassembly (406);
- identification of the IL-8 and the growth related oncogen as a part of the HER2-induced cytokine signature in breast cancer (407);

- identification of the cytokine expression signature in the interstitial fluid that perfuses the tumour microenvironment: i) interleukins (IL-8, IL-10, IL-12, IL-13, IL-16); ii) growth factors (TGF-β1/2/3, TNF-α/β, VEGF, PDGF); iii) oncostatin M, monocyte chemo-attractant proteins 1-3, neurotrophins etc. (408);
- the proteins involved in the development of doxorubicin resistance in the MDA-MB-231 cell line model. A decrease in the expression of mitogen-activated protein kinase, cyclin D2, cytokeratin 18, cyclin B1, and heterogeneous nuclear ribonucleoprotein m3-m4 were associated with doxorubicin resistance (409).

Given that both the MDA-MB-231 and HCC1806 cells used in the antibody array represent the basal-like breast cancer subtype, we were able to compare the array outputs. This also allowed us to monitor the level of consistency of the NCT depletion-induced effects in two distinct triple negative breast cancer cell lines.

### 4.3.1. XP725 Profiler Array reveals NCT regulated signaling networks in MDA-MB-231 and HCC1806 breast cancer cells

MDA-MB-231 cells were treated with the Control and *NCT* siRNA for 72 h and the degree of NCT protein inhibition was confirmed by western blotting. HCC1806-Luc1 and HCC1806-NCTsh cells were cultured to 70-80% confluence and processed for protein extraction. Protein lysates from both cell lines (control and NCT depleted), were labeled with the Cy3 and Cy5 fluorochroms, respectively, and hybridised to the array platform (XP725 Profiler Array, Sigma). This array consisted of 725 monoclonal antibodies spotted in duplicate on the nitrocellulose membrane. The level of NCT knockdown in MDA-MB-231 cells treated with *NCT* siRNA and in HCC1806-NCTsh cells was confirmed by western blotting prior to proceeding with the hybridisation of the samples onto the antibody array slide (Figure 39).

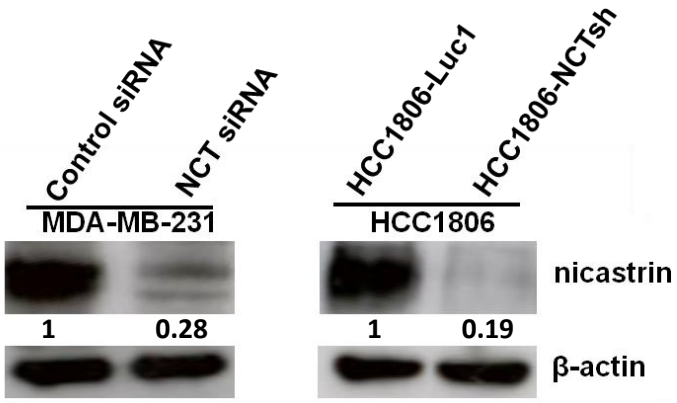


**Figure 39.Confirmation of nicastrin protein downregulation in the samples hybridised on the XP725 antibody array.** MDA-MB-231 cells were treated with *Control* siRNA and *NCT* siRNA for 72 h. HCC1806 cells were cultured to 70-80% confluence and harvested for protein lysis extraction. Western blotting was used to examine the level of nicastrin knockdown in both cell lines. β-actin was used as a loading control. The intensity of the bands was quantified using the Image J software. Numbers below the bands represent fold change compared to the control siRNA/shRNA samples, relative to the loading control.

The signal obtained from each spot of the scanned array slide was dependent on the abundance of the corresponding antigen in the applied sample, as well as on the quality/preservation of the individual spots. Nicastrin depletion affected expression of multiple proteins which participate in known cellular signaling pathways that regulate cancer cell proliferation, invasion and apoptosis. Most of the changes induced by transient *NCT* silencing in MDA-MB-231 cells were mirrored in the HCC1806-NCTsh, stable depleted cell line, to the same extent or to a higher degree (Table 7-10 and Annex 1)

### *4.3.1.4. Proinvasive proteins regulated by nicastrin silencing*

| Table 7. | Sigma | Fold Change | | p-value | |
|---|---|---|---|---|---|
| **Protein** | **Antibody ID** | **MDA231 NCTsi** | **HCC1806-NCTsh** | **MDA-MB-231** | **HCC1806-NCTsh** |
| **β-actin** | A1978 | 1.02 | 1.05 | | |
| **Myosin Ib Nuclear** | M3567 | -2.7 | -2.94 | 3.93E-05 | 0.0006 |
| **Myosin IIA** | M8064 | -2.42 | -2.22 | 5.16E-05 | 0.001 |
| **Myosin Light Chain Kinase** | M7905 | -2.04 | -2.56 | 8.78E-05 | 0.0009 |
| **Myosin Va** | M4812 | -2.94 | -3.22 | 1.70E-07 | 5.56E-06 |
| **Myosin VI** | M0691 | -2.94 | -3.125 | 9.61E-08 | 8.88E-06 |
| **Zip Kinase** | Z0134 | -4 | -6.67 | 1.91E-05 | 0.0003 |
| **Rsk1** | R5145 | -1.85 | -2.22 | 0.0008 | 0.0005 |
| **RhoE** | R6153 | 1.2 | 5.6 | 0.029 | 0.048 |
| **Smad4** | S3934 | -1.85 | -2.38 | 0.0001 | 0.001 |
| **Transforming Growth Factor-b pan** | T9429 | 5.5 | | 0.005 | |
| **Zyxin** | Z0377 | 2.5 | 4.5 | 5.21E-06 | 0.0009 |
| **FAK pTyr577** | F8926 | -3.44 | -8.33 | 2.55E-05 | 0.0002 |
| **Sp1** | S9809 | -3 | -3.33 | 3.08E-05 | 0.0005 |
| **Fas ligand** | F2051 | -2.56 | -3.44 | 1.40E-07 | 5.68E-06 |
| **cRaf pSer621** | R1151 | -4 | 7.14 | 1.94E-05 | 0.0002 |
| **Fibronectin** | F3648 | -2.38 | -3.57 | 0.008 | 0.003 |

Protein lysates of MDA-MB-231 cells treated with the *Control* and *NCT* siRNA for 72h, as well as lysates from HCC1806-Luc1 and HCC1806-NCTsh cells were prepared and extracts with protein concentrations ≥ 1.0 mg/ml were used for fluorescent labeling with Cy3 and Cy5 fluorochroms. Only samples with a dye-to-protein molar ratio >2 were applied to the antibody microarray. The hybridised antibody microarray slides were scanned using a GenePix Personal 4100A Microarray Scanner (Axon Instruments, Union City, CA) with 532 and 635 nm lasers. Primary analysis was done with the GenePix Pro (version 4.1) software package (Axon Instruments). Images of the scanned antibody microarrays were gridded and linked to a protein print list. Absent spots were flagged automatically by GenePix Pro; however, all spots were manually reviewed. The log ratios of Cy5 to Cy3 were determined for each spot to estimate the relative concentration of each protein. Values were normalised according to the manufacturer's protocol to the values of a chosen normalising protein, in this case β-actin. Only samples showing > 2-fold upregulation or downregulation in expression were deemed significant. This cut-off was selected as it has been used previously in antibody microarray experiments (410). Empty cells in the table reflect the undetected sample in a particular cell line. This may be due to loss of antibody activity by denaturation during printing or array storage or low levels of the respective antigen in the sample. The tables (Table 7-10) list the proteins that are up- or down-regulated by at least 2-fold in at least one of the cell lines used. Full antibody list: www.sigmaaldrich.com/etc/medialib/docs/Sigma-Aldrich/General_Information/xp725_ab_list.pdf

Myosins are a large family of structurally diverse actin-dependent molecules involved in cell migration through acto-myosin dynamics. Acto-myosin cytoskeleton has a fundamental role in the activation of migration and disassembly of cell-cell adhesions. Myosin IIa colocalises with metastasin-1 at the leading edge of cancer cells. Depletion of myosin IIA using siRNA impairs cancer cell migration (411). Upregulation of myosin Va by *Snail* is involved in cancer cell metastasis (412). Myosin VI is overexpressed in aggressive prostate and ovarian cancers. RNA-mediated myosin VI knockdown results in impaired *in vitro* migration (413). Myosin light chain kinase promotes transcellular intravasation of breast cancer cells through the underlying endothelial cells, facilitating invasion (414). Myosin light chain kinase is also responsible for high proliferative ability of breast cancer cells via the p38 pathway (415). All of the above myosin molecules were downregulated by NCT inhibition, suggesting that NCT could be regulating breast cancer cell motility/invasiveness through the network of myosin proteins.

The ZIP kinase, inhibited by NCT depletion, has an important function in cell motility and migration. It is necessary for the phosphorylation and the activity of myosin II, which is essential for maintaining acto-myosin contractility during cell motility. Attenuation of the ZIP kinase using siRNA in fibroblast cells results in the failure of stable myosin filament formation in stress fiber structure thus changing cytoskeletal structure and cell morphology, which inferrs decreased motility (416).

Small GTPase Rho signaling pathways underpin the motility of breast cancer cells during the invasive growth and metastasis (417). The RSK1 protein, which was downregulated by NCT depletion, drives p27 phosphorylation which promotes RhoA activity and increases cell motility (418). RhoE, upregulated by stable NCT knockdown, is an antagonist of the RhoA, and leads to the formation of highly sealed tight junctions in mammary epithelial tumour cells (419), and was upregulated by NCT inhibition. Smad4 is a signal transducer for TGF-β signaling. Smad4 inhibition, here observed upon NCT knockdown, inhibits TGF-β-induced EMT, and in MDA-MB-231 breast cancer xenograft models, *Smad4* siRNA strongly inhibits the frequency of bone metastasis (420).

Focal adhesions are actin-rich structures that enable cells to adhere to the extracellular matrix. Zyxin is a zinc-binding phospho-protein that concentrates at focal adhesions and along the actin cytoskeleton. It is important in the execution of the EMT program as it redistributes to points of cadherin-based adhesion at the end of individual actin cables in cells that have been induced to undergo EMT. So far it has been demonstrated that cells expressing zyxin fail to initiate EMT, and show significantly delayed scattering time (248 min) compared to zyxin knockdown cells (162 min) (421). It is intriguing that we observed an increase in zyxin protein levels in MDA-MB-231 (2.5-fold) and HCC1806 cells (4.5-fold) upon NCT knockdown, as zyxin-mediated effects appear to be a part of the mechanism of NCT depletion-mediated inhibition on EMT.

Cancer cell surface associated fibronectin induces secretion of MMPs by the extracellular matrix, a step which facilitates cancer cell invasion into the surrounding stroma (422). Nicastrin depletion reduces cancer cell-associated fibronectin levels, thereby proposing an additional mechanism for NCT siRNA induced reduction of breast cancer cell invasion.

Focal adhesion kinase (FAK) is an intracellular protein-tyrosine kinase that regulates formation and disassembly of cell-cell focal contacts, required for efficient cell movement. It acts as an integrator of cell motility-associated signaling events. FAK phosphorylation on tyrosine 577 is consistent with activation of Src signaling and is commonly linked to changes in cell motility. FAK-mediated cell invasion is associated with the accumulation of activated FAK (phosphorylated at Tyr-397, 576, and 577) in both growing and retracting lamellipodia and pseudopodia (423). Efficient inhibition of activated FAK is achieved by NCT depletion (3.4-fold in MDA-MB-231 and 8.3-fold in HCC1806 cells) in invasive breast cancer cells.

The transcriptional factor Sp1 plays an important role in invasion and metastasis of tumours. In breast cancer tissue *in vivo*, as well as in invasive MDA-MB-231 cells, Sp1 overexpression stimulates the proinvasive urokinase-type plasminogen activator and its receptor (424). An antibody array analysis also revealed that CDK4 was one of the interacting partners of Sp1, capable of inducing Sp1 mRNA levels (425). Concurrent decrease in CDK4 we have observed in the antibody microarray, may suggest a plausible mechanism of the Sp1 protein reduction upon NCT silencing. Furthermore, Sp1 positively regulates CD147 mRNA levels in lung cancer cells (426), a protein which is a reported

regulator of GS activity and one we have found downregulated in MDA-MB-231 breast cancer cell line by NCT siRNA. Therefore, reduction of Sp1 may be a causative factor in the CD147 reduction in MDA-MB-231 cells.

The Fas-ligand secreted by tumour cells binds to the Fas-receptors on T-cells which infiltrate the tumour stroma causing apoptosis of these immune effector cells as a means of cancer immune evasion (427). Fas-ligand expression in the primary tumour is considerably less frequent among breast cancer patients with bone metastases, compared to women without skeletal spread. Many treatments, like tamoxifen, lower the amount of the Fas-ligand, creating an immune permissive environment and facilitating killing of cancer cells by activated lymohocytes (428). NCT depletion could therefore be facilitating the cytotoxic effects of immune effector cells in a similar manner, as it also lowers Fas ligand protein levels.

#### *4.3.1.1. Cell-cycle and cell apoptosis regulating proteins affected by nicastrin silencing*

| Table 8. | Sigma | Fold Change | | p-value | |
|---|---|---|---|---|---|
| **Protein** | **Antibody ID** | **MDA231 NCTsi** | **HCC1806-NCTsh** | **MDA-MB-231** | **HCC1806-NCTsh** |
| **β-actin** | A1978 | 1.02 | 1.05 | | |
| **Bcl2** | B3170 | -1.47 | -2.02 | 0.0005 | 0.01 |
| **BclxL** | B9304 | -2.70 | -2.94 | 2.01E-07 | 1.03E-05 |
| **BID** | B4305 | -3.22 | -2.85 | 4.23E-05 | 8.60E-05 |
| **BUB1** | B0561 | 1.27 | 2.9 | 0.003 | 0.002 |
| **cMyc** | C3956 | -2.32 | -2.63 | 9.77E-05 | 0.0009 |
| **Cdk1** | C4973 | 1.6 | 4.00 | 0.006 | 0.01 |
| **Cdk4** | C8218 | -1.53 | -2.22 | 0.0003 | 0.001 |
| **DRAK1** | D1314 | -5 | -9 | 1.52E-05 | 0.0002 |
| **E2F1** | E8901 | -2.43 | -2.85 | 3.35E-05 | 0.0006 |
| **E2F2** | E8776 | -2.43 | -2.77 | 5.45E-05 | 0.0008 |
| **E2F4** | E8526 | -2.63 | -3 | 4.14E-05 | 0.0007 |
| **GADD153** | G6916 | -3 | -3.125 | 2.98E-05 | 0.0006 |
| **PUMA bbc3** | P4618 | -3 | -3.22 | 5.73E-07 | 1.12E-05 |
| **MTBP** | M3566 | -4.5 | -4.76 | 1.68E-05 | 0.0003 |

In both cell lines, the MDA-MB-231 and HCC1806, NCT inhibition affected the cellular apoptotic machinery, as demonstrated by a downregulation of the anti-apoptotic proteins Bcl-2 and Bcl-xl. These effects were more pronounced in the HCC1806 cells upon stable NCT inhibition. Bcl-2 is known to block programmed cell death in combination with its anti-apoptotic family member Bcl-xl, and pro-apoptotic Bad, Bax, and Bid proteins (429). We observed a downregulation of the pro-apoptotic protein Bid. The p53 upregulated modulator of apoptosis (PUMA) also known as Bcl-2-binding component 3 (bbc3), is a pro-apoptotic protein, member of the Bcl-2 protein family (430). The array detected a downregulation of PUMA bbc3 upon NCT silencing in both cell lines, which together with Bid downregulation, could potentially be acting as a negative feed-back mechanism in response to the pro-apoptotic stimuli inferred by NCT inhibition.

The MDM2 binding protein (MTBP) promotes MDM2-mediated ubiquitination and degradation of p53. Its effects have been studied in MCF-7 cells where transfection of the human MTBP results in the proteasomal degradation and inhibition of the p53 tumour suppressor (431). We demonstrates that NCT silencing induced inhibition of MTBP by > 4-fold, indicating that NCT could be promoting the p53-mediated tumour-suppressor functions in breast cancer cells via the MTBP-mediated regulation of p53 degradation.

Cyclin-dependent kinases (CDKs) are a family of protein kinases first discovered for their role in regulating the cell cycle. CDK4 is a genetically validated therapeutic target in cancer, and much efforts have been invested in developing selective CDK4 inhibitors as anti-cancer agents (432). Furthermore, a combination of a CDK4 inhibitor and a GSI (MRK-003) has significantly additive anti-tumourigenic effects in a T-ALL model, as the addition of a CDK4 inhibitor reduces MRK-003 $GI_{50}$ values by 6-8-fold (209). CDK1 activity in cancer cells reflects the activation state of the spindle assembly checkpoints and is required for execution of the chemotherapy-induced cancer cell death (433). Nicastrin inhibition induced a downregulation of the CDK4 by 2.2-fold and an upregulation of CDK1 by 4-fold in HCC1806-NCTsh cells, while the same trend was noted in MDA-MB-231 cells only to a lesser degree, indicating that CDKs may be important downstream effectors in of the NCT-mediated effects on cell survival.

Disturbed mitotic checkpoints are a common trait of many human cancers and can lead to chromosomal instability and aneuploidy, a feature present in over 90% of all solid tumours (434). One of the regulators of mitotic checkpoints is the Bub1 serine/threonine kinase, essential for preventing cell cycle progression into anaphase in the presence of spindle damage. Reduced expression of Bub1 has been identified in several human tumours such as colon, esophageal, gastric and breast cancer (435). Indications for possible Bub1 involvement in tumourigenesis also stem from animal experiments, where mice with reduced Bub1 expression show an increase in tumour susceptibility (436). Bub1 was upregulated 2.9-fold in response to stable NCT inhibition.

The E2F transcriptional factor proteins regulate the activity of promoters containing the E2F binding sites. E2F factors target the genes that regulate cell cycle progression. Mitogenic stimulation leads to activation of the E2F-dependent transcription and the S-phase entry (437). Low E2F1 transcript levels are a strong determinant of favorable breast cancer outcome (438), and expression of E2F4 in invasive breast carcinomas is associated with poor prognosis (439). Nicastrin inhibition led to a downregulation of E2F1, E2F2 and E2F4 by > 2-fold in both analysed cell lines. C-myc is a cellular proto-oncogene and known transcriptional target of Notch1 (123). It interacts with E2F transcription factors and CDKs in the regulation of cell cycle progression and programmed cell death (440). C-myc downregulation in cells leads inhibition of cell proliferation characterized by S phase delay. The observed downregulation of c-myc levels upon NCT silencing may be a Notch-mediated effect, as well as an effect mediated effect through E2F/CDK regulators.

The growth arrest and DNA damage inducible gene 153 (GADD153) is a transcription factor which belongs to the CCAAT/enhancer binding protein family (C/EBP family). The protein levels of C/EBP family members are significantly higher (15-times) in triple negative breast cancer tissue (441), while GADD153 mRNA levels are also increased in breast cancer tissue compared to normal breast (442). GADD153 overexpression alone is not sufficient to induce tumourigenesis but it does induce cancer cell hyperplasia, rendering the cells vulnerable to further oncogenic hits (441). GADD153 protein levels were reduced > 3-fold by the NCT knockdown.

The death-associated protein kinase (DRAK1), downregulated by NCT silencing in MDA-MB-231 and HCC1806 cells, is a serine/threonine kinase which is a positive mediator of programmed cell death through its catalytic activity (443). In an *in vivo* experimental lung cancer model, the overexpression of DAP kinase sensitises cancer cells to apoptotic stimuli and inhibits metastatic progression, providing a mechanism that links apoptosis to metastasis (444). The mechanism of DRAK1 downregulation upon NTC silencing in breast cancer cells remains unknown, however, we anticipate that this may be a cellular mechanism of resistance to anti-proliferative and anti-invasive effects of NCT inhibition.

#### *4.3.1.2. Histon deacetylases affected by nicastrin silencing*

| Table 9. | Sigma | Fold Change | | p-value | |
|---|---|---|---|---|---|
| **Protein** | **Antibody ID** | **MDA231 NCTsi** | **HCC1806-NCTsh** | **MDA-MB-231** | **HCC1806-NCTsh** |
| **β-actin** | A1978 | 1.02 | 1.05 | | |
| **HDAC3** | H6537 | -2.7 | -3 | 0.0006 | 0.007 |
| **HDAC4** | H9411 | -2.12 | -2.56 | 1.03E-06 | 5.41E-05 |
| **HDAC10** | H3413 | -2.56 | -2.5 | 4.28E-05 | 0.0009 |

Classical histone deacetylases (HDACs) are a class of enzymes that remove acetyl groups from an ε-N-acetyl lysine amino acid on a histone, and are a promising novel class of anti-cancer drug targets. First HDAC inhibitors have been evaluated in clinical trials and showed activity against several cancer types. HDAC1 knockdown causes cell cycle arrest, growth inhibition and apoptosis. HDAC3 inhibition induces expression of differentiation genes and disrupts the cell cycle. HDAC4 is upregulated in breast cancer compared with renal, bladder, colorectal cancer, and its knockdown inhibits expression and functional activity of HIF-1α. HDAC10 knockdown down-regulates VEGFR (445). Nicastrin inhibition causes a reduction of HDAC3/4/10 protein levels by ≥ 2.5-fold, suggesting that its effects on gene transcription may be executed via this group of transcriptional regulators.

### *4.3.1.5. Oncogenic pathways affected by nicastrin silencing*

| Table 10. | Sigma | Fold Change | | p-value | |
|---|---|---|---|---|---|
| **Protein** | **Antibody ID** | **MDA231 NCTsi** | **HCC1806-NCTsh** | **MDA-MB-231** | **HCC1806-NCTsh** |
| **β-actin** | A1978 | 1.02 | 1.05 | | |
| **MAP Kinase Erk1/Erk2** | M5670 | -1.85 | -2.38 | 0.0001 | 0.001 |
| **MAP Kinase Kinase MEK** | M5795 | -2 | -2.08 | 9.98E-05 | 0.001 |
| **JAB1** | J3020 | -2.94 | -3.125 | 0.0002 | 0.001 |
| **Protein Kinase Ca** | P4334 | -2.04 | -2.22 | 8.85E-05 | 0.001 |
| **Protein Kinase Cb2** | P3203 | -3.125 | -3.22 | 2.97E-05 | 0.0005 |
| **Protein Kinase Cd** | P8333 | -2.27 | -2.7 | 6.38E-05 | 0.0007 |
| **Protein Kinase C** | P0713 | -2.04 | -2.63 | 7.09E-07 | 1.32E-05 |
| **cRaf pSer621** | R1151 | -4 | 7.14 | 1.94E-05 | 0.0002 |
| **S6 Kinase** | S4047 | -1.96 | -2.63 | 9.76E-05 | 0.0008 |
| **mTOR** | T2949 | -2.49 | -2.94 | 4.57E-05 | 0.0006 |
| **Nicastrin** | N1660 | -1.67 | -1.42 | 0.0002 | 0.01 |
| **Presenilin 1** | P7854 | -1.49 | -1.44 | 0.0002 | 0.0005 |
| **Notch1** | N6786 | -1.47 | 1.1 | 0.0006 | 0.97 |
| **p21WAF1Cip1** | P1484 | -2.56 | -2.7 | 4.10E-05 | 0.0007 |

Protein kinase C (PKC) family consists of at least 12 serine-threonine kinases with an established oncogenic potential. Most common iso-enzymes displaying altered expression during cancer progression are PKC-a, -b and -d (446). The fact that PKC inhibition prevents Notch1 upregulation (447), and that NCT downregulation in MDA-MB-231 and HCC1806 cells acts as a negative regulator of PKC isoforms expression, proposes a complex bi-directional cross-talk between the GS and the PKC.

The c-Jun activation domain-binding protein-1 (JAB-1) is is a direct target of the EGFR signaling in ERα negative breast cancer cells. MDA-MB-231 and HCC1806 cells are representative of the triple negative breast cancer where the EGFR pathway is active (448). We have previously shown that NCT depletion in HCC1806 cells reduces protein levels of EGFR, and JAB1 downregulation may be a confirmation that the downstream effects of the EGFR pathway are equally inactivated upon NCT silencing.

The MAP kinase cascade is a critical signal transduction pathway in transmitting extracellular signals to the nucleus. The fact that we have observed downregulation of active MAPK on the antibody array (MEK and ERK1/2), corroborated our previous observation that

NCT inhibition interferes with the ERK1/2 activation. We have previously noted as well that NCT silencing inhibits the Akt phosphorylation at Ser473 residue. The array revealed that an important down-stream effector of both the Akt and the MAPK pathways, the S6 kinase (449), was downregulated by NCT depletion.

The Raf proteins provide a link between Ras/MAPK signaling and ERK activation. Direct binding of Raf to active Ras (Ras-GTP) results in c-Raf recruitment to the plasma membrane. Phosphorylation of c-Raf at residue Ser621 occurs at the plasma membrane and appears to be essential for c-Raf activation (450, 451). The array has indicated that transient NCT silencing in MDA-MB-231 cells inhibited c-Raf, which is consistent with the inhibition of the MAPK/ERK cascade, while in stably depleted cells its phoshorylation is increased, potentially acting to compensate the inhibition of the MAPK pathway inferred by chronic NCT depletion.

Mammalian target of rapamycin (mTOR) pathway was downregulated > 2.4 fold in both cell lines upon NCT ablation. mTOR is a direct target of the activated Akt pathway, which is attenuated upon NCT silencing. Attenuation of Notch signaling in breast cancer cells has been shown to inhibit the PI3K/Akt-mTOR axis (383). Furthermore, MCF-7 cells exhibiting aberrant Notch activity display resistance to chemotherapy due to mTOR pathway hyperactivation, which can be reversed by an mTOR inhibitor (385). Therefore, the effects we have observed on the Akt/mTOR are a likely Notch-mediated effect.

Interestingly, the degree of NCT inhibition we have detected by western blotting was higher than the one reflected on the array. Also, our data have shown that Notch1-ICD was significantly reduced in both cell lines upon NCT silencing, which was bearly observed in the MDA-MB-231 cells and absent in the HCC1806 set (Table 10). This may reflect the different antibodies used. We have performed western blotting using an antibody specifically raised against the cleaved Notch1 at Val1744 residue, while the Sigma N6786 antibody recognises both the full-length and the cleaved Notch1, the difference in the gel mobility of which (300 kDa and 110 kDa, respectively) cannot be reflected on the array spot. Furthermore, we have shown that NCT silencing in MDA-MB-231 and HCC1806 cells induces p21 upregulation. The array produced an opposite result. All these differences and inconsistencies observed may also reflect technical issues (hybridisation efficacy, scanning, spot preservation) with the particular areas on the platform.

Furthermore, greater reliability of the array data may be obtained if the array is repeated with inclusion of the 'dye-swapping' step, which entails alternative labeling of the samples with Cy3 and Cy5. Each protein sample is labeled with each dye and respective pairs are hybridised onto two separate array slides per cell line. Both slides for each cell line are scanned and the ratio of the two dye signals is calculated and compared for each antibody-antigen pair (404).

## 4.4. Discussion

In this chapter we have analysed the effects of stable NCT depletion in the triple negative, basal-like, HCC1806 breast cancer cell line. As in the context of transient NCT silencing using siRNA in MDA-MB-231 cells, stable NCT knockdown in HCC1806 cells resulted in the disruption of the GS enzyme complex and activity. Namely, protein levels of PS1, Aph-1 and PEN2 were reduced, with concurrent decrease in the cleaved Notch1 protein. This result confirms the relevance of NCT in maintaining the stability and functionality of the GS in breast cancer cells. Furthermore, the Akt pathway downstream of NCT/Notch was attenuated. As in MDA-MB-231 cells, NCT silencing resulted in a marked reduction of vimentin protein levels and cell invasion capacity. In terms of the functional effects, and extending the characterisation of the HCC1806-NCTsh cells, originally generated by the group of Prof. M Loren (USA), we have shown that NCT stable depletion induced a slower turnover rate of HCC1806 cells. We have shown that the proliferation marker Ki67 was markedly downregulated in HCC1806-NCTsh cels compared to the NCT expressing counterpart, which is line with the observed slower proliferation of HCC1806-NCTsh cells. Although a comparable percentage of cells was identified in the S-phase, in both the HCC1806-Luc1 and HCC1806-NCTsh cells in the work of Dong et al.(164), the reduced rate of cell division may be caused by slower S-phase progression in HCC1806-NCTsh cells. In order to address this issue in the future experiments, the rate of cell proliferation, calculated from the bi-variate BrdU/DNA flow cytometric data will be evaluated, in order to estimate the S-phase duration (377).

Given the importance that has been attributed to the Notch signaling in maintaining and perpetuating the population cancer stem cells (110, 176), and in view of the fact that NCT depletion markedly inhibited active Notch1 in HCC1806 cells, we decided to extend our

research efforts into investigating whether NCT depletion affected breast cancer stem cells. In order to achieve this, we performed cell sorting using the CD44 and CD24 as markers of the cancer stem cell phenotype, in both the HCC1806-Luc1 and HCC1806-NCTsh cells. This experiment was previously not performed in MDA-MB-231 cells, as the context of transient NCT silencing by means of siRNA represented a disadvantageous setting where the full extent of prolonged, stable NCT depletion would not be appreciated. Cell population baring the $CD44^{+}/CD24^{-}$ phenotype from either cell line was considered to be enriched for breast cancer stem cells. The mammosphere forming experiment evaluated the capability of stem cells from HCC1806-Luc1 and HCC1806-NCTsh cells to form proliferative sphere structures in anchorage independent growth conditions, a characteristic inherent for cells with stem cell-like properties. Indeed, NCT inhibition reduced the mammosphere formation efficacy, indicating that NCT may be relevant for breast cancer stem cell propagation. This effect may be mediated through NCT regulation of Notch, as we have further shown that NCT depletion inhibits protein levels of active Notch4, which is primarily responsible for Notch-induced propagation of breast cancer stem cells *in vitro* and *in vivo* (176). In further support of the fact that inhibition of NCT may act to suppress breast cancer stem cells, and considering that cancer cells acquire 'stemness' features through EMT transformation (90), we observed a marked downregulation of the *bone fide* EMT promoter genes (*Vimentin*, *SIP1*, *SNAIL*) in HCC1806-NCTsh stem cells compared to the NCT expressing counterpart.

Finally, in this chapter, we presented data from the protein array we performed to investigate the global effects of NCT silencing on the proteome of MDA-MB-231 and HCC1806 cells. In our hands, the protein array has proven to be a research tool which does not yield highly consistent results when compared to western blotting. However, some of the data obtained from this protein array are intriguing, and if validated by western blotting will represent important information about NCT downstream pathways, which may be involved in regulating cell invasion and proliferation. As a priority, we will focus on validating the observed changes in the protein levels of the myosin family members (myosin Ib, II, Va, VI, and myosin light chain), which are required for the acto-myosin contractility and cancer cell motility/invasion (452). Validation of the data would enable us to gain further insight into the mechanism(s) by which NCT could be regulating cell motility and invasion.

.

# CHAPTER 5

# Results

## Comparison of nicastrin silencing and Notch receptor silencing effects on gene expression in MDA-MB-231 cells

## 5.1. Nicastrin regulates a Notch independent gene set in MDA-MB-231 cells

In order to determine to which extent the effects of NCT silencing are mediated through the GS/Notch-dependent signaling, we developed a collaboration with Prof. L. Miele (University of Mississippi Cancer Institute, USA), and conducted a gene array screen comparing the effect of NCT depletion in MDA-MB-231 cells with the changes inferred by the treatment of MDA-MB-231 cells with the siRNA of individual Notch receptors.

In our laboratory, we have treated MDA-MB-231 cells with *NCT* siRNA and *NCT* knockdown was validated by RT-qPCR. In order to compare and contrast the global gene changes induced by NCT downregulation vs. those induced by gene silencing of Notch receptors, the group of Prof. L. Miele have treated the same cell line with individual siRNAs for Notch1, Notch2 and Notch4. The mRNA from all samples, run in biological duplicates, was reverse transcribed and hybridised to an Affymetrix 2.0 platform. The array was performed by the Northwestern University Genomics Core Facility in Chicago, USA.

Data analysis has thus far been been completed for 387 genes from the Affymetrix gene array, and encompasses genes that are predominantly regulated by either *NCT* siRNA or *Notch2* siRNA. Genes up- or downregulated by $\geq$ 2-fold were considered significantly affected by either type of treatment. Results have shown that: i) 56.9% (n = 220) genes were not affected by *Notch1/2/4* siRNA or *NCT* siRNA; ii) 16.5% (n = 64) genes were regulated only by NCT siRNA (Table 11), while 16.5% (n = 64) genes were regulated by *Notch2* siRNA only; iii) 10.1% (n = 39) were shared between *Notch2* siRNA and *NCT* siRNA (Figure 40, Annex 2). This 387 of analysed genes did not contain genes affected by *Notch1/4* siRNA or genes shared between all Notch receptors and NCT. The analysis of those genes is pending and will undoubtedly reveal more intriguing results. While keeping in mind that the Affymetrix gene array analysis is still incomplete, the results analyses to date suggest that NCT regulates a subset of genes that are not modulated by Notch, and/or that there are context-dependent GS enzyme activities, which are defined by distinct affinities to different Notch receptors.

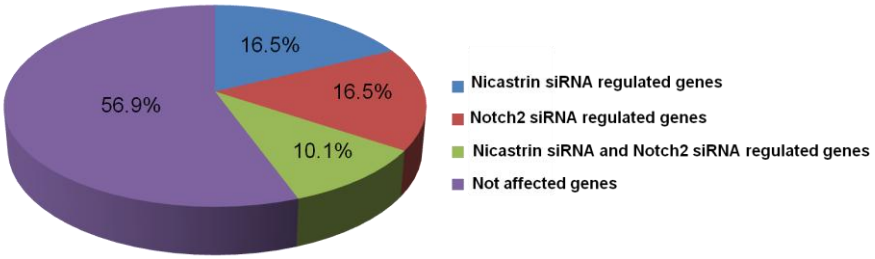


**Figure 40.Pie chart depicting the percentages of genes regulated by NCT siRNA and Notch siRNA in MDA-MB-231 cells.** Data analysis has been completed for the 387 genes from the Affymetrix gene array. Regulation by ± 2-fold was considered significant. 56.9% (n = 220) genes were not affected by *Notch1/2/4* siRNA or *NCT* siRNA. 16.5% (n = 64) genes were regulated by *Notch2* siRNA only, while 16.5% (n = 64) genes were regulated only by *NCT* siRNA. 10.1% (n = 39) were regulated by both *Notch2* siRNA and *NCT* siRNA.

**Table 11.Genes exclusively regulated by *NCT* siRNA**

| | | Fold Change | | | | |
|---|---|---|---|---|---|---|
| **Gene Symbol** | **Gene Discription** | **Notch1 siRNA** | **Notch2 siRNA** | **Notch4 siRNA** | **NCT siRNA** | **p-value NCTsiRNA vs. ControlsiRNA** |
| **MT2A** | metallothionein 2A | -1.97 | -3.02 | -1.04 | **2.94** | 0.00029 |
| **IL10RB** | interleukin 10 receptor, beta | -1.46 | -1.61 | -1.13 | **-2.37** | 3.84E-05 |
| **PHLDA1** | pleckstrin homology-like domain | -1.42 | -2.50 | 1.11 | **2.86** | 2.54E-07 |
| **ASNS** | asparagine synthetase | 1.41 | 2.46 | -1.04 | **6.20** | 7.86E-07 |
| **CST4** | cystatin S | -1.35 | -1.59 | -1.42 | **8.13** | 1.82E-09 |
| **E2F2** | E2F transcription factor 2 | -1.34 | 1.50 | -1.32 | **-2.06** | 9.61E-06 |
| **MGLL** | monoglyceride lipase | 1.34 | 1.61 | 1.09 | **4.28** | 3.92E-08 |
| **MT1X** | metallothionein 1X | -1.33 | -5.76 | 1.25 | **2.42** | 0.00016 |
| **BUB1** | budding uninhibited by benzimidazoles 1 | -1.28 | 1.78 | 1.06 | **-2.16** | 0.00067 |
| **KHDRBS3** | KH domain RNA binding signal transduction associated 3 | -1.22 | 1.55 | -1.13 | **10.15** | 5.76E-09 |
| **EIF4E2** | eukaryotic translation initiation factor 4E | 1.21 | -1.70 | -1.03 | **-2.01** | 1.74E-06 |
| **SPANXA1** | sperm protein associated X-linked A1 | 1.17 | -1.55 | 1.16 | **12.54** | 9.71E-12 |
| **TUBB2A** | tubulin, beta 2A | -1.16 | -1.94 | -1.03 | **-2.00** | 0.00509 |
| **AKR1B1** | aldo-keto reductase family 1, member B1 | -1.15 | 1.81 | -1.07 | **-3.19** | 3.74E-05 |
| **ID2** | inhibitor of DNA binding 2, dominant negative helix-loop-helix protein | 1.09 | -1.66 | 1.54 | **-2.68** | 0.00068 |
| **GNG11** | guanine nucleotide binding gamma 11 | 1.08 | -1.66 | -1.27 | **-3.98** | 1.65E-08 |
| **UBE2T** | ubiquitin-conjugating enzyme E2T | -1.05 | -1.75 | -1.18 | **-3.19** | 2.69E-07 |
| **ARHGDIB** | Rho GDP dissociation inhibitor (GDI) beta | 1.05 | 1.96 | 1.26 | **2.39** | 2.43E-06 |
| **SPANXB2** | SPANX family, member B2 | -1.02 | -1.32 | -1.04 | **8.03** | 2.86E-10 |

**Array experiment**.MDA-MB-231 cells were treated with *Control* and *NCT* siRNA for 72h. mRNA was sent to Prof Lucio Miele, USA, where their own MDA-MB-231 cells were treated with the Notch siRNAs. Values represent fold change between NCT siRNA and Control siRNA; and Notch siRNAs vs. respective controls. The four types of treatment were therefore not normalised to the same control siRNA, and direct comparisons between the two types of treatment have to be validated, due to the fact that although the same cell line was used, the MDA-MB-231 cells did not originate from the same laboratory.

### 5.1.1. Common genes affected by NCT siRNA and a gamma-secretase inhibitor

In addition to comparing the effects induced by *NCT* siRNA with the individual Notch receptor silencing, we also obtained information about the common genes regulated by NCT siRNA and a clinically tested GSI (Merck). The array performed by the group of Prof. L. Miele identified an 18-gene signature characteristic for the GSI-MRK0752 treatment in MDA-MB-231 cells. The GSI used was not an aldehyde peptide and it had no proteasome inhibitory activity. Of these 18 genes, 13 were also affected by *NCT* siRNA in the same direction (Table 12). The remaining 5 genes were only affected by the GSI, and hence represent information proprietary to our collaborators. At present, we do not possess information about the genes differentially regulated between the NCT silencing and GSI treatment. Therefore, the data obtained thus far comparing NCT siRNA and GSI effects in MDA-MB-231 cells is limited, and precludes arriving to a conclusion that NCT siRNA regulates a distinct set of genes compared to the GSI. Interestingly, both treatments induced a potent downregulation of the *ABCA1* gene, which encodes a multi-drug resistant protein, i.e. a membrane pump which mediates efflux of anti-cancer drugs. This suggests that targeting the GS enzyme via a GSI or NCT inhibition may facilitate overcoming resistance to certain types of cancer therapeutics. The effect of silencing *NCT* was even more profound than that of the GSI on some of the genes in the signature, e.g. on an FGF antagonist *SPRY1* (upregulated 4.75-fold upon NCT siRNA vs. 1.73-fold upon GSI treatment) and *ANXA8L2* (downregulated 3.19-fold vs. 1.54-fold).

**Table 12.Genes regulated by GSI and *NCT* siRNA**

| Gene Symbol | Gene Description | NCT siRNA | GSI | p-value |
|---|---|---|---|---|
| **ABCA1** | ATP-binding cassette, sub-family A member 1 | -3.3 | -7.06 | 9.24E-08 |
| **SC4MOL** | sterol-C4-methyl oxidase-like | 2.14 | 2.79 | 3.73E-06 |
| **IL6** | interleukin 6 (interferon, beta 2) | -1.87 | -2.13 | 1.28E-05 |
| **SQLE** | squalene epoxidase | 1.79 | 2.26 | 3.41E-05 |
| **EPAS1** | endothelial PAS domain protein 1 | 1.34 | -2.07 | 1.01E-05 |
| **TNFSF10** | tumour necrosis factor (ligand) superfamily 10 | -3.00 | -2.02 | 6.33E-06 |
| **MCM4** | minichromosome maintenance complex 4 | -1.43 | -1.87 | 1.70E-05 |
| **HNRNPAB** | heterogeneous nuclear ribonucleoprotein A/B | -1.55 | -1.8 | 3.68E-05 |
| **SPRY1** | sprouty homolog 1, antagonist of FGF signaling | 4.75 | 1.73 | 1.80E-05 |
| **ELOVL6** | ELOVL family member 6 | -1.53 | 1.61 | 1.40E-05 |
| **DCTPP1** | dCTP pyrophosphatase 1 | -1.93 | -1.56 | 2.24E-05 |
| **ANXA8L2** | annexin A8-like 2 | -3.19 | -1.54 | 1.78E-05 |
| **C5orf41** | chromosome 5 open reading frame 41 | 2.34 | 1.51 | 2.86E-05 |

The *ABCA1* multidrug resistance gene encodes the ATP hydrolysing cellular transporter, which is able to export a wide variety of natural and synthetic compounds from the cells (453). Drug resistance is a major obstacle in achieving the response to chemotherapy and ABCA1 is often overexpressed in many human malignancies, including breast cancer, representing a causal factor of resistance to apoptosis-inducing agents (454, 455). *ABCA1* was downregulated by the NCT siRNA and GSI by 3.3- and 7-fold, respectively.

*TNFSF10* (TRAIL) is a p53-transcriptional target gene, which activates Caspase 8 via the death receptor DR5. It could be a mediator of apoptosis induced by GSI and/or NCT knockdown (456). The protein encoded by the gene is the tumour necrosis factor-related apoptosis-inducing ligand (457). Impairment of the TRAIL-mediated apoptotic pathway contributes to oncogenesis by promoting survival of cells that could accumulate severe chromosomal alterations (458). *TNFSF10* was downregulated by the NCT siRNA and GSI by 3- and 2-fold, respectively.

Microarray studies have linked annexin A8 (*ANXA8L2*) mRNA expression to a ‘basal cell-like’ subset of breast cancers. High expression of this gene in invasive breast carcinomas was shown to have has a significant adverse effect on disease-free and overall survival (459). *ANXA8L2* was downregulated by the NCT siRNA and GSI by 3.19- and 1.54-fold, respectively.

Sprouty (*SPRY*) is a negative regulator of the fibroblast growth factor (FGF) pathway signaling. Sprouty binds to, and displaces Shp2 from FRS2 and Grb2, preventing subsequent activation of Ras and Raf pathways, resulting in the net inhibition of the MAPK/ERK2 activation (460). A majority of breast cancers (~80 %) show a downregulation of *SPRY1* and *SPRY2* mRNA levels (461). *SPRY1* was upregulated by the NCT siRNA and GSI by 4.75- and 1.73-fold, respectively.

### 5.3.2 Validation of gene array data

In order to validate our gene array data, we repeated the *NCT* siRNA treatment of MDA-MB-231 cells and performed RT-q-PCR analysis for the chosen genes. We also performed RT-q-PCR analysis in the stably depleted HCC1806-NCTsh cell line, in order to investigate if the effects of *NCT* silencing are reproducible in another cell line which represents the basal B like breast cancer. Furthermore, we anticipated that some of the genes may be more profoundly affected in the conditions of the stable, rather than the transient NCT depletion (Figure 41).

Even though the degree of *NCT* silencing was comparable to that of the samples used for the Affymetrix array, from the genes we have attempted to validate thus far, we were not able to reproduce the effects on *SPRY1* and *CTGF* genes upon *NCT* inhibition in MDA-MB-231 cells (Figure 41a). However the effect was observed in the HCC1806-NCTsh cell line, where NCT depletion induced an 8.5-fold increase in *SPRY1* and a 13.5-fold increase in *CTGF* gene levels compared to HCC1806-Luc1 (Figure 41b). Effects on *CST4, TNFSF10* and *SPANXB2* were validated in the MDA-MB-231 cells. *CST4* was also not regulated by NCT depletion in HCC1806-NCTsh cells. Failure to reproduce some of the array data may be due to the difference between the probes used in the gene array vs. primers used for the RT-qPCR experiment. Also there are reported splice variants of the *SPRY1* gene (462) and single nucleotide polymorphisms of the *CTGF* (www.ensembl.org), which if present in any of our cell lines, coupled with the differences in primers we used and probes used on the gene array, may have been the cause of failure to detect the same degree of regulation as achieved by the array probes. Design of alternate primer sets for the genes in question will be conducted in order to address this hypothesis.

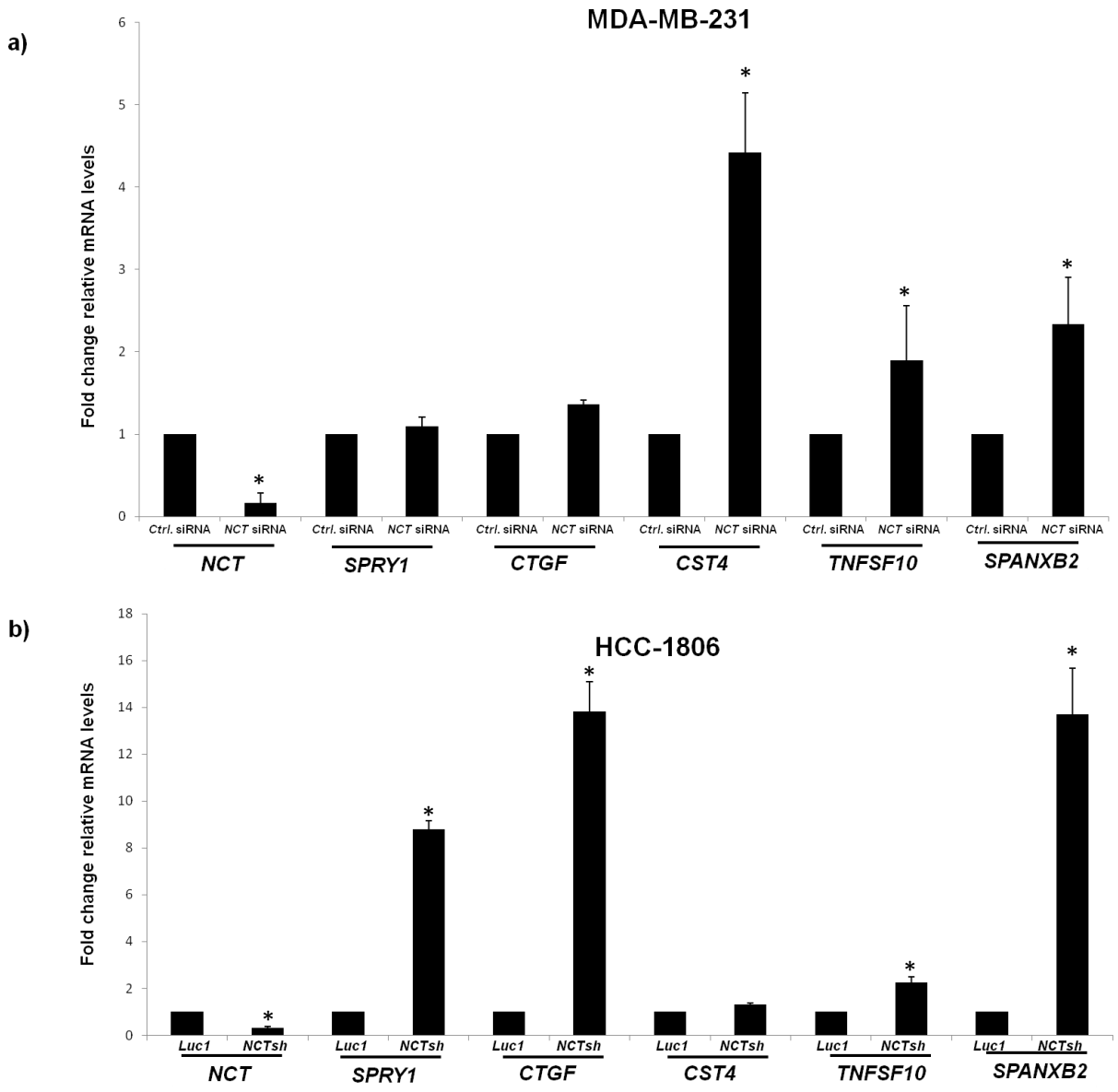


**Figure 41.RT-qPCR validation of the Affymetrix gene array in MDA-MB-231 and HCC1806 cells. Fold change of relative mRNA levels of *NCT, SPRY1, CTGF, CST4, TNFSF10* and *SPANXB2* is shown. a)** MDA-MB-231 cells were transfected with the *Control* and *NCT* siRNA at 40 nmol concentration and after 72 h cells were harvested for mRNA extraction. Bars represent mean value of the mRNA fold-change ± SEM from three separate experiments, each in triplicate. GAPDH was used for normalising. *NCT*, *p = 0.0002*; SPRY1*, *p = 0.35*; CTGF*, *p = 9.88E-05; *CST4*, *p = 0.001; *TNFSF10*, *p = 0.036 and *SPANXB2*, *p = 0.015; **b)** HCC1806-Luc1 and HCC1806-NCTsh cells were cultured to 70-80 % confluence and harvested for mRNA extraction**.** Bars represent mean value of the mRNA fold-change ± SEM from three separate experiments, each in triplicate. GAPDH was used for normalising. *NCT*, *p = 0.003*; SPRY1*, *p = 0.001*; CTGF*, *p = 0.005*; CST4*, *p = 0.02*; TNFSF10*, *p = 0.02 and *SPANXB2*, *p = 0.001.

## 5.4. Discussion

We have employed gene array analysis as a tool to investigate global transcriptome changes in MDA-MB-231 cells upon transient NCT silencing. Furthermore, we sought to compare the effects of the nicastrin knockdown to that induced by a gamma-secretase inhibitor and silencing of individual Notch receptors. Although the array analyses are not fully complete, the data obtained thus far indicate that NCT may regulate a subset of genes which are not affected by Notch receptors.

*SPANXA1* and *SPANXB2* are cancer/testis-associated genes, which are located in a cluster on chromosome X. They are not only expressed in the germ cells, but also in a number of tumours (463). Overexpression of Fra-2 (a Fos-related AP1 transcription factor that is implicated in progression of cancer) in MCF-7 cells, promotes cancer cell invasion, an effect accompanied by a substantial, 4.75-fold reduction of the SPANX genes (464). *NCT* siRNA induces an increased in SPANXA1 and SPANXB2 by 12.5- and 8-fold, respectively.

Guanine nucleotide binding protein gamma 11 gene (*GNG11*) expression has been identified as one of the markers of the EMT and a gene whose expression correlates with the basal B subtype of breast cancer (54). *NCT* siRNA inhibited *GNG11* by 3.9-fold.

Non-muscle myosin II-B (*MYH10*) plays a major role in cell motility by regulating the retraction phase of the migratory cycle. Downregulation of *MYH10* in human malignancies counteracts invasion of cancer cells (465). NCT siRNA downregulated the expression of the *MYH10* gene by 2.4-fold.

Connective tissue growth factor (*CTGF*) expression is associated with tumour development and progression. There is growing body of evidence that CTGF may regulate cancer cell migration, invasion, angiogenesis, and anoikis. Furthermore, CTGF expression is positively correlated with the basal B subtype of breast cancer and is considered an EMT promoting gene (54), as well as a factor facilitating bone metastasis in breast cancer (466). *NCT* siRNA upregulated CTGF expression by 3.5-fold (Annex 2), potentially reflecting a compensatory cellular mechanism against the anti-invasive effects induced by the *NCT* silencing.

The Rho GDP dissociation inhibitor beta (D4-GDI/*ARHGDIB*) is a member of a major class of RhoGTPase regulators, RhoGDIs. RhoGDIs have a cell context dependent role in either inhibiting Rho activities by retaining Rho effectors in their inactive form (467), or promoting their function by facilitating cellular transport to the plasma membrane (468). D4-GDI has 78% homology to other Rho-GDIs. It binds and inhibits Rac2 in cells via its N-terminal domain. It has been identified as a metastasis suppressor gene in bladder cancer. With regards to the expression and role of D4-GDI in breast cancer, the data is conflicting (468). In breast cancer, its expression is higher in invasive MDA-MB-231 than in the non-invasive MCF-7 cells, however its knockdown has no effect on cellular invasive capacity. It is therefore proposed that its role in inhibiting or promoting Rho activity may be dependent on the stage of cancer progression, as well as cancer type. *NCT* siRNA increased *ARHGDIB* expression by 2.4-fold. The actual implications of the elevated D4-GDI levels on Rho activity in breast cancer cells, in the context of NCT silencing, needs to be addressed by investigating the level of Rac activity, as well as monitoring the cellular localisation of the Rho effector proteins.

The aldo-keto reductase1 B1 (*AKR1B1*) is overexpressed in human malignancies such as liver, breast, and lung cancer. It plays a role in the development and progression of cancer through carbonyl detoxification, retinoic acid homeostatic regulation, and lipid metabolic control. Therefore, AKR1B1 inhibitors have been highlighted as a novel class of antitumour agents (469). NCT inhibition reduced AKR1B1 levels by 3.2-fold.

Breast cancer patients with tumours that are negative for PHLDA1 protein expression have a shorter disease-free survival ($p < 0.001$) and overall survival ($p < 0.001$) than patients with tumours that are positive for PHLDA1 protein (470). *NCT* siRNA induced upregulation of *PHLDA1* by 2.86-fold.

Cystatin S (*CST4*) belongs to the family of tumour suppressors which undergo methylation-dependent, epigenetic silencing in human malignancies (471). *NCT* siRNA increased expression of the *CST4* by 8.1-fold.

Ubiquitin-conjugating enzyme E2T (*UBE2T*) has a critical role in the development and progression of breast cancer, as it plays a role in controlling the function of various cellular proteins, including critical regulators of signal transduction, cell proliferation, and apoptosis. It also represents a potential therapeutic target.

Its function relates to the breast cancer susceptibility gene, BRCA1, which is lost in some breast cancers due to genetic mutation, epigenetic silencing, or haploinsufficiency. *UBE2T* siRNA upregulates BRCA1 protein levels in breast cells, as a part of its anti-tumour effect (472). *NCT* siRNA reduced *UBE2T* expression by 3.2-fold.

A screen which utilised the National Cancer Institute bank of 60 cancer cell lines (NCI-60) has demonstrated that the expression of the *ASNS* gene correlates with the sensitivity of cancer cells to treatment with L-asparaginase (bacterial enzyme used to treat acute lymphoblastic leukemia). Absence of this gene selectively starves cells that cannot synthesize sufficient asparagine for their own needs (473). *NCT* siRNA caused upregulation of the *ASNS* gene by 6.2-fold.

Taken together, the gene array demonstrated that nicastrin silencing may regulate genes which function as a part of the cellular pathways which mediate cancer cell migration and invasion. Many of these genes have already been documented as drivers of the EMT (54), and denominators of common breast cancer metastasis signatures: i) *TNFSF10* and *ARHGDIB* in the MDA-MB-231 lung cancer model and human tumours; ii) *SPANX* and *CTGF* in the MDA-MB-231 lung and bone metastasis model; iii) *ANXA* in the MDA-MB-435 cell line breast cancer model (474). Interestingly, NCT depletion induced a potent upregulation of tumour suppressor genes, like *CST4* and *SPRY1*. Some of the effects we have observed may be induced as a result of the cellular negative feed-back mechanism. For example, the fact that the proinvasive CTGF gene was significantly increased may possibly be a response to invasion inhibitory effects induced by *NCT* siRNA treatment. Genes regulated by NCT do not belong to one cellular pathway, rather many of them interact and cross-talk. Therefore, the level of the functional output of NCT-mediated transcriptome modulation is a reflection of the cumulative effects on its targets. Given the diverse expression of NCT targets, the functional consequences of its inhibition may also be cell-context dependent. Importantly, our data have revealed that while many NCT downstream effects are mediated through the GS complex and Notch signaling, NCT possesses a proprietary set of target genes which are not affected by Notch receptors.

# CHAPTER 6

# Results

# Clinical implications of nicastrin expression in human breast cancer tissue

## 6.1. Introduction

Tumour pathology provides useful insights into breast cancer biology and into the relevance of potential new biomarkers. Biomarkers are determinants of the tumour molecular profile, its aggressiveness and the likelihood of response to certain therapies. They can be measured from the tumour tissue or other biological samples (i.e. patient serum) and can be determined by DNA, mRNA or protein expression analyses. Immunohistochemistry (IHC) remains the method of choice for determining the expression levels of protein biomarkers in cancer tissue (475). Biomarkers can be stratified into:

- Diagnostic (screening) biomarkers:

They are used to detect and identify a given type of cancer. These markers are expected to have high specificity and sensitivity (e.g. CA-125 for ovarian cancer, CA15-3 for breast cancer, CA19-9 for colon cancer etc.)

- Prognostic biomarkers:
  They are determined once the diagnosis has been confirmed for the purpose of predicting the probable course of the disease in terms of recurrence, i.e. disease aggressiveness (tumour grade, ERα, HER2 status etc.).

- Predictive biomarkers:
  They serve to predict the response to a drug before the treatment is initiated. These markers classify patients as likely responders or non-responders to a particular type of treatment.

A valid biomarker needs to be specific and sensitive. Specificity refers to the proportion of control individuals who test negative for the biomarker. Sensitivity is the proportion of individuals with confirmed disease who test positive for the biomarker.

Despite continuous effort, only a few tissue biomarkers of breast cancer have entered routine use (ERα, PR, HER2), and in some laboratories E-cadherin, EGFR and p53 (476). Furthermore, ERα and HER2 are not just biomarkers but also therapeutic targets in breast cancer. However, diseases like the triple negative breast cancer, which lack expression of the common biomarkers, are the primary focus of laborious efforts to discover new determinants of tumour aggressiveness and prognosis, and thereby new therapeutic target.

## 6.2. Immunohistochemistry of nicastrin expression in breast tissue

Led by our data showing marked NCT upregulation in breast cancer cell lines compared to a non-transformed mammary epithelium cell line, we hypothesised that NCT would be upregulated in human breast cancer tissue compared to normal breast tissue as well. To explore this, we obtained normal breast tissue from reduction mammoplasties, as well as samples of benign breast disease (fibroadenoma), and a tissue microarray (TMA) containing 1050 breast cancer cases with known clinico-pathological outcomes. This allowed us to assess the suitability of NCT as a therapeutic target in breast cancer as well.

Nicastrin antibody (N-1660), raised against the C-terminus of the protein (691-709 a.a.) (220), was used to optimise the IHC staining on full-faced sections of the normal breast and breast cancer tissue. Specificity of the IHC staining was verified using pre-incubation with the NCT blocking peptide. Representative images of the NCT staining pattern and intensity are shown in Figure 42. Scoring was done on the basis of staining intensity as being negative = 0, weakly positive = 1+, moderate = 2+, and strong = 3+. We then dichotomised the groups into NCT low expressors containing cases with scores 0 and 1+, and NCT high expressors, encompassing 2+ and 3+ scores (Figure 42).

Normal breast tissues from reduction mammoplasties (n = 40) were examined and NCT was absent (IHC score 0) in 30/40 cases, and expressed at very low levels (IHC score 1+) in the remaining 10 cases. Benign breast disease (fibroadenoma) tissue (n = 10) equally displayed absence of NCT in the luminal cell compartment, while the basal cells showed an upregulation of NCT staining intensity (Figure 42).

Nicastrin immunostaining in breast cancer TMAs showed predominant cytoplasmic localisation with variable cell membrane staining. Informative data were obtained in 1050 tissue cores, of which 52.5% showed low (0 and 1+ intensity score) and 47.5% showed high (2+ and 3+ score) expression (Table 13). We further obtained paired primary tumour and lymph node samples (n = 15) and observed that NCT expression was retained in the lymph node metastasis at the same level as annotated to the primary tumour.

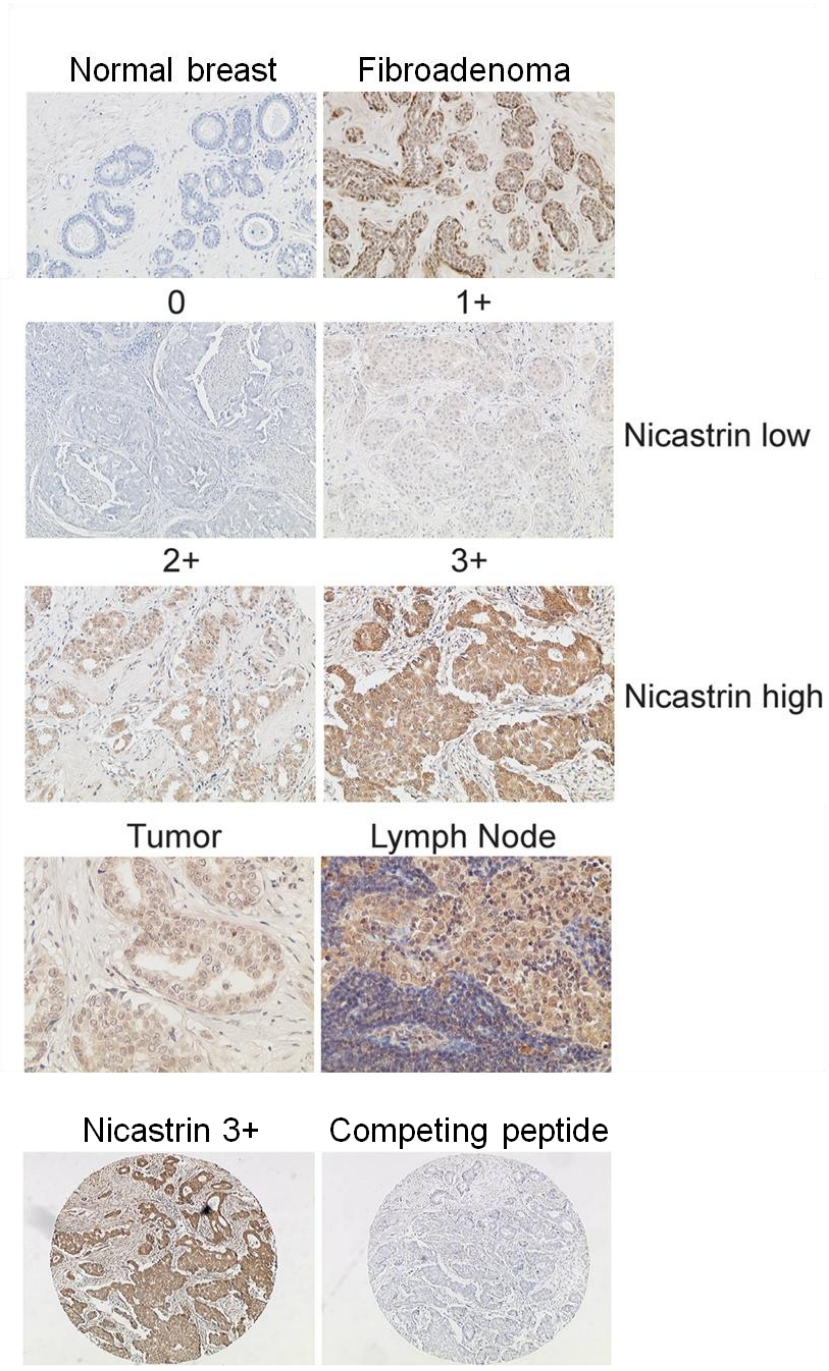


**Figure 42.Nicastrin expression is upregulated in breast cancer compared to normal breast tissue**. Representative images of normal breast tissue (n = 40), fibroadenoma (n = 10), showing absence of nicastrin expression and expression in myopepithelial cells respectively. Nicastrin expression in breast cancer tissue (n = 1050). Representative images of nicastrin null, 1+, 2+ and 3+ staining in breast tumours. Nicastrin expression is preserved in lymph node metastasis (n = 15). Pre-incubation with competing peptide confirms the specificity of the N-1660 antibody.

**Table 13.Expression of nicastrin in breast cancer tissue**

| Nicastrin intensity score | Number of cases | Percent (%) |
|---|---|---|
| **0** | 54 | 5.2 |
| **1** | 497 | 47.3 |
| **2** | 349 | 33.2 |
| **3** | 150 | 14.3 |
| **Total** | 1050 | 100 |

Given the comprehensive characterisation of the breast cancer tissue cohort we used, we were able to correlate NCT expression with other known clinical and pathological parameters (Table 14). High NCT expression positively correlated with the ERα and PR hormonal receptors ($p < 0.001$). There was a direct correlation with cytokeratin 18 ($p < 0.001$) and E-cadherin ($p< 0.01$), and inverse with basal cytokeratines 5/6 ($p = 0.01$). Nicastrin expression correlated with patient age ($p = 0.031$), where patients > 50 years were more likely to have tumours expressing high NCT levels. Surprisingly, nicastrin expression inversely correlated with tumour grade ($p < 0.001$). More nicastrin abundance was recorded in both grade 1 and particularly grade 2 tumours. With respect to tumour type, NCT appeared to be significantly upregulated in tubular carcinomas (n = 208/1050), with 61% (n = 127/208) showing high expression, versus 39% (n = 81/208) with low levels ($p = 0.002$). In patients with invasive ductal carcinoma (624/1050), 54.3% (n = 339/624) had high and 45.7% (n = 285/624) low NCT levels. No correlation was observed with tumour size (Table 14).

**Table 14.Patients' characteristics and tumour biomarkers showing nicastrin expression**

| Variable/biomarker | Nicastrin expression | | *p*-value |
|---|---|---|---|
| | Low (%) | High (%) | |
| Patients age (years) | | | |
| ≤50 | 231 (41.8) | 173 (35.3) | 0.031 |
| >50 | 321 (58.2) | 325 (64.7) | |
| Grade | | | |
| 1 | 70 (12.8) | 96 (19.4) | <0.001 |
| 2 | 166 (30.3) | 187 (37.7) | |
| 3 | 312 (56.9) | 213 (42.9) | |
| Stage | | | |
| 1 | 337 (51.8) | 313 (48.2) | 0.827 |
| 2 | 164 (52.9) | 146 (47.1) | |
| 3 | 48 (55.2) | 39 (44.8) | |
| Tumour type | | | |
| Tubular | 81 (39) | 127 (61) | 0.002 |
| Invasive ductal | 285 (45.7) | 339 (54.3) | |
| Estrogen receptor | | | |
| Negative | 170 (61.8) | 105 (38.2) | <0.001 |
| Positive | 355 (49.2) | 367 (50.8) | |
| Progesterone receptor | | | |
| Negative | 251 (59.6) | 170 (40.4) | <0.001 |
| Positive | 270 (47.7) | 296 (52.3) | |
| HER2 receptor | | | |
| 0/1+/ | 503 (53.4) | 439 (46.6) | 0.076 |
| 2+/3+ | 33 (42.3) | 45 (57.7) | |
| Cytokeratin 18 | | | |
| Negative | 67 (13.3) | 437 (86.7) | <0.001 |
| Positive | 30 (6.4) | 439 (93.6) | |
| Cytokeratin 5/6 | | | |
| Negative | 432 (50.7) | 420 (49.3) | 0.01 |
| Positive | 96 (61.9) | 51 (38.1) | |
| E-cadherin | | | |
| Negative | 219 (60.2) | 145 (39.8) | < 0.01 |
| Positive | 309 (48.1) | 333 (51.9) | |

Kaplan-Meier survival analysis was then performed to evaluate a potential impact of NCT expression on disease-free and overall survival (breast cancer specific survival). High NCT expression was not predictive of disease-free survival, nor of breast cancer specific survival (overall survival) in the whole dataset (p = 0.664). Equally, we saw no impact of high nicastrin levels on overall survival in the ERα positive subset of patients (p = 0.183). In further pre-defined subset analysis, high NCT levels had borderline predictive value for overall survival at 5 years (p = 0.05) in the ERα negative patients (n = 275/1050) (Figure 43). Nicastrin expression did not retain significance in a multivariate analysis model combined with tumour grade, stage, and size. Nicastrin expression did not predict outcome to systemic adjuvant treatments (endocrine or chemotherapy).

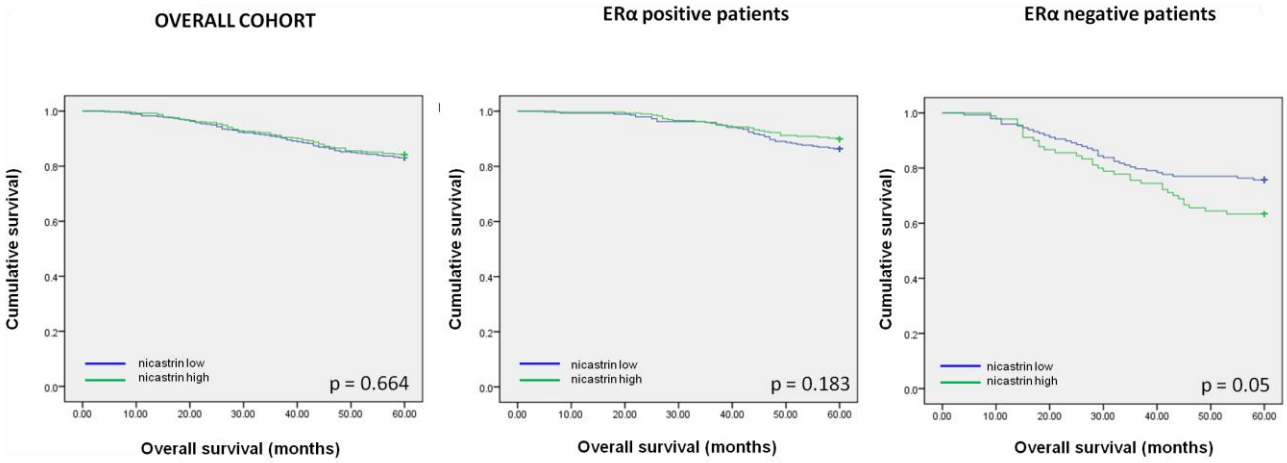


**Figure 43**.Kaplan-Meier model comparing breast cancer specific survival in breast cancer patients according to nicastrin protein expression. **a)** Entire analysed cohort (p = 0.664). **b)** ERα positive patients (p = 0.183). **c)** ERα negative patients (p = 0.05)

Furthermore, we analysed sections of primary breast cancer tissue (n = 40), which contained the *in situ* and the invasive component represented on one full faced tissue preparation. Immunostaining for NCT has revealed that in 8/40 cases (20%), NCT was absent from the non-invasive, *in situ* tumour, while it was upregulated in the invasive breast cancer tissue counterpart (Figure 44).

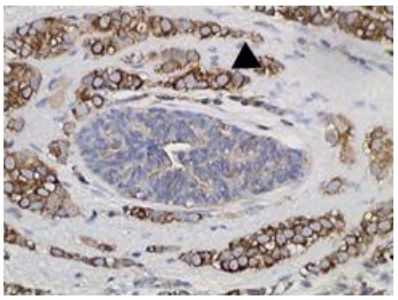

**Figure 44.Differential expression of NCT in *in situ* and invasive breast cancer.** Representative image of a full faced breast cancer tissue section showing NCT expression the *in situ* (white arrow) and invasive breast cancer (black arrow head). Magnification x100.

We have also obtained fresh primary breast cancer tissue and axillary lymph nodes containing breast cancer metastases, which were processed using the magnetic beads coated with an epithelial marker in order to purify and enrich the preparation for epithelial tumour cells. Obtained purified cells were often insufficient to yield the sample suitable for protein extraction. However, we managed to probe two tumours and two metastatic lymph node samples for NCT protein expression. MDA-MB-231 cell whole cell lysates were used as a positive control. The tumour (TU2) and the lymph node (LN2) lanes annotate a paired sample from the primary tumour and the corresponding lymph node metastasis, respectively (Figure 45). Here, albeit at low levels, we were able to show that NCT expression is preserved in the lymph node metastasis to the same level as in the primary tumour. Interestingly, the visualised NCT band in the primary tissue corresponded to the mature NCT, as the immature NCT band was absent, unlike in MDA-MB-231 cells where both NCT forms were detected. This is similar to the previously reported data where only the mature NCT band was detected from whole cell lysates of mouse cortical neurons (248).

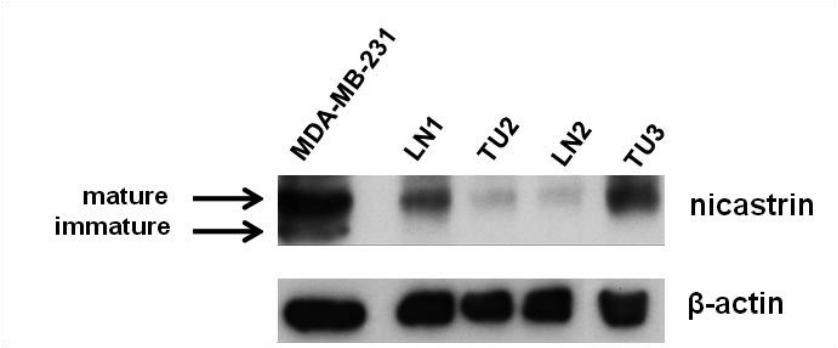


**Figure 45.Western blotting demonstrating NCT protein expression in primary tissue.** MDA-MB-231 whole cell lysates were used as positive control. Primary breast cancer tissue (TU) and metastatic lymph nodes (LN) were processed according to the Dynal beads separation protocol and preparations enriched for epithelial tumour cells were obtained. 30 μg of protein was loaded in each lane. β-actin served as the loading control.

## 6.3. Nicastrin expression in the normal tissue of other organs

Expression of NCT was next investigated in the normal tissue from other organs. Nicastrin was expressed in the normal skin (IHC score = 2+; n = 12), normal liver (1+/2+; n = 7), renal tubules (1+/2+; n = 7), heart muscle ( 2+, n = 2), vaginal portion of the cervix ( 2+, n = 2), but absent or expressed at low levels in the normal prostate (0/1+; n = 12), colon ( 0/1+, n = 7), lung (0, n = 7), testis (0/1+, n = 5), endometrium (1+, n = 5), cerebrum (1+, n = 7), thyroid (0, n = 5), and renal glomeruli (0, n = 7) (Figure 46).

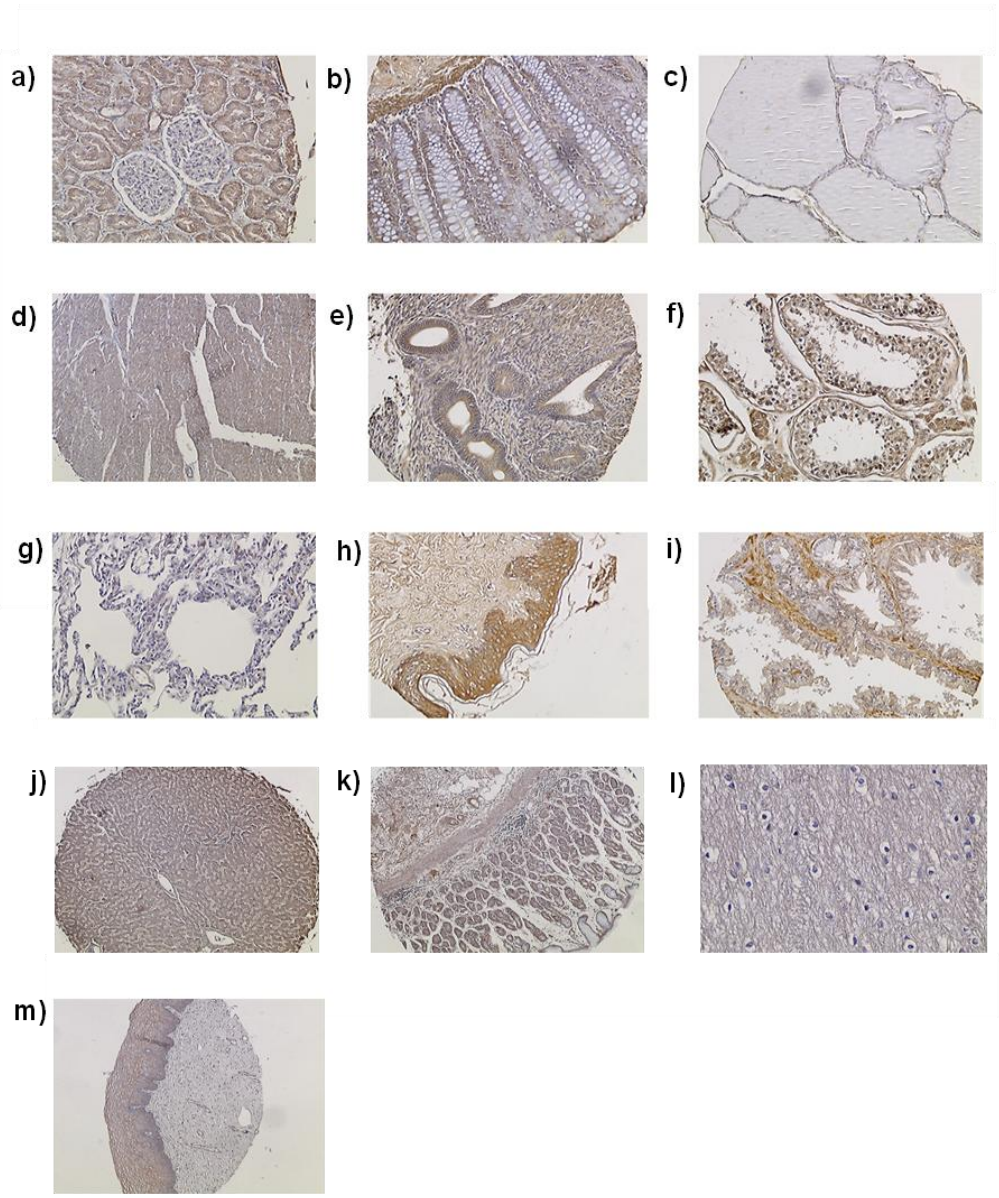


**Figure 46.IHC staining showing NCT expression in normal tissues. a)** kidney; **b)** colon; **c)** thyroid; **d)** heart; **e)** endometrium; **f)** testis; **g)** lung; **h)** skin; **i)** prostate; **j)** liver; **k)** stomach; **l)** cerebral white matter; **m)** vaginal cervix. Magnification is x 100. For vaginal cervix, skin and liver Magnification is x 40.

## 6.4. Discussion

Even though it has been demonstrated that overexpression of active Notch is a characteristic of a subset of breast cancers, where it confers worse survival (158, 477), activity of the GS enzyme or expression of its components (NCT, PS, PEN2, Aph-1) in breast cancer tissue has not yet been examined. In this chapter we have demonstrated that NCT protein is not expressed in epithelial cells of the normal breast tissue, while it is markedly upregulated in breast cancer tissue. Furthermore, analysis of benign breast lesions, fibroadenomas, showed increased NCT expression in the basal cell compartment, while the luminal cells maintained NCT negativity. Several studies have considered fibroadenomas as a risk factor for developing breast cancer (478). In fibroadenomas, genes related to collagen synthesis, fibrosis and growth factors are overexpressed compared to the normal mammary gland. This stroma is deemed capable to provide a permissible milieu for the malignant transformation of adjacent epithelium (479). Upregulation of NCT in the basal cells of fibroadenomas may be a response to pro-oncogenic signals derived from fibroadenoma-related stroma, and an example of the importance of the extracellular matrix-breast tissue cross-talk in malignant cell transformation.

Of the 1050 analysed breast cancer cases, 47.5% exhibited high NCT expression. Nicastrin expression correlated significantly with that of the ERα, PR and the luminal marker CK18, linking its expression with the luminal breast cancers. Its high expression was associated with ductal carcinomas, which is in line with the positive association of NCT and E-cadherin levels, as E-cadherin is used as one of the markers distinguishing ductal from lobular breast cancers (480). In our *in vitro* experiments, we have observed NCT expression in ERα negative cell lines (MDA-MB-231, HCC1806 and SKBR3), as well as ERα positive cell lines (MCF-7 and BT474). Nicastrin silencing reduced proliferation of MCF-7 cells, and BT474 cells expressed mature NCT which migrated at a higher molecular weight. These data, together with the fact that we saw a trend towards a direct correlation between HER2 and high NCT expression ($p = 0.076$), proposes that NCT might be important in luminal A (MCF-7) and luminal B (BT-474) breast cancers as well. The fact that survival analysis failed to identify an impact of high NCT levels in the ERα positive cohort suggests that the hormonal treatment these patient have received (tamoxifen), may have alleviated the 'oncogenic' impact of high NCT expression.

A similar observation has recently been reported by Giamas et al., where even though high expression of a tyrosine kinase LMTK3 correlated inversely with ERα levels in the same cohort used for NCT expression analysis, LMTK3 abundance predicted for worse outcome of ERα positive patients treated with tamoxifen (481). Regarding potential estrogenic regulation of *NCT*, with the help of Dr Jason Carol (Cambridge, UK), we have observed that there are potential estrogen response elements 20-30 kb upstream of the *NCT* promoter in two ERα positive cell lines (Figure 47). If ERα is regulating *NCT*, these may be the cis-regulatory elements. These are non-coding DNA sequence in or near a gene required for proper spatio-temporal expression of that gene, often containing binding sites for transcription factors. The NURSA gene expression tool, which gives a *p*-value to any estrogen regulated gene changes, based on multiple combined studies (http://www.nursa.org/gems), suggested that in MCF-7 cells, *NCT* is downregulated by estrogen. Therefore, it is worth exploring in more detail a possible cross-talk between NCT and ERα in breast cancer cells.

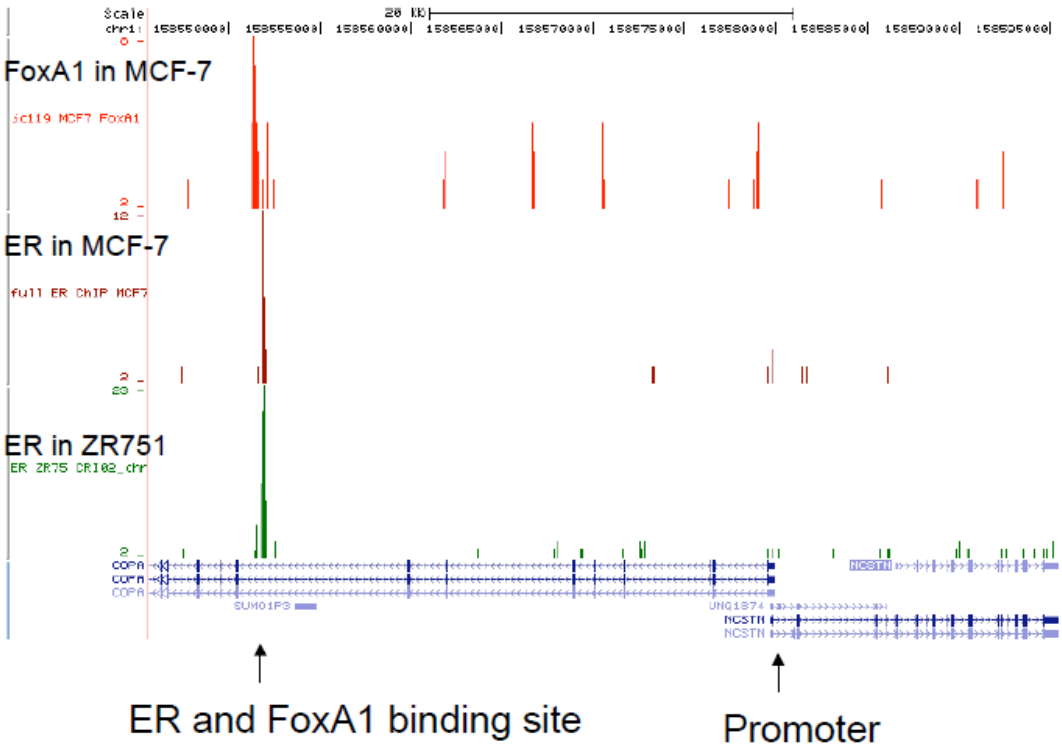


**Figure 47.Estrogen response elements near the promoter of *NCT* gene.** Bio-informatics analyses in the NCT promoter revealed a potential ERE motif located ~20-30 kb upstream of the transcriptional start site of the gene. The coloured boxes represent ERα binding sites in the three cell lines.

Of the 1050 patients, 23.8% (n = 250) were ERα negative. ERα negative breast cancers are by nature more aggressive (482). Being deprived of anti-hormonal therapy as a treatment option, these patients receive only chemotherapy after surgical excision of the primary tumour, and anti-HER2 therapy is provided if HER2 is overexpressed and/or amplified. High NCT levels in the ERα negative subgroup were predictive of worse breast cancer specific survival at 5 years, suggesting that NCT contributes to the disease aggressiveness of this particular breast cancer subtype. This is in line with our *in vitro* data using MDA-MB-231 cells and HCC1806 cells, representative of the ERα negative breast cancer model (367), as well as the MCF10A cells overexpressing NCT, where NCT appears to help maintain the EMT state. Furthermore, since Notch1 overexpression has been linked to the basal breast cancers, which are ERα negative (158), and we have observed an impact of NCT abundance in this same subset of patients, it may be worth assessing the Notch1-ICD expression in our patient cohort and investigating whether it positively correlates to that of NCT. Furthermore, we will investigate whether PS1 expression follows the trend of NCT in this patient group, as this will allow us to gain insight if the adverse impact on overall survival we have observed is conferred due to NCT high levels, or to the overall high expression levels of the GS in the breast cancer tissue. Previous reports have investigated NCT expression in non-human tissues by western blotting and PCR. The most elaborate study of NCT expression in mouse tissues identified significant levels in the skeletal muscle, heart and lung, as well as a prominence of lower molecular weight NCT glycoforms in the brain and liver (220). Our analysis of NCT expression in a panel of normal human tissues indicated a moderate expression in the renal tubules, liver and heart, with a higher expression in the skin. Lung and colon tissues did not demonstrate immunorectivity for NCT. Since the antibody used to detect NCT in mouse tissues was the same one we used, N-1660 directed against the C-terminus of NCT, it appears that NCT exhibits species-dependent tissue expression. Evaluating tissue distribution of a potential therapeutic target is of vital importance as it helps predict possible sites/organs of side-effects. Our data suggest that targeting NCT might induce certain consequences in the skin. Previous reports have noted that inhibition of GS in a NCT knockdown mouse model gives rise to proliferative skin lesions and skin tumours (370). Therefore, should an anti-NCT therapy be utilised in the treatment of breast cancer, a therapeutic window may need to be identified which would allow for achievement of clinical benefit, while avoiding treatment related toxicities.

# CHAPTER 7

# Results

# Development and characterisation of anti-nicastrin monoclonal antibodies

## 7.1. Introduction

An optimal target for monoclonal antibody (MAb) therapy in cancer is a molecule expressed on the cell surface of the tumour cells, whose expression and function contribute to the development and/or progression of the disease, and the inhibition of which selectively targets the cancer cells while inducing minimal side-effects.

Monoclonal antibodies serve two important functions: i) they bind to the target protein (antigen) and modulate its expression and/or function; ii) they bind immune effector cells or elements of the complement system, inducing cytotoxic or immunological effects (32). Apart from their specific mode of action, another advantage of MAbs as biological therapy module over small molecules is that they persist in the circulation with long half-lives and enable lower frequency of administration (483). The most commonly targeted tumour-associated antigens are the growth factor receptors, frequently overexpressed in human malignancies (19). Anti-HER2 MAb (trastuzumab) is the best example of this type of biological treatment. It is approved for the treatment of both primary and metastatic breast cancers that display overexpression of the HER2 protein, and/or amplification of the HER2 gene (484). Many new MAbs are in clinical trials and in preclinical investigations. Recently, a MAb against N-cadherin extracellular domain has been proposed for the treatment of prostate cancer (483).

We hypothesised that NCT would be a candidate target for the development of antagonistic MAbs based on the following facts:

i) NCT is a transmembrane protein with a large extracellular domain which harbours important functional domains
ii) NCT is overexpressed in breast cancer tissue compared to the normal breast
iii) NCT expression confers worse overall survival in ERα negative breast cancer patients
iv) NCT silencing inhibits invasion and proliferation of breast cancer cells.

In this chapter we describe the characterisation and functional effects of anti-NCT antibodies.

## 7.2. The advantages and disadvantages of polyclonal and monoclonal antibodies

Antibodies are produced by lymphocytes upon exposure to a specific antigen. Numerous epitopes are recognised by a large number of lymphocytes which proliferate and differentiate into plasma cells, and the consequent antibody response is polyclonal. Polyclonal Abs (PcAbs) are hetrogeneous and can be generated much more rapidly and cost-effectively. However, the quantity of PcAbs that can be obtained is dependent on the size of the animal used as a host and its lifespan (485).

In contrast, monoclonal antibodies (MAbs) are produced by a single B lymphocyte clone. Their purity levels are higher, they are homogeneous and consistent. Fusion of the myeloma cells and spleen cells upon immunisation of the host, yields hybridoma cell lines, each capable of producing a single MAb clone as an indefinite source. The hybridoma supernatants are then screened and selected against the antigen, and subsequently expanded. Generation of hybridomas, production and purification of MAbs is more costly and time-consuming. However, the mono-specificity renders MAbs superior to the PcAbs as they are able to serve as therapeutics, as well as valuable tools for mapping functional epitopes on the antigen, and for potential structural analysis (485).

## 7.3. Anti-NCT polyclonal antibody (PcAb)

For the purpose of conducting proof of principle experiments, we generated anti-NCT PcAbs and firstly investigated whether they recognised endogenous NCT in breast cancer cells. For this purpose, we performed FACS analysis on non-permeabilised MCF-7 and MDA-MB-231 cells and confirmed that the anti-NCT PcAb 4631 successfully bound to the cell surface NCT ectodomain (Figure 48a) in both cell lines. We next performed western blotting using whole cell lysates of MCF-7 and MDA-MB-231 cells and observed that the PcAbs were able to detect the mature, immature and the non-glycosylated forms of NCT (Figure 48b). PcAb 4631 was used in the following experiments. Since we based our decision to primarily focus on NCT function in ERα negative cells based on the fact that NCT abundance in the ERα negative patient population conferred worse survival, we performed the functional experiments with anti-NCT antibodies using MDA-MB-231 cells.

We treated MDA-MB-231 with increasing concentrations of the PcAb and demonstrated that it induced a dose-dependent anti-proliferative effect. An inhibition of 25.9±1.3% was induced by the 25 μg/ml dose, while 50 μg/ml and 100 μg/ml inhibited breast cancer cell proliferation by 35.2±1.8% and 50±2.9%, respectively (Figure 48c). Furthermore, cell cycle analysis indicated that the mechanism by which the anti-NCT PcAb achieved the anti-proliferative effect was via induction of the cellular sub-G1 arrest, mimicking the effect of NCT genetic silencing (Figure 48d). In addition, blocking NCT using the PcAb reduced Bcl-2 levels, which is in line with the sub-G1 cellular accumulation, disrupted the GS complex activity, as demonstrated by the marked reduction in Notch1-ICD levels, and reduced protein levels of the Akt (Figure 49).

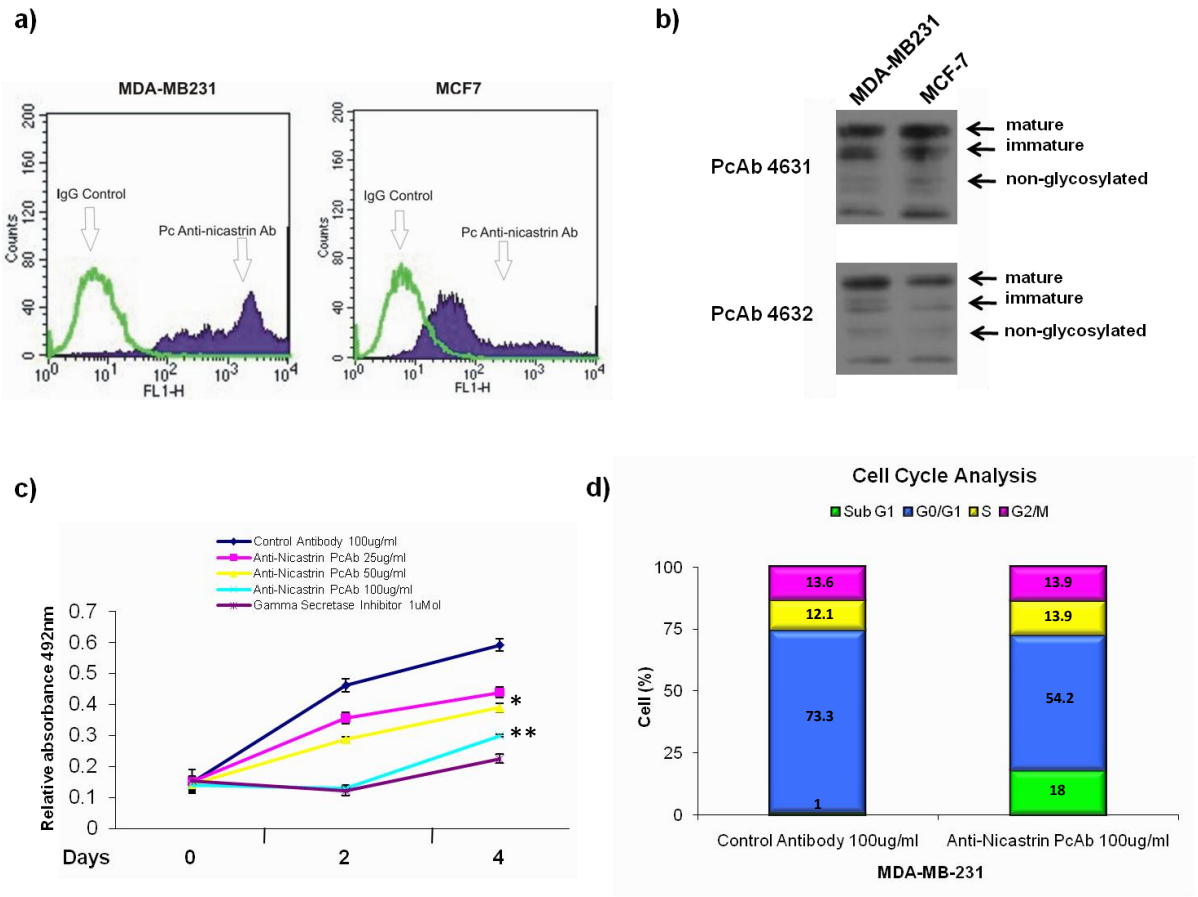


**Figure 48**.**Anti-nicastrin PcAb inhibit proliferation of MDA-MB-231 cells. a)** Anti-NCT PcAb recognises endogenous cell surface NCT on breast cancer cells. Non-permiabilised MCF-7 and MDA-MB231 cells were incubated with 100 µg/ml of the anti-NCT PcAb (4631) followed by the secondary anti-rabbit-FITC conjugated secondary antibody. FACS analysis were performed on the FACSCalibur, BD. **b)** Western blotting showing that the anti-NCT PcAbs (4631 and 4632) at the dose of 1 µg/ml recognise endogenous NCT in MCF-7 and MDA-MB-231 cell lysates. **c)** MDA-MB-231 cells were plated (3 x $10^3$/well) in 96-well plates and treated with increasing doses (25-50-100 µg/ml) of the anti-NCT PcAb**.** Rabbit IgG isotype control was used as a negative control at the equivalent of the highest anti-NCT PcAb concentration (100 µg/ml). GSI1 at 1µM was used as a positive control. Anti-NCT PcAb inhibits proliferation of MDA-MB-231 cells in a dose-dependent manner: 25 µg/ml (25.9±1.3%), 50 µg/ml (35.2±1.8%), 100 µg/ml (50±2.9%). Error bars represent SEM from two independent experiments, each in quadruplicate; *p = 0.03; **p = 0.02. **d)** MDA-MB-231 cells were plated in 6-well plates (2 x $10^5$/well) and treated with the anti-NCT PcAb (100 µg/ml) and Rabbit IgG as an isotype control for 24 h. Cells were then processed for cell cycle analysis using the CycleTEST Plus DNA Reagent Kit.

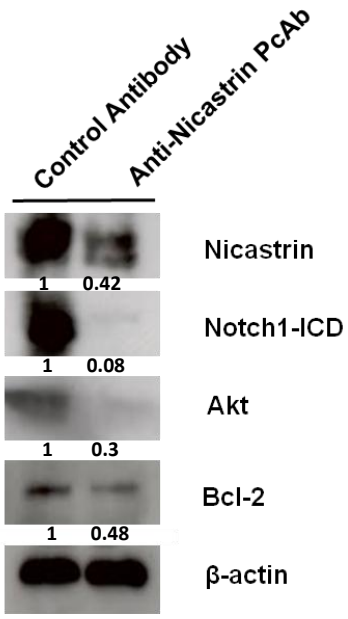


**Figure 49.Treatment of MDA-MB-231 cells with the anti-NCT PcAb reduces NCT protein levels and inhibits Notch1.** Western blotting showing the effects of the anti-NCT PcAb (100 μg/ml) on NCT, Bcl-2 and Akt and Notch1-ICD. β-actin was used as the loading control. The intensity of bands was quantified using Image J software. Numbers below the bands represent fold change compared to MDA-MB-231 Control antibody treated cells, relative to the loading control.

### 7.3.2. Anti-NCT PcAb inhibits breast cancer cell invasion

We next measured the invasive capacity of MDA-MB-231 cells treated with increasing concentrations of the anti-NCT PcAb (10-100 μg/ml). Compared to the rabbit IgG isotype control, the anti-NCT PcAb was a potent inhibitor of cell invasion in a dose dependent manner. Namely, the dose of 25 μg/ml induced a 36±3.8% reduction, while 50 μg/ml and 100 μg/ml inhibited cell invasion by 54±2.9% and 57.2±2.3%, respectively (Figure 50a). When the anti-NCT PcAb was preincubated with the NCT recombinant protein, used as the immunising antigen, the inhibitory effect on cell invasion was rescued, signifying the reliance of the anti-invasiveness effect of the PcAb on targeting NCT (Figure 50b).

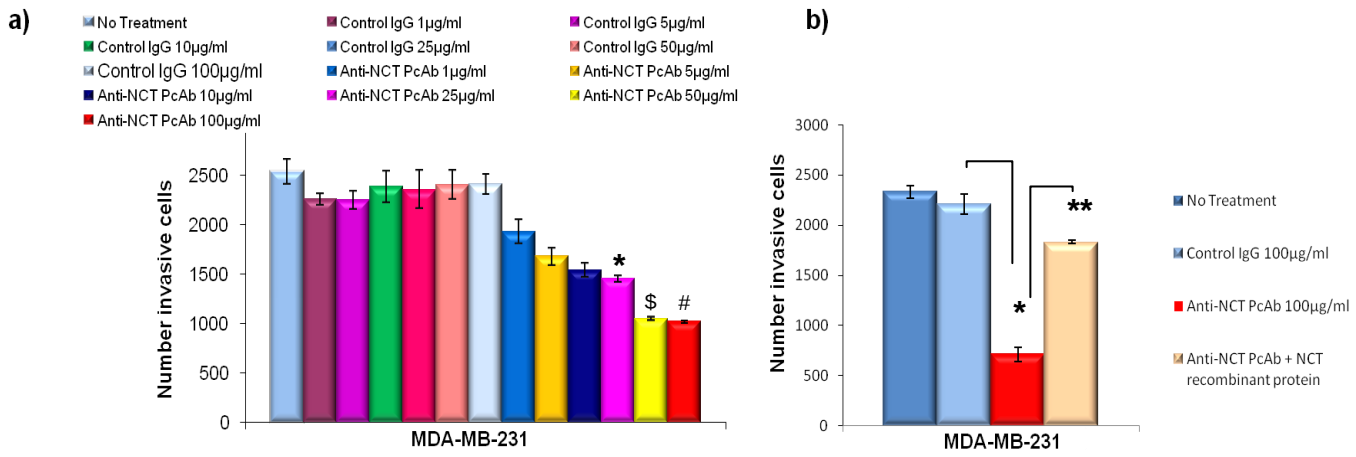


**Figure 50.Effects of the anti-NCT PcAb on breast cancer cell invasion *in vitro*. a)** Effects of anti-NCT PcAb on the invasion of MDA-MB231 cells, in a dose dependent manner. Doses of 25–100 µg/ml produce a significant inhibition (25 µg/ml = 36±3.8%, *p = 0.009; 50 µg/ml = 54±2.9%, $^{\$}$p < 0.001; 100 µg/ml = 57.2±2.3%, $^{\#}$p < 0.001). Error bars represent SEM from three independent experiments, each in triplicate. **b)** Pre-incubation of the anti-NCT Pc-Ab at the dose of 100 µg/ml with 20 µg/ml of the NCT recombinant protein used as an antigen to produce the PcAb, rescued the PcAb-induced inhibition of cell invasion. Error bars represent SEM from three independent experiments, each in triplicate. * p = 0.0003; **p = 0.004.

Taken together, we have shown that inhibition of NCT using the targeted Ab approach, which can potentially be exploited for development of an anti-NCT Ab therapeutic, is able to induce the anti-proliferative and anti-invasive effects similar to the levels generated by purely experimental NCT genetic silencing.

## 7.4. Production and selection of anti-NCT monoclonal antibodies

Anti-NCT monoclonal antibodies (MAbs) were raised by genetic immunisation of rats using a cDNA, encoding for the extracellular domain of NCT (34-669 a.a.). This cDNA was cloned into proprietary expression vector (Genovac), specially developed to maximise an immune response in mammals and to allow screening of the resulting immune sera. The immunisation constructs were introduced into the animals' skin using a Genegun. Once an immune response had been identified, lymphocytes were removed for fusion with mouse myeloma cells and hybridoma supernatant screening. We opted for genetic immunisation, as this novel technique simplifies and shortens the MAb production procedure, by eliminating the step of producing and purifying the protein immunogen.

The second advantage of genetic vaccination is that it more closely resembles activation of an immune response upon an infection with a pathogen, which increases the magnitude of antibody production (486).

In order to decide which hybridomas to take forward and based on the efficacy of the previous experiments with anti-NCT PcAbs, we decided to introduce a dual discrimination approach, where we would select those clones that recognised endogenous NCT and inhibited invasion of MDA-MB-231 cells. We have therefore screened the 21 MAb clones by FACS and the transwell invasion assay. From the 21 clones originally selected as being positive by FACS analysis against the cell line transfected with the NCT cDNA (Genovac) (Figure 51), we found that ten clones (1E2, 1H4, 2H6, 6H5, 6H11, 9G7, 9F1, 10C5, 10C11, 10E9) recognised endogenous NCT on non-permeabilised MDA-MB-231 cells (Figure 52). This could be explained by the fact that we have used the cells in a non-permeabilised condition in order to monitor the binding capacity to the cell surface antigen, mimicking the desired *in vivo* conditions. Furthermore, the concentration of the NCT antigen on the cell surface of MDA-MB-231 cells may have been a limiting factor, compared to the concentration of NCT in the transfected, Genovac propriety cell line, which was an artificial system generated to overexpress NCT.

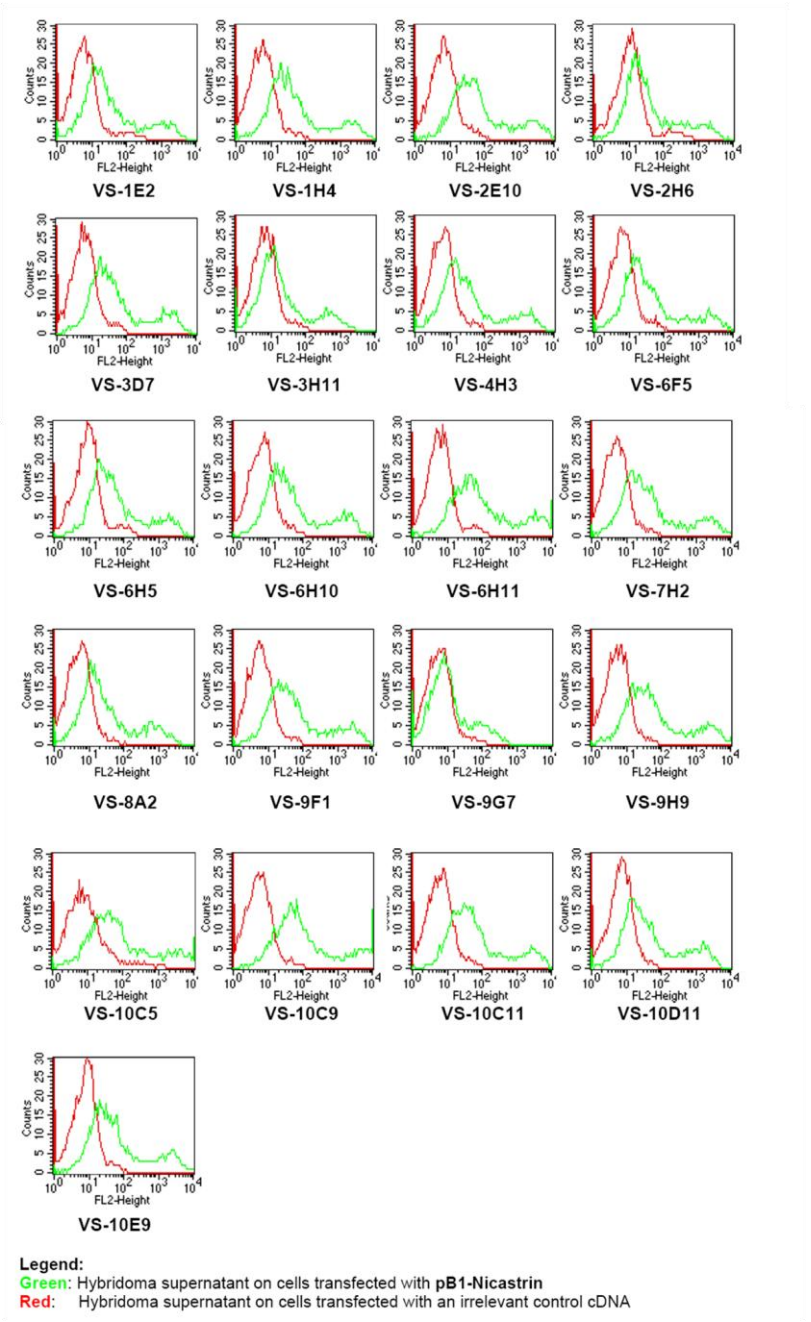


**Figure 51.FACS analysis of hybridoma supernatants (Genovac).** Antibodies were raised by genetic immunisation of WISTAR rats using the cDNA, encoding for the ECD of nicastrin (34-669 a.a). This cDNA was cloned into a proprietary GENOVAC expression vector developed to maximise an immune response in mammals and to allow screening of the resulting immune sera. The immunisation constructs were introduced into the animals using a Genegun. Following DNA boosts, test sera were taken from the animals and tested for the presence of antibodies in a transient transfection assay in flow cytometry against the corresponding GENOVAC screening vector. Labels bellow the histograms annotate the MAb clone reference number.

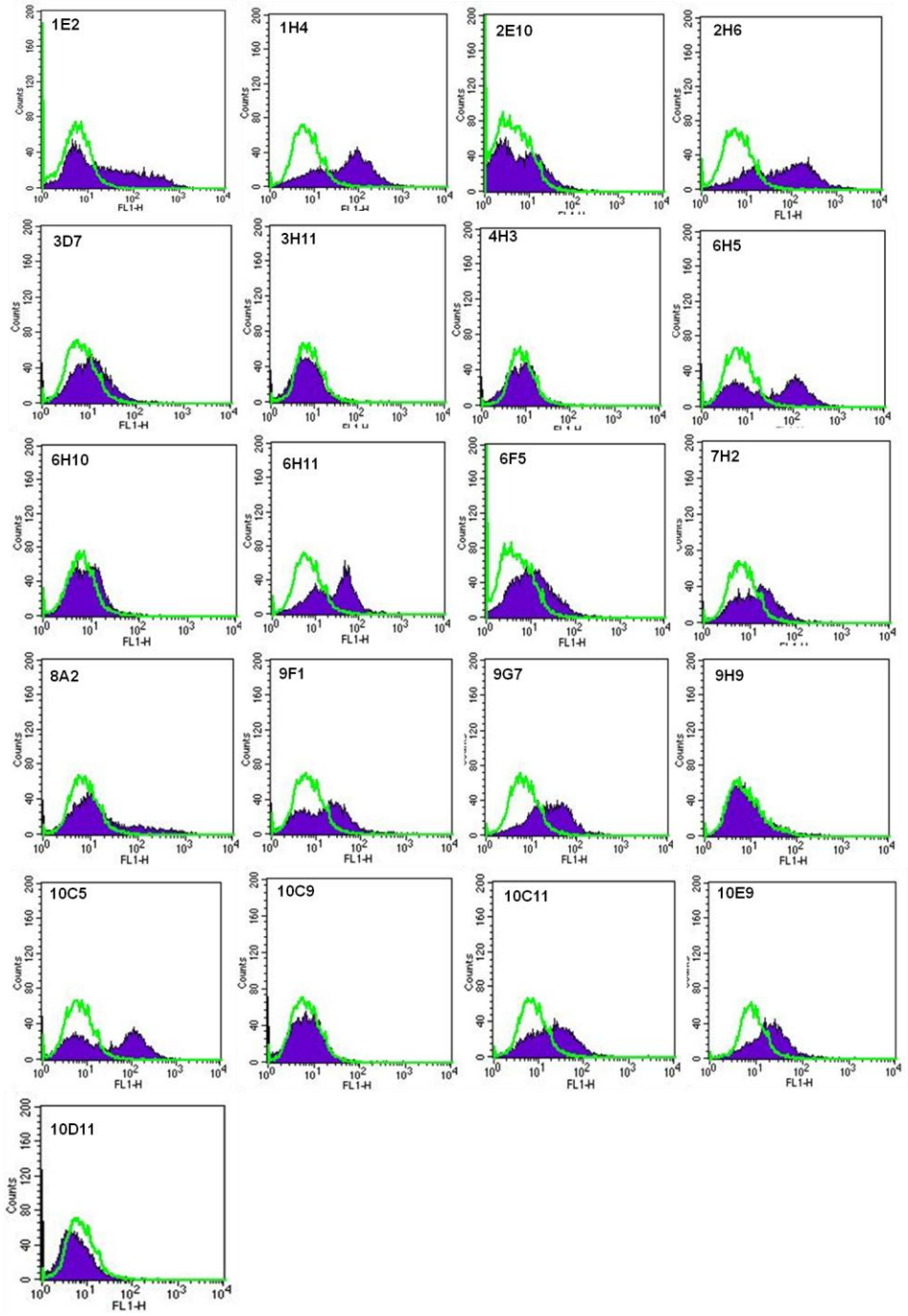


**Figure 52.FACS analysis assessing the binding efficacy of the 21 anti-nicastrin MAb clones.** MDA-MB-231 cells were grown to 70-80% confluence. Cells were incubated with the supernatants obtained from the first round of hybridoma cloning (Figure 48) and with the rat IgG2b as the isotype control antibody at an arbitrary concentration of 50 µg/ml. The concentration of the MAbs in the preparations was at this phase unknown. Secondary anti-Rat-FITC conjugated antibody was used. FACS analysis was performed using the FACSCalibur, BD. The labels in the top left-hand corner of the histograms annotate the MAb clone reference number. **Blue:** Rat IgG2b isotype control; **Green:** MAb supernatants.

We further analysed the potency of the cultivated clones to inhibit invasion of MDA-MB-231 cells. The clones that failed to recognise endogenous NCT in the FACS experiments also failed to produce a marked anti-invasive effect. From the ten clones which were positive by FACS, seven produced a reduction in the cell invasion: 1H4 (44±12.4%), 2H6 (60±5.6%), 6H5 (39±2.6%), 6H11 (40±6.4%), 9G7 (42±11.2%), 10C5 (65±10.2%) and 10C11 (50±10.3%), while three clones (1E2, 9F1 and 10E9) had no effect (Figure 53).

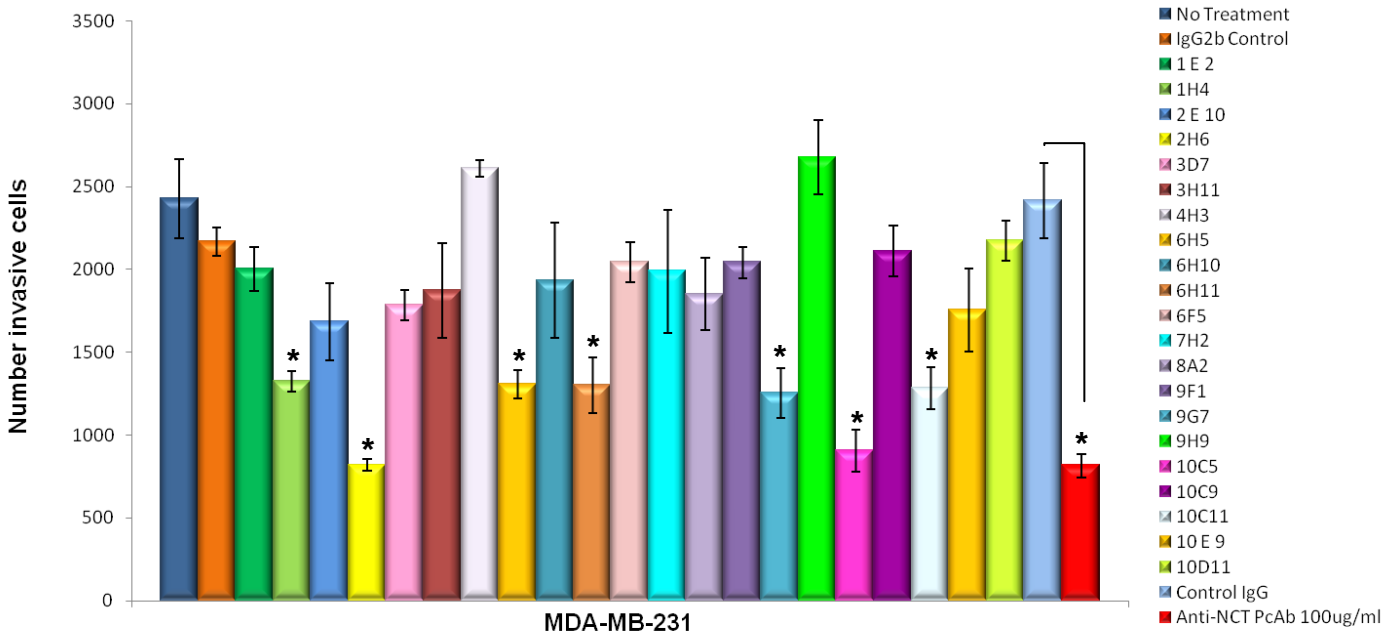


**Figure 53**.**Anti-nicastrin monoclonal antibodies affect MDA-MB-231cell invasion.** MDA-MB-231 cells were treated with indicated anti-NCT MAbs and subjected to the transwell invasion assay for 72 h. Bars represent mean number of invaded cells ± SEM from three separate experiments, each in triplicate. Statistical difference from IgG2b isotype control antibody. 1H4, *p = 0.01; 2H6, *p = 0.0005; 6H5, *p = 0.01; 6H11, *p = 0.01; 9G7, *p = 0.01; 10C5, *p = 0.02; 10C11, *p = 0.004. Anti-nicastrin PcAb (100 μg/μl) was used as a positive control,*p < 0.001.

We have therefore decided to take the clones 1E2, 2H6, 10C5 and 10C11 into the second round of subcloning to generate pure hybridomas. The 1E2 clone was chosen in order to represent a ‘negative control’ anti-NCT MAb, based on the criteria that it recognised the antigen but failed to induce a functional consequence.

## 7.5. Characterisation of the anti-NCT MAbs clones (1E2, 2H6, 10C5 and 10C11)

We further tested the chosen anti-NCT MAb clones upon the second round of subcloning. In order to evaluate whether the supernatants contained any Ab molecules, we subjected them to denaturation and ran the samples on a 10% SDS-PAGE, followed by the transfer into a PVDF membrane and Ponceau staining. We were able to observe two distinct bands in all four samples, at ~50 kDa and ~25 kDa, corresponding to the heavy- and the light- Ab chains. We could not estimate the MAb concentration, but the abundance of the bands appeared comparable. The dominating band at ~50 kDa reflected the presence of the serum albumin from the hybridoma culture media, and possibly obscured the 50 kDa heavy chain Ab band (Figure 54).

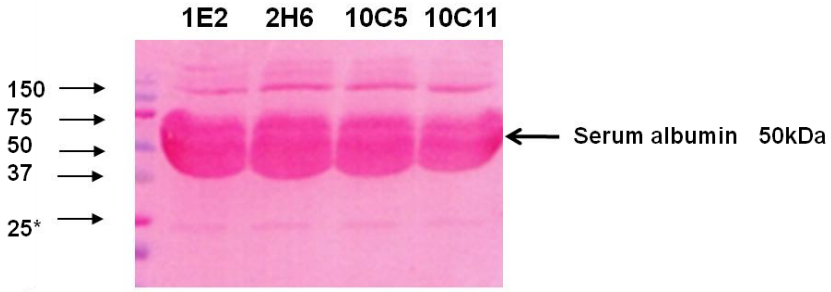


**Figure 54.**MAb clone supernatants (1E2, 2H6, 10C5 and 10C11) from the second round of sub-cloning were denatured and run on a 10% SDS-PAGE under reducing conditions. Upon transfer to a PVDF membrane, Ponceau staining revealed the presence of the heavy- and the light- MAb chains in each samples, at ~50 kDa and ~25 kDa, respectively. Protein observed in abundance at ~ 50kDa corresponds to the serum albumin, originating from the hybridoma culture media (ISF-1).

We than repeated the cell invasion assay using the 1E2, 2H6, 10C5 and 10C11 supernatants from the second round of subcloning. Furthermore, we have expanded the scope of the experiments by treating the MDA-MB-231 cells with the MAbs clones and investigating their capacity to inhibit cell proliferation as well. As previously observed, the 2H6, 10C5 and 10C11 clones consistently produced an anti-invasive effect, while the 1E2 had no impact on cell invasion (Figure 55a). This functionality of the MAbs was mirrored in a proliferation assay.

The growth rate of the MDA-MB-231 cells treated with the 1E2 clone was unchanged compared to control, while the clones 2H6 and 10C5 induced a 23.7±5.5% and 25.8±5.5% inhibition of cell proliferation, respectively, and the 10C11 clone impeded cell growth by 40±3.3% over the period of 3 days (Figure 55b).

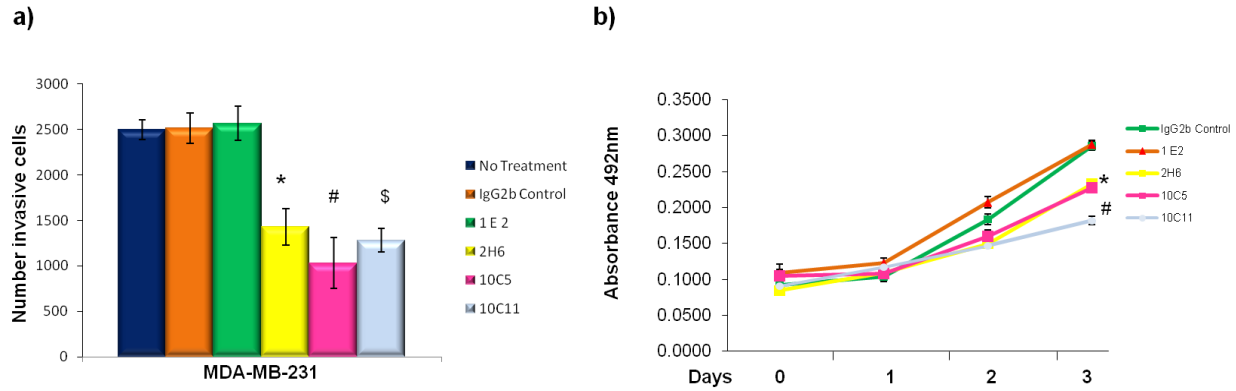


**Figure 55.Cell proliferation and invasion assays using anti-NCT MAb clones. a)** MDA-MB-231 cells were grown to 70-80% confluence. Cells were detached using EDTA, washed once with PBS and pre-incubated with anti-NCT MAbs supernatants derived from the second round of sub-cloning. Rat IgG2b isotype control was used in as a negative control. After incubation, cells (5 x $10^4$/well) were plated in the upper wells of the transwell invasion plate. The lower chamber contained the chemo-attractant. Cells were incubated for 72 h at 37 °C, and number of invaded cells from the lower chamber was counted using the Casy counter. Bars represent mean number of invaded cells ± SEM from three separate experiments. Statistical difference from IgG2b isotype control antibody: 2H6 (47.7±7.7, *p = 0.014); 10C5 (60±10.1%, $^{\#}$ p = 0.01); 10C11 (50±5.3%, $^{\$}$ p =0.004). **b)** MDA-MB-231 cells processed the same as above and pre-incubated with anti-NCT MAbs supernatants derived from the second round of sub-cloning at RT for 30 min. Rat IgG2b isotype control was used as negative control Ab. Cells were plated (3 x $10^3$/well) in 96-well plates and this time point corresponded to Day 0. MAb treatment was supplemented every day, and the SRB assay was performed until Day 6. Absorbance was measured at 492 nm. Error bars correspond to SEM from two independent experiments, each in quadruplicate. The p-values are in relation to IgG2b isotype control: 2H6 (23.7±5.5%, *p = 0.04); 10C5 (25.8±5.5%, *p = 0.04); 10C11 (40±3.4%, $^{\#}$ p = 0.02).

## 7.6. Characterisation of the purified anti-NCT MAbs

Having reproduced the effectiveness of the chosen MAb clones from the second round of sublcloning, the production of 1E2, 2H6, 10C5 and 10C11 MAbs was scaled up using serum-free hybridoma culture conditions, and MAbs were affinity purified using a protein A column (Genovac). We confirmed that the purified, endotoxin free MAbs of a known concentration, bound endogenous NCT on MDA-MB-231 cells (Figure 56e), and furthermore explored whether they recognised distinct NCT glycofoms by western blotting.

Interestingly, we observed that the clones 1E2 and 10C11 were able to pick-up the deglycosylated NCT as well as its immature and mature forms in all four breast cancer cell lines used (MCF-7, MDA-MB-231, BT474, HCC1806), while the 2H6 clone recognised the immature and the deglycosylated forms. However, only the 10C5 clone distinguished the deglycosylated form of NCT in all samples (Figure 56 a-d). This result is highly intriguing since it implies that in breast cancer cells some amount of partially glycosylated NCT reaches the cell surface, since the 10C5 clone recognised NCT on the cell surface of MDA-MB-231 cells. We have also observed a higher mobility of the mature NCT in BT474 cells (Figure 56a), as detected by MAbs 1E2, suggesting that the mature NCT in this particular cell line might be undergoing additional post-translational modifications, like phosphorylation. Intriguingly, this was the only HER2 positive cell line in the panel, suggesting that the cross-talk between NCT and HER2 may be worth exploring. We have also confirmed that the purified MAbs were able to recognise the cell surface NCT on MDA-MB-231 cells (Figure 56e & f).

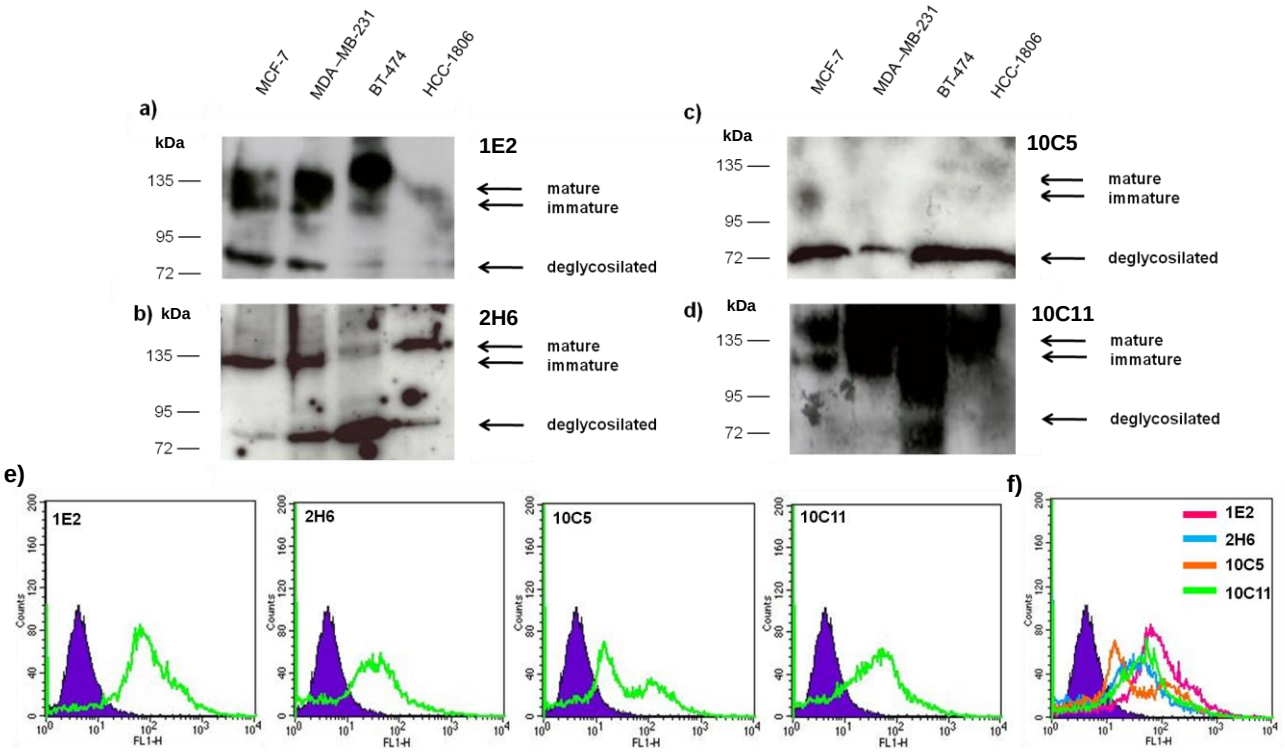


**Figure 56.Western blotting using MAb IgGs.** Whole cell lysates from MCF-7, MDA-MB-231, BT-474 and HCC1806 cells were prepared and run on a 10% SDS-PAGE under reducing conditions, and probed with **a)** 1E2; **b)** 2H6; **c)** 10C5 and; **d)** 10C11 at 4 μg/ml concentration. The signal was detected using the secondary anti-Rat HPR antibody. Arrows indicate expected molecular weight for the deglycosylated, immature and mature NCT. **e)** Non-permeabilised MDA-MB-231 cells were incubated with the Rat IgG2b isotype control (blue) and purified anti-NCT MAbs at 100 μg/ml concentration (green line). Anti-Rat-FITC conjugate was used as a secondary antibody. Histograms indicate a shift upon binding of the anti-NCT MAbs to NCT on MDA-MB-231 cells. Labels in the upper left hand corner of the histograms annotate the MAb. **f)** Overlay of the individual histograms. Color bars in the upper right hand corner of the histogram correspond to the lines and are accompanied by respective MAb labels.

We next investigated the anti-invasive and anti-proliferative effect of the purified clones in MDA-MB-231 cells. Clones 2H6, 10C5 and 10C11 were potent inhibitors of cell invasion with the dose of 50 μg/ml and 200 μg/ml inducing a similar degree of inhibition of invasion: 2H6 (66±10%), 10C5 (48±9.2%) and 10C11 (51.2±3.4%) (Figure 57a). The 1E2 MAb had no effect on either cell invasion or proliferation. The dose of 200 μg/ml was used in the proliferation assay and induced a 28.2±5.2% inhibition of cell growth with the 2H6 and 25.3±8.2% with the 10C5 clone, while a 57.2±5.3% impediment of cell growth was observed with the 10C11 MAb (Figure 57b).

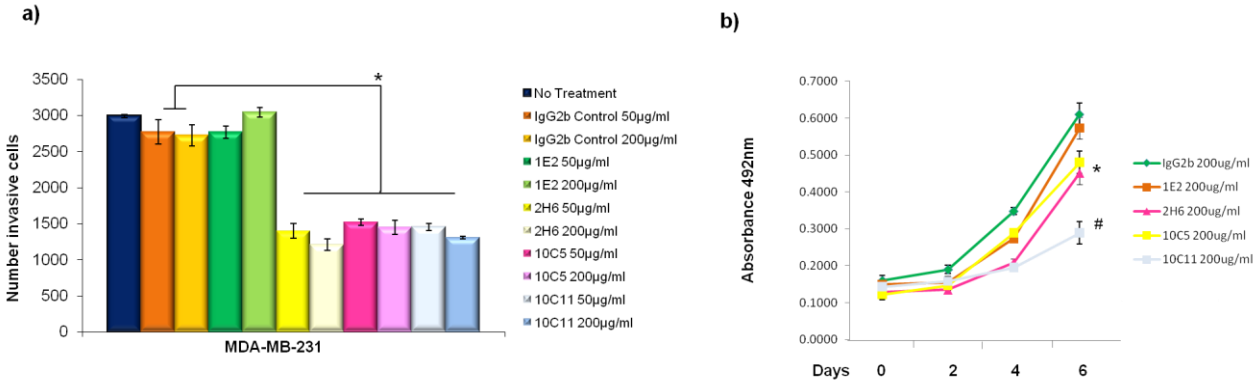


**Figure 57.Cell proliferation and invasion assays using purified anti-NCT MAbs. a)** MDA-MB-231 cells were grown to 70-80% confluence and detached using EDTA. Cells were washed once with PBS and pre-incubated with purified MAbs (1E2, 2H6, 10C5 and 10C11) at RT for 30 min. Rat IgG2b isotype control was used as a negative control Ab. Cells (5 x $10^4$/well) were plated in the upper wells of the transwell invasion plate. The lower chamber contained the chemo-attractant. Cells were incubated for 72 h at 37 °C, and number of invaded cells from the lower chamber was counted using the Casy counter. Bars represent mean number of invaded cells ± SEM from three separate experiments. Statistical difference from the respective concentration of the IgG2b isotype control (2H6 50 µg/ml, p = 0.005; 2H6 200 µg/ml, p = 4.95E-05; 10C5 50 µg/ml, p = 0.0001; 10C5 200 µg/ml, p = 0.0002; 10C11 50 µg/ml, p = 0.0007; 10C11 200 µg/ml, p = 0.0002). **b)** MDA-MB-231 cells were processed in the same way as stated above and pre-incubated with purified MAbs (1E2, 2H6, 10C5 and 10C11), at RT for 30 min. Rat IgG2b isotype control was used as negative control Ab. Cells were plated (3 x $10^3$/well) in 96-well plates and this time point corresponded to Day 0. MAb treatment was supplemented and the SRB assay was performed every 2 days until Day 6. Measurements were performed at 492 nm. Error bars represent SEM from two independent experiments, each one in quadruplicate, *$p < 0.05$, $^{\#}p < 0.02$.

Since our data have shown that NCT silencing reduces vimentin protein levels and affects cell invasion, we next investigated whether anti-NCT MAbs were inducing similar downstream effects. Western blotting of MDA-MB-231 cells treated for 72 h with the MAbs at the concentration of 200 µg/ml showed a reduction of vimentin protein levels. The 2H6 MAb was most potent in inhibiting this proinvasive protein, consistent with its potency to inhibit breast cancer cell invasion (Figure 58).

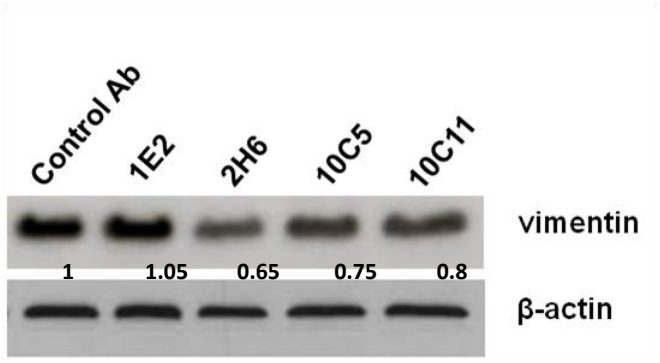


**Figure 58.Treatment of MDA-MB-231 cells with anti-NCT MAbs reduced vimentin protein levels.** MDA-MB-231 cells were treated with anti-NCT MAbs 1E2, 2H6, 10C5 and 10C11 (200 μg/ml) for 72 h. Cells were then lysed and protein extracts were examined for vimentin protein expression by Western blotting. β-actin was used as the loading control. The intensity of bands was quantified using Image J software. Numbers below the bands represent fold change compared to the IgG2b control antibody treated samples, relative to the loading control.

We next cultured MDA-MB-231 cells in 3D Matrigel chambers and supplemented the culture media containing 2% Matrigel with 200 μg/ml of each MAb. The treatment was replenished every 2 days and at day 6, we performed phase contrast imaging of the formed acini-like structures. As previously observed in HCC1806-NCTsh cells grown in 3D Matrigel, the MDA-MB-231 cells treated with anti-NCT MAbs 2H6, 10C5 and 10C11 underwent growth arrest and produced more regular and rounded acini-like structures, compared to the appearance of the control treated cells (66). This effect was consistent with the 2D proliferation assay, but strikingly the 1E2 MAb also induced a modest anti-proliferative effect in 3D conditions (Figure 59). Having observed a change in the 3D acini morphology induced by anti-NCT MAbs, we next sought to investigate the effects on cellular polarity. During tumour progression, tissue polarity is lost as a function of deregulated oncogenic signaling. The PI3K/Akt pathway is one of the main regulators of cellular polarity during malignant transformation, and chemical inhibition of this pathway results in re-establishment of the apico-lateral tight junctions and the reorganisation of the actin cytoskeleton (70). Using the basal extracellular matrix receptor, α6-integrin, aberrantly localised to the cytoplasm in the control cells, we demonstrated that treatment with anti-NCT MAbs restored basal tissue polarity in MDA-MB-231 cells, as judged by the membrane relocalisation of α6-integrin (Figure 60). Since the Akt pathway was inhibited by the treatment of MDA-MB-231 cells with the anti-NCT PcAb, we speculate that the effect of the MAb treatment on cell polarity may be, at least in part, induced by impaired Akt downstream of NCT.

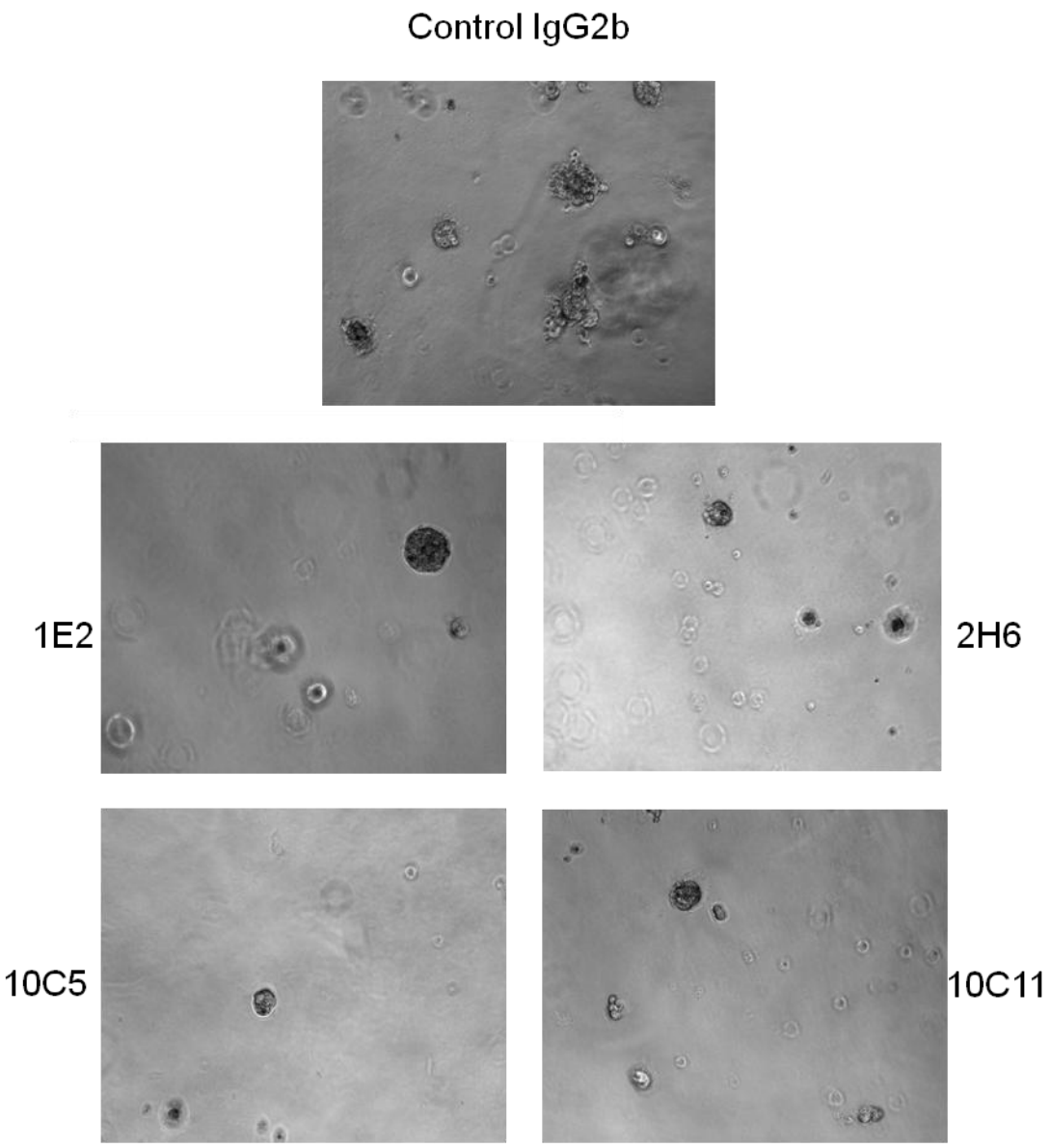


**Figure 59.Treatment of MDA-MB-231 cells with anti-NCT MAbs inhibits growth of acini-like structures**. MDA-MB-231 cells (1 x $10^3$/chamber) were plated in the 3D Matrigel overlay experiment. Cells were cultured in the media containing 2% Matrigel, supplemented with the isotype control Rat IgG2b antibody and the 1E2, 2H6, 10C5 and 10C11 MAbs at 200 μg/ml. Treatment was added upon plating and every 48 h until Day 6. Cells were then imaged using the phase contrast microscopy. Magnification x10.

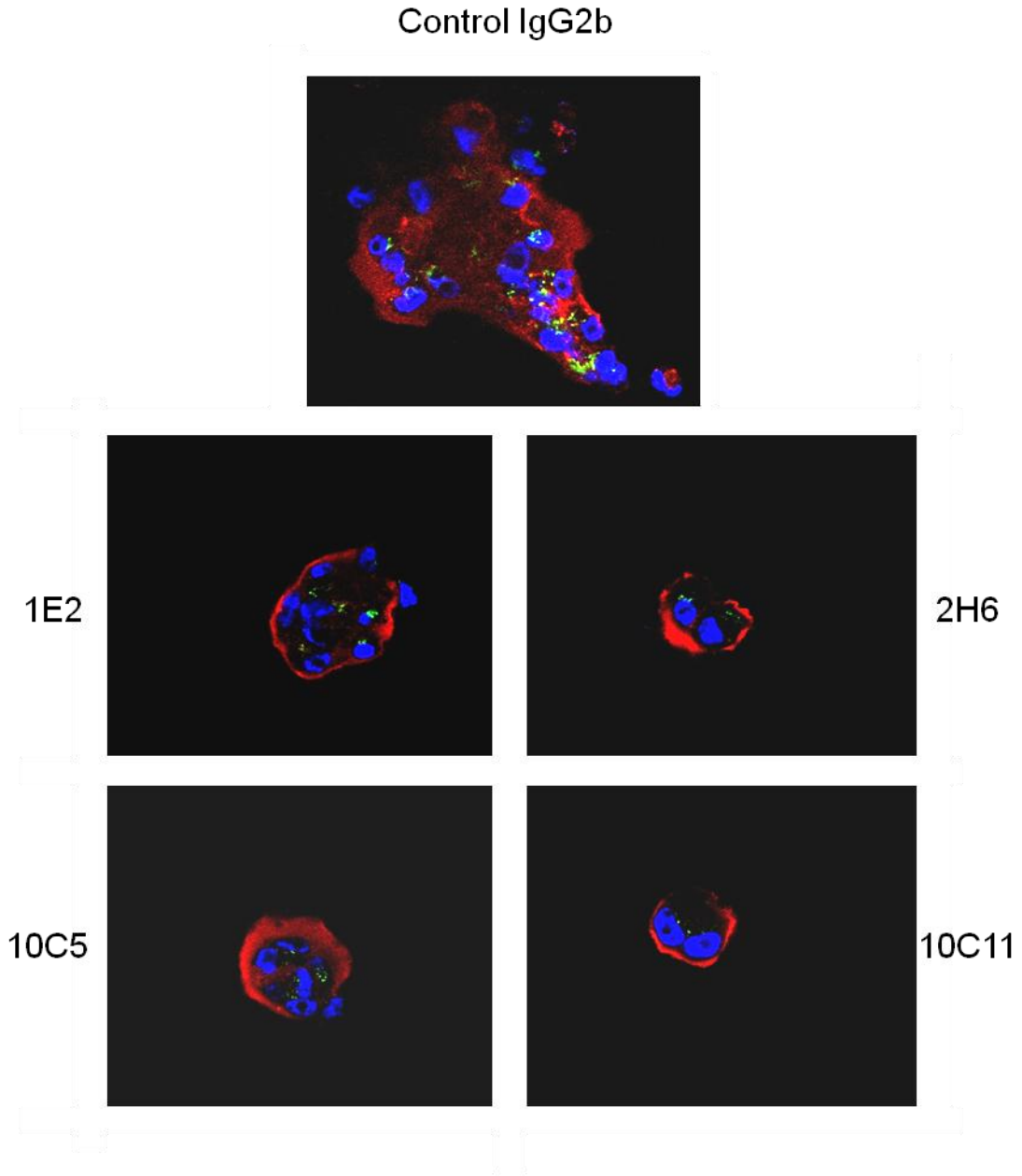


**Figure 60.Treatment of MDA-MB-231 cells with the anti-NCT MAbs induces repolarisation of the α6-integrin.** MDA-MB-231 cells (1 x $10^3$/chamber) were plated in the 3D Matrigel overlay experiment. Cells were cultured in the media containing 2% Matrigel, supplemented with the isotype control Rat IgG2b antibody and the 1E2, 2H6, 10C5 and 10C11 MAbs at 200 μg/ml. Treatment was added upon plating and every 48 h until Day 6. Cells were then fixed, permeabilised and stained with anti-α6-intergin (red), anti-GM130 (green) antibodies. Alexa Flour 488 goat anti-rabbit, and Alexa Fluor 555 goat anti-mouse (Invitrogen) were used as secondary antibodies. DAPI (blue) was used to counterstain the nuclei. Magnification x40.

## 7.7. Determination of the binding properties of anti-NCT MAbs

Tumour-targeting specificity of MAbs requires the target antigen to be primarily expressed on the tumour cells, while the efficacy requires sufficient binding affinity and sustainable tumour retention. The concept that MAbs must have high affinity in order to be therapeutically potent is being somewhat challenged (487). The 'binding-site barrier' model predicts that as the strength of the antigen-antibody bond increases, the amount of MAb diffusing into a solid tumour decreases (30). Antigen expression and internalisation can also have profound effects on MAb penetration into tumours (28), and intrinsic affinity of MAb IgG molecules is an important determinant of their accumulation and penetration into solid tissue**.** It has been observed, however, that the higher-affinity antibodies also exhibit a higher degree of internalisation and catabolism by peri-vascular cells in both *in vitro* and *in vivo* studies (487). Therefore, a balance between antibody affinity and antigen density is required for optimal therapeutic effects.

Enzymatically generated Fab fragments, lacking the Fc region responsible for most effector MAb functions, fail to produce meaningful therapeutic responses. Their *in vivo* blood clearance and catabolism are far more rapid than for whole IgG molecules, while accumulation in the tumour is diminished (488) (489). They are, therefore, as stand-alone molecules, less suitable as cancer therapeutics, but nevertheless, useful tools for *in vitro* investigation of MAb binding properties.

We have, therefore, generated and purified antibody Fab fragments from all four whole IgG molecules (1E2, 2H6, 10C5 and 10C11), using a papain digestion method (Chapter 2). Successful digestion of whole IgGs is shown (Figure 61).

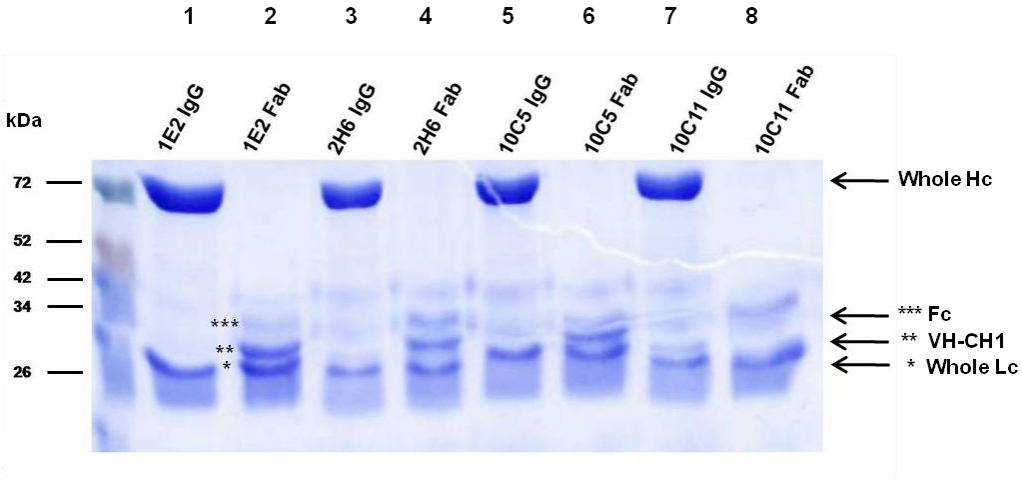


**Figure 61.Coomassie gel.** Fab fragments were made from 1E2, 2H6, 10C5 and 10C11whole IgG molecules using a papain-mediated digestion and purification on the protein A column (Pierce). Whole IgG and Fabs from all four MAbs were denatured, and samples were run on a 10% SDS-PAGE under reducing conditions. The gel was stained using Coomassie blue. Whole IgG lanes: (1-3-5-7) show the presence of the whole heavy chain (Hc) and the light chains (Lc). Digested IgG: lanes (2-4-6-8) show the presence of *Fab fragments at ~25kDa, as well as ** VH-CH1 fragments and the *** Fc fragments.

This allowed a detailed characterisation of the MAb binding affinity and specificity, without the complication of bivalent avidity effects of whole IgGs. Fab fragments from all four clones as well as whole IgGs were subjected to the binding activity analysis by means of ELISA (Figure 62, Table 15).

### 7.7.1. Dissociation constant ($K_d$) determination of full IgGs and Fab fragments by ELISA

The binding of Fab fragments from all four clones as well as whole IgGs was measured directly by ELISA. The antigen used was the mammalian NCT ECD-Fc fusion protein (Fusion Antibodies). The $K_d$ was determined to be 0.61 nM (high affinity) for the 10C11 clone, and 3.7 nM (moderate affinity) for the 1E2 clone using whole MAbs. Clones 2H6 and 10C5 had 21.6 nM and non-detectable $K_d$ values, respectively (Figure 62a, Table 15a). The binding affinity reduced upon Fab fragmentation and measured 624 nM for the 1E2 clone and 222 nM for 10C11, while values were not detectable for the 2H6 and 10C5 Fab fragments (Figure 62, Table 15b). This suggests a significant enhancement of binding affinity due to bivalent cross-linking.

**Table 15.$K_d$ values of anti-NCT MAb whole IgG2b- and Fab- molecules**

**a)**

| IgG2b | $K_d$ (nM) | SD |
|---|---|---|
| **1E2** | 3.7 | 0.83 |
| **2H6** | 21.6 | 0.6 |
| **10C5** | ND | - |
| **10C11** | 0.61 | 0.15 |

**b)**

| Fab | $K_d$ (nM) | SD |
|---|---|---|
| **1E2** | 624 | 92 |
| **2H6** | ND | - |
| **10C5** | ND | - |
| **10C11** | 222 | 9.1 |

### 7.7.2. Titration FACS and cell based $K_d$ calculation

Cell-based quantitative FACS was performed using MDA-MB-231 cells. This allowed MAb binding to the endogenous, native, cell-surface antigen and determination of a cell-based $K_d$. It was established to be 69 nM for the 1E2 clone, 57 nM for the 2H6, 536 nM for the 10C5 clone and 72 nM for the 10C11 clone (Figure 62c). As well as being physiologically relevant, the $K_d$ values obtained indicated that the binding of the MAbs *in vivo* was predominantly monovalent.

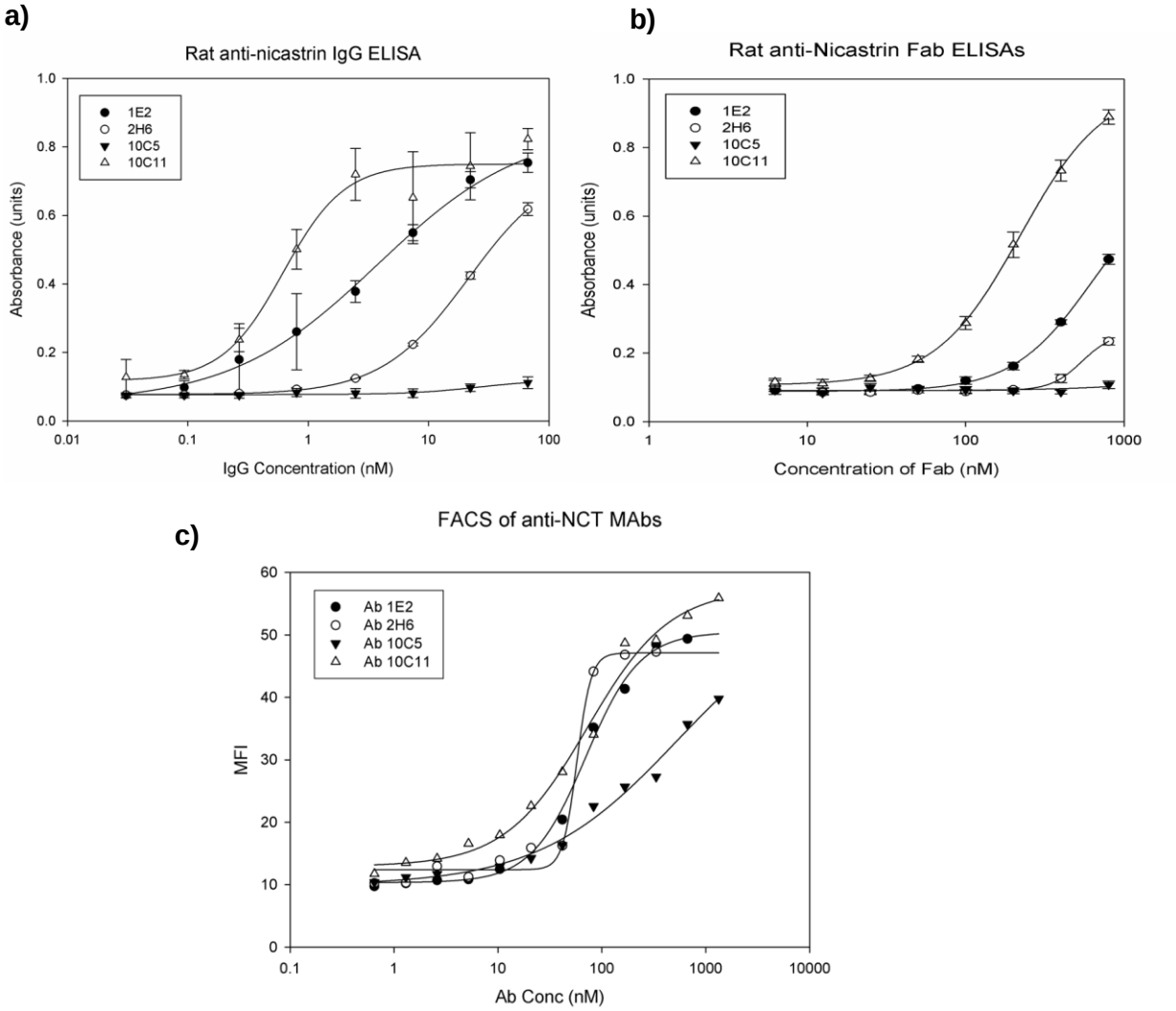


**Figure 62.Determination of MAb Kd values in a non-cell bases ELISA assay and the cell-based FACS experiment. a)** The binding of Fab fragments from all four clones and, **b)** whole IgGs was measured by ELISA. Recombinant human NCT-Fc antigen was coated on 96-well microtiter plates (5 µg/ml). Purified IgGs and Fabs were used with a two-fold serial titration (1 mM to 0.01 nM), followed by secondary detecting antibodies and colorimetric substrate (POD, Roche). Reaction was quenched by adding 1N $H_2SO_4$, and the signal was measured at 492 nm. **c)** Cell-based FACS titration was performed by incubating non-permeablised MDA-MB-231cells with each IgG as a primary antibody in two fold serial dilution (1 mM to 0.01 nM), followed by the secondary anti-Rat FITC-conjugated antibody. Non-cell based, and cell-based dissociation constant ($K_d$) were determined by fitting the binding curves to sigmoidal 1:1 binding curves and extrapolating the 50% binding concentration (SigmaPlot v10.0).

### 7.7.3. BIACore Surface Plasmon Resonance Analysis

BIACore is designed for the routine analysis of biomolecular interactions. Surface plasmon resonance (SPR) detects reflective index changes close to the surface of the BIACore chip. Since all biomolecules have refractive properties, no labeling is required. SPR detects binding events as changes in mass at the chip surface. This method, therefore, enables real time kinetics measurement and qualitative rankings of MAbs. The association rate ($K_a$) reflects the rate of complex formation and MAb recognition capacity towards the cognate antigen, while the dissociation rate ($K_d$) reflects the stability, i.e. fraction of the complex that decoys per second (490). The principle of the assay is shown in Figure 63.

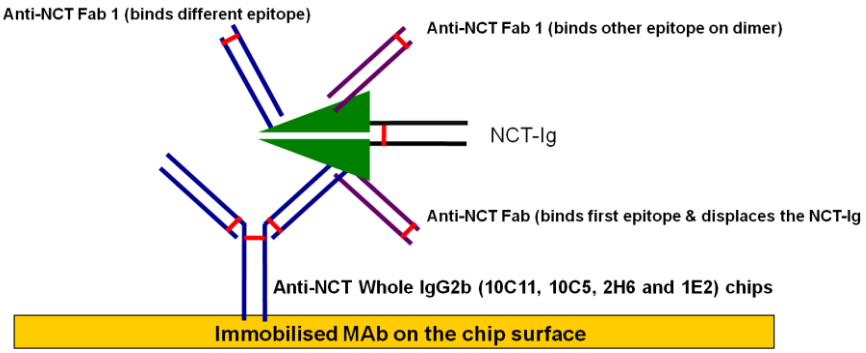


**Figure 63.The principle of epitope mapping by the surface Plasmon resonance (BIACore).**

BIACore 3000 was used to epitope map the anti-NCT MAbs by determining which ones compete for binding to the NCT antigen. An indicated MAb was immobilised onto the surface of the BIACore chip which was then exposed to the flow of the human NCT-Fc protein (Figure 63). The sensogram registered a consequent increase in the chip weight corresponding to the association part of the curve. Next, a chosen Fab fragment was injected and flown over the chip surface. If the binding sites of the Fab were occupied by the immobilised IgG, then a dissociation (descending) curve was observed, indicating that the IgG and the Fab bound overlapping or same epitopes. If additional binding was observed (ascending curve), it indicated that the IgG and the Fab bound distinct epitopes. Indeed, we observed that 10C11 and 1E2 clones are binding overlapping epitopes (Annex 3a-c-d; displaced binding), while 10C11 and 2H6 clones are directed against spatially distinct regions

on the NCT protein (Annex 3b; additive binding). Other permutations of the immobilised MAb IgGs and Fab fragments in the competition binding BIACore assay are under way. Additionally, given that the 10C11 clone has thus far proven to possess the best binding affinity, we have also performed BIACore analysis of the 10C11 MAb binding kinetics. A range of NCT-Ig antigen concentrations were flowed over the surface of the immobilised 10C11 MAb to give a series of associations and dissociations from which the association rate constant ($K_{on}$) of 4 x $10^3$ $M^{-1}$ $s^{-1}$ and the dissociation rate constant was ($K_{off}$) of 6 x $10^{-4}$ $s^{-1}$ were determined. Consequently a $K_d$ of 149 nm was calculated, which was comparable to the ELISA $K_d$ analysis (Annex 3e).

### 7.7.4. Isolation of IgG antibody Fv-DNA sequences from hybridoma cell lines

Knowledge of the MAb sequence is important for the purpose of engineering higher affinity derivatives and humanised antibodies. The 1E2, 2H6, 10C5 and 10C11 hybridoma clones were grown in culture and cells from each clone were harvested for mRNA isolation. RT-PCR was carried out on all clones using primers designed to amplify the variable heavy- and light-domain sub-genes (361). Restriction sites introduced by the primers can enable the Fv-DNA to be inserted at the 3'-terminus of DNA coding for a bacterial leader sequence in many commercial expression vectors. After cloning the $V_H$ and $V_L$ genes into the pCR®2.1 vector, the restriction fragments were analysed by gel electrophoresis, and subsequently sent for sequencing using M13 primers (sequences provided in Chapter 2). This will allow for definite identification of the critical, antigen binding domains of the antibody variable domains and complementarity determination regions (CDR) (Figure 64).

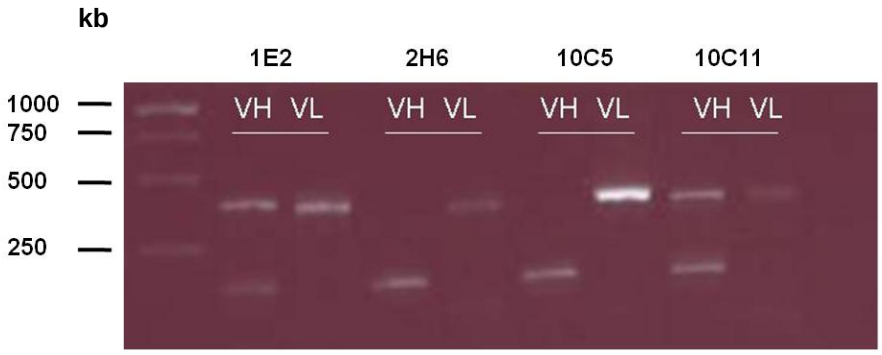


**Figure 64.Agarose gel electrophoresis of amplified MAb DNA (1E2, 2H6, 10C5 and 10C11).** Results for the heavy chain (VH) and the light chain (VL) amplification are shown. Expected PCR transcripts are visualized at ~ 350 kb. The temperature of hybridisation during the PCR was 52 °C. Amplification was successful for of 1E2 and 10C11 (VH & VL), 2H6 VL and 10C5 VL, while no product was detected for 2H6 VH and 10C5 VH. This indicates the need to further optimise the PCR conditions.

## 7.6. Discussion

An anti-NCT PcAb was developed against the DAP domain of the NCT protein (261-502 a.a.), which harbours the functionally relevant DYIGS region and the E333 site, involved in GS substrate recognition, and NCT maturation (302). NCT-Pc Ab recognised endogenous, cell-surface NCT on breast cancer cells and inhibited cell proliferation, as well as cell invasion, both in a dose-dependent manner. Moreover, treatment of MDA-MB-231 cells with the PcAb reduced NCT protein levels and inhibited GS activity, as demonstrated by the lack of Notch1-ICD generation. We have also shown that the Akt pathway downstream of NCT was attenuated. These data served as a strong proof of principle that NCT could be targeted in breast cancer cells by means of a blocking antibody.

We therefore developed anti-NCT MAbs by genetic immunisation of rats using the cDNA encoding for NCT ectodomain. From 21 positively screened hybridomas using a Genovac propriety cell line where NCT had been artificially overexpressed, we identified ten clones which recognised endogenous, cell-surface NCT on breast cells. Consequently, seven of those were also able to inhibit breast cancer cell invasion, as screened by using the transwell cell invasion assay. Clone 1E2, which bound NCT on MDA-MB-231 cells, but failed to infer a functional inhibitory effect on cell invasion was subcloned and expanded to

be used as a ‘negative MAb control’. Positive clones taken forward were 2H6, 10C5 and 10C11.

The transwell cell invasion assay, has been widely implemented for screening inhibitors of cellular migration and invasion, and provides affordable and reproducible results. Matrigel is used as the standard matrix to coat the polycarbonate filter inserts. The standard pore size of 8 μm ensures that the cells do not passively fall into the bottom well but rather pass through by actively ‘squeezing’ through the pores (491, 492). Furthermore, this 3D model of cell invasion has advantages over 2D cultures in mimicking more physiological conditions with respect to dimensionality, architecture and cell polarity *in vivo* (493).

The doses of MAb used for the treatment of MDA-MB-231 cells were 50 μg/ml and 200 μg/ml for the invasion assay, and 200 μg/ml in all other assays. This high dose was chosen due to the fact that we were anticipating low antigen density of the cell surface, due to the reported GS spatial paradox and segregation into plasma membrane lipid rafts (242, 247). The same rational led us to hypothesise that the proximity of the neighbouring NCT molecules on the cell membrane would not be sufficient to allow for the bivalent binding of the MAbs, therefore we aimed to maximise the magnitude of MAb-antigen interaction by delivering increased amounts of the MAb.

In the functional assays, purified clones 2H6 and 10C5 produced a comparable anti-proliferative effect in MDA-MB-231 cells, while 10C11 was more potent. All three clones inhibited cell invasion to a similar degree at both 50 μg/ml and 200 μg/ml dose. This suggests firstly, that the degree of functional inhibition of cell invasion saturates at or below the dose of 50 μg/ml, and secondly, given the degree of inhibition at an equivalent dose, that the anti-invasive effect of the anti-NCT MAbs could be predominant over their anti-proliferative effect. The anti-invasive effects may be mediated by the observed reduction of vimentin protein levels and the induction of cancer cell repolarisation. Further characterisation of the MAbs using a non-cell based ELISA assay and the cell-based FACS analysis, confirmed that the preferred mode of physiological IgG binding is monovalent (Figure 65), and that the 10C5 clone is not the best candidate MAb due to the high $K_d$ value. This information is valuable for the design of functional *in vitro* experiments as well as *in vivo* studies to determine MAb dose selection.

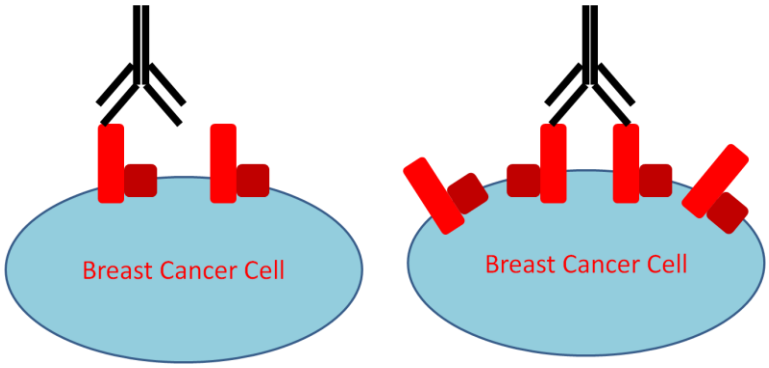


**Figure 65.The concept of monovalent and bivalent MAb-antigen binding.** Monovalent binding engages one arm of the MAb heavy- and light-chain variable regions for interaction with the antigen. Bivalent binding engages variable domains on both MAb arms. Antigen density of the cell membrane can be a limiting factor preventing bivalent binding.

Interestingly, what emanated from the competition based BIACore analyses was that the 1E2 and 10C11 clones bind overlapping epitopes on the NCT antigen. Coupled with the fact that the 1E2 MAb did not infer significant inhibitory effects, this suggests that the non-overlapping region between the two MAbs may be functionally important. Importantly, 2H6 and 10C11 MAbs recognised distinct regions on NCT. Having in mind that the 10C11 clone was a more potent inhibitor of cell proliferation than the 2H6 MAb, while both had comparable impact on invasion, it is plausible that the 10C11 binding epitope on NCT is particularly relevant for mediating cell survival, while the region corresponding to the 2H6 binding site primarily mediates cell invasion.

The developed MAbs further differed in their ability to recognise NCT glycoforms. The 1E2 and 10C11 MAbs recognised all three NCT forms (deglycosylated, immature and mature) (220), while the 2H6 was superior in recognising the immature and the deglycosylated NCT. Remarkably, the 10C5 antibody only recognised the deglycosylated NCT. It has been demonstrated *in vitro* that only the fully post-translationally modified NCT reaches the cell surface (292). The fact that the 10C5 MAb was able to recognise NCT on the cell surface of MDA-MB-231 cells, as well as to induce functional effects in conditions where MDA-MB-231 cells were not permeabilised, leaves us with a hypothesis that a certain amount of not fully glycosylated NCT might reach the plasma membrane in breast cancer cells.

# CHAPTER 8

# General Discussion

## 8.1. Nicastrin silencing in breast cancer cells disrupts the gamma-secretase complex and affects cell adhesion and invasion regulators

The marked upregulation of NCT protein expression in human breast cancer cell lines compared to normal breast cells prompted our efforts to employ the NCT siRNA targeting approach and elucidate whether NCT is functionally important in breast cancer cells. Nicastrin has thus far primarily been characterised and investigated as a member of the GS enzyme quartet, partnering with PS, PEN2 and Aph-1 to form a functionally active proteolytic complex (494). Given the diversity and the sheer number of GS substrates (190), the activity of which is inhibited by impaired GS function upon NCT silencing, both the anti-proliferative and the anti-invasive aspects of NCT inhibition could be interpreted as being indirectly caused by deregulated GS substrate function. This is an entirely plausible argument, since we have been able to demonstrate that, as in other cellular systems (164), NCT silencing in breast cancer cells inhibits Notch signaling, but also affects mediators of cell apoptosis, adhesion and invasion, which are cellular processes affected by other GS substrates as well: CD44, HER4, E-cadherin, EpCAM etc.

Our main observation upon NCT silencing in MCF-7 and MDA-MB-231 cells was the effect on cell adhesion and invasion proteins. The mechanism underlying the effects on cell-cell adhesions by NCT silencing appears to involve the regulation of E-cadherin and p120ctn localisation to the cell membrane. Since NCT inhibition also reduces cellular levels of PS1, which binds E-cadherin on the same motif involved in E-cadherin binding to p120ctn, we hypothesise that absence of PS1 allows for enhanced E-cadherin-p120ctn interaction, which facilitates cell adhesion (372). As for the effects on cell invasion, the most pronounced modulation was observed in the case of vimentin protein and mRNA levels, both of which were markedly decreased upon NCT silencing, and significantly increased upon its overexpression. This may be mediated via the coordinately modulated mRNA levels of the promoter of vimentin transcription, *SIP1*. As a major promoter of breast cancer cell invasion, vimentin maintains mesenchymal cell shape and behavior. Its overexpression in MCF-7 cells and MCF10A cells is sufficient to induce phenotypic changes characterised by elongation and reduction in cell height, which enable the invading cells to be more resilient and survive the shear mechanical stress associated with detachment from the primary tumour and invading through the tissue to form metastatic deposits (495).

The anti-invasive effects of NCT silencing observed in MDA-MB-231 and HCC1806 basal-like breast cancer cell lines reflect the changes in cell shape and distribution. Immunofluorescence imaging and phase contrast microscopy have demonstrated that NCT-depleted MDA-MB-231 and HCC1806 cells lose their scattered distribution and assume a more cobble-stone like shape, with formation of cell-cell junctions.

Cancer cell invasion can be mediated by two main forms of cell movement, the elongated and the amoeboid. These two forms can be interchangeable and depend on the cell intrinsic properties, position of cancer cells within the tumour, as well as on the signals from the tumour surroundings. Elongated, mesenchymal movement is driven by Rac-dependent signaling, integrin molecules, matrix-metalloproteases and proteolytic disintegration of the extracellular matrix (ECM). The acto-myosin contractility in amoeboid motility represents the force behind the formation of bleb-like protrusions on the cell membrane, enabling the cells to push and squeeze through the ECM without much need for ECM proteolysis (496). Inhibition of one of these forms of movement has been known to induce a switch to the alternate mechanism. Ideally, one would aim to inhibit both the amoeboid and the mesenchymal motility in order to abrogate formation of metastasis successfully (452). Recently, a model of MDA-MB-231 cell migration has shown that these cells predominantly engage in amoeboid cell movement during invasion through the 3D matrix, with myosin IIa accumulating at the rear of the cell. The RhoA-ROCK1 signaling axis promotes acto-myosin contractility during amoeboid movement (497), while RhoE inhibits motility by acting as a negative regulator of ROCK1-mediated signaling (498). Our protein array data have shown that NCT silencing could be upregulating RhoE levels and inhibiting myosin IIa, which suggests that the mechanism of anti-invasive effects of NCT depletion could be mediated through attenuation of amoeboid cell movement.

In addition, the immunofluorescence imaging of MDA-MB-231 cells indicated that some cells adopt the elongated phenotype on a 2D substratum, when the locomotive force is predominantly generated by Rac1, in support of mesenchymal movement (452). This data, coupled with our RT-qPCR analysis upon NCT silencing and overexpression, which demonstrated that NCT modulates expression of integrins and MMP7 metalloprotease, both of which mediate Rac-induced motility, may serve as an indication that mesenchymal cell movement might be affected by NCT silencing as well. Interestingly, a Rac1 activating protin DOCK3 (499, 500), which is a member of the DOCK180 family of guanine nucleotide

exchange factors that facilitates GTP loading of Rac1 at the plasma membrane, has been identified as a binding partner of PS1 in neuronal cells (501). It was shown that overexpression of PS1 in Alzheimer's disease induces relocalisation of DOCK3 from the cytoplasm to the cell membrane (501). If PS1 and DOCK3 were interacting and colocalising at the plasma membrane in breast cancer cells as well, it could implicate PS1 and by inference GS, as potential regulators of Rac1, and thereby mesenchymal cell movement. If the PS1-DOCK3 interaction at the cell membrane observed in neurons, translates to the breast cancer cell model, then a hypothesis could be postulated that NCT depletion-induced reduction of PS1 acts as a mechanism to downregulate DOCK3, thereby attenuating Rac1 mediated cell invasion.

## 8.2. Stable nicastrin depletion in triple-negative breast cancer cells HCC1806 reduces the proportion of the stem-cell-like population and inhibits their invasive traits

The importance of targeting breast cancer stem cells in order to achieve more durable effects of anti-cancer therapy, and ultimately prolong patient survival, has been established. Multiple neo-adjuvant clinical trials in breast cancer patients have shown that neither chemotherapy nor hormonal therapy are entirely successful in eradicating tumour initiating cells, but rather they increase the cancer stem cell pool in the residual tumour tissue (502). In 2003, the work of Al Hajj et al. described CD44 and CD24 as relevant markers of this cell population within a tumour, and since then the $CD44^{+}/CD24^{low/-}$ phenotype has been widely used to isolate and characterise breast cancer stem cells *in vitro* and *in vivo* (87). Breast cancer stem cells express invasive features characterised by high vimentin and Slug levels and absence of E-cadherin (503).

It has been demonstrated that Notch signaling also contributes to the maintenance and expansion of the breast cancer stem cell pool (110). Targeting Notch by direct siRNA and using GSIs potently reduced mammosphere formation (176, 504). Mammosphere formation in MCF-7, MDA-MB-231, BT-474, and SKBR3 cells was abolished by using a non-aldehyde containing GSI, MRK003, resulting in cell death after 7-10 days in all cell lines. Equally, Notch1 siRNA prevented mammosphere formation (504). Differential activity of Notch1 and Notch4 receptors has been observed in mammospheres from the sorted MCF-7 and MDA-

MB-231 cells. Notch4 signaling was found to have a greater effect on breast cancer stem cell activity than Notch1 (176), and Notch inhibition by a GSI (MK-0752) reduced breast cancer stem cell number and activity (176). Our data using CD44/CD24 immunosorting in HCC1806-Luc1 and HCC1806-NCTsh cell lines, recapitulated the finding of the differential activity between Notch1 and Notch4 in breast cancer stem-cells, and further implicated NCT as a regulator of this cell population. The stem-cell pool was reduced in NCT depleted cells, and even though Notch4 mRNA levels remained high, NCT ablation reduced protein levels of the active Notch4. Our observations further expand by demonstrating that NCT acts as a potent inhibitor of cell invasion inducers in breast cancer stem cells including, v*imentin*, *SIP1* and *Snail*. It would be of interst to examine the effect of Notch4 siRNA on these markers of cell invasion in the context of breast cancer stem cells, and gain insight whether NCT silencing is acting to regulate them via Notch, or possibly in a Notch-independent manner.

Recently, the issue of cancer stem cell plasticity has been addressed in the context of the breast cancer stem cell phenotype. It has been demonstrated that like the $CD44^+/CD24^-$ population, which propagates *in vitro* and *in vivo*, giving rise to a proportion of $CD44^+/CD24^+$ cells, the $CD44^+/CD24^+$ cells, initially deemed non-tumourigenic, are also able to interconvert and produce $CD44^+/CD24^-$ cells *in vitro* and in xenograft models of breast cancer (503, 505). The stem cell-like potential and interconversion appears to be mediated through the Activin/Nodal signaling pathway. Hence the authors propose that successful breast cancer stem cell targeting should aim to disable the Activin/Nodal signaling which would then impair this interconversion, thus preventing the $CD44^+/CD24^+$ to give rise to more invasive $CD44^+/CD24^-$ cells (503). Interestingly, Nodal is a direct target of the Notch pathway (506), and its expression in breast cancer tissue correlates with disease progression (507). Furthermore, Notch4 silencing potently downregulates Nodal in malignant melanoma (508). Therefore, we will explore the impact of NCT depletion on the levels of Nodal in breast cancer stem cells.

In summary, considering the fact that NCT inhibition was able to reduce proliferation and invasion of differentiated breast cancer cells, and to impede proinvasive proteins in breast cancer stem cells defined by the CD44/CD24 phenotype, we speculate that the anti-NCT therapy in breast cancer may not only target the bulk of the primary tumour, but might also be potent in reducing the number and the invasive potential of breast cancer stem cells, deemed responsible for cancer relapse.

## 8.3. Nicastrin inhibition regulates a subset of Notch-independent genes in MDA-MB-231 cells

Since the discovery of the roles for intracellular domains of GS substrates in gene transcription (Notch-ICD, APP-ICD etc.), the notion of GS as a major player in pathologically altered gene transcription has been extensively studied. Comparison of differentially regulated genes in Chinese hamster ovary (CHO) cells, in conditions where GS has been overexpressed vs. inhibited has revealed several affected functional gene clusters underlying GS-mediated cellular biology (222). We have similarly investigated genes that are transcriptionally susceptible to NCT activity in breast cancer MDA-MB-231 cells, by comparing global transcriptional changes between conditions of NCT silencing and silencing of the individual Notch receptors.

Interestingly, some genes that appeared significantly affected in our experiment were also identified by the work of Magold et al. who investigated genes modulated between conditions of GS overexpression vs. GS inhibition in CHO cells. One of the genes with 3-fold increased transcription under enhanced GS activity compared to inhibited GS activity was Bub1. In line with that, Bub1 was downregulated in our experiments by NCT silencing. Furthermore, vimentin and SPARC (secreted protein acidic and rich in cysteine), both genes involved in promoting EMT (53), were downregulated upon GS overexpression in CHO cells. In contrast to this, GS inhibition was ~previously shown to downregulate vimentin via Notch inhibition in salivary epithelial cells (391), and we have consistently found vimentin to be potently inhibited by NCT depletion in both MDA-MB-231 and HCC1806 cells. CD44 and E-cadherin genes were downregulated by 3-fold, while Notch3 and Hes1 were increased under enhanced GS activity by 5-fold and 7-fold, respectively in CHO cells overexpressing GS (222). Of the genes involved in cellular migration, MYH10 transcript levels were 3-fold decreased, and we have found the same qualitative change of the MYH10 upon NCT silencing, which reduced GS activity. The fact that MYH10, vimentin and E-cadherin were regulated by NCT silencing in the same direction as they were by GS overexpression in CHO cells, which have been extensively used for the characterisation of the GS complex (326), proposes that GS/NCT activity may be highly cell context dependent, and at the same time emphasises the importance of NCT siRNA-induced anti-invasive effects in breast cancer cells. It is important though to emphasise that the comparisons in CHO cells were made

between two extreme conditions of GS overexpression vs. inhibition, while we have compared NCT siRNA effects with control, 'base-line' levels, which could account for the differences.

Furthermore, a recent microarray experiment has identified genes regulated by overexpression of active Notch1 in non-transformed breast cells MCF10A, and highlighted the importance of the Notch signal strength in induction of either malignant cell transformation (intermediate levels of Notch) or entosis (high levels of Notch) (390). The intergrin gene signature was prominently modulated by Notch1 induction, in line with the observed loss of cell-cell adhesions. Similarly, we have demonstrated that NCT stable knockdown increases integrin A4 and decreases integrin B2 mRNA, which therefore may be a Notch1-mediated effect in HCC1806-NCTsh cells.

Interestingly, genes that we found regulated only by *NCT* silencing and not *Notch1* siRNA in MDA-MB-231 cells, were found regulated in the inverse fashion in MCF10A cells by Notch1 overexpression. These are *PHLDA1* and *ASNS* which were downregulated by 2-fold upon transfection of MCF10A with Notch1-ICD, and upregulated 2.86-fold and 6.2-fold, respectively by *NCT* depletion. Also, the *E2F2* gene was inhibited by *NCT* silencing while its upregulation was noted upon Notch1 activity induction in non-malignant breast cells. These data suggest that the dependence of certain genes on NCT or Notch1 signaling may be dependent on the actual degree of Notch activation/inhibition, particularly since the importance of the Notch activity levels to induce differential cellular effects has been demonstrated. Furthermore, comparison of gene signatures in normal and breast cancer tissue revealed a malignancy-risk gene signature of 109 upregulated and 31 downregulated genes (509). Among the upregulated genes, some were those that we found affected by NCT silencing. For example, *Bub1* and *UBE2T* were found 2.7- and 4.9-fold upregulated in breast cancer compared to normal breast tissue (509), while we found that they were downregulated by NCT siRNA by 2.2- and 3.2-fold, respectively. This suggests that NCT silencing may indeed be relevant for reversing some of the molecular changes acquired by malignant transformation of breast cells. Once we obtain complete Affymetrix gene array analysis, more of such genes may become apparent. It is also important to bear in mind that NCT silencing may be modulating the observed Notch-independent gene set in MDA-MB-231 cells via regulation of other GS substartes. This could be addressed by performing siRNA for selected GS substrates, such as HER4, CD44, EpCAM, N-cadherin etc., and investigating the effect

on the genes we have here attributed to being susceptible to NCT depletion. As transcriptional activity of genes translates into molecular functions, mapping the interactions of proteins encoded by the genes we validate, and proteins revealed in the antibody array we have performed, could more precisely highlight the cellular pathways mediated by NCT in breast cancer cells.

## 8.4. Nicastrin is overexpressed in breast cancer tissue compared to normal breast

Expression of GS components (NCT, PS, Aph-1 and PEN2) has thus far not been examined in breast cancer tissue. An indication that overall GS activity may be elevated in breast cancers, stems from the fact that activated Notch1 is overexpressed in a subset of breast cancer patients, where it predicts for worse overall survival (477). We have analysed NCT expression in human breast tissue using an antibody raised against the C-terminal portion of NCT that has previously been used for analysis of NCT expression in mouse tissue by IHC (220). We confirmed the antibody specificity in breast cancer tissue by pre-incubation with the competing peptide, which abrogated the immunoreactivity altogether.

We have observed that NCT is not present in the normal breast, while its levels appeared increased in the basal cell compartment of fibroadenomas and were increased in epithelial cells of breast cancer tissue. The intensity of NCT staining was dichotomised to NCT low and NCT high expressors. In the 1050 breast cancer tissue specimens examined, high NCT expression, detected in 47.5% of the examined cases, was predictive of worse overall survival in the ERα negative patient subset.

This result directed our focus towards investigating the role of NCT in aggressive breast cancer, since the ERα negative tumours are clinically, as well as *in vitro*, more invasive than their ERα positive counterpart. Corroborating the importance of high NCT expression in invasive breast cancer, we demonstrated an elevation of NCT expression in the invasive component, compared to the associated *in situ* carcinoma on the full-faced sections of tumours, and have also showed that NCT abundance is retained in the breast cancer lymph node metastasis. Taking this into consideration, and having shown that targeting NCT using siRNA and specific monoclonal antibodies was able to inhibit the invasive cellular features at the molecular, phenotypic and functional level *in vitro*, we formed a hypothesis that targeting

NCT to inhibit aggressive breast cancer may be a therapeutic approach worth investigating further.

Our IHC data equally highlighted the need to characterise the mechanism(s) responsible for inducing high NCT expression in breast cancer. The fact that NCT levels appeared elevated in the basal cell compartment of fibroadenomas proposes that the stromal-derived factors may regulate NCT expression in breast epithelium in a paracrine manner. The importance of fibroblasts surrounding the breast epithelial tissue has recently been reiterated by the work which demonstrated that the stromal fibroblast compartment of breast tumours potently regulates stem-cell related genes in breast cancer cells (510). Namely, cocluture of breast cancer derived fibroblasts with MCF-7 cells in mammosphere-growth permissive conditions potently promoted expression of cancer stem-cell related genes, including Notch1, compared to the coculture models with normal breast tissue fibroblsts (510). Regulation of NCT gene expression has so far been examined in a panel of neuronal cell lines, where none of the cytokines or growth/differentiation factors used to treat the cells (TNF-α, IL-1β, brain-derived neurotropic factor, PMA) had any effect on NCT transcription. Therefore, comparable coculture experiments, as well as treating breast epithelial cells which do not express high NCT levels (MCF10A) with a repertoir of factors (TGF-β, HGF, FGF, EGF TNF-α, VEGF, etc.) derived from breast cancer associated stroma (511), is warranted, in order to evaluate their potential to upregulate NCT mRNA and/or protein levels.

Furthermore, our IHC analysis highlighted a direct correlation between high NCT expression and ERα positivity in breast cancer tissue. We suspect that the lack of predictive capacity of high NCT expression for survival of ERα positive breast cancers comes from the fact that benefit from hormonal therapy given to these patients could have abrogated adverse impact of high NCT levels. Our *in vitro* data where NCT siRNA was able to inhibit the proliferation of ERα positive, MCF-7 breast cancer cells, as well as preliminary analysis (www.nursa.org), which indicated that estrogen may be able to regulated NCT gene expression in breast cancer cells, highlight that investigating the molecular and functional implications of NCT expression in hormono-sensitive breast cancer may be important.

## 8.5. Anti-nicastrin monoclonal antibodies as potential means of targeting nicastrin in invasive breast cancer cells

Our *in vitro* and *in vivo* data have revealed that NCT may be an important signaling molecule in breast cancer cells. Coupled with the fact that NCT architecture reveals a prominent extracellular domain which harbours important functional domains, we have hypothesised that an antagonistic monoclonal antibody would be a valid therapeutic to inhibit NCT function(s) in breast cancer cells.

Selected anti-NCT MAbs proved to be potent inhibitors of breast cancer cell invasion and inducers of breast cancer cell repolarisation. All functionally effective MAbs (2H6, 10C5 and 10C11) recognised NCT on the surface of breast cancer cells but had a differential potential to recognise NCT glycosylated forms in whole cell lysates. Particularly, the 10C5 MAb detected only the deglycosylated NCT form by western blotting, prompting us to hypothesise that there could be a certain amount of partially glycosylated NCT which functions at the plasma membrane. It is also possible that the mature NCT conformation, which is consistent with increased glycosylation, represents steric hindrance for reactivity of this MAb with the peptide backbone.

The differential reactivity of anti-NCT antibodies raised against distinct peptide epitopes has been recognised in membrane lysate preparations from adult and embryonic mouse brain-derived neural stem cells. NCT ectodomain antibody (331–346 a.a.) showed reactivity with immature and deglycosylated NCT, while a C-terminal antibody (691–709 a.a.) detected mature NCT of ~145 kDa, in addition to lower molecular weight forms. Antibody generated to the hydrophobic region adjacent to the signal peptide on the NCT N-terminal region (32-44 a.a.) detected NCT as two major bands, a stronger band at ~125 kDa, and a weaker band at ~145 kDa in the embryonic brain tissue, demonstrating thereby less reactivity for the more mature NCT forms (220).

The differential ability of MAbs raised against distinct regions of an antigen may be explained by the unique sensitivity of each MAb to detect post-translational modifications (PTMs) of a protein they were raised against. This suggests that caution must be taken when choosing a MAb to detect highly modified proteins, such as NCT. An example of this are MAbs raised against recombinant osteopontin using phage display (512).

Osteopontin is a secreted phosphoglycoprotein found in a variety of tissues and body fluids, and a CD44 ligand. Degree of osteopontin phosphorylation plays a role in determining its physiological function, similar to the impact that the level of NCT glycosylation has on its ability to form a functional GS complex and localise to the cell membrane. All tested MAbs raised against osteopontin recognised the protein derived from conditioned medium of Ras-transformed fibroblasts, while only one MAb (AK2A1) reacted with the protein secreted by the non-transfromed cells, which contains 17 additional phosphate modifications. However, even the AK2A1 MAb failed to recognise urin-derived osteopontin, which is additionally glycosylated, and may therefore contain unique modifications which are able to specifically inhibit AK2A1 binding (512). Glycosylation motifs of NCT may therefore be inhibiting the binding of the 10C5 anti-NCT MAb, rendering it incapable to identify higher molecular weight NCT isoforms. Anti-NCT MAb binding sensitivity to PTMs may be the feature that is determining their ability to identify subtle differences in the protein structure, thereby highlighting their usefulness.

Thus far, the glycosylation profile or the presence of other PTMs of NCT (e.g. phosphorylation) in breast cancer tissue has not been investigated. In our future experiments we can apply NCT deglycosylation treatments (EndoH and PNGase) to breast cancer cells, in order to remove the high mannose moieties and total N-linked sugars, respectively, and test the binding ability of the MAbs in a cell based ELISA assay, by western blotting, as well as perform immunofluoresence colocalisation studies incorporating markers of cellular compartments (calnexin for the ER; GM130 for the Golgi). This may yield important information about expression levels and cellular distribution pattern of NCT glycosylation forms in breast cancer cells. Immunohistochemistry staining of breast cancer tissue is a methodology that cannot permit us to subject the tissue sections to manipulations such as deglycosylation treatments. Hence, analysis of NCT glycoforms' expression levels would only be feasible with MAbs raised against specific NCT glycoforms, which is not the case with the MAbs that we currently have at our disposal. However, we can apply the anti-NCT MAbs to immunostain breast cancer tissues, using consecutive sections of the same breast cancer TMA (University of Nottingham, UK). That would enable us to directly compare and contrast the staining pattern/intensity.

It would be of particular interest to evaluate eventual differences in the staining obtained using the 1E2/10C11 MAbs which recognise mature NCT and the 10C5 MAb, which on a western blot picks up only the deglycosylated form. Correlation of the staining intensity with the known breast cancer prognostic and predictive parameters, as well as disease-free and overall survival, could potentially reveal a differential impact of the NCT levels picked up by distinct MAbs, on survival, or a differential relation to relevant breast cancer biomarkers (ERα, PR, HER2, tumour grade etc.).

Considering the fact that the anti-NCT MAbs elicit anti-invasive and anti-proliferative effects in breast cancer cells, it would be important to determine the exact epitopes on the NCT-ECD to which these MAbs bind, as they apparently map important functional domains of the NCT protein. Phage libraries displaying millions of peptides are extremely useful tools for mapping sequential (continuous) and conformational (discontinuous) epitopes of antibodies (513, 514). Another strategy is chemical cross linking followed by mass spectrometry (MS) (515). Cross-linking reagents generate patterns (covalent bonds between reactive amino acid side chains that are located in close proximity of each other), that are easily observed by MS, which is helpful in distinguishing cross-linker-modified peptides from unmodified peptides after proteolytic digestion.

The cross-linked complex is subjected to tryptic digest, and since proteolysis does not lead to dissociation of immune complexes, an epitope can be identified by MS, as the method of choice for a rapid, specific and sensitive detection of protein/protein interactions stabilised by cross-linking (515, 516).

In order to progress the best candidate anti-NCT MAb into well designed *in vivo* experiments and further design a clinically applicable therapeutic, features including antibody affinity, stability, effector functions, half-life, tissue penetration and distribution should be optimised (517). Furthermore, characteristics of NCT as an antigen in breast cancer tissue are equally important, as the balance between the antigen density, internalisation and antibody dissociation, affects therapeutic effects (488).

The high cell-based $K_d$ values of the anti-NCT MAbs in MDA-MB-231 cells (> 50 nM) indicate that the mode of binding to cell surface NCT is primarily monovalent, most likely due to low antigen density. As such, they cannot at present be considered as desirable therapeutic tools. For example, the $K_d$ value of the humanised anti-HER2 MAb (trastuzumab)

in SKBR3 cells, is 5 nM (518). We will examine the relative cell-surface abundance of NCT in other breast cancer cell line models (MCF-7, BT-474, SKBR3, HCC-1806) by performing the FACS titration assay. Since antigen density is an important parameter that needs to be considered for *in vivo* binding studies, this information will guide MAb dose selection for xenograft model experiments, as it will indicate whether the MAbs engage in monovalent or bivalent binding across the panel the breast cancer cell lines. Generally, if the target protein density is low so that only one arm of the IgG molecule can bind, the antibody-antigen interaction cannot be retained if antibody affinity is low. With high-affinity antibodies the strength of the interaction between a single binding site and the antigen is sufficient to retain antibody with only monovalent binding, and the antibody is bound effectively, irrespective of the antigen density (488).

Thus far, turnover of NCT has been examined in the MEF cells using metabolic labeling (cell surface biotinylation) followed by the pulse-chase experiment. It has been established that the turnover of both mature and immature NCT is slow (> 24 h) in wild type and PS-deficient MEFs, emphasising that stability of NCT is not dependent on PS (248). We will perform this experiment in breast cancer cells in order to compare NCT membrane cycling dynamics with the off-rate of the MAbs, because if the antigen internalisation rate on the cell surface is faster than the off-rate of the MAb, then the MAb is internalised in the complex with the antigen and degraded (24).

If the antibody affinity is very high it can represents a limiting factor for homogenous tissue distribution, inducing MAb accumulation at the tumour periphery in line with the 'site-barrier' model (30). This has been well demonstrated by investigating tissue permeability of anti-HER2 MAbs designed to recognise the same HER2 antigen epitope but with variable affinities ($K_d$ values ranging from 270 to 0.56 nM) (487). Lowest affinity MAb ($K_d$ = 270 nM) had the best tumour penetration profile. Moderate affinity ($K_d$ = 23 nM) was associated with the highest tumour accumulation, whereas high affinity ($K_d$ = 0.56 nM) was found to produce the lowest tumour accumulation and confinement to the perivascular space and tumour rim (487). However, HER2 is the only target that has been studied in this way, so this may not be applicable to all (especially non-internalising) antigens. Therefore, tissue permeability of anti-NCT MAbs will be evaluated as a part of the *in vivo* xenograft model biodistribution studies, using immunohistochemistry penetration methodology, which enables

measurement of MAb distribution in relation to the tumour associated blood vessels visualised by co-staining with anti-CD31 antibody (487).

Another important determinant of therapeutic MAbs is their mode of action. The therapeutic efficacy of anti-NCT MAbs will be dependent on their antigen binding ability as well as their ability to trigger effector activity in the form of ADCC and/or CDC, which is an aspect of their mode of action which will be assessed.

Increasing the affinity of an antibody would allow lower doses to elicit a more profound biological activity which in turn would increase the therapeutic window and lower dose related toxicity. The approaches to improve antibody affinity can be divided into two categories. One is to create libraries of mutated CDRs or the entire variable domains by random CDR mutagenesis, chain shuffling, or DNA shuffling, and select for higher affinity variants. The other approach is to make small libraries by hot spot mutagenesis, mimicking the *in vivo* affinity maturation. Hot-spots are the amino acids that make a major contribution to the antibody-antigen interaction, and they are usually located in the central part of the epitope-paratope (antibody region recognising the antigen epitope) interaction site (517). Using an effective method of selection, it is possible to obtain recombinant antibodies with dissociation constant values reaching $10^{-10}$ M and below (21).

Before engaging in the process of increasing antibody affinity, one should equally consider the clinical relevance of the process, especially if the relative density of an antigen on the target and non-target tissues is different. In such a case, it could be possible to select antibodies of specific affinity and valence to differentiate the target tissue. For example, if an epitope is present at a higher density on the tumour cells than in benign tissues, a lower affinity antibody would be a desirable therapeutic because bivalent binding could be used to discriminate between the two tissues (21). Therefore, biodistribution analysis and investigation of NCT antigen density on other tissues would be of great importance. Thus far, there are two main sites of concern regarding treatment related toxicities linked to NCT inhibition, the skin and the hematopoetic system, both observed in mouse models upon generation of NCT knockout strains. Namely, proliferative skin lesions and myeloproliferative disorder resembling chronic myeloid leukemia (splenic enlargement, leukocytosis and monocytosis in peripheral blood, myeloid infiltrates in the bone marrow and liver) occurred in $NCT^{-/-}$ mice (154, 370).

We have detected NCT expression in normal skin, suggesting that the skin-related toxicity could be common in humans. Expression of NCT in human lymphocytes needs to be addressed. Nicastrin silencing in the context of the work performed by the groups of Liu et al. and Klinakis et al. acted as a means of Notch inhibition, which served to implicate Notch as both an oncogene and tumour suppressor in different hematological malignancies. Nevertheless, their work emphasises the importance of optimising the therapeutic window when considering NCT inhibition with MAbs as a therapeutic strategy, so to avoid treatment related toxicities and induction of other malignancies while treating breast cancer.

# 8. Final comment

In the course of this thesis we have analysed the biological and clinical implications of nicastrin expression in breast cancer cells and tissue. Taken together, the results presented here have identified nicastrin as a potential novel therapeutic target in breast cancer. Nicastrin fulfills certain criteria in order to be considered as a target for monoclonal antibody therapy: i) It is differentially expressed between normal breast and breast cancer tissue; ii) High nicastrin expression confers worse overall survival in ERα negative breast cancer patients, indicating its relevance in aggressive breast tumours; iii) Nicastrin inhibition attenuates breast cancer cell invasion and proliferation; iv) Nicastrin possesses an extracellular domain which harbours important functional sites and could be targetable by an antagonistic antibody.

Based on the work encompassed in this thesis, we suggest that nicastrin function in breast cancer cells is important to maintain the stability and function of the gamma-secretase complex. We also propose that nicastrin is an important mediator of breast cancer cell spread, as its expression correlated with aggressive disease and its inhibition attenuated breast cancer cell invasion. Anti-invasive and anti-proliferative effects inferred by nicastrin silencing and anti-nicastrin monoclonal antibodies in breast cancer cells are, in large part certainly a consequence of the GS/Notch inhibition. Whether nicastrin possesses relevant GS/Notch-independent functions in breast cancer cells, as proposed by the gene array that compared nicastrin silencing effects to those inferred by inhibiting Notch receptors, remains to be investigated. In addition, our further experiments will involve: i) characterisation of the nicastrin downstream signaling effects which mediate breast cancer cell invasion; ii) characterisation of the nicastrin antigen as a potential target for a monoclonal antibody (cell surface expression and turnover dynamics); iii) characterisation of the developed monoclonal antibodies in terms of epitope mapping, mode of binding, biodistribution and improving their binding affinity; iv) application of the anti-nicastrin monoclonal antibodies in *in vivo* breast cancer xenograft models.

# ANNEX 1

| XP725 Profiler Array | Sigma | Fold Change | |
|---|---|---|---|
| **Protein** | **Antibody ID** | **MDA231 NCTsi** | **HCC1806 NCTsh** |
| **β-actin** | A1978 | 0.98 | 0.9 |
| **AP2a** | A0844 | -2.00 | -2.00 |
| **AP Edonuclease** | A2105 | 1.53 | 2.91 |
| **ATF1** | A7833 | -2.32 | -2.43 |
| **ATF2** | A4086 | -2.27 | -2.27 |
| **ATF2 pThr69 71** | A4095 | -2.43 | -2.56 |
| **BACH1** | B1310 | 2.6 | 5.21 |
| **cJun pSer63** | J2128 | | -8.3 |
| **caspase 6** | C7599 | -2.77 | -3.12 |
| **caspase 7** | C7724 | -2.63 | -3 |
| **a-catenin** | C2081 | -1.81 | -2.43 |
| **bCatenin pSer33** | C2363 | -2.22 | -2.17 |
| **Cathepsin D** | C0715 | 2 | 3.9 |
| **Clathrin Heavy Chain** | C1960 | 1.1 | 2.2 |
| **Connexin 32** | C3470 | -2.5 | -2.77 |
| **DcR2** | D3188 | -2.56 | -3.00 |
| **DcR3** | D1814 | 1.8 | 2.6 |
| **DEDAF** | D3316 | -2.17 | -1.96 |
| **Desmosomal protein** | D1286 | 1.2 | 2.5 |
| **Episialin** | E0143 | 1.25 | 2.1 |
| **FKHRL1 FOXO3a** | F2178 | -2.32 | -2.77 |
| **FRS2** | F9052 | -2.22 | -2.5 |
| **G9a Methyltransferase** | G6919 | 1 | 2 |
| **GATA1** | G0290 | -2.63 | -2.63 |
| **Glutamate receptor NMDAR** | G9038 | -2.7 | -2.43 |
| **HAT1** | H7161 | -2.63 | -2.32 |
| **methyl Histone H3 MeLys9** | H7162 | -2.85 | -2.85 |
| **Histone H3 pSer28** | H9908 | -2.94 | -3 |
| **hSNF5 INI1** | H9912 | -2.7 | -3 |
| **IKKa** | I6139 | -2.04 | -2.04 |
| **ILP2** | I4782 | -2.63 | -2.63 |
| **L1CAM** | L4543 | 1.1 | 2.78 |
| **Laminin** | L9393 | -3.22 | -3.125 |
| **Leptin** | L3410 | -2.7 | -2.7 |
| **MBD4** | M9817 | -2.43 | -2.32 |
| **LRRK2 (PARK8)** | L3044 | 3.02 | 5.25 |
| **Nerve growth factor receptor p75** | N3908 | -3.125 | -3.44 |
| **Neurofibromin** | N3662 | -1.92 | -2.43 |
| **Nitric Oxide Synthase Endothelial** | N9532 | -2.08 | -2.43 |
| **Nitrotyrosin** | N0409 | -2.38 | -2.22 |
| **PARP** | P7605 | -2.5 | -2.5 |
| **PCAF** | P7493 | -2.32 | -2.17 |
| **Phospholipase C g1** | P8104 | -2.63 | -2.43 |
| **PINCH1** | P9371 | 1.23 | 3.36 |
| **PRMT4** | P4995 | -2.7 | -2.7 |
| **Rab9** | R5404 | 1 | 3.5 |
| **Reelin** | R4904 | -2.43 | -2.5 |
| **RICK** | R9650 | -2.63 | -2.77 |
| **RIP Receptor Interacting Protein** | R8274 | -2.38 | -2.77 |
| **Serine Threonine Protein Phosphatase 1g1** | P7609 | 2.8 | |

| | | | |
|---|---|---|---|
| **Serine Threonine Protein Phosphatase 2 A Bg** | P5359 | 4.4 | |
| **Sir2** | S5313 | -2.7 | -3.22 |
| **Spred2** | S7320 | 1.8 | 4.6 |
| **SUMO1** | S5446 | -3.33 | -3.57 |
| **TOM22** | T6319 | -2.63 | -2.77 |
| **Pinin** | P0084 | -2.43 | -4.16 |

Protein lysates of MDA-MB-231 cells treated with the *Control* and *NCT* siRNA for 72 h, as well as lysates from HCC1806-Luc1 and HCC1806-NCTsh cells were prepared and extracts with protein concentrations ≥ 1.0 mg/ml were used for fluorescent labeling with Cy3 and Cy5 fluorochroms. Only samples with a dye-to-protein molar ratio > 2 were applied to the antibody microarray. The hybridised antibody microarray slides were scanned using a GenePix Personal 4100A Microarray Scanner (Axon Instruments, Union City, CA) with 532 and 635 nm lasers. Primary analysis was done with the GenePix Pro (version 4.1) software package (Axon Instruments). Images of the scanned antibody microarrays were gridded and linked to a protein print list. Absent spots were flagged automatically by GenePix Pro; however, all spots were manually reviewed. The log ratios of Cy5 to Cy3 were determined for each spot to estimate the relative concentration of each protein. Values were normalised according to the manufacturer's protocol to the values of a chosen normalising protein, in this case β-actin. Only samples showing > 2-fold upregulation or downregulation in expression are deemed significant. This cut-off was selected because it is has been used previously in antibody microarray experiments (410). Empty cells in the table reflect the undetected sample in a particular cell line. This may be due to loss of antibody activity by denaturation during printing or array storage or low levels of the respective antigen in the sample. The table lists the proteins that are up- or down- regulated by at least 2-fold in at least one of the cell lines used. Full antibody list:
www.sigmaaldrich.com/etc/medialib/docs/Sigma-Aldrich/General_Information/xp725_ab_list.pdf

# ANNEX 2

## A. Genes regulated by NCT siRNA in MDA-MB-231 cells

| | | Fold Change | | | | |
|---|---|---|---|---|---|---|
| Gene Symbol | Gene Discription | Notch1 siRNA | Notch2 siRNA | Notch4 siRNA | NCT siRNA | p-value NCTsiRNA vs. ControlsiRNA |
| **HSPE1** | heat shock 10kDa protein 1 | 1.62 | -1.72 | 1.31 | **-2.58** | 0.04156 |
| **DYNLT3** | dynein, light chain, Tctex-type 3 | 1.62 | 1.84 | 1.11 | **2.06** | 0.00038 |
| **MYOF** | Myoferlin | -1.44 | 1.58 | 1.07 | **2.25** | 7.96E-05 |
| **NFE2L3** | nuclear factor (erythroid-derived 2)like 3 | -1.55 | 1.70 | -1.28 | **-2.17** | 0.00102 |
| **BRP44** | brain protein 44 | -1.45 | -1.51 | -1.26 | **-2.05** | 7.87E-06 |
| **CLTB** | clathrin, light chain (Lcb) | 1.44 | 1.53 | -1.04 | **2.36** | 4.90E-06 |
| **WFS1** | Wolfram syndrome 1 –wolframin | -1.36 | 1.87 | 1.10 | **4.93** | 6.52E-08 |
| **PLOD2** | procollagen-lysine, 2-oxoglutarate 5-dioxygenase 2 | -1.35 | 1.61 | 1.36 | **2.12** | 4.08E-06 |
| **LOC1001319** | hypothetical LOC100131909 | 1.35 | 1.71 | 1.09 | **2.26** | 8.73E-06 |
| **ABCB9** | ATP-binding cassette B, member 9 | -1.34 | 1.33 | 1.00 | **2.00** | 6.17E-07 |
| **SEPW1** | selenoprotein W, 1 | -1.33 | -1.67 | -1.07 | **-2.12** | 4.92E-08 |
| **BCAR3** | breast cancer anti-estrogen resistance 3 | -1.32 | 1.96 | 1.29 | **2.18** | 0.00012 |
| **LRRC61** | leucine rich repeat containing 61 | -1.31 | -1.76 | -1.38 | **-2.93** | 3.78E-07 |
| **RIPK2** | receptor-interacting ser/thr kinase 2 | 1.31 | 1.63 | 1.31 | **2.08** | 0.00019 |
| **C13orf15** | chromosome 13 open reading frame 15 | -1.31 | 1.88 | 1.01 | **3.99** | 1.43E-07 |
| **MANF** | mesencephalic astrocyte neurotrophic factor | -1.30 | -1.50 | -1.28 | **3.34** | 1.58E-06 |
| **GPT2** | glutamic pyruvate transaminase 2 | 1.30 | 1.66 | 1.01 | **3.06** | 1.18E-05 |
| **LOC1001342** | similar to mitogen-activated kinase | 1.30 | 1.91 | 1.48 | **2.12** | 1.81E-06 |
| **PAWR** | PRKC, apoptosis, WT1, regulator | -1.26 | 1.58 | 1.36 | **2.35** | 6.57E-07 |
| **PSMB2** | proteasome subunit, beta type, 2 | -1.26 | -1.77 | -1.30 | **-2.27** | 4.01E-05 |
| **ADCY3** | adenylate cyclase 3 | 1.23 | 1.59 | 1.48 | **-2.02** | 9.52E-06 |
| **IL1RAPL1** | interleukin 1 receptor accessory protein1 | -1.23 | 1.82 | 1.17 | **2.47** | 8.63E-06 |
| **PVRL3** | poliovirus receptor-related 3 | 1.20 | 1.24 | 1.11 | **2.22** | 3.08E-05 |
| **ITPRIP** | inositol 1,4,5-triphosphate receptor | -1.19 | 1.65 | 1.12 | **2.01** | 1.45E-05 |
| **CCPG1** | cell cycle progression 1 | 1.17 | 1.62 | 1.42 | **2.14** | 1.83E-06 |
| **PXDN** | peroxidasin homolog (Drosophila) | 1.15 | 1.60 | -1.18 | **2.32** | 0.00030 |
| **ZNF598** | zinc finger protein 598 | 1.14 | 1.79 | 1.23 | **2.30** | 1.46E-07 |
| **SHMT2** | serine hydroxymethyltransferase 2 | -1.13 | 1.51 | -1.06 | **2.60** | 2.11E-06 |
| **DYNLT1** | dynein, light chain, Tctex-type 1 | 1.12 | -1.86 | -1.04 | **-2.24** | 5.11E-05 |
| **POMP** | proteasome maturation protein | -1.12 | -1.78 | -1.18 | **-2.06** | 3.42E-05 |
| **LY6E** | lymphocyte antigen 6 complex, locus E | 1.11 | -1.84 | -1.20 | **-2.63** | 9.49E-07 |
| **SLC24A6** | solute carrier family 24, member 6 | 1.10 | 1.51 | -1.25 | **2.93** | 4.88E-07 |
| **MRPL22** | mitochondrial ribosomal protein L22 | 1.09 | -1.49 | -1.33 | **-2.34** | 6.50E-06 |
| **NME1** | non-metastatic cells 1, protein (NM23A) | 1.08 | -1.80 | -1.30 | **-2.20** | 2.94E-07 |
| **IGSF3** | immunoglobulin superfamily, member 3 | 1.08 | 1.77 | -1.45 | **-2.29** | 1.66E-06 |
| **LDLR** | low density lipoprotein receptor | 1.08 | 1.85 | 1.37 | **3.06** | 3.90E-07 |
| **NUCB1** | nucleobindin 1 | 1.07 | 1.73 | 1.27 | **2.60** | 0.00020 |
| **GPR177** | G protein-coupled receptor 177 | 1.07 | 1.44 | -1.07 | **2.53** | 2.12E-07 |
| **VGLL4** | vestigial like 4 (Drosophila) | 1.06 | 1.68 | 1.21 | **2.06** | 4.39E-07 |

| | | | | | | |
|---|---|---|---|---|---|---|
| **PTS** | 6-pyruvoyltetrahydropterin synthase | 1.05 | -1.89 | -1.43 | **-2.39** | 0.00370 |
| **PRKRIR** | protein-kinase RNA dependent inhibitor | 1.05 | -2.94 | 1.29 | **2.34** | 6.15E-07 |
| **LITAF** | lipopolysaccharide-induced TNF factor | 1.04 | -1.99 | -1.13 | **-2.34** | 2.00E-05 |
| **MAGOH** | mago-nashi homolog | 1.04 | -1.95 | -1.19 | **-2.27** | 2.60E-06 |
| **ZFAND5** | zinc finger, AN1-type domain 5 | 1.02 | 1.89 | 1.25 | **2.26** | 1.03E-06 |
| **EML3** | echinoderm microtubule associated protein like 3 | -1.02 | 1.88 | 1.32 | **2.00** | 8.65E-05 |

## B . Genes regulated by NCT siRNA and Notch2 siRNA in MDA-MB-231 cells

| Gene Symbol | Gene Description | Notch1 siRNA | Notch2 siRNA | Notch4 siRNA | NCT siRNA | p-value Notch2 siRNA | p-value NCT siRNA |
|---|---|---|---|---|---|---|---|
| **RFTN1** | raftlin, lipid raft linker 1 | -1.49 | 2.20 | -1.04 | 2.23 | 0.003 | 0.0002 |
| **KRT7** | keratin 7 | 1.46 | -2.46 | -1.20 | -2.62 | 0.000328 | 0.000211 |
| **SLC3A2** | solute carrier family 3 member 2 | 1.43 | 2.35 | 1.24 | 3.06 | 1.46E-06 | 1.97E-07 |
| **TRPC4AP** | transient receptor cation channel | 1.41 | 2.17 | 1.385 | 2.33 | 5.91E-06 | 3.11E-06 |
| **LOC64531** | coiled-coil-helix-coiled-coil-helix domain | -1.41 | -3.10 | -1.46 | -2.10 | 0.000108 | 0.001609 |
| **S100A4** | S100 calcium binding protein A4 | -1.32 | -3.04 | -1.16 | -2.06 | 5.13E-07 | 1.21E-05 |
| **CD97** | CD97 molecule | 1.30 | 3.17 | 1.45 | 2.41 | 3.50E-08 | 2.69E-07 |
| **CSK** | c-src tyrosine kinase | 1.27 | 2.43 | 1.24 | 2.00 | 1.08E-06 | 6.02E-06 |
| **CLCN7** | chloride channel 7 | 1.26 | 2.37 | 1.26 | 2.54 | 1.11E-05 | 6.30E-06 |
| **NINJ2** | ninjurin 2 | -1.25 | -2.14 | -1.06 | -2.86 | 0.000417 | 4.71E-05 |
| **TCTEX1D** | Tctex1 domain containing 2 | -1.25 | -2.50 | -1.27 | -2.65 | 3.97E-06 | 2.51E-06 |
| **NDUFB3** | NADH dehydrogenase 1 beta 3 | 1.25 | -3.27 | -1.07 | -2.49 | 1.54E-06 | 1.03E-05 |
| **ETS1** | erythroblastosis virus E26 oncogene | 1.24 | 2.37 | 1.46 | 3.57 | 1.88E-05 | 1.12E-06 |
| **NEDD4L** | neural precursor cell expressed, developmentally downregulated 4 | -1.23 | 2.27 | -1.10 | 2.73 | 2.23E-06 | 4.82E-07 |
| **RPS24** | ribosomal protein S24 | -1.22 | -4.06 | -1.36 | -2.87 | 1.11E-08 | 9.54E-08 |
| **PCBD1** | pterin-4 alpha-carbinolamine dehydratase/dimerization cofactor of hepatocyte nuclear factor 1 alpha | -1.22 | -2.06 | -1.12 | -2.35 | 4.72E-05 | 1.45E-05 |
| **RPL26** | ribosomal protein L26 | -1.22 | -3.10 | -1.47 | -3.98 | 3.10E-05 | 7.43E-06 |
| **C7orf59** | chromosome 7 open read frame 59 | -1.21 | -2.76 | -1.45 | -2.10 | 2.11E-07 | 2.21E-06 |
| **NDUFB2** | NADH dehydrogenase 1 beta 2 | -1.20 | -2.42 | -1.06 | -2.09 | 2.15E-06 | 7.88E-06 |
| **GNG12** | guanine nucleotide binding protein (G protein), gamma 12 | 1.19 | 2.01 | -1.00 | 2.00 | 4.52E-05 | 4.84E-05 |
| **DERL1** | Der1-like domain family, member 1 | -1.19 | 3.06 | 1.11 | 2.14 | 6.97E-06 | 0.000103 |
| **ATP6V0A** | ATPase, H+ transport-lysosomal V0 | 1.16 | 2.21 | 1.40 | 3.46 | 8.11E-08 | 2.76E-09 |
| **LGMN** | Legumain | -1.15 | 2.01 | 1.06 | 2.04 | 5.51E-06 | 4.88E-06 |
| **VEGFC** | vascular endothelial growth factor C | -1.14 | 2.11 | 1.43 | 4.40 | 6.69E-05 | 4.58E-07 |
| **GMDS** | GDP-mannose 4,6-dehydratase | 1.10 | 2.76 | 1.07 | 2.38 | 6.06E-07 | 1.96E-06 |
| **ULK1** | unc-51-like kinase 1 (C. elegans) | 1.09 | 2.11 | 1.19 | 2.21 | 1.62E-06 | 1.07E-06 |
| **C8orf59** | chromosome 8 open reading frame | 1.09 | -3.47 | 1.04 | -2.61 | 0.001667 | 0.006988 |
| **ACTN1** | actinin, alpha 1 | 1.08 | 4.01 | 1.22 | 2.18 | 3.43E-05 | 0.001515 |

| | | | | | | | |
|---|---|---|---|---|---|---|---|
| **TMEM66** | transmembrane protein 66 | 1.07 | 2.03 | 1.29 | 2.36 | 3.98E-05 | 1.03E-05 |
| **C14orf2** | chromosome 14 open reading frame 2 | -1.07 | -3.30 | -1.23 | -2.21 | 8.42E-07 | 1.64E-05 |
| **FRMD6** | FERM domain containing 6 | 1.07 | 2.33 | -1.06 | 2.96 | 1.82E-05 | 3.01E-06 |
| **DBI** | diazepam binding inhibitor | -1.04 | -2.51 | -1.18 | -2.13 | 8.89E-08 | 3.83E-07 |
| **TM4SF1** | transmembrane 4 L six family 1 | -1.04 | 2.01 | 1.32 | 2.16 | 1.19E-06 | 5.54E-07 |
| **CCNI** | cyclin I | 1.03 | 2.59 | 1.05 | 2.00 | 1.92E-05 | 0.00017 |
| **CTGF** | connective tissue growth factor | 1.02 | 3.87 | 1.38 | 3.51 | 2.23E-06 | 3.84E-06 |
| **CCDC58** | coiled-coil domain containing 58 | 1.02 | -2.06 | -1.39 | -2.10 | 0.000334 | 0.000291 |
| **LOC729973** | hypothetical LOC729973 | 1.01 | -3.66 | -1.35 | -2.28 | 2.09E-05 | 0.00043 |
| **SLIT2** | slit homolog 2 (Drosophila) | 1.01 | 2.62 | 1.02 | 2.64 | 3.63E-07 | 3.38E-07 |
| **CBX5** | chromobox homolog 5 | 1.00 | -2.30 | -1.30 | -3.06 | 2.41E-07 | 2.65E-08 |

**Array experiment**.MDA-MB-231 cells were treated with *Control* and *NCT* siRNA for 72 h. mRNA was sent to Prof Lucio Miele, USA, where their own MDA-MB-231 cells were treated with the Merck GSI. Values represent fold change between *NCT* siRNA vs. *Control* siRNA; and *Notch2* siRNA vs. *Control* siRNA. The two types of treatment were therefore not normalised to the same control, and direct comparisons between the two types of treatment have to be validated, due to the fact that although the same cell line was used, the MDA-MB-231 cells did not originate from the same laboratory.

# ANNEX 3

a)

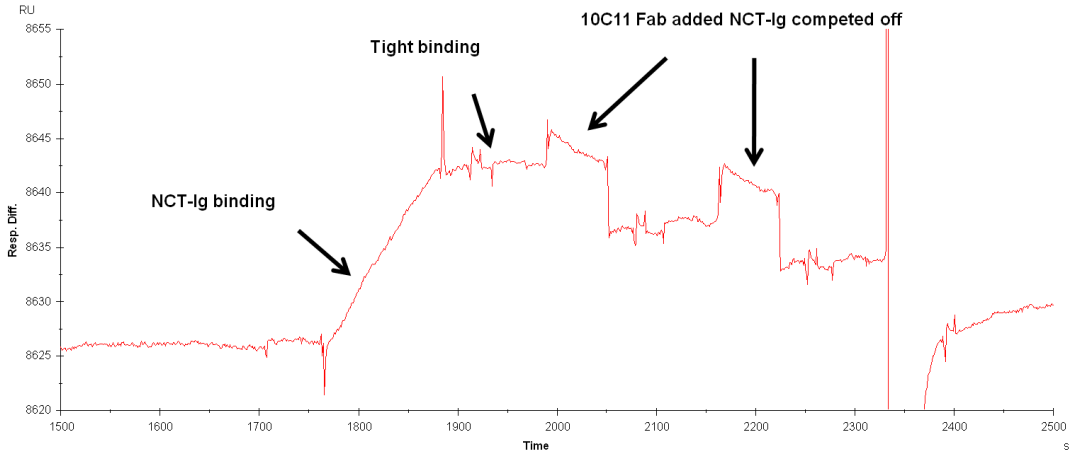


10C11 MAb

b)

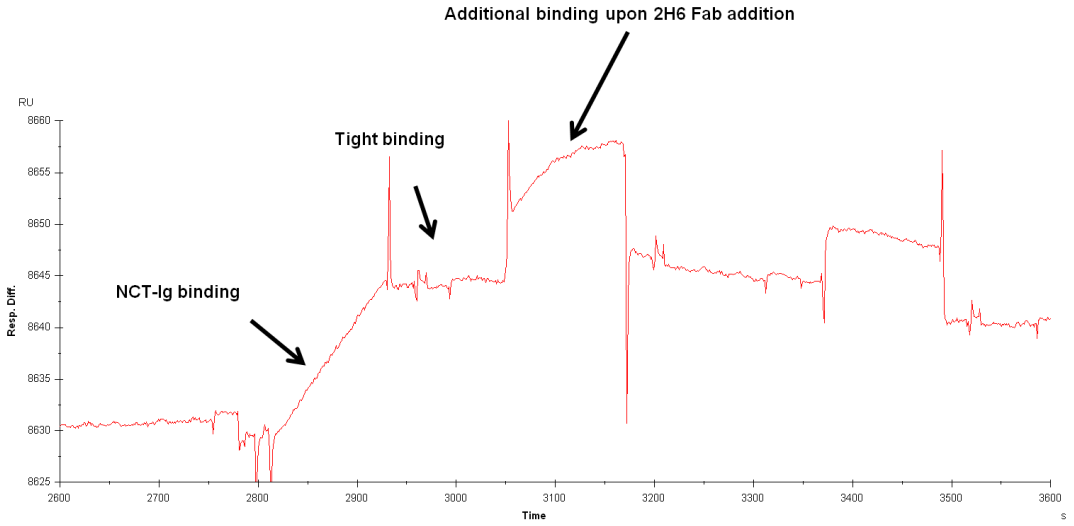


10C11 MAb

c)

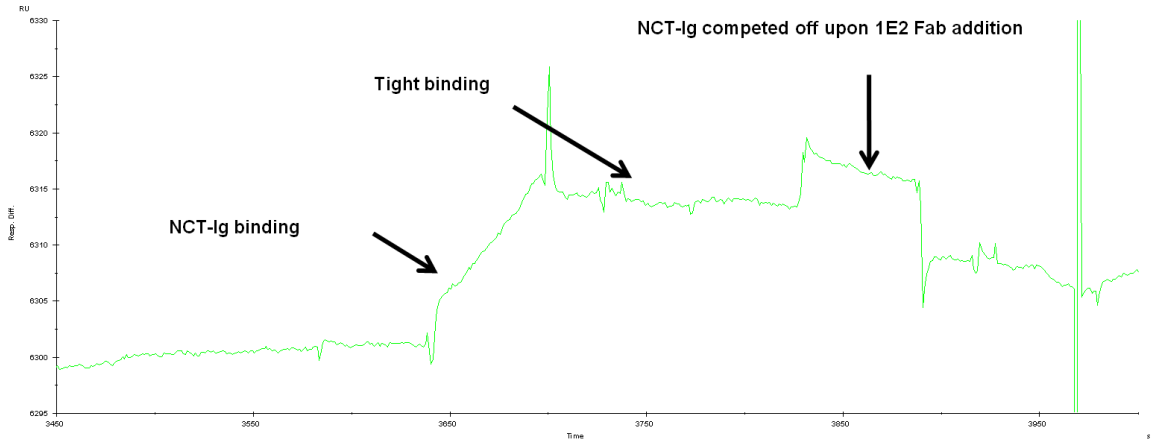


1E2 MAb

d)

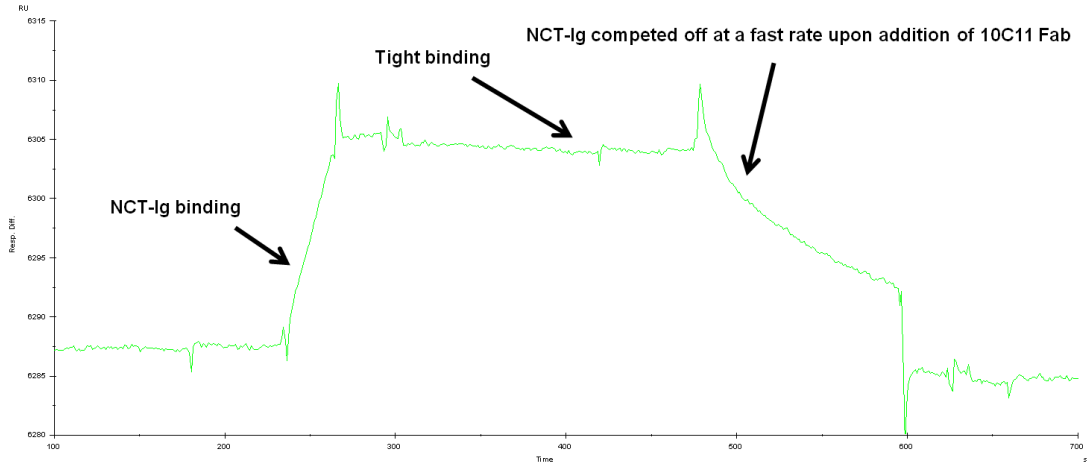


1E2 MAb

**Sensogram of anti-NCT MAbs binding to the human NCT-Fc protein.**
**a,b)** 10C11 and **c,d)** 1E2 MAbs were immobilised using NHS-EDC coupling on the surface of a separate BIACore CM5 chip. This was followed by a 2 min flow of the human NCT-Fc antigen (15 µg/ml), which resulted in formation of antigen-antibody binding, represented by the initial ascending slope on the sensograms. Indication 'tight binding' reflects the strength of the IgG-antigen interaction (flat line with slow decay). Next, each IgG chip was subjected to a 1 min flow of an indicated Fab (25 µg/ml) for the purpose of deciphering the degree of competitive binding between the antibodies. Binding was measured at a flow rate of 10 µl/min for 5 min at RT. Dissociation was initiated upon replacement of the analyte solution with buffer. Response (flow cell, Fc2) is indicated as resonance units (RU) and is corrected for nonspecific binding to a blank chip (flow cell, Fc1). Net binding = Fc 2-1.

**e)**

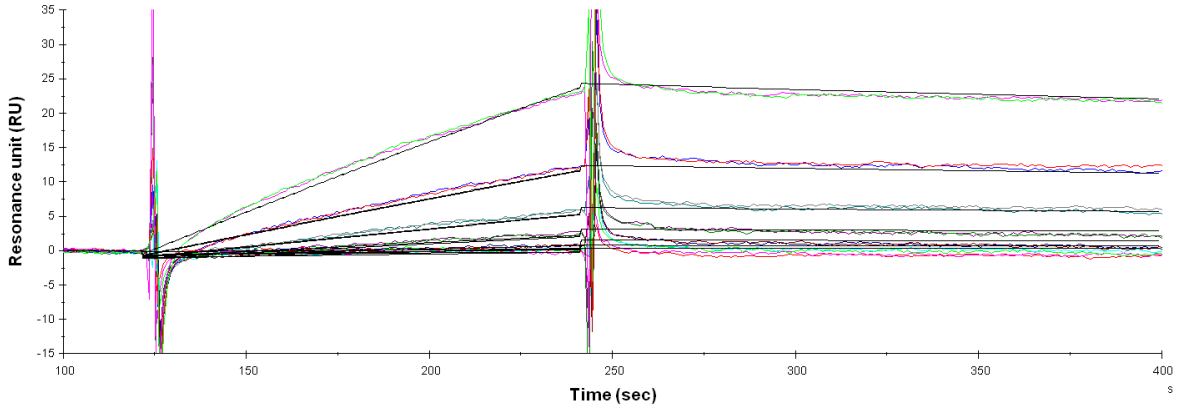


**BIACore analysis of the 10C11 MAb binding kinetics.** A range of NCT-Ig antigen concentrations were flowed over the surface of the immobilised 10C11 MAb to give a series of associations and dissociations from which the association rate constant ($K_{on}$) of 4 x $10^{3}$ $M^{-1}$ $s^{-1}$ and the the dissociation rate constant was ($K_{off}$) of 6 x $10^{-4}$ $s^{-1}$ were determined. Consequently a $K_d$ of 149 nm was calculated.

# REFERENCES


1. Bray F, Moller B. Predicting the future burden of cancer. Nat Rev Cancer 2006; 6: 63-74.
2. Ott JJ, Ullrich A, Mascarenhas M, Stevens GA. Global cancer incidence and mortality caused by behavior and infection. J Public Health 2010 (Oxf).
3. Statistical Information Team CRU. 2009.
4. Bray F, McCarron P, Parkin DM. The changing global patterns of female breast cancer incidence and mortality. Breast Cancer Res 2004; 6: 229-39.
5. Helmrich SP, Shapiro S, Rosenberg L, et al. Risk factors for breast cancer. Am J Epidemiol 1983; 117: 35-45.
6. Ferlay J, Shin HR, Bray F, Forman D, Mathers C, Parkin DM. Estimates of worldwide burden of cancer in 2008: GLOBOCAN 2008. Int J Cancer.
7. Bertucci F, Birnbaum D. Reasons for breast cancer heterogeneity. J Biol 2008; 7: 6.
8. Hanahan D, Weinberg RA. The hallmarks of cancer. Cell 2000; 100: 57-70.
9. Vogelstein B, Kinzler KW. Cancer genes and the pathways they control. Nat Med 2004; 10: 789-99.
10. Weinstein IB, Joe A. Oncogene addiction. Cancer Res 2008; 68: 3077-80; discussion 80.
11. Correa Geyer F, Reis-Filho JS. Microarray-based gene expression profiling as a clinical tool for breast cancer management: are we there yet? Int J Surg Pathol 2009; 17: 285-302.
12. WHO clasification of Tumours. Pathology and genetics of tumours of the breast and female genital organs. Lyon Press, Lyon 2003 2003.
13. Weigelt B, Reis-Filho JS. Histological and molecular types of breast cancer: is there a unifying taxonomy? Nat Rev Clin Oncol 2009; 6: 718-30.
14. Wellings SR, Jensen HM. On the origin and progression of ductal carcinoma in the human breast. J Natl Cancer Inst 1973; 50: 1111-8.
15. Sorlie T, Perou CM, Tibshirani R, et al. Gene expression patterns of breast carcinomas distinguish tumor subclasses with clinical implications. Proc Natl Acad Sci U S A 2001; 98: 10869-74.
16. Reichert JM, Rosensweig CJ, Faden LB, Dewitz MC. Monoclonal antibody successes in the clinic. Nat Biotechnol 2005; 23: 1073-8.
17. Strebhardt K, Ullrich A. Paul Ehrlich's magic bullet concept: 100 years of progress. Nat Rev Cancer 2008; 8: 473-80.
18. Kohler G, Milstein C. Continuous cultures of fused cells secreting antibody of predefined specificity. Nature 1975; 256: 495-7.
19. Adams GP, Weiner LM. Monoclonal antibody therapy of cancer. Nat Biotechnol 2005; 23: 1147-57.
20. Reichert JM. Monoclonal antibodies in the clinic. Nat Biotechnol 2001; 19: 819-22.
21. Altshuler EP, Serebryanaya DV, Katrukha AG. Generation of recombinant antibodies and means for increasing their affinity. Biochemistry 2010 (Mosc); 75: 1584-605.
22. Carter P. Improving the efficacy of antibody-based cancer therapies. Nat Rev Cancer 2001; 1: 118-29.
23. Ross JS, Gray K, Gray GS, Worland PJ, Rolfe M. Anticancer antibodies. Am J Clin Pathol 2003; 119: 472-85.
24. Rudnick SI, Adams GP. Affinity and avidity in antibody-based tumor targeting. Cancer Biother Radiopharm 2009; 24: 155-61.
25. Reilly RM, Sandhu J, Alvarez-Diez TM, Gallinger S, Kirsh J, Stern H. Problems of delivery of monoclonal antibodies. Pharmaceutical and pharmacokinetic solutions. Clin Pharmacokinet 1995; 28: 126-42.

26. Adams GP, Schier R, Marshall K, et al. Increased affinity leads to improved selective tumor delivery of single-chain Fv antibodies. Cancer Res 1998; 58: 485-90.

27. Thurber GM, Schmidt MM, Wittrup KD. Antibody tumor penetration: transport opposed by systemic and antigen-mediated clearance. Adv Drug Deliv Rev 2008; 60: 1421-34.

28. Ackerman ME, Pawlowski D, Wittrup KD. Effect of antigen turnover rate and expression level on antibody penetration into tumor spheroids. Mol Cancer Ther 2008; 7: 2233-40.

29. Kyriakos RJ, Shih LB, Ong GL, Patel K, Goldenberg DM, Mattes MJ. The fate of antibodies bound to the surface of tumor cells in vitro. Cancer Res 1992; 52: 835-42.

30. Fujimori K, Covell DG, Fletcher JE, Weinstein JN. A modeling analysis of monoclonal antibody percolation through tumors: a binding-site barrier. J Nucl Med 1990; 31: 1191-8.

31. Juweid M, Neumann R, Paik C, et al. Micropharmacology of monoclonal antibodies in solid tumors: direct experimental evidence for a binding site barrier. Cancer Res 1992; 52: 5144-53.

32. Tabrizi MA, Tseng CM, Roskos LK. Elimination mechanisms of therapeutic monoclonal antibodies. Drug Discov Today 2006; 11: 81-8.

33. Tassev DV, Cheung NK. Monoclonal antibody therapies for solid tumors. Expert Opin Biol Ther 2009; 9: 341-53.

34. Slamon DJ, Leyland-Jones B, Shak S, et al. Use of chemotherapy plus a monoclonal antibody against HER2 for metastatic breast cancer that overexpresses HER2. N Engl J Med 2001; 344: 783-92.

35. Hurwitz H, Fehrenbacher L, Novotny W, et al. Bevacizumab plus irinotecan, fluorouracil, and leucovorin for metastatic colorectal cancer. N Engl J Med 2004; 350: 2335-42.

36. Kalluri R, Weinberg RA. The basics of epithelial-mesenchymal transition. J Clin Invest 2009; 119: 1420-8.

37. Hay ED. An overview of epithelio-mesenchymal transformation. Acta Anat (Basel) 1995; 154: 8-20.

38. Zeisberg M, Shah AA, Kalluri R. Bone morphogenic protein-7 induces mesenchymal to epithelial transition in adult renal fibroblasts and facilitates regeneration of injured kidney. J Biol Chem 2005; 280: 8094-100.

39. Acloque H, Adams MS, Fishwick K, Bronner-Fraser M, Nieto MA. Epithelial-mesenchymal transitions: the importance of changing cell state in development and disease. J Clin Invest 2009; 119: 1438-49.

40. Keshamouni VG, Schiemann WP. Epithelial-mesenchymal transition in tumor metastasis: a method to the madness. Future Oncol 2009; 5: 1109-11.

41. Thiery JP. Epithelial-mesenchymal transitions in tumour progression. Nat Rev Cancer 2002; 2: 442-54.

42. Moreno-Bueno G, Cubillo E, Sarrio D, et al. Genetic profiling of epithelial cells expressing E-cadherin repressors reveals a distinct role for Snail, Slug, and E47 factors in epithelial-mesenchymal transition. Cancer Res 2006; 66: 9543-56.

43. Taube JH, Herschkowitz JI, Komurov K, et al. Core epithelial-to-mesenchymal transition interactome gene-expression signature is associated with claudin-low and metaplastic breast cancer subtypes. Proc Natl Acad Sci U S A 2010; 107: 15449-54.

44. Jechlinger M, Grunert S, Beug H. Mechanisms in epithelial plasticity and metastasis: insights from 3D cultures and expression profiling. J Mammary Gland Biol Neoplasia 2002; 7: 415-32.

45. Shi Y, Massague J. Mechanisms of TGF-beta signaling from cell membrane to the nucleus. Cell 2003; 113: 685-700.

46. Niessen K, Fu Y, Chang L, Hoodless PA, McFadden D, Karsan A. Slug is a direct Notch target required for initiation of cardiac cushion cellularization. J Cell Biol 2008; 182: 315-25.

47. Medici D, Hay ED, Olsen BR. Snail and Slug promote epithelial-mesenchymal transition through beta-catenin-T-cell factor-4-dependent expression of transforming growth factor-beta3. Mol Biol Cell 2008; 19: 4875-87.

48. Kokudo T, Suzuki Y, Yoshimatsu Y, Yamazaki T, Watabe T, Miyazono K. Snail is required for TGFbeta-induced endothelial-mesenchymal transition of embryonic stem cell-derived endothelial cells. J Cell Sci 2008; 121: 3317-24.

49. Gregory PA, Bracken CP, Bert AG, Goodall GJ. MicroRNAs as regulators of epithelial-mesenchymal transition. Cell Cycle 2008; 7: 3112-8.

50. Cannito S, Novo E, Compagnone A, et al. Redox mechanisms switch on hypoxia-dependent epithelial-mesenchymal transition in cancer cells. Carcinogenesis 2008; 29: 2267-78.

51. Radisky ES, Radisky DC. Matrix metalloproteinase-induced epithelial-mesenchymal transition in breast cancer. J Mammary Gland Biol Neoplasia 2010; 15: 201-12.

52. Wheelock MJ, Shintani Y, Maeda M, Fukumoto Y, Johnson KR. Cadherin switching. J Cell Sci 2008; 121: 727-35.

53. Kokkinos MI, Wafai R, Wong MK, Newgreen DF, Thompson EW, Waltham M. Vimentin and epithelial-mesenchymal transition in human breast cancer--observations in vitro and in vivo. Cells Tissues Organs 2007; 185: 191-203.

54. Blick T, Widodo E, Hugo H, et al. Epithelial mesenchymal transition traits in human breast cancer cell lines. Clin Exp Metastasis 2008; 25: 629-42.

55. Neve RM, Chin K, Fridlyand J, et al. A collection of breast cancer cell lines for the study of functionally distinct cancer subtypes. Cancer Cell 2006; 10: 515-27.

56. Miyazono K, ten Dijke P, Heldin CH. TGF-beta signaling by Smad proteins. Adv Immunol 2000; 75: 115-57.

57. Kim K, Lu Z, Hay ED. Direct evidence for a role of beta-catenin/LEF-1 signaling pathway in induction of EMT. Cell Biol Int 2002; 26: 463-76.

58. Lehmann K, Janda E, Pierreux CE, et al. Raf induces TGFbeta production while blocking its apoptotic but not invasive responses: a mechanism leading to increased malignancy in epithelial cells. Genes Dev 2000; 14: 2610-22.

59. Masszi A, Di Ciano C, Sirokmany G, et al. Central role for Rho in TGF-beta1-induced alpha-smooth muscle actin expression during epithelial-mesenchymal transition. Am J Physiol Renal Physiol 2003; 284: F911-24.

60. Cho HJ, Yoo J. Rho activation is required for transforming growth factor-beta-induced epithelial-mesenchymal transition in lens epithelial cells. Cell Biol Int 2007; 31: 1225-30.

61. Fuxe J, Vincent T, de Herreros AG. Transcriptional crosstalk between TGFbeta and stem cell pathways in tumor cell invasion: Role of EMT promoting Smad complexes. Cell Cycle 2010; 9.

62. Sarrio D, Rodriguez-Pinilla SM, Hardisson D, Cano A, Moreno-Bueno G, Palacios J. Epithelial-mesenchymal transition in breast cancer relates to the basal-like phenotype. Cancer Res 2008; 68: 989-97.

63. Nielsen TO, Hsu FD, Jensen K, et al. Immunohistochemical and clinical characterization of the basal-like subtype of invasive breast carcinoma. Clin Cancer Res 2004; 10: 5367-74.

64. Rakha EA, El-Sayed ME, Green AR, Paish EC, Lee AH, Ellis IO. Breast carcinoma with basal differentiation: a proposal for pathology definition based on basal cytokeratin expression. Histopathology 2007; 50: 434-8.

65. Bissell MJ, Radisky DC, Rizki A, Weaver VM, Petersen OW. The organizing principle: microenvironmental influences in the normal and malignant breast. Differentiation 2002; 70: 537-46.

66. Kenny PA, Lee GY, Myers CA, et al. The morphologies of breast cancer cell lines in three-dimensional assays correlate with their profiles of gene expression. Mol Oncol 2007; 1: 84-96.

67. Lee GY, Kenny PA, Lee EH, Bissell MJ. Three-dimensional culture models of normal and malignant breast epithelial cells. Nat Methods 2007; 4: 359-65.

68. Debnath J, Muthuswamy SK, Brugge JS. Morphogenesis and oncogenesis of MCF-10A mammary epithelial acini grown in three-dimensional basement membrane cultures. Methods 2003; 30: 256-68.

69. Wang F, Hansen RK, Radisky D, et al. Phenotypic reversion or death of cancer cells by altering signaling pathways in three-dimensional contexts. J Natl Cancer Inst 2002; 94: 1494-503.

70. Liu H, Radisky DC, Wang F, Bissell MJ. Polarity and proliferation are controlled by distinct signaling pathways downstream of PI3-kinase in breast epithelial tumor cells. J Cell Biol 2004; 164: 603-12.

71. Creighton CJ, Chang JC, Rosen JM. Epithelial-mesenchymal transition (EMT) in tumor-initiating cells and its clinical implications in breast cancer. J Mammary Gland Biol Neoplasia 2010; 15: 253-60.

72. Thiery JP, Sleeman JP. Complex networks orchestrate epithelial-mesenchymal transitions. Nat Rev Mol Cell Biol 2006; 7: 131-42.

73. Pierce GB. Teratocarcinoma: model for a developmental concept of cancer. Curr Top Dev Biol 1967; 2: 223-46.

74. Reya T, Morrison SJ, Clarke MF, Weissman IL. Stem cells, cancer, and cancer stem cells. Nature 2001; 414: 105-11.

75. Osborne C, Wilson P, Tripathy D. Oncogenes and tumor suppressor genes in breast cancer: potential diagnostic and therapeutic applications. Oncologist 2004; 9: 361-77.

76. Rosen LS, Ashurst HL, Chap L. Targeting signal transduction pathways in metastatic breast cancer: a comprehensive review. Oncologist 2010; 15: 216-35.

77. Reynolds BA, Weiss S. Clonal and population analyses demonstrate that an EGF-responsive mammalian embryonic CNS precursor is a stem cell. Dev Biol 1996; 175: 1-13.

78. Wicha MS, Liu S, Dontu G. Cancer stem cells: an old idea--a paradigm shift. Cancer Res 2006; 66: 1883-90; discussion 95-6.

79. Woodward WA, Chen MS, Behbod F, Rosen JM. On mammary stem cells. J Cell Sci 2005; 118: 3585-94.

80. Kalirai H, Clarke RB. Human breast epithelial stem cells and their regulation. J Pathol 2006; 208: 7-16.

81. Goodell MA, Rosenzweig M, Kim H, et al. Dye efflux studies suggest that hematopoietic stem cells expressing low or undetectable levels of CD34 antigen exist in multiple species. Nat Med 1997; 3: 1337-45.

82. Welm BE, Tepera SB, Venezia T, Graubert TA, Rosen JM, Goodell MA. Sca-1(pos) cells in the mouse mammary gland represent an enriched progenitor cell population. Dev Biol 2002; 245: 42-56.

83. Smalley MJ, Clarke RB. The mammary gland "side population": a putative stem/progenitor cell marker? J Mammary Gland Biol Neoplasia 2005; 10: 37-47.

84. Clayton H, Titley I, Vivanco M. Growth and differentiation of progenitor/stem cells derived from the human mammary gland. Exp Cell Res 2004; 297: 444-60.

85. Reynolds BA, Tetzlaff W, Weiss S. A multipotent EGF-responsive striatal embryonic progenitor cell produces neurons and astrocytes. J Neurosci 1992; 12: 4565-74.

86. Johansson CB, Momma S, Clarke DL, Risling M, Lendahl U, Frisen J. Identification of a neural stem cell in the adult mammalian central nervous system. Cell 1999; 96: 25-34.

87. Al-Hajj M, Wicha MS, Benito-Hernandez A, Morrison SJ, Clarke MF. Prospective identification of tumorigenic breast cancer cells. Proc Natl Acad Sci U S A 2003; 100: 3983-8.

88. Kristiansen G, Winzer KJ, Mayordomo E, et al. CD24 expression is a new prognostic marker in breast cancer. Clin Cancer Res 2003; 9: 4906-13.

89. Abraham BK, Fritz P, McClellan M, Hauptvogel P, Athelogou M, Brauch H. Prevalence of CD44+/CD24-/low cells in breast cancer may not be associated with clinical outcome but may favor distant metastasis. Clin Cancer Res 2005; 11: 1154-9.

90. Mani SA, Guo W, Liao MJ, et al. The epithelial-mesenchymal transition generates cells with properties of stem cells. Cell 2008; 133: 704-15.

91. Ginestier C, Hur MH, Charafe-Jauffret E, et al. ALDH1 is a marker of normal and malignant human mammary stem cells and a predictor of poor clinical outcome. Cell Stem Cell 2007; 1: 555-67.

92. Marcato P, Dean CA, Pan D, et al. Aldehyde Dehydrogenase Activity of Breast Cancer Stem Cells is Primarily Due to Isoform ALDH1A3 and Its Expression is Predictive of Metastasis. Stem Cells 2010.

93. Morimoto K, Kim SJ, Tanei T, et al. Stem cell marker aldehyde dehydrogenase 1-positive breast cancers are characterized by negative estrogen receptor, positive human epidermal growth factor receptor type 2, and high Ki67 expression. Cancer Sci 2009; 100: 1062-8.

94. Zhou L, Jiang Y, Yan T, et al. The prognostic role of cancer stem cells in breast cancer: a meta-analysis of published literatures. Breast Cancer Res Treat; 122: 795-801.

95. Lynch MD, Cariati M, Purushotham AD. Breast cancer, stem cells and prospects for therapy. Breast Cancer Res 2006; 8: 211.

96. Wright MH, Robles AI, Herschkowitz JI, et al. Molecular analysis reveals heterogeneity of mouse mammary tumors conditionally mutant for Brca1. Mol Cancer 2008; 7: 29.

97. Morel AP, Lievre M, Thomas C, Hinkal G, Ansieau S, Puisieux A. Generation of breast cancer stem cells through epithelial-mesenchymal transition. PLoS One 2008; 3: e2888.

98. Shimono Y, Zabala M, Cho RW, et al. Downregulation of miRNA-200c links breast cancer stem cells with normal stem cells. Cell 2009; 138: 592-603.

99. Li X, Lewis MT, Huang J, et al. Intrinsic resistance of tumorigenic breast cancer cells to chemotherapy. J Natl Cancer Inst 2008; 100: 672-9.

100. Creighton CJ, Li X, Landis M, et al. Residual breast cancers after conventional therapy display mesenchymal as well as tumor-initiating features. Proc Natl Acad Sci U S A 2009; 106: 13820-5.

101. Cheng GZ, Chan J, Wang Q, Zhang W, Sun CD, Wang LH. Twist transcriptionally up-regulates AKT2 in breast cancer cells leading to increased migration, invasion, and resistance to paclitaxel. Cancer Res 2007; 67: 1979-87.

102. Yang AD, Fan F, Camp ER, et al. Chronic oxaliplatin resistance induces epithelial-to-mesenchymal transition in colorectal cancer cell lines. Clin Cancer Res 2006; 12: 4147-53.

103. Tewes M, Aktas B, Welt A, et al. Molecular profiling and predictive value of circulating tumor cells in patients with metastatic breast cancer: an option for monitoring response to breast cancer related therapies. Breast Cancer Res Treat 2009; 115: 581-90.

104. Aktas B, Tewes M, Fehm T, Hauch S, Kimmig R, Kasimir-Bauer S. Stem cell and epithelial-mesenchymal transition markers are frequently overexpressed in circulating tumor cells of metastatic breast cancer patients. Breast Cancer Res 2009; 11: R46.

105. Raimondi C, Gradilone A, Naso G, et al. Epithelial-mesenchymal transition and stemness features in circulating tumor cells from breast cancer patients. Breast Cancer Res Treat 2010.

106. Munz M, Baeuerle PA, Gires O. The emerging role of EpCAM in cancer and stem cell signaling. Cancer Res 2009; 69: 5627-9.

107. Brabletz T, Jung A, Spaderna S, Hlubek F, Kirchner T. Opinion: migrating cancer stem cells - an integrated concept of malignant tumour progression. Nat Rev Cancer 2005; 5: 744-9.

108. Merchant AA, Matsui W. Targeting Hedgehog--a cancer stem cell pathway. Clin Cancer Res; 16: 3130-40.

109. Takahashi-Yanaga F, Kahn M. Targeting Wnt signaling: can we safely eradicate cancer stem cells? Clin Cancer Res 2010; 16: 3153-62.

110. Pannuti A, Foreman K, Rizzo P, et al. Targeting Notch to target cancer stem cells. Clin Cancer Res 2010; 16: 3141-52.

111. Liu S, Dontu G, Wicha MS. Mammary stem cells, self-renewal pathways, and carcinogenesis. Breast Cancer Res 2005; 7: 86-95.

112. Jones RJ, Matsui WH, Smith BD. Cancer stem cells: are we missing the target? J Natl Cancer Inst 2004; 96: 583-5.

113. Rizzo P, Osipo C, Foreman K, Golde T, Osborne B, Miele L. Rational targeting of Notch signaling in cancer. Oncogene 2008; 27: 5124-31.

114. Weinmaster G. The ins and outs of notch signaling. Mol Cell Neurosci 1997; 9: 91-102.

115. Miele L. Notch signaling. Clin Cancer Res 2006; 12: 1074-9.

116. Callahan R, Egan SE. Notch signaling in mammary development and oncogenesis. J Mammary Gland Biol Neoplasia 2004; 9: 145-63.

117. Blaumueller CM, Qi H, Zagouras P, Artavanis-Tsakonas S. Intracellular cleavage of Notch leads to a heterodimeric receptor on the plasma membrane. Cell 1997; 90: 281-91.

118. Xu A, Lei L, Irvine KD. Regions of Drosophila Notch that contribute to ligand binding and the modulatory influence of Fringe. J Biol Chem 2005; 280: 30158-65.

119. Logeat F, Bessia C, Brou C, et al. The Notch1 receptor is cleaved constitutively by a furin-like convertase. Proc Natl Acad Sci U S A 1998; 95: 8108-12.

120. Parks AL, Klueg KM, Stout JR, Muskavitch MA. Ligand endocytosis drives receptor dissociation and activation in the Notch pathway. Development 2000; 127: 1373-85.

121. Iso T, Kedes L, Hamamori Y. HES and HERP families: multiple effectors of the Notch signaling pathway. J Cell Physiol 2003; 194: 237-55.

122. Ronchini C, Capobianco AJ. Induction of cyclin D1 transcription and CDK2 activity by Notch(ic): implication for cell cycle disruption in transformation by Notch(ic). Mol Cell Biol 2001; 21: 5925-34.

123. Weng AP, Millholland JM, Yashiro-Ohtani Y, et al. c-Myc is an important direct target of Notch1 in T-cell acute lymphoblastic leukemia/lymphoma. Genes Dev 2006; 20: 2096-109.

124. Klinakis A, Szabolcs M, Politi K, Kiaris H, Artavanis-Tsakonas S, Efstratiadis A. Myc is a Notch1 transcriptional target and a requisite for Notch1-induced mammary tumorigenesis in mice. Proc Natl Acad Sci U S A 2006; 103: 9262-7.

125. Rangarajan A, Talora C, Okuyama R, et al. Notch signaling is a direct determinant of keratinocyte growth arrest and entry into differentiation. EMBO J 2001; 20: 3427-36.

126. Deftos ML, He YW, Ojala EW, Bevan MJ. Correlating notch signaling with thymocyte maturation. Immunity 1998; 9: 777-86.

127. Tagami S, Okochi M, Yanagida K, et al. Regulation of Notch signaling by dynamic changes in the precision of S3 cleavage of Notch-1. Mol Cell Biol 2008; 28: 165-76.

128. Pece S, Serresi M, Santolini E, et al. Loss of negative regulation by Numb over Notch is relevant to human breast carcinogenesis. J Cell Biol 2004; 167: 215-21.

129. McGill MA, Dho SE, Weinmaster G, McGlade CJ. Numb regulates post-endocytic trafficking and degradation of Notch1. J Biol Chem 2009; 284: 26427-38.

130. Rennstam K, McMichael N, Berglund P, et al. Numb protein expression correlates with a basal-like phenotype and cancer stem cell markers in primary breast cancer. Breast Cancer Res Treat 2010; 122: 315-24.

131. Mine T, Matsueda S, Li Y, et al. Breast cancer cells expressing stem cell markers CD44+ CD24 lo are eliminated by Numb-1 peptide-activated T cells. Cancer Immunol Immunother 2009; 58: 1185-94.

132. Zeng Q, Li S, Chepeha DB, et al. Crosstalk between tumor and endothelial cells promotes tumor angiogenesis by MAPK activation of Notch signaling. Cancer Cell 2005; 8: 13-23.

133. Wang Z, Li Y, Kong D, Sarkar FH. The role of Notch signaling pathway in epithelial-mesenchymal transition (EMT) during development and tumor aggressiveness. Curr Drug Targets 2010; 11: 745-51.

134. Sundaram MV. The love-hate relationship between Ras and Notch. Genes Dev 2005; 19: 1825-39.

135. Weijzen S, Rizzo P, Braid M, et al. Activation of Notch-1 signaling maintains the neoplastic phenotype in human Ras-transformed cells. Nat Med 2002; 8: 979-86.

136. Parr C, Watkins G, Jiang WG. The possible correlation of Notch-1 and Notch-2 with clinical outcome and tumour clinicopathological parameters in human breast cancer. Int J Mol Med 2004; 14: 779-86.

137. Weng AP, Ferrando AA, Lee W, et al. Activating mutations of NOTCH1 in human T cell acute lymphoblastic leukemia. Science 2004; 306: 269-71.

138. Rosati E, Sabatini R, Rampino G, et al. Constitutively activated Notch signaling is involved in survival and apoptosis resistance of B-CLL cells. Blood 2009; 113: 856-65.

139. Zweidler-McKay PA, He Y, Xu L, et al. Notch signaling is a potent inducer of growth arrest and apoptosis in a wide range of B-cell malignancies. Blood 2005; 106: 3898-906.

140. Nefedova Y, Cheng P, Alsina M, Dalton WS, Gabrilovich DI. Involvement of Notch-1 signaling in bone marrow stroma-mediated de novo drug resistance of myeloma and other malignant lymphoid cell lines. Blood 2004; 103: 3503-10.

141. Westhoff B, Colaluca IN, D'Ario G, et al. Alterations of the Notch pathway in lung cancer. Proc Natl Acad Sci U S A 2009; 106: 22293-8.

142. Park JT, Li M, Nakayama K, et al. Notch3 gene amplification in ovarian cancer. Cancer Res 2006; 66: 6312-8.

143. Konishi J, Kawaguchi KS, Vo H, et al. Gamma-secretase inhibitor prevents Notch3 activation and reduces proliferation in human lung cancers. Cancer Res 2007; 67: 8051-7.

144. Jung SG, Kwon YD, Song JA, et al. Prognostic significance of Notch 3 gene expression in ovarian serous carcinoma. Cancer Sci 2010; 101: 1977-83.

145. Lin JT, Chen MK, Yeh KT, et al. Association of high levels of Jagged-1 and Notch-1 expression with poor prognosis in head and neck cancer. Ann Surg Oncol 2010; 17: 2976-83.

146. Meng RD, Shelton CC, Li YM, et al. gamma-Secretase inhibitors abrogate oxaliplatin-induced activation of the Notch-1 signaling pathway in colon cancer cells resulting in enhanced chemosensitivity. Cancer Res 2009; 69: 573-82.

147. Villaronga MA, Bevan CL, Belandia B. Notch signaling: a potential therapeutic target in prostate cancer. Curr Cancer Drug Targets 2008; 8: 566-80.

148. Bin Hafeez B, Adhami VM, Asim M, et al. Targeted knockdown of Notch1 inhibits invasion of human prostate cancer cells concomitant with inhibition of matrix metalloproteinase-9 and urokinase plasminogen activator. Clin Cancer Res 2009; 15: 452-9.

149. Wang Z, Li Y, Banerjee S, et al. Down-regulation of Notch-1 and Jagged-1 inhibits prostate cancer cell growth, migration and invasion, and induces apoptosis via inactivation of Akt, mTOR, and NF-kappaB signaling pathways. J Cell Biochem 2010; 109: 726-36.

150. Yao J, Qian C. Inhibition of Notch3 enhances sensitivity to gemcitabine in pancreatic cancer through an inactivation of PI3K/Akt-dependent pathway. Med Oncol 2010; 27: 1017-22.

151. Wang J, Wakeman TP, Lathia JD, et al. Notch promotes radioresistance of glioma stem cells. Stem Cells 2010; 28: 17-28.

152. Dotto GP. Notch tumor suppressor function. Oncogene 2008; 27: 5115-23.

153. O'Neill CF, Urs S, Cinelli C, et al. Notch2 signaling induces apoptosis and inhibits human MDA-MB-231 xenograft growth. Am J Pathol 2007; 171: 1023-36.

154. Klinakis A, Lobry C, Abdel-Wahab O, et al. A novel tumour-suppressor function for the Notch pathway in myeloid leukaemia. Nature 2010; 473: 230-3.

155. Stylianou S, Clarke RB, Brennan K. Aberrant activation of notch signaling in human breast cancer. Cancer Res 2006; 66: 1517-25.

156. Farnie G, Clarke RB. Mammary stem cells and breast cancer--role of Notch signalling. Stem Cell Rev 2007; 3: 169-75.

157. Farnie G, Clarke RB, Spence K, et al. Novel cell culture technique for primary ductal carcinoma in situ: role of Notch and epidermal growth factor receptor signaling pathways. J Natl Cancer Inst 2007; 99: 616-27.

158. Lee CW, Simin K, Liu Q, et al. A functional Notch-survivin gene signature in basal breast cancer. Breast Cancer Res 2008; 10: R97.

159. Song LL, Peng Y, Yun J, et al. Notch-1 associates with IKKalpha and regulates IKK activity in cervical cancer cells. Oncogene 2008; 27: 5833-44.

160. Ring A, Dowsett M. Mechanisms of tamoxifen resistance. Endocr Relat Cancer 2004; 11: 643-58.

161. Lee CW, Raskett CM, Prudovsky I, Altieri DC. Molecular dependence of estrogen receptor-negative breast cancer on a notch-survivin signaling axis. Cancer Res 2008; 68: 5273-81.

162. Chen Y, Li D, Liu H, et al. Notch-1 signaling facilitates survivin expression in human non-small cell lung cancer cells. Cancer Biol Ther 2011; 11: 14-21.

163. Osipo C, Patel P, Rizzo P, et al. ErbB-2 inhibition activates Notch-1 and sensitizes breast cancer cells to a gamma-secretase inhibitor. Oncogene 2008; 27: 5019-32.

164. Dong Y, Li A, Wang J, Weber JD, Michel LS. Synthetic lethality through combined Notch-epidermal growth factor receptor pathway inhibition in basal-like breast cancer. Cancer Res 2010; 70: 5465-74.

165. Mittal S, Subramanyam D, Dey D, Kumar RV, Rangarajan A. Cooperation of Notch and Ras/MAPK signaling pathways in human breast carcinogenesis. Mol Cancer 2009; 8: 128.

166. Baranwal S, Alahari SK. Molecular mechanisms controlling E-cadherin expression in breast cancer. Biochem Biophys Res Commun 2009; 384: 6-11.

167. Chen J, Imanaka N, Griffin JD. Hypoxia potentiates Notch signaling in breast cancer leading to decreased E-cadherin expression and increased cell migration and invasion. Br J Cancer 2010; 102: 351-60.

168. Leong KG, Niessen K, Kulic I, et al. Jagged1-mediated Notch activation induces epithelial-to-mesenchymal transition through Slug-induced repression of E-cadherin. J Exp Med 2007; 204: 2935-48.

169. Sahlgren C, Gustafsson MV, Jin S, Poellinger L, Lendahl U. Notch signaling mediates hypoxia-induced tumor cell migration and invasion. Proc Natl Acad Sci U S A 2008; 105: 6392-7.

170. Lee JH, Suk J, Park J, et al. Notch signal activates hypoxia pathway through HES1-dependent SRC/signal transducers and activators of transcription 3 pathway. Mol Cancer Res 2009; 7: 1663-71.

171. Zavadil J, Cermak L, Soto-Nieves N, Bottinger EP. Integration of TGF-beta/Smad and Jagged1/Notch signalling in epithelial-to-mesenchymal transition. EMBO J 2004; 23: 1155-65.

172. Wang Z, Kong D, Banerjee S, et al. Down-regulation of platelet-derived growth factor-D inhibits cell growth and angiogenesis through inactivation of Notch-1 and nuclear factor-kappaB signaling. Cancer Res 2007; 67: 11377-85.

173. Clark EA, Golub TR, Lander ES, Hynes RO. Genomic analysis of metastasis reveals an essential role for RhoC. Nature 2000; 406: 532-5.

174. Kleer CG, van Golen KL, Zhang Y, Wu ZF, Rubin MA, Merajver SD. Characterization of RhoC expression in benign and malignant breast disease: a potential new marker for small breast carcinomas with metastatic ability. Am J Pathol 2002; 160: 579-84.

175. Srivastava S, Ramdass B, Nagarajan S, Rehman M, Mukherjee G, Krishna S. Notch1 regulates the functional contribution of RhoC to cervical carcinoma progression. Br J Cancer 2010; 102: 196-205.

176. Harrison H, Farnie G, Howell SJ, et al. Regulation of breast cancer stem cell activity by signaling through the Notch4 receptor. Cancer Res 2010; 70: 709-18.

177. Sansone P, Storci G, Giovannini C, et al. p66Shc/Notch-3 interplay controls self-renewal and hypoxia survival in human stem/progenitor cells of the mammary gland expanded in vitro as mammospheres. Stem Cells 2007; 25: 807-15.

178. Tao L, Roberts AL, Dunphy KA, Bigelow C, Yan H, Jerry DJ. Repression of Mammary Stem/Progenitor Cells by p53 Is Mediated by Notch and Separable from Apoptotic Activity. Stem Cells 2011; 29: 119-27.

179. Du Z, Li J, Wang L, et al. Overexpression of DeltaNp63alpha induces a stem cell phenotype in MCF7 breast carcinoma cell line through the Notch pathway. Cancer Sci 2010; 101: 2417-24.

180. Noguera-Troise I, Daly C, Papadopoulos NJ, et al. Blockade of Dll4 inhibits tumour growth by promoting non-productive angiogenesis. Novartis Found Symp 2007; 283: 106-20; discussion 21-5, 238-41.

181. Nickoloff BJ, Qin JZ, Chaturvedi V, Denning MF, Bonish B, Miele L. Jagged-1 mediated activation of notch signaling induces complete maturation of human keratinocytes through NF-kappaB and PPARgamma. Cell Death Differ 2002; 9: 842-55.

182. Pitsouli C, Delidakis C. The interplay between DSL proteins and ubiquitin ligases in Notch signaling. Development 2005; 132: 4041-50.

183. Wu Y, Cain-Hom C, Choy L, et al. Therapeutic antibody targeting of individual Notch receptors. Nature 2010; 464: 1052-7.

184. Moss ML, Stoeck A, Yan W, Dempsey PJ. ADAM10 as a target for anti-cancer therapy. Curr Pharm Biotechnol 2008; 9: 2-8.

185. Imbimbo BP. Therapeutic potential of gamma-secretase inhibitors and modulators. Curr Top Med Chem 2008; 8: 54-61.

186. Shih Ie M, Wang TL. Notch signaling, gamma-secretase inhibitors, and cancer therapy. Cancer Res 2007; 67: 1879-82.

187. Oehlrich D, Berthelot DJ, Gijsen HJ. Gamma-Secretase Modulators as Potential Disease Modifying Anti-Alzheimer's Drugs. J Med Chem 2010

188. Lleo A, Berezovska O, Herl L, et al. Nonsteroidal anti-inflammatory drugs lower Abeta42 and change presenilin 1 conformation. Nat Med 2004; 10: 1065-6.

189. Kukar TL, Ladd TB, Bann MA, et al. Substrate-targeting gamma-secretase modulators. Nature 2008; 453: 925-9.

190. De Strooper B, Annaert W. Novel research horizons for presenilins and gamma-secretases in cell biology and disease. Annu Rev Cell Dev Biol 2010; 26: 235-60.

191. Li YM, Xu M, Lai MT, et al. Photoactivated gamma-secretase inhibitors directed to the active site covalently label presenilin 1. Nature 2000; 405: 689-94.

192. Esler WP, Kimberly WT, Ostaszewski BL, et al. Activity-dependent isolation of the presenilin- gamma -secretase complex reveals nicastrin and a gamma substrate. Proc Natl Acad Sci U S A 2002; 99: 2720-5.

193. Kornilova AY, Bihel F, Das C, Wolfe MS. The initial substrate-binding site of gamma-secretase is located on presenilin near the active site. Proc Natl Acad Sci U S A 2005; 102: 3230-5.

194. Morohashi Y, Kan T, Tominari Y, et al. C-terminal fragment of presenilin is the molecular target of a dipeptidic gamma-secretase-specific inhibitor DAPT (N-[N-(3,5-difluorophenacetyl)-L-alanyl]-S-phenylglycine t-butyl ester). J Biol Chem 2006; 281: 14670-6.

195. Seiffert D, Bradley JD, Rominger CM, et al. Presenilin-1 and -2 are molecular targets for gamma-secretase inhibitors. J Biol Chem 2000; 275: 34086-91.

196. Fauq AH, Simpson K, Maharvi GM, Golde T, Das P. A multigram chemical synthesis of the gamma-secretase inhibitor LY411575 and its diastereoisomers. Bioorg Med Chem Lett 2007; 17: 6392-5.

197. Best JD, Jay MT, Otu F, et al. In vivo characterization of Abeta(40) changes in brain and cerebrospinal fluid using the novel gamma-secretase inhibitor N-[cis-4-[(4-chlorophenyl)sulfonyl]-4-(2,5-difluorophenyl)cyclohexyl]-1,1, 1-trifluoromethanesulfonamide (MRK-560) in the rat. J Pharmacol Exp Ther 2006; 317: 786-90.

198. Fleisher AS, Raman R, Siemers ER, et al. Phase 2 safety trial targeting amyloid beta production with a gamma-secretase inhibitor in Alzheimer disease. Arch Neurol 2008; 65: 1031-8.

199. Henley DB, May PC, Dean RA, Siemers ER. Development of semagacestat (LY450139), a functional gamma-secretase inhibitor, for the treatment of Alzheimer's disease. Expert Opin Pharmacother 2009; 10: 1657-64.

200. Zheng M, Wang J, Lubinski J, et al. Studies on the pharmacokinetics and metabolism of a gamma-secretase inhibitor BMS-299897, and exploratory investigation of CYP enzyme induction. Xenobiotica 2009; 39: 544-55.

201. Akiyoshi T, Nakamura M, Yanai K, et al. Gamma-secretase inhibitors enhance taxane-induced mitotic arrest and apoptosis in colon cancer cells. Gastroenterology 2008; 134: 131-44.

202. Wei P, Walls M, Qiu M, et al. Evaluation of selective gamma-secretase inhibitor PF-03084014 for its antitumor efficacy and gastrointestinal safety to guide optimal clinical trial design. Mol Cancer Ther 2010; 9: 1618-28.

203. Albain KS CC, Rajan P, Zlobin A, Gogellas C, Bova D, Lo SS, Robinson P, Sarker S, Gaynor ER, Cooper R, Aranha G, Czaplicki K, Busby B,Rizzo P, Chisamore M, Demuth T, Blackman S, Watters J, Stiff P, Fuqua SAW, Miele L. Combination of Notch Inhibitor MK-0752 and Endocrine Therapy for Early Stage ER+ Breast Cancer in Presurgical Window Pilot Study. Proceedings of the 2010 San Antonio Breast Cancer Conference; 2010 Dec 8-12; San Antonio, Texas: SABCS 2010 Abstract number PD05-12 2010

204. Evin G, Sernee MF, Masters CL. Inhibition of gamma-secretase as a therapeutic intervention for Alzheimer's disease: prospects, limitations and strategies. CNS Drugs 2006; 20: 351-72.

205. Real PJ, Tosello V, Palomero T, et al. Gamma-secretase inhibitors reverse glucocorticoid resistance in T cell acute lymphoblastic leukemia. Nat Med 2009; 15: 50-8.

206. Slodkowska EA, Ross JS. MammaPrint 70-gene signature: another milestone in personalized medical care for breast cancer patients. Expert Rev Mol Diagn 2009; 9: 417-22.

207. Conlin AK, Seidman AD. Use of the Oncotype DX 21-gene assay to guide adjuvant decision making in early-stage breast cancer. Mol Diagn Ther 2007; 11: 355-60.

208. Watters JW, Cheng C, Majumder PK, et al. De novo discovery of a gamma-secretase inhibitor response signature using a novel in vivo breast tumor model. Cancer Res 2009; 69: 8949-57.

209. Rao SS, O'Neil J, Liberator CD, et al. Inhibition of NOTCH signaling by gamma secretase inhibitor engages the RB pathway and elicits cell cycle exit in T-cell acute lymphoblastic leukemia cells. Cancer Res 2009; 69: 3060-8.

210. He W, Luistro L, Carvajal D, et al. High tumor levels of IL6 and IL8 abrogate preclinical efficacy of the gamma-secretase inhibitor, RO4929097. Mol Oncol 2011; 5(3):292-301.

211. Shelton CC, Tian Y, Frattini MG, Li YM. An exo-cell assay for examining real-time gamma-secretase activity and inhibition. Mol Neurodegener 2009; 4: 22.

212. Jorissen E, De Strooper B. Gamma-secretase and the intramembrane proteolysis of Notch. Curr Top Dev Biol 2010; 92: 201-30.

213. De Strooper B. Aph-1, Pen-2, and Nicastrin with Presenilin generate an active gamma-Secretase complex. Neuron 2003; 38: 9-12.

214. Spasic D, Annaert W. Building gamma-secretase: the bits and pieces. J Cell Sci 2008; 121: 413-20.

215. Steiner H. Uncovering gamma-secretase. Curr Alzheimer Res 2004; 1: 175-81.

216. Hebert SS, Serneels L, Dejaegere T, et al. Coordinated and widespread expression of gamma-secretase in vivo: evidence for size and molecular heterogeneity. Neurobiol Dis 2004; 17: 260-72.

217. Serneels L, Dejaegere T, Craessaerts K, et al. Differential contribution of the three Aph1 genes to gamma-secretase activity in vivo. Proc Natl Acad Sci U S A 2005; 102: 1719-24.

218. Serneels L, Van Biervliet J, Craessaerts K, et al. gamma-Secretase heterogeneity in the Aph1 subunit: relevance for Alzheimer's disease. Science 2009; 324: 639-42.

219. Donoviel DB, Hadjantonakis AK, Ikeda M, Zheng H, Hyslop PS, Bernstein A. Mice lacking both presenilin genes exhibit early embryonic patterning defects. Genes Dev 1999; 13: 2801-10.

220. Ilaya NT, Evin G, Masters CL, Culvenor JG. Nicastrin expression in mouse peripheral tissues is not co-ordinated with presenilin and is high in muscle. J Neurochem 2004; 91: 230-7.

221. Sarasa L, Gallego C, Monleon I, et al. Cloning, sequencing and expression in the dog of the main amyloid precursor protein isoforms and some of the enzymes related with their processing. Neuroscience 2010; 171: 1091-101.

222. Magold AI, Cacquevel M, Fraering PC. Gene expression profiling in cells with enhanced gamma-secretase activity. PLoS One 2009; 4: e6952.

223. Capell A, Kaether C, Edbauer D, et al. Nicastrin interacts with gamma-secretase complex components via the N-terminal part of its transmembrane domain. J Biol Chem 2003; 278: 52519-23.

224. Sato K, Sato M, Nakano A. Rer1p, a retrieval receptor for ER membrane proteins, recognizes transmembrane domains in multiple modes. Mol Biol Cell 2003; 14: 3605-16.

225. Spasic D, Raemaekers T, Dillen K, et al. Rer1p competes with APH-1 for binding to nicastrin and regulates gamma-secretase complex assembly in the early secretory pathway. J Cell Biol 2007; 176: 629-40.

226. Kaether C, Scheuermann J, Fassler M, et al. Endoplasmic reticulum retention of the gamma-secretase complex component Pen2 by Rer1. EMBO Rep 2007; 8: 743-8.

227. LaVoie MJ, Fraering PC, Ostaszewski BL, et al. Assembly of the gamma-secretase complex involves early formation of an intermediate subcomplex of Aph-1 and nicastrin. J Biol Chem 2003; 278: 37213-22.

228. Kaether C, Capell A, Edbauer D, et al. The presenilin C-terminus is required for ER-retention, nicastrin-binding and gamma-secretase activity. EMBO J 2004; 23: 4738-48.

229. Fassler M, Zocher M, Klare S, et al. Masking of transmembrane-based retention signals controls ER export of gamma-secretase. Traffic 2010; 11: 250-8.

230. Kaether C, Haass C, Steiner H. Assembly, trafficking and function of gamma-secretase. Neurodegener Dis 2006; 3: 275-83.

231. Knappenberger KS, Tian G, Ye X, et al. Mechanism of gamma-secretase cleavage activation: is gamma-secretase regulated through autoinhibition involving the presenilin-1 exon 9 loop? Biochemistry 2004; 43: 6208-18.

232. Fraering PC, LaVoie MJ, Ye W, et al. Detergent-dependent dissociation of active gamma-secretase reveals an interaction between Pen-2 and PS1-NTF and offers a model for subunit organization within the complex. Biochemistry 2004; 43: 323-33.

233. Sato T, Diehl TS, Narayanan S, et al. Active gamma-secretase complexes contain only one of each component. J Biol Chem 2007; 282: 33985-93.

234. Zhou S, Zhou H, Walian PJ, Jap BK. CD147 is a regulatory subunit of the gamma-secretase complex in Alzheimer's disease amyloid beta-peptide production. Proc Natl Acad Sci U S A 2005; 102: 7499-504.

235. Pardossi-Piquard R, Bohm C, Chen F, et al. TMP21 transmembrane domain regulates gamma-secretase cleavage. J Biol Chem 2009; 284: 28634-41.

236. Winkler E, Hobson S, Fukumori A, et al. Purification, pharmacological modulation, and biochemical characterization of interactors of endogenous human gamma-secretase. Biochemistry 2009; 48: 1183-97.

237. Tsui-Pierchala BA, Encinas M, Milbrandt J, Johnson EM, Jr. Lipid rafts in neuronal signaling and function. Trends Neurosci 2002; 25: 412-7.

238. Lajoie P, Nabi IR. Lipid rafts, caveolae, and their endocytosis. Int Rev Cell Mol Biol 2010; 282: 135-63.

239. Williamson R, Thompson AJ, Abu M, et al. Isolation of detergent resistant microdomains from cultured neurons: detergent dependent alterations in protein composition. BMC Neurosci 2010; 11: 120.

240. Urano Y, Hayashi I, Isoo N, et al. Association of active gamma-secretase complex with lipid rafts. J Lipid Res 2005; 46: 904-12.

241. Li YM, Lai MT, Xu M, et al. Presenilin 1 is linked with gamma-secretase activity in the detergent solubilized state. Proc Natl Acad Sci U S A 2000; 97: 6138-43.

242. Vetrivel KS, Cheng H, Kim SH, et al. Spatial segregation of gamma-secretase and substrates in distinct membrane domains. J Biol Chem 2005; 280: 25892-900.

243. Osenkowski P, Ye W, Wang R, Wolfe MS, Selkoe DJ. Direct and potent regulation of gamma-secretase by its lipid microenvironment. J Biol Chem 2008; 283: 22529-40.

244. Capell A, Beher D, Prokop S, et al. Gamma-secretase complex assembly within the early secretory pathway. J Biol Chem 2005; 280: 6471-8.

245. Annaert W, De Strooper B. Presenilins: molecular switches between proteolysis and signal transduction. Trends Neurosci 1999; 22: 439-43.

246. Baulac S, LaVoie MJ, Kimberly WT, et al. Functional gamma-secretase complex assembly in Golgi/trans-Golgi network: interactions among presenilin, nicastrin, Aph1, Pen-2, and gamma-secretase substrates. Neurobiol Dis 2003; 14: 194-204.

247. Siman R, Velji J. Localisation of presenilin-nicastrin complexes and gamma-secretase activity to the trans-Golgi network. J Neurochem 2003; 84: 1143-53.

248. Herreman A, Van Gassen G, Bentahir M, et al. gamma-Secretase activity requires the presenilin-dependent trafficking of nicastrin through the Golgi apparatus but not its complex glycosylation. J Cell Sci 2003; 116: 1127-36.

249. Jutras I, Laplante A, Boulais J, Brunet S, Thinakaran G, Desjardins M. Gamma-secretase is a functional component of phagosomes. J Biol Chem 2005; 280: 36310-7.

250. Liao YF, Wang BJ, Cheng HT, Kuo LH, Wolfe MS. Tumor necrosis factor-alpha, interleukin-1beta, and interferon-gamma stimulate gamma-secretase-mediated cleavage of amyloid precursor protein through a JNK-dependent MAPK pathway. J Biol Chem 2004; 279: 49523-32.

251. Pasternak SH, Bagshaw RD, Guiral M, et al. Presenilin-1, nicastrin, amyloid precursor protein, and gamma-secretase activity are co-localized in the lysosomal membrane. J Biol Chem 2003; 278: 26687-94.

252. Bagshaw RD, Pasternak SH, Mahuran DJ, Callahan JW. Nicastrin is a resident lysosomal membrane protein. Biochem Biophys Res Commun 2003; 300: 615-8.

253. Fukumori A, Okochi M, Tagami S, et al. Presenilin-dependent gamma-secretase on plasma membrane and endosomes is functionally distinct. Biochemistry 2006; 45: 4907-14.

254. Hansson CA, Frykman S, Farmery MR, et al. Nicastrin, presenilin, APH-1, and PEN-2 form active gamma-secretase complexes in mitochondria. J Biol Chem 2004; 279: 51654-60.

255. Lazarov VK, Fraering PC, Ye W, Wolfe MS, Selkoe DJ, Li H. Electron microscopic structure of purified, active gamma-secretase reveals an aqueous intramembrane chamber and two pores. Proc Natl Acad Sci U S A 2006; 103: 6889-94.

256. Ogura T, Mio K, Hayashi I, et al. Three-dimensional structure of the gamma-secretase complex. Biochem Biophys Res Commun 2006; 343: 525-34.

257. Osenkowski P, Li H, Ye W, et al. Cryoelectron microscopy structure of purified gamma-secretase at 12 A resolution. J Mol Biol 2009; 385: 642-52.

258. Renzi F, Zhang X, Rice WJ, et al. Structure of {gamma}-secretase and its trimeric pre-activation intermediate by single-particle electron microscopy. J Biol Chem 2011; 286(24):21440-9

259. Steiner H, Than M, Bode W, Haass C. Pore-forming scissors? A first structural glimpse of gamma-secretase. Trends Biochem Sci 2006; 31: 491-3.

260. Hemming ML, Elias JE, Gygi SP, Selkoe DJ. Proteomic profiling of gamma-secretase substrates and mapping of substrate requirements. PLoS Biol 2008; 6: e257.

261. Yamasaki A, Eimer S, Okochi M, et al. The GxGD motif of presenilin contributes to catalytic function and substrate identification of gamma-secretase. J Neurosci 2006; 26: 3821-8.

262. Perez-Revuelta BI, Fukumori A, Lammich S, Yamasaki A, Haass C, Steiner H. Requirement for small side chain residues within the GxGD-motif of presenilin for gamma-secretase substrate cleavage. J Neurochem 2010; 112: 940-50.

263. Tolia A, Horre K, De Strooper B. Transmembrane domain 9 of presenilin determines the dynamic conformation of the catalytic site of gamma-secretase. J Biol Chem 2008; 283: 19793-803.

264. van Roy F, Berx G. The cell-cell adhesion molecule E-cadherin. Cell Mol Life Sci 2008.

265. Semb H, Christofori G. The tumor-suppressor function of E-cadherin. Am J Hum Genet 1998; 63: 1588-93.

266. Kowalski PJ, Rubin MA, Kleer CG. E-cadherin expression in primary carcinomas of the breast and its distant metastases. Breast Cancer Res 2003; 5: R217-22.

267. Thiery JP, Morgan M. Breast cancer progression with a Twist. Nat Med 2004; 10: 777-8.

268. Onder TT, Gupta PB, Mani SA, Yang J, Lander ES, Weinberg RA. Loss of E-cadherin promotes metastasis via multiple downstream transcriptional pathways. Cancer Res 2008; 68: 3645-54.

269. Ferber EC, Kajita M, Wadlow A, et al. A role for the cleaved cytoplasmic domain of E-cadherin in the nucleus. J Biol Chem 2008; 283: 12691-700.

270. Kiss A, Troyanovsky RB, Troyanovsky SM. p120-catenin is a key component of the cadherin-gamma-secretase supercomplex. Mol Biol Cell 2008; 19: 4042-50.

271. Yanagisawa M, Huveldt D, Kreinest P, et al. A p120 catenin isoform switch affects Rho activity, induces tumor cell invasion, and predicts metastatic disease. J Biol Chem 2008; 283: 18344-54.

272. Martin S, Jansen F, Bokelmann J, Kolb H. Soluble CD44 splice variants in metastasizing human breast cancer. Int J Cancer 1997; 74: 443-5.

273. Murakami D, Okamoto I, Nagano O, et al. Presenilin-dependent gamma-secretase activity mediates the intramembranous cleavage of CD44. Oncogene 2003; 22: 1511-6.

274. Oliferenko S, Kaverina I, Small JV, Huber LA. Hyaluronic acid (HA) binding to CD44 activates Rac1 and induces lamellipodia outgrowth. J Cell Biol 2000; 148: 1159-64.

275. Pillozzi S, Brizzi MF, Bernabei PA, et al. VEGFR-1 (FLT-1), beta1 integrin, and hERG K+ channel for a macromolecular signaling complex in acute myeloid leukemia: role in cell migration and clinical outcome. Blood 2007; 110: 1238-50.

276. Rahimi N, Golde TE, Meyer RD. Identification of ligand-induced proteolytic cleavage and ectodomain shedding of VEGFR-1/FLT1 in leukemic cancer cells. Cancer Res 2009; 69: 2607-14.

277. Mezquita B, Mezquita J, Pau M, Mezquita C. A novel intracellular isoform of VEGFR-1 activates Src and promotes cell invasion in MDA-MB-231 breast cancer cells. J Cell Biochem 2010; 110: 732-42.

278. Yarden Y, Sliwkowski MX. Untangling the ErbB signalling network. Nat Rev Mol Cell Biol 2001; 2: 127-37.

279. Ni CY, Yuan H, Carpenter G. Role of the ErbB-4 carboxyl terminus in gamma-secretase cleavage. J Biol Chem 2003; 278: 4561-5.

280. Zhou W, Carpenter G. Heregulin-dependent trafficking and cleavage of ErbB-4. J Biol Chem 2000; 275: 34737-43.

281. Srinivasan R, Gillett CE, Barnes DM, Gullick WJ. Nuclear expression of the c-erbB-4/HER-4 growth factor receptor in invasive breast cancers. Cancer Res 2000; 60: 1483-7.

282. Jones FE. HER4 intracellular domain (4ICD) activity in the developing mammary gland and breast cancer. J Mammary Gland Biol Neoplasia 2008; 13: 247-58.

283. Vidal GA, Naresh A, Marrero L, Jones FE. Presenilin-dependent gamma-secretase processing regulates multiple ERBB4/HER4 activities. J Biol Chem 2005; 280: 19777-83.

284. Zhu Y, Sullivan LL, Nair SS, et al. Coregulation of estrogen receptor by ERBB4/HER4 establishes a growth-promoting autocrine signal in breast tumor cells. Cancer Res 2006; 66: 7991-8.

285. Rokicki J, Das PM, Giltnane JM, et al. The ERalpha coactivator, HER4/4ICD, regulates progesterone receptor expression in normal and malignant breast epithelium. Mol Cancer 2010; 9: 150.

286. Naresh A, Thor AD, Edgerton SM, Torkko KC, Kumar R, Jones FE. The HER4/4ICD estrogen receptor coactivator and BH3-only protein is an effector of tamoxifen-induced apoptosis. Cancer Res 2008; 68: 6387-95.

287. Maetzel D, Denzel S, Mack B, et al. Nuclear signalling by tumour-associated antigen EpCAM. Nat Cell Biol 2009; 11: 162-71.

288. Ralhan R, Cao J, Lim T, Macmillan C, Freeman JL, Walfish PG. EpCAM nuclear localisation identifies aggressive thyroid cancer and is a marker for poor prognosis. BMC Cancer 2010; 10: 331.

289. Hazan RB, Qiao R, Keren R, Badano I, Suyama K. Cadherin switch in tumor progression. Ann N Y Acad Sci 2004; 1014: 155-63.

290. Uemura K, Kihara T, Kuzuya A, et al. Characterization of sequential N-cadherin cleavage by ADAM10 and PS1. Neurosci Lett 2006; 402: 278-83.

291. Marambaud P, Wen PH, Dutt A, et al. A CBP binding transcriptional repressor produced by the PS1/epsilon-cleavage of N-cadherin is inhibited by PS1 FAD mutations. Cell 2003; 114: 635-45.

292. Yang DS, Tandon A, Chen F, et al. Mature glycosylation and trafficking of nicastrin modulate its binding to presenilins. J Biol Chem 2002; 277: 28135-42.

293. Confaloni A, Terreni L, Piscopo P, et al. Nicastrin gene in familial and sporadic Alzheimer's disease. Neurosci Lett 2003; 353: 61-5.

294. George RA, Spriggs RV, Bartlett GJ, et al. Effective function annotation through catalytic residue conservation. Proc Natl Acad Sci U S A 2005; 102: 12299-304.

295. Fagan R, Swindells M, Overington J, Weir M. Nicastrin, a presenilin-interacting protein, contains an aminopeptidase/transferrin receptor superfamily domain. Trends Biochem Sci 2001; 26: 213-4.

296. Yu G, Nishimura M, Arawaka S, et al. Nicastrin modulates presenilin-mediated notch/glp-1 signal transduction and betaAPP processing. Nature 2000; 407: 48-54.

297. Dermaut B, Theuns J, Sleegers K, et al. The gene encoding nicastrin, a major gamma-secretase component, modifies risk for familial early-onset Alzheimer disease in a Dutch population-based sample. Am J Hum Genet 2002; 70: 1568-74.

298. Tomita T, Katayama R, Takikawa R, Iwatsubo T. Complex N-glycosylated form of nicastrin is stabilized and selectively bound to presenilin fragments. FEBS Lett 2002; 520: 117-21.

299. Shah S, Lee SF, Tabuchi K, et al. Nicastrin functions as a gamma-secretase-substrate receptor. Cell 2005; 122: 435-47.

300. Chen F, Yu G, Arawaka S, et al. Nicastrin binds to membrane-tethered Notch. Nat Cell Biol 2001; 3: 751-4.

301. Chavez-Gutierrez L, Tolia A, Maes E, Li T, Wong PC, de Strooper B. Glu(332) in the Nicastrin ectodomain is essential for gamma-secretase complex maturation but not for its activity. J Biol Chem 2008; 283: 20096-105.

302. Dries DR, Shah S, Han YH, et al. Glu-333 of nicastrin directly participates in gamma-secretase activity. J Biol Chem 2009; 284: 29714-24.

303. Walker ES, Martinez M, Wang J, Goate A. Conserved residues in juxtamembrane region of the extracellular domain of nicastrin are essential for gamma-secretase complex formation. J Neurochem 2006; 98: 300-9.

304. Cruts M, Van Broeckhoven C. Presenilin mutations in Alzheimer's disease. Hum Mutat 1998; 11: 183-90.

305. Bertram L, McQueen MB, Mullin K, Blacker D, Tanzi RE. Systematic meta-analyses of Alzheimer disease genetic association studies: the AlzGene database. Nat Genet 2007; 39: 17-23.

306. Helisalmi S, Dermaut B, Hiltunen M, et al. Possible association of nicastrin polymorphisms and Alzheimer disease in the Finnish population. Neurology 2004; 63: 173-5.

307. Cousin E, Hannequin D, Mace S, et al. No replication of the association between the Nicastrin gene and familial early-onset Alzheimer's disease. Neurosci Lett 2003; 353: 153-5.

308. Zhong L, Dong-hai Q, Hong-ying L, Qing-feng L. Analysis of the nicastrin promoter rs10752637 polymorphism and its association with Alzheimer's disease. Eur J Neurosci 2009; 30: 1831-6.

309. Ma Z, Han D, Zuo X, Wang F, Jia J. Association between promoter polymorphisms of the nicastrin gene and sporadic Alzheimer's disease in North Chinese Han population. Neurosci Lett 2009; 458: 136-9.

310. Lupton MK, Proitsi P, Danillidou M, et al. Deep sequencing of the nicastrin gene in pooled DNA, the identification of genetic variants that affect risk of Alzheimer's disease. PLoS One 2010; 6: e17298.

311. Confaloni A, Crestini A, Albani D, et al. Rat nicastrin gene: cDNA isolation, mRNA variants and expression pattern analysis. Brain Res Mol Brain Res 2005; 136: 12-22.

312. Schell T, Kulozik AE, Hentze MW. Integration of splicing, transport and translation to achieve mRNA quality control by the nonsense-mediated decay pathway. Genome Biol 2002; 3: REVIEWS1006.

313. Peirce MJ, Wait R, Begum S, Saklatvala J, Cope AP. Expression profiling of lymphocyte plasma membrane proteins. Mol Cell Proteomics 2004; 3: 56-65.

314. Chung HM, Struhl G. Nicastrin is required for Presenilin-mediated transmembrane cleavage in Drosophila. Nat Cell Biol 2001; 3: 1129-32.

315. Zhang YW, Luo WJ, Wang H, et al. Nicastrin is critical for stability and trafficking but not association of other presenilin/gamma-secretase components. J Biol Chem 2005; 280: 17020-6.

316. Shirotani K, Edbauer D, Capell A, Schmitz J, Steiner H, Haass C. Gamma-secretase activity is associated with a conformational change of nicastrin. J Biol Chem 2003; 278: 16474-7.

317. Shirotani K, Edbauer D, Kostka M, Steiner H, Haass C. Immature nicastrin stabilizes APH-1 independent of PEN-2 and presenilin: identification of nicastrin mutants that selectively interact with APH-1. J Neurochem 2004; 89: 1520-7.

318. Zhao G, Liu Z, Ilagan MX, Kopan R. Gamma-secretase composed of PS1/Pen2/Aph1a can cleave notch and amyloid precursor protein in the absence of nicastrin. J Neurosci 2010; 30: 1648-56.

319. Futai E, Yagishita S, Ishiura S. Nicastrin is dispensable for gamma-secretase protease activity in the presence of specific presenilin mutations. J Biol Chem 2009; 284: 13013-22.

320. Blom N, Sicheritz-Ponten T, Gupta R, Gammeltoft S, Brunak S. Prediction of post-translational glycosylation and phosphorylation of proteins from the amino acid sequence. Proteomics 2004; 4: 1633-49.

321. An HJ, Froehlich JW, Lebrilla CB. Determination of glycosylation sites and site-specific heterogeneity in glycoproteins. Curr Opin Chem Biol 2009; 13: 421-6.

322. Leem JY, Vijayan S, Han P, et al. Presenilin 1 is required for maturation and cell surface accumulation of nicastrin. J Biol Chem 2002; 277: 19236-40.

323. Kornfeld R, Kornfeld S. Assembly of asparagine-linked oligosaccharides. Annu Rev Biochem 1985; 54: 631-64.

324. Chen R, Jiang X, Sun D, et al. Glycoproteomics analysis of human liver tissue by combination of multiple enzyme digestion and hydrazide chemistry. J Proteome Res 2009; 8: 651-61.

325. Wollscheid B, Bausch-Fluck D, Henderson C, et al. Mass-spectrometric identification and relative quantification of N-linked cell surface glycoproteins. Nat Biotechnol 2009; 27: 378-86.

326. Kimberly WT, LaVoie MJ, Ostaszewski BL, Ye W, Wolfe MS, Selkoe DJ. Complex N-linked glycosylated nicastrin associates with active gamma-secretase and undergoes tight cellular regulation. J Biol Chem 2002; 277: 35113-7.

327. Arawaka S, Hasegawa H, Tandon A, et al. The levels of mature glycosylated nicastrin are regulated and correlate with gamma-secretase processing of amyloid beta-precursor protein. J Neurochem 2002; 83: 1065-71.

328. Iwanaga T, Tsutsumi R, Noritake J, Fukata Y, Fukata M. Dynamic protein palmitoylation in cellular signaling. Prog Lipid Res 2009; 48: 117-27.

329. Basu. Protein palmitoylation and dynamic modulation of protein function. Current Science 2004; 87.

330. Cheng H, Vetrivel KS, Drisdel RC, et al. S-palmitoylation of gamma-secretase subunits nicastrin and APH-1. J Biol Chem 2009; 284: 1373-84.

331. Kim SK, Park HJ, Hong HS, Baik EJ, Jung MW, Mook-Jung I. ERK1/2 is an endogenous negative regulator of the gamma-secretase activity. FASEB J 2006; 20: 157-9.

332. Tung YT, Hsu WM, Wang BJ, et al. Sodium selenite inhibits gamma-secretase activity through activation of ERK. Neurosci Lett 2008; 440: 38-43.

333. Giamas G, Man YL, Hirner H, et al. Kinases as targets in the treatment of solid tumors. Cell Signal 2010; 22: 984-1002.

334. Kuo LH, Hu MK, Hsu WM, et al. Tumor necrosis factor-alpha-elicited stimulation of gamma-secretase is mediated by c-Jun N-terminal kinase-dependent phosphorylation of presenilin and nicastrin. Mol Biol Cell 2008; 19: 4201-12.

335. Hattori C, Asai M, Oma Y, et al. BACE1 interacts with nicastrin. Biochem Biophys Res Commun 2002; 293: 1228-32.

336. Pardossi-Piquard R, Dunys J, Yu G, St George-Hyslop P, Alves da Costa C, Checler F. Neprilysin activity and expression are controlled by nicastrin. J Neurochem 2006; 97: 1052-6.

337. Hu Y, Ye Y, Fortini ME. Nicastrin is required for gamma-secretase cleavage of the Drosophila Notch receptor. Dev Cell 2002; 2: 69-78.

338. Lopez-Schier H, St Johnston D. Drosophila nicastrin is essential for the intramembranous cleavage of notch. Dev Cell 2002; 2: 79-89.

339. Li J, Fici GJ, Mao CA, et al. Positive and negative regulation of the gamma-secretase activity by nicastrin in a murine model. J Biol Chem 2003; 278: 33445-9.

340. Nguyen V, Hawkins C, Bergeron C, et al. Loss of nicastrin elicits an apoptotic phenotype in mouse embryos. Brain Res 2006; 1086: 76-84.

341. Rozmahel R, Mount HT, Chen F, et al. Alleles at the Nicastrin locus modify presenilin 1-deficiency phenotype. Proc Natl Acad Sci U S A 2002; 99: 14452-7.

342. Pardossi-Piquard R, Dunys J, Giaime E, et al. p53-dependent control of cell death by nicastrin: lack of requirement for presenilin-dependent gamma-secretase complex. J Neurochem 2009; 109: 225-37.

343. Dunys J, Kawarai T, Sevalle J, et al. p53-Dependent Aph-1 and Pen-2 anti-apoptotic phenotype requires the integrity of the gamma-secretase complex but is independent of its activity. J Biol Chem 2007; 282: 10516-25.

344. Checler F, Dunys J, Pardossi-Piquard R, Alves da Costa C. p53 is regulated by and regulates members of the gamma-secretase complex. Neurodegener Dis 2010; 7: 50-5.

345. Hwang DY, Kim YK, Lim CJ, Cho JS. Mutant nicastrin protein can induce the cytochrome c release and the Bax expression. Int J Neurosci 2004; 114: 1277-89.

346. Ciechanover A. Proteolysis: from the lysosome to ubiquitin and the proteasome. Nat Rev Mol Cell Biol 2005; 6: 79-87.

347. He G, Qing H, Tong Y, Cai F, Ishiura S, Song W. Degradation of nicastrin involves both proteasome and lysosome. J Neurochem 2007; 101: 982-92.

348. Massey LK, Mah AL, Monteiro MJ. Ubiquilin regulates presenilin endoproteolysis and modulates gamma-secretase components, Pen-2 and nicastrin. Biochem J 2005; 391: 513-25.

349. Maeda T, Marutani T, Zou K, et al. An E3 ubiquitin ligase, Synoviolin, is involved in the degradation of immature nicastrin, and regulates the production of amyloid beta-protein. FEBS J 2009; 276: 5832-40.

350. Deary IJ, Hamilton G, Hayward C, et al. Nicastrin gene polymorphisms, cognitive ability level and cognitive ageing. Neurosci Lett 2005; 373: 110-4.

351. Tabuchi K, Chen G, Sudhof TC, Shen J. Conditional forebrain inactivation of nicastrin causes progressive memory impairment and age-related neurodegeneration. J Neurosci 2009; 29: 7290-301.

352. Wang B, Yang W, Wen W, et al. Gamma-secretase gene mutations in familial acne inversa. Science 2010; 330: 1065.

353. Brijbassi S, Amtul Z, Newbigging S, Westaway D, St George-Hyslop P, Rozmahel RF. Excess of nicastrin in brain results in heterozygosity having no effect on endogenous APP processing and amyloid peptide levels in vivo. Neurobiol Dis 2007; 25: 291-6.

354. Nadler Y, Alexandrovich A, Grigoriadis N, et al. Increased expression of the gamma-secretase components presenilin-1 and nicastrin in activated astrocytes and microglia following traumatic brain injury. Glia 2008; 56: 552-67.

355. Givogri MI, de Planell M, Galbiati F, et al. Notch signaling in astrocytes and neuroblasts of the adult subventricular zone in health and after cortical injury. Dev Neurosci 2006; 28: 81-91.

356. Hayashi I, Takatori S, Urano Y, et al. Single chain variable fragment against nicastrin inhibits the gamma-secretase activity. J Biol Chem 2009; 284: 27838-47.

357. Sturge J, Wienke D, East L, Jones GE, Isacke CM. GPI-anchored uPAR requires Endo180 for rapid directional sensing during chemotaxis. J Cell Biol 2003; 162: 789-94.

358. Sturge J, Wienke D, Isacke CM. Endosomes generate localized Rho-ROCK-MLC2-based contractile signals via Endo180 to promote adhesion disassembly. J Cell Biol 2006; 175: 337-47.

359. Dontu G, Abdallah WM, Foley JM, et al. In vitro propagation and transcriptional profiling of human mammary stem/progenitor cells. Genes Dev 2003; 17: 1253-70.

360. McShane LM, Altman DG, Sauerbrei W, Taube SE, Gion M, Clark GM. Reporting recommendations for tumor marker prognostic studies (REMARK). J Natl Cancer Inst 2005; 97: 1180-4.

361. Dubel S, Breitling F, Fuchs P, et al. Isolation of IgG antibody Fv-DNA from various mouse and rat hybridoma cell lines using the polymerase chain reaction with a simple set of primers. J Immunol Methods 1994; 175: 89-95.

362. Yang J, Weinberg RA. Epithelial-mesenchymal transition: at the crossroads of development and tumor metastasis. Dev Cell 2008; 14: 818-29.

363. Kopan R, Ilagan MX. Gamma-secretase: proteasome of the membrane? Nat Rev Mol Cell Biol 2004; 5: 499-504.

364. PM LR. Phase I pharmacokinetic (PK), and pharmacodynamic (PD) trial of the novel oral Notch inhibitor MK-0752 in patients (pts) with advanced breast cancer (BC) and other solid tumors.

Journal of Clinical Oncology 2006 ASCO Annual Meeting Proceedings Part I 2006; 24.

365. Murphy MP, Das P, Nyborg AC, et al. Overexpression of nicastrin increases Abeta production. FASEB J 2003; 17: 1138-40.

366. Bhaskaran N, Lin KW, Gautier A, Woksepp H, Hellman U, Souchelnytskyi S. Comparative proteome profiling of MCF10A and 184A1 human breast epithelial cells emphasized involvement of CDK4 and cyclin D3 in cell proliferation. Proteomics Clin Appl 2009; 3: 68-77.

367. Kao J, Salari K, Bocanegra M, et al. Molecular profiling of breast cancer cell lines defines relevant tumor models and provides a resource for cancer gene discovery. PLoS One 2009; 4: e6146.

368. Sotiriou C, Neo SY, McShane LM, et al. Breast cancer classification and prognosis based on gene expression profiles from a population-based study. Proc Natl Acad Sci U S A 2003; 100: 10393-8.

369. Rasul S, Balasubramanian R, Filipovic A, Slade MJ, Yague E, Coombes RC. Inhibition of gamma-secretase induces G2/M arrest and triggers apoptosis in breast cancer cells. Br J Cancer 2009; 100: 1879-88.

370. Li T, Wen H, Brayton C, et al. Epidermal growth factor receptor and notch pathways participate in the tumor suppressor function of gamma-secretase. J Biol Chem 2007; 282: 32264-73.

371. Davis MA, Ireton RC, Reynolds AB. A core function for p120-catenin in cadherin turnover. J Cell Biol 2003; 163: 525-34.

372. Baki L, Marambaud P, Efthimiopoulos S, et al. Presenilin-1 binds cytoplasmic epithelial cadherin, inhibits cadherin/p120 association, and regulates stability and function of the cadherin/catenin adhesion complex. Proc Natl Acad Sci U S A 2001; 98: 2381-6.

373. Marambaud P, Shioi J, Serban G, et al. A presenilin-1/gamma-secretase cleavage releases the E-cadherin intracellular domain and regulates disassembly of adherens junctions. EMBO J 2002; 21: 1948-56.

374. McInroy L, Maatta A. Down-regulation of vimentin expression inhibits carcinoma cell migration and adhesion. Biochem Biophys Res Commun 2007; 360: 109-14.

375. Ridley AJ, Schwartz MA, Burridge K, et al. Cell migration: integrating signals from front to back. Science 2003; 302: 1704-9.

376. Nystrom ML, McCulloch D, Weinreb PH, et al. Cyclooxygenase-2 inhibition suppresses alphavbeta6 integrin-dependent oral squamous carcinoma invasion. Cancer Res 2006; 66: 10833-42.

377. Istfan NW, Person KS, Holick MF, Chen TC. 1alpha,25-Dihydroxyvitamin D and fish oil synergistically inhibit G1/S-phase transition in prostate cancer cells. J Steroid Biochem Mol Biol 2007; 103: 726-30.

378. Fitzgerald K, Harrington A, Leder P. Ras pathway signals are required for notch-mediated oncogenesis. Oncogene 2000; 19: 4191-8.

379. Gutierrez A, Look AT. NOTCH and PI3K-AKT pathways intertwined. Cancer Cell 2007; 12: 411-3.

380. Kang DE, Yoon IS, Repetto E, et al. Presenilins mediate phosphatidylinositol 3-kinase/AKT and ERK activation via select signaling receptors. Selectivity of PS2 in platelet-derived growth factor signaling. J Biol Chem 2005; 280: 31537-47.

381. Jin SM, Cho HJ, Jung MW, Mook-Jung I. DNA damage-inducing agent-elicited gamma-secretase activity is dependent on Bax/Bcl-2 pathway but not on caspase cascades. Cell Death Differ 2007; 14: 189-92.

382. Tanaka M, Setoguchi T, Hirotsu M, et al. Inhibition of Notch pathway prevents osteosarcoma growth by cell cycle regulation. Br J Cancer 2009; 100: 1957-65.

383. Efferson CL, Winkelmann CT, Ware C, et al. Downregulation of Notch pathway by a gamma-secretase inhibitor attenuates AKT/mammalian target of rapamycin signaling and glucose uptake in an ERBB2 transgenic breast cancer model. Cancer Res 2010; 70: 2476-84.

384. Wendel HG, De Stanchina E, Fridman JS, et al. Survival signalling by Akt and eIF4E in oncogenesis and cancer therapy. Nature 2004; 428: 332-7.

385. Mungamuri SK, Yang X, Thor AD, Somasundaram K. Survival signaling by Notch1: mammalian target of rapamycin (mTOR)-dependent inhibition of p53. Cancer Res 2006; 66: 4715-24.

386. Soni A, Akcakanat A, Singh G, et al. eIF4E knockdown decreases breast cancer cell growth without activating Akt signaling. Mol Cancer Ther 2008; 7: 1782-8.

387. Nabeshima K, Iwasaki H, Koga K, Hojo H, Suzumiya J, Kikuchi M. Emmprin (basigin/CD147): matrix metalloproteinase modulator and multifunctional cell recognition molecule that plays a critical role in cancer progression. Pathol Int 2006; 56: 359-67.

388. Li QQ, Wang WJ, Xu JD, et al. Involvement of CD147 in regulation of multidrug resistance to P-gp substrate drugs and in vitro invasion in breast cancer cells. Cancer Sci 2007; 98: 1064-9.

389. Edbauer D, Winkler E, Haass C, Steiner H. Presenilin and nicastrin regulate each other and determine amyloid beta-peptide production via complex formation. Proc Natl Acad Sci U S A 2002; 99: 8666-71.

390. Mazzone M, Selfors LM, Albeck J, et al. Dose-dependent induction of distinct phenotypic responses to Notch pathway activation in mammary epithelial cells. Proc Natl Acad Sci U S A 2010; 107: 5012-7.

391. Dang H, Lin AL, Zhang B, Zhang HM, Katz MS, Yeh CK. Role for Notch signaling in salivary acinar cell growth and differentiation. Dev Dyn 2009; 238: 724-31.

392. Aoyagi-Ikeda K, Maeno T, Matsui H, et al. Notch Induces Myofibroblast Differentiation of Alveolar Epithelial Cells via TGF-ss/Smad3 Pathway. Am J Respir Cell Mol Biol 2010.

393. Sergina NV, Rausch M, Wang D, et al. Escape from HER-family tyrosine kinase inhibitor therapy by the kinase-inactive HER3. Nature 2007; 445: 437-41.

394. el-Deiry WS, Tokino T, Velculescu VE, et al. WAF1, a potential mediator of p53 tumor suppression. Cell 1993; 75: 817-25.

395. Harrison H, Farnie G, Brennan KR, Clarke RB. Breast cancer stem cells: something out of notching? Cancer Res 2010; 70: 8973-6.

396. Dontu G, Al-Hajj M, Abdallah WM, Clarke MF, Wicha MS. Stem cells in normal breast development and breast cancer. Cell Prolif 2003; 36 Suppl 1: 59-72.

397. Liu R, Wang X, Chen GY, et al. The prognostic role of a gene signature from tumorigenic breast-cancer cells. N Engl J Med 2007; 356: 217-26.

398. Morris MR, Ricketts C, Gentle D, et al. Identification of candidate tumour suppressor genes frequently methylated in renal cell carcinoma. Oncogene 2010; 29: 2104-17.

399. Woods Ignatoski KM, Grewal NK, Markwart S, Livant DL, Ethier SP. p38MAPK induces cell surface alpha4 integrin downregulation to facilitate erbB-2-mediated invasion. Neoplasia 2003; 5: 128-34.

400. Ivetic A, Ridley AJ. The telling tail of L-selectin. Biochem Soc Trans 2004; 32: 1118-21.

401. Laubli H, Borsig L. Selectins as mediators of lung metastasis. Cancer Microenviron 2010; 3: 97-105.

402. Ramachandran N, Srivastava S, Labaer J. Applications of protein microarrays for biomarker discovery. Proteomics Clin Appl 2008; 2: 1444-59.

403. Kopf E, Zharhary D. Antibody arrays--an emerging tool in cancer proteomics. Int J Biochem Cell Biol 2007; 39: 1305-17.

404. Hudelist G, Pacher-Zavisin M, Singer CF, et al. Use of high-throughput protein array for profiling of differentially expressed proteins in normal and malignant breast tissue. Breast Cancer Res Treat 2004; 86: 281-91.

405. Lin Y, Huang R, Chen L, et al. Identification of interleukin-8 as estrogen receptor-regulated factor involved in breast cancer invasion and angiogenesis by protein arrays. Int J Cancer 2004; 109: 507-15.

406. Yang JY, Zong CS, Xia W, et al. MDM2 promotes cell motility and invasiveness by regulating E-cadherin degradation. Mol Cell Biol 2006; 26: 7269-82.

407. Vazquez-Martin A, Colomer R, Menendez JA. Protein array technology to detect HER2 (erbB-2)-induced 'cytokine signature' in breast cancer. Eur J Cancer 2007; 43: 1117-24.

408. Celis JE, Gromov P, Cabezon T, et al. Proteomic characterization of the interstitial fluid perfusing the breast tumor microenvironment: a novel resource for biomarker and therapeutic target discovery. Mol Cell Proteomics 2004; 3: 327-44.

409. Smith L, Watson MB, O'Kane SL, Drew PJ, Lind MJ, Cawkwell L. The analysis of doxorubicin resistance in human breast cancer cells using antibody microarrays. Mol Cancer Ther 2006; 5: 2115-20.

410. Ghobrial IM, McCormick DJ, Kaufmann SH, et al. Proteomic analysis of mantle-cell lymphoma by protein microarray. Blood 2005; 105: 3722-30.

411. Betapudi V, Licate LS, Egelhoff TT. Distinct roles of nonmuscle myosin II isoforms in the regulation of MDA-MB-231 breast cancer cell spreading and migration. Cancer Res 2006; 66: 4725-33.

412. Lan L, Han H, Zuo H, et al. Upregulation of myosin Va by Snail is involved in cancer cell migration and metastasis. Int J Cancer 2010; 126: 53-64.

413. Dunn TA, Chen S, Faith DA, et al. A novel role of myosin VI in human prostate cancer. Am J Pathol 2006; 169: 1843-54.

414. Khuon S, Liang L, Dettman RW, Sporn PH, Wysolmerski RB, Chew TL. Myosin light chain kinase mediates transcellular intravasation of breast cancer cells through the underlying endothelial cells: a three-dimensional FRET study. J Cell Sci 2010; 123: 431-40.

415. Cui WJ, Liu Y, Zhou XL, Wang FZ, Zhang XD, Ye LH. Myosin light chain kinase is responsible for high proliferative ability of breast cancer cells via anti-apoptosis involving p38 pathway. Acta Pharmacol Sin 2010; 31: 725-32.

416. Komatsu S, Ikebe M. ZIP kinase is responsible for the phosphorylation of myosin II and necessary for cell motility in mammalian fibroblasts. J Cell Biol 2004; 165: 243-54.

417. Burbelo P, Wellstein A, Pestell RG. Altered Rho GTPase signaling pathways in breast cancer cells. Breast Cancer Res Treat 2004; 84: 43-8.

418. Larrea MD, Hong F, Wander SA, et al. RSK1 drives p27Kip1 phosphorylation at T198 to promote RhoA inhibition and increase cell motility. Proc Natl Acad Sci U S A 2009; 106: 9268-73.

419. Rubenstein NM, Chan JF, Kim JY, Hansen SH, Firestone GL. Rnd3/RhoE induces tight junction formation in mammary epithelial tumor cells. Exp Cell Res 2005; 305: 74-82.

420. Deckers M, van Dinther M, Buijs J, et al. The tumor suppressor Smad4 is required for transforming growth factor beta-induced epithelial to mesenchymal transition and bone metastasis of breast cancer cells. Cancer Res 2006; 66: 2202-9.

421. Sperry RB, Bishop NH, Bramwell JJ, et al. Zyxin controls migration in epithelial-mesenchymal transition by mediating actin-membrane linkages at cell-cell junctions. J Cell Physiol 2010; 222: 612-24.

422. Saad S, Gottlieb DJ, Bradstock KF, Overall CM, Bendall LJ. Cancer cell-associated fibronectin induces release of matrix metalloproteinase-2 from normal fibroblasts. Cancer Res 2002; 62: 283-9.

423. Lim Y, Lim ST, Tomar A, et al. PyK2 and FAK connections to p190Rho guanine nucleotide exchange factor regulate RhoA activity, focal adhesion formation, and cell motility. J Cell Biol 2008; 180: 187-203.

424. Zannetti A, Del Vecchio S, Carriero MV, et al. Coordinate up-regulation of Sp1 DNA-binding activity and urokinase receptor expression in breast carcinoma. Cancer Res 2000; 60: 1546-51.

425. Tapias A, Ciudad CJ, Roninson IB, Noe V. Regulation of Sp1 by cell cycle related proteins. Cell Cycle 2008; 7: 2856-67.

426. Kong LM, Liao CG, Fei F, Guo X, Xing JL, Chen ZN. Transcription factor Sp1 regulates expression of cancer-associated molecule CD147 in human lung cancer. Cancer Sci 2010; 101: 1463-70.

427. Mor G, Kohen F, Garcia-Velasco J, et al. Regulation of fas ligand expression in breast cancer cells by estrogen: functional differences between estradiol and tamoxifen. J Steroid Biochem Mol Biol 2000; 73: 185-94.

428. Hofmann MH, Heinrich J, Radziwill G, Moelling K. A short hairpin DNA analogous to miR-125b inhibits C-Raf expression, proliferation, and survival of breast cancer cells. Mol Cancer Res 2009; 7: 1635-44.

429. Korsmeyer SJ. BCL-2 gene family and the regulation of programmed cell death. Cancer Res 1999; 59: 1693s-700s.

430. Nakano K, Vousden KH. PUMA, a novel proapoptotic gene, is induced by p53. Mol Cell 2001; 7: 683-94.

431. Brady M, Vlatkovic N, Boyd MT. Regulation of p53 and MDM2 activity by MTBP. Mol Cell Biol 2005; 25: 545-53.

432. Liu N, Fang H, Li Y, Xu W. Recent research in selective cyclin-dependent kinase 4 inhibitors for anti-cancer treatment. Curr Med Chem 2009; 16: 4869-88.

433. Nakayama S, Torikoshi Y, Takahashi T, et al. Prediction of paclitaxel sensitivity by CDK1 and CDK2 activity in human breast cancer cells. Breast Cancer Res 2009; 11: R12.

434. Williams BR, Amon A. Aneuploidy: cancer's fatal flaw? Cancer Res 2009; 69: 5289-91.

435. Klebig C, Korinth D, Meraldi P. Bub1 regulates chromosome segregation in a kinetochore-independent manner. J Cell Biol 2009; 185: 841-58.

436. Jeganathan K, Malureanu L, Baker DJ, Abraham SC, van Deursen JM. Bub1 mediates cell death in response to chromosome missegregation and acts to suppress spontaneous tumorigenesis. J Cell Biol 2007; 179: 255-67.

437. Muller H, Helin K. The E2F transcription factors: key regulators of cell proliferation. Biochim Biophys Acta 2000; 1470: M1-12.

438. Vuaroqueaux V, Urban P, Labuhn M, et al. Low E2F1 transcript levels are a strong determinant of favorable breast cancer outcome. Breast Cancer Res 2007; 9: R33.

439. Rakha EA, Pinder SE, Paish EC, Robertson JF, Ellis IO. Expression of E2F-4 in invasive breast carcinomas is associated with poor prognosis. J Pathol 2004; 203: 754-61.

440. Mateyak MK, Obaya AJ, Sedivy JM. c-Myc regulates cyclin D-Cdk4 and -Cdk6 activity but affects cell cycle progression at multiple independent points. Mol Cell Biol 1999; 19: 4672-83.

441. Zahnow CA. CCAAT/enhancer binding proteins in normal mammary development and breast cancer. Breast Cancer Res 2002; 4: 113-21.

442. Arnal M, Solary E, Brunet-Lecomte P, Lizard-Nacol S. Expression of the gadd153 gene in normal and tumor breast tissues by a sensitive RT-PCR method. Int J Mol Med 1999; 4: 545-8.

443. Kawai T, Matsumoto M, Takeda K, Sanjo H, Akira S. ZIP kinase, a novel serine/threonine kinase which mediates apoptosis. Mol Cell Biol 1998; 18: 1642-51.

444. Inbal B, Cohen O, Polak-Charcon S, et al. DAP kinase links the control of apoptosis to metastasis. Nature 1997; 390: 180-4.

445. Witt O, Deubzer HE, Milde T, Oehme I. HDAC family: What are the cancer relevant targets? Cancer Lett 2009; 277: 8-21.

446. Koivunen J, Aaltonen V, Peltonen J. Protein kinase C (PKC) family in cancer progression. Cancer Lett 2006; 235: 1-10.

447. Fujimori K, Kadoyama K, Urade Y. Protein kinase C activates human lipocalin-type prostaglandin D synthase gene expression through de-repression of notch-HES signaling and enhancement of AP-2 beta function in brain-derived TE671 cells. J Biol Chem 2005; 280: 18452-61.

448. Wang J, Barnes RO, West NR, Olson M, Chu JE, Watson PH. Jab1 is a target of EGFR signaling in ERalpha-negative breast cancer. Breast Cancer Res 2008; 10: R51.

449. Carriere A, Ray H, Blenis J, Roux PP. The RSK factors of activating the Ras/MAPK signaling cascade. Front Biosci 2008; 13: 4258-75.

450. Light Y, Paterson H, Marais R. 14-3-3 antagonizes Ras-mediated Raf-1 recruitment to the plasma membrane to maintain signaling fidelity. Mol Cell Biol 2002; 22: 4984-96.

451. Kolch W. Meaningful relationships: the regulation of the Ras/Raf/MEK/ERK pathway by protein interactions. Biochem J 2000; 351 Pt 2: 289-305.

452. Yamazaki D, Kurisu S, Takenawa T. Involvement of Rac and Rho signaling in cancer cell motility in 3D substrates. Oncogene 2009; 28: 1570-83.

453. Deeley RG, Westlake C, Cole SP. Transmembrane transport of endo- and xenobiotics by mammalian ATP-binding cassette multidrug resistance proteins. Physiol Rev 2006; 86: 849-99.

454. Bachmeier BE, Iancu CM, Killian PH, et al. Overexpression of the ATP binding cassette gene ABCA1 determines resistance to Curcumin in M14 melanoma cells. Mol Cancer 2009; 8: 129.

455. Park S, Shimizu C, Shimoyama T, et al. Gene expression profiling of ATP-binding cassette (ABC) transporters as a predictor of the pathologic response to neoadjuvant chemotherapy in breast cancer patients. Breast Cancer Res Treat 2006; 99: 9-17.

456. Yu W, Tiwary R, Li J, et al. Alpha-TEA induces apoptosis of human breast cancer cells via activation of TRAIL/DR5 death receptor pathway. Mol Carcinog 2010; 49: 964-73.

457. Kuribayashi K, Krigsfeld G, Wang W, et al. TNFSF10 (TRAIL), a p53 target gene that mediates p53-dependent cell death. Cancer Biol Ther 2008; 7: 2034-8.

458. Turchi L, Aberdam E, Mazure N, et al. Hif-2alpha mediates UV-induced apoptosis through a novel ATF3-dependent death pathway. Cell Death Differ 2008; 15: 1472-80.

459. Stein T, Price KN, Morris JS, et al. Annexin A8 is up-regulated during mouse mammary gland involution and predicts poor survival in breast cancer. Clin Cancer Res 2005; 11: 6872-9.

460. Lo TL, Fong CW, Yusoff P, et al. Sprouty and cancer: the first terms report. Cancer Lett 2006; 242: 141-50.

461. Lo TL, Yusoff P, Fong CW, et al. The ras/mitogen-activated protein kinase pathway inhibitor and likely tumor suppressor proteins, sprouty 1 and sprouty 2 are deregulated in breast cancer. Cancer Res 2004; 64: 6127-36.

462. Wang L, Ji C, Wu H, et al. Identification and expression analysis of a novel splice variant of human Sprouty1 gene. Int J Mol Med 2003; 12: 783-7.

463. Salemi M, Calogero AE, Zaccarello G, et al. Expression of SPANX proteins in normal prostatic tissue and in prostate cancer. Eur J Histochem 2010; 54: e41.

464. Milde-Langosch K, Janke S, Wagner I, et al. Role of Fra-2 in breast cancer: influence on tumor cell invasion and motility. Breast Cancer Res Treat 2008; 107: 337-47.

465. Jacobs K, Van Gele M, Forsyth R, et al. P-cadherin counteracts myosin II-B function: implications in melanoma progression. Mol Cancer 2010; 9: 255.

466. Chu CY, Chang CC, Prakash E, Kuo ML. Connective tissue growth factor (CTGF) and cancer progression. J Biomed Sci 2008; 15: 675-85.

467. Scherle P, Behrens T, Staudt LM. Ly-GDI, a GDP-dissociation inhibitor of the RhoA GTP-binding protein, is expressed preferentially in lymphocytes. Proc Natl Acad Sci U S A 1993; 90: 7568-72.

468. Zhang B. Rho GDP dissociation inhibitors as potential targets for anticancer treatment. Drug Resist Updat 2006; 9: 134-41.

469. Liu J, Wen G, Cao D. Aldo-keto reductase family 1 member B1 inhibitors: old drugs with new perspectives. Recent Pat Anticancer Drug Discov 2009; 4: 246-53.

470. Nagai MA, Fregnani JH, Netto MM, Brentani MM, Soares FA. Down-regulation of PHLDA1 gene expression is associated with breast cancer progression. Breast Cancer Res Treat 2007; 106: 49-56.

471. Rivenbark AG, Coleman WB. Epigenetic regulation of cystatins in cancer. Front Biosci 2009; 14: 453-62.

472. Ueki T, Park JH, Nishidate T, et al. Ubiquitination and downregulation of BRCA1 by ubiquitin-conjugating enzyme E2T overexpression in human breast cancer cells. Cancer Res 2009; 69: 8752-60.

473. Lorenzi PL, Reinhold WC, Rudelius M, et al. Asparagine synthetase as a causal, predictive biomarker for L-asparaginase activity in ovarian cancer cells. Mol Cancer Ther 2006; 5: 2613-23.

474. Urquidi V, Goodison S. Genomic signatures of breast cancer metastasis. Cytogenet Genome Res 2007; 118: 116-29.

475. Walker RA. Immunohistochemical markers as predictive tools for breast cancer. J Clin Pathol 2008; 61: 689-96.

476. Harris L, Fritsche H, Mennel R, et al. American Society of Clinical Oncology 2007 update of recommendations for the use of tumor markers in breast cancer. J Clin Oncol 2007; 25: 5287-312.

477. Reedijk M, Odorcic S, Chang L, et al. High-level coexpression of JAG1 and NOTCH1 is observed in human breast cancer and is associated with poor overall survival. Cancer Res 2005; 65: 8530-7.

478. El-Wakeel H, Umpleby HC. Systematic review of fibroadenoma as a risk factor for breast cancer. Breast 2003; 12: 302-7.

479. Marxfeld H, Staedtler F, Harleman JH. Gene expression in fibroadenomas of the rat mammary gland in contrast to spontaneous adenocarcinomas and normal mammary gland. Exp Toxicol Pathol 2006; 58: 145-50.

480. Acs G, Lawton TJ, Rebbeck TR, LiVolsi VA, Zhang PJ. Differential expression of E-cadherin in lobular and ductal neoplasms of the breast and its biologic and diagnostic implications. Am J Clin Pathol 2001; 115: 85-98.

481. Giamas G FA, Jacob J, Messier W, Zang H, Yang D, Zang W, Shifa BA, Photiou A, Stewart-Tralau C, Castelano L, Green A, Coombes RC, Ellis IO, Simak A, Lenz HJ, Stebbing J. Kinome screening for regulators of the estrogen receptor identifies LMTK3 as a new therapeutic target in breast cancer. Nature Medicine 2011; Epub ahead of print.

482. Sheikh MS, Garcia M, Pujol P, Fontana JA, Rochefort H. Why are estrogen-receptor-negative breast cancers more aggressive than the estrogen-receptor-positive breast cancers? Invasion Metastasis 1994; 14: 329-36.

483. Tanaka H, Kono E, Tran CP, et al. Monoclonal antibody targeting of N-cadherin inhibits prostate cancer growth, metastasis and castration resistance. Nat Med 2010; 16: 1414-20.

484. Cobleigh MA, Vogel CL, Tripathy D, et al. Multinational study of the efficacy and safety of humanized anti-HER2 monoclonal antibody in women who have HER2-overexpressing metastatic breast cancer that has progressed after chemotherapy for metastatic disease. J Clin Oncol 1999; 17: 2639-48.

485. Lipman NS, Jackson LR, Trudel LJ, Weis-Garcia F. Monoclonal versus polyclonal antibodies: distinguishing characteristics, applications, and information resources. ILAR J 2005; 46: 258-68.

486. Tang DC, DeVit M, Johnston SA. Genetic immunisation is a simple method for eliciting an immune response. Nature 1992; 356: 152-4.

487. Rudnick SI, Lou J, Shaller CC, et al. Influence of affinity and antigen internalization on the uptake and penetration of Anti-HER2 antibodies in solid tumors. Cancer Res 2011; 71(6): 2250-9.

488. Zuckier LS, Berkowitz EZ, Sattenberg RJ, Zhao QH, Deng HF, Scharff MD. Influence of affinity and antigen density on antibody localisation in a modifiable tumor targeting model. Cancer Res 2000; 60: 7008-13.

489. Hopf U, Meyer zum Buschenfelde KH, Dierich MP. Demonstration of binding sites for IgG Fc and the third complement component (C3) on isolated hepatocytes. J Immunol 1976; 117: 639-45.

490. Homola J. Present and future of surface plasmon resonance biosensors. Anal Bioanal Chem 2003; 377: 528-39.

491. Albini A, Benelli R. The chemoinvasion assay: a method to assess tumor and endothelial cell invasion and its modulation. Nat Protoc 2007; 2: 504-11.

492. Albini A, Noonan DM. The 'chemoinvasion' assay, 25 years and still going strong: the use of reconstituted basement membranes to study cell invasion and angiogenesis. Curr Opin Cell Biol 2010; 22: 677-89.

493. Even-Ram S, Yamada KM. Cell migration in 3D matrix. Curr Opin Cell Biol 2005; 17: 524-32.

494. De Strooper B. Nicastrin: gatekeeper of the gamma-secretase complex. Cell 2005; 122: 318-20.

495. Mendez MG, Kojima S, Goldman RD. Vimentin induces changes in cell shape, motility, and adhesion during the epithelial to mesenchymal transition. FASEB J 2010; 24: 1838-51.

496. Croft DR, Olson MF. Regulating the conversion between rounded and elongated modes of cancer cell movement. Cancer Cell 2008; 14: 349-51.

497. Poincloux R, Collin O, Lizarraga F, et al. Contractility of the cell rear drives invasion of breast tumor cells in 3D Matrigel. Proc Natl Acad Sci U S A 2011; 108(5): 1943-8.

498. Riento K, Guasch RM, Garg R, Jin B, Ridley AJ. RhoE binds to ROCK I and inhibits downstream signaling. Mol Cell Biol 2003; 23: 4219-29.

499. Sanz-Moreno V, Gadea G, Ahn J, et al. Rac activation and inactivation control plasticity of tumor cell movement. Cell 2008; 135: 510-23.

500. Namekata K, Enokido Y, Iwasawa K, Kimura H. MOCA induces membrane spreading by activating Rac1. J Biol Chem 2004; 279: 14331-7.

501. Kashiwa A, Yoshida H, Lee S, et al. Isolation and characterization of novel presenilin binding protein. J Neurochem 2000; 75: 109-16.

502. Lacerda L, Pusztai L, Woodward WA. The role of tumor initiating cells in drug resistance of breast cancer: Implications for future therapeutic approaches. Drug Resist Updat 2010; 13: 99-108.

503. Meyer MJ, Fleming JM, Ali MA, Pesesky MW, Ginsburg E, Vonderhaar BK. Dynamic regulation of CD24 and the invasive, CD44posCD24neg phenotype in breast cancer cell lines. Breast Cancer Res 2009; 11: R82.

504. Grudzien P, Lo S, Albain KS, et al. Inhibition of Notch signaling reduces the stem-like population of breast cancer cells and prevents mammosphere formation. Anticancer Res 2010; 30: 3853-67.

505. Chang J LM, Schott A, Pavlick A, Debrolecki H, Korkaya X, Zhang A, Froehlich A, Rodriguez M, Rimawi M, Wisha M, Lewis M, Hayes D. Targeting Intrinsically-Resistant Breast Cancer Stem Cells with Gamma-Secretase Inhibitors. Cancer Research 2009; 69: Supplement 3.

506. Strizzi L, Hardy KM, Seftor EA, et al. Development and cancer: at the crossroads of Nodal and Notch signaling. Cancer Res 2009; 69: 7131-4.

507. Postovit LM, Margaryan NV, Seftor EA, et al. Human embryonic stem cell microenvironment suppresses the tumorigenic phenotype of aggressive cancer cells. Proc Natl Acad Sci U S A 2008; 105: 4329-34.

508. Postovit LM, Seftor EA, Seftor RE, Hendrix MJ. Targeting Nodal in malignant melanoma cells. Expert Opin Ther Targets 2007; 11: 497-505.

509. Chen DT, Nasir A, Culhane A, et al. Proliferative genes dominate malignancy-risk gene signature in histologically-normal breast tissue. Breast Cancer Res Treat 2010; 119: 335-46.

510. Zhang F, Song C, Ma Y, Tang L, Xu Y, Wang H. Effect of fibroblasts on breast cancer cell mammosphere formation and regulation of stem cell-related gene expression. Int J Mol Med 2011; 28(3):365-371

511. Olsen CJ, Moreira J, Lukanidin EM, Ambartsumian NS. Human mammary fibroblasts stimulate invasion of breast cancer cells in a three-dimensional culture and increase stroma development in mouse xenografts. BMC Cancer 2010; 10: 444.

512. Kazanecki CC, Kowalski AJ, Ding T, Rittling SR, Denhardt DT. Characterization of anti-osteopontin monoclonal antibodies: Binding sensitivity to post-translational modifications. J Cell Biochem 2007; 102: 925-35.

513. Carmen S, Jermutus L. Concepts in antibody phage display. Brief Funct Genomic Proteomic 2002; 1: 189-203.

514. Bottger V. Epitope mapping using phage display peptide libraries. Methods in Molecular Biology, Epitope mapping protocols 2009; 524.

515. Pimenova T, Nazabal A, Roschitzki B, Seebacher J, Rinner O, Zenobi R. Epitope mapping on bovine prion protein using chemical cross-linking and mass spectrometry. J Mass Spectrom 2008; 43: 185-95.

516. Van de Water J, Deininger SO, Macht M, Przybylski M, Gershwin ME. Detection of molecular determinants and epitope mapping using MALDI-TOF mass spectrometry. Clin Immunol Immunopathol 1997; 85: 229-35.

517. Kim SJ, Park Y, Hong HJ. Antibody engineering for the development of therapeutic antibodies. Mol Cells 2005; 20: 17-29.

518. Goldenberg MM. Trastuzumab, a recombinant DNA-derived humanized monoclonal antibody, a novel agent for the treatment of metastatic breast cancer. Clin Ther 1999; 21: 309-18.